



The  
University  
Of  
Sheffield.

# **The Development of Low Band Gap Conjugated Polymers for Application in Electronic Devices**

**Majed Othman A. Alawad**

A thesis submitted to  
The university of Sheffield  
As partial fulfillment for the degree of Doctor of Philosophy

**Department of Chemistry**

**May 2019**

“Hitch your wagon to a star”

“إِذَا غَامَرْتَ فِي شَرْفِ مَرُومِ النُّجُومِ فَلَا تَقْنَعْ بِمَا دُونَ”

**Al-Mutanabbi**

***To my mother, who would be happy with this work!***

## **Declaration**

This thesis submitted for the degree of doctorate of philosophy (PhD) at the University of Sheffield, having been submitted for no other degree. It records the research carried out at the University of Sheffield from January 2015 to December 2018. It is entirely my original work, unless where referenced

Signed .....

Date .....

>>  
**ACKNOWLEDGMENTS**

With a great sense of gratitude, I would like to first offer my sincere thanks to the Almighty Allah, who gave me the patience and the opportunity to achieve my father's dream. I would especially like to thank my beloved mom, Norah Alnugaithan, for praying every day for my success, especially during my scholarship journey. Life is nothing without you, Mom, and even if I wrote a thesis about you, I would not be able to cover a fraction of your love, sacrifice, and support. May God bless you with good health and a long life. My sincere thanks are also due to my beautiful wife, Batool Alrashoodi, for recovering my lost dreams and helping me believe in them again. You are my dream, my love, and my life, and you always will be. I wish you all the best of luck in all of your future endeavours. My sincerest appreciation goes to all my loved ones—my sisters, brothers, and nieces—for their invaluable encouragement and endless support for me throughout my education. You are the breath of my life; my life would be so hard without you.

I heartily thank my supervisor, Dr Ahmed Iraqi, for his tremendous advice, conversation, and guidance throughout every stage of my Ph.D. I am also grateful to my wonderful colleagues in Dr Iraqi's lab; they make the work environment fun and more productive. I would also like to acknowledge all of the highly valuable people in the Department of Chemistry at the University of Sheffield. I cannot name you all, but my very great appreciation must be extended to the amazing technicians: Dr Sandra for helping with the high temperature NMR measurements; Stephen for helping in elemental analysis; Rob for helping with GPC and TGA measurements; and Simon and Sharon for MS and XRD measurements.

My deep thanks also go to Dr Suleiman Alisae, Dr Bakhet Alquarshi, Dr Omar Mohammed Esmaeel, and Mr Bader Altayeb, all of whom have had a great impact on me through their assistance and support in my time of need. I wish you all the best for your futures.

Finally, I would like to express my deep sense of gratitude towards the King Abdulaziz City for Science and Technology for their financial support of my entire scholarship journey.

>>  
**ABSTRACT**

Sunlight, or solar energy, can play an active role in generating electricity and supplying global energy needs, as most renewable energy derives from the sun and can be utilized for a set of commercial or industrial applications. The use of this energy has been extensively studied using photovoltaic devices. Conjugated polymers can assist in utilizing sunlight for electronic applications. This area of research has recently become attractive to many researchers. In their attempts to shed light and develop efficient materials for use in this field, researchers have designed a number of different monomers that can be used either as donors or acceptors, and then copolymerised them using transition metal-catalysts to afford polymers with tailored properties for use in electronic devices.

In this thesis, efforts to design new generations of polymers for use in solar cells have involved thieno[3,4-*c*]pyrrole-4,6-dione (TPD) backbone as the acceptor unit in the alternating push-pull conjugated polymer, and included a variety of donor units (thiophene and fluorene) that couple in a similar fashion to those highlighted for P3HTs (**[RIR] PT<sub>OP</sub>-TPD<sub>BP</sub>**, **[RIR] PT<sub>OP</sub>-TPD<sub>O</sub>**, **[RR] PT<sub>OP</sub>-TPD<sub>O</sub>**, **[T-T] PT<sub>2OP</sub>-TPD<sub>O</sub>**, and **[H-H] PT<sub>2OP</sub>-TPD<sub>O</sub>**) and which use hydrophilic/hydrophobic substituents as side chains along the copolymer backbones (**PF<sub>OXY</sub>DT-TPD<sub>OXY</sub>**, **PF<sub>OXY</sub>DT-TPD<sub>DMO</sub>**, **PF<sub>O</sub>DT-TPD<sub>DMO</sub>**, **PF<sub>O</sub>DT-TPD<sub>OXY</sub>**, **PT<sub>OXY</sub>-TPD<sub>OXY</sub>**, **PT<sub>OXY</sub>-TPD<sub>DMO</sub>**, and **PT<sub>ODD</sub>-TPD<sub>DMO</sub>**).

All copolymers were characterised using Proton Nuclear Magnetic Resonance, Gel Permeation Chromatography, UV-visible absorption spectroscopy, Cyclic Voltammetry, Thermal Gravimetric Analysis, and Powder X-Ray Diffraction. The optical properties were carefully studied and discussed. The optical band gaps of these copolymers were in the range of 1.80 eV to 2.12 eV. Thermal Gravimetric Analysis revealed that all the copolymers showed an excellent thermal stability. Powder X-Ray Diffraction studies indicated that the hydrophilic side chains promote a better chain packing of polymer chains with shorter interlayer distance than their alkylated counterparts.



**>>  
TABLE OF CONTENTS**

|  |             |
|--|-------------|
| <b>ACKNOWLEDGMENTS</b>   | <b>V</b>    |
| <b>ABSTRACT</b>  | <b>VII</b>  |
| <b>TABLE OF CONTENTS</b>   | <b>IX</b>   |
| <b>TABLE OF FIGURES</b>  | <b>XV</b>   |
| <b>TABLE OF SCHEMES</b>  | <b>XX</b>   |
| <b>TABLE OF TABLES</b>   | <b>XXII</b> |
| <b>GLOSSARY OF ABBREVIATIONS AND TERMS</b>   | <b>XXIV</b> |
| <br>   |             |
| <b><u>CHAPTER I INTRODUCTION</u></b>   | <b>1</b>    |
| <b>1.1 INTRODUCTION</b>  | <b>2</b>    |
| <b>1.2 BACKGROUND AND DEVELOPMENT OF CONDUCTIVE POLYMERS</b>                             | <b>2</b>    |
| <b>1.3 <math>\pi</math>- CONJUGATED POLYMERS AND SEMICONDUCTOR PROPERTIES</b>            | <b>4</b>    |
| <b>1.4 ELECTRONIC CONDUCTION IN SEMICONDUCTOR POLYMERS</b>                               | <b>6</b>    |
| <b>1.5 APPLICATIONS OF CONJUGATED SYSTEMS IN ORGANIC ELECTRONIC AND PHOTONIC DEVICES</b> | <b>9</b>    |
| <b>1.5.1 ORGANIC FIELD EFFECT TRANSISTORS (OFETs)</b>                                    | <b>9</b>    |
| <b>1.5.2 POLYMER LIGHT-EMITTING DIODES (PLEDs)</b>                                       | <b>10</b>   |
| <b>1.5.3 ORGANIC SOLAR CELLS (OSCs)</b>  | <b>12</b>   |
| <b>1.5.3.1 BASIC OPERATION OF PHOTOVOLTAIC CELLS</b>                                     | <b>12</b>   |
| <b>1.5.3.2 DEVICE ARCHITECTURES</b>  | <b>13</b>   |
| <b>1.5.3.2.1 SINGLE-LAYER DEVICE</b>   | <b>13</b>   |
| <b>1.5.3.2.2 BI-LAYER HETEROJUNCTION</b>   | <b>14</b>   |
| <b>1.5.3.2.3 BULK HETEROJUNCTION</b>   | <b>15</b>   |
| <b>1.6 SYNTHESIS OF CONJUGATED POLYMERS</b>  | <b>16</b>   |
| <b>1.6.1 SUZUKI COUPLING</b>   | <b>17</b>   |
| <b>1.6.2 DIRECT(HETERO)AROMATIC ARYLATION COUPLING</b>                                   | <b>18</b>   |
| <b>1.7 CHARACTERISTICS OF A SOLAR CELL</b>   | <b>19</b>   |
| <b>1.8 STRUCTURE-PROPERTY RELATIONSHIPS OF CONJUGATED POLYMERS</b>                       | <b>21</b>   |
| <b>1.8.1 MOLECULAR ENERGY LEVELS OF THE POLYMER SOLAR CELLS</b>                          | <b>21</b>   |
| <b>1.8.2 SIDE CHAINS: OUTSIDE THE CONTEXT OF SOLUBILITY</b>                              | <b>23</b>   |
| <b>1.8.3 REGIOREGULARITY OF THE POLYMERS</b>   | <b>26</b>   |
| <b>1.8.4 ELECTRIC DIPOLE MOMENTS</b>   | <b>28</b>   |
| <b>1.9 LOW BAND GAP-BASED DONOR-ACCEPTOR COPOLYMERS</b>                                  | <b>31</b>   |
| <b>1.9.1 POLY(THIENO[3,4-C]PYRROLE-4,6-DIONE) CONTAINING ELECTRON-DONATING MOIETIES</b>  | <b>31</b>   |
| <b>1.9.2 POLY(FLUORENE) CONTAINING ELECTRON-ACCEPTING MOIETIES</b>                       | <b>36</b>   |
| <b>1.10 AIMS OF THE WORK</b>   | <b>40</b>   |
| <b>1.11 REFERENCES</b>   | <b>43</b>   |

|  |           |
|--|-----------|
| <b><u>CHAPTER II EFFECTS OF REGIOREGULARITY OF THIENYL-TPD POLYMERS ON THE OPTICAL AND ELECTRONIC PROPERTIES</u></b>                                   | <b>51</b> |
| 2.1 INTRODUCTION   | 52        |
| 2.2 RESULTS AND DISCUSSIONS  | 55        |
| 2.2.1 MONOMER SYNTHESIS  | 55        |
| 2.2.2 POLYMERS SYNTHESIS AND CHARACTERISATION  | 64        |
| 2.2.3 POLYMERS OPTICAL PROPERTIES  | 66        |
| 2.2.4 POLYMERS ELECTROCHEMICAL PROPERTIES  | 67        |
| 2.2.5 POLYMERS THERMAL PROPERTIES  | 68        |
| 2.2.6 POLYMERS MOLECULAR STRUCTURE   | 69        |
| 2.3. CONCLUSIONS   | 72        |
| 2.4 REFERENCES   | 73        |
| <br>   |           |
| <b><u>CHAPTER III EXAMINING THE EFFECT OF TRI (ETHYLENE GLYCOL) AS SIDE CHAIN OF CONJUGATED POLYMERS ON THEIR CHEMICAL AND PHYSICAL PROPERTIES</u></b> | <b>75</b> |
| 3.1 INTRODUCTION   | 76        |
| 3.2. RESULTS AND DISCUSSION  | 79        |
| 3.2.1 MONOMER SYNTHESIS  | 79        |
| 3.2.2 POLYMERS SYNTHESIS AND CHARACTERISATION  | 84        |
| 3.2.3 POLYMERS OPTICAL PROPERTIES  | 86        |
| 3.2.4 POLYMERS ELECTROCHEMICAL PROPERTIES  | 87        |
| 3.2.5 POLYMERS THERMAL PROPERTIES  | 89        |
| 3.2.6 POLYMERS MOLECULAR STRUCTURE   | 90        |
| 3.3 CONCLUSION   | 91        |
| 3.4 REFERENCES   | 93        |
| <br>   |           |
| <b><u>CHAPTER IV EFFECTS OF TRIETHYLENE GLYCOL SUBSTITUTION PATTERN ON THE PROPERTIES OF THIENYL/THIENO-PYRROLE ALTERNATING COPOLYMERS</u></b>         | <b>95</b> |
| 4.1. INTRODUCTION  | 96        |
| 4.2 RESULTS AND DISCUSSION   | 99        |
| 4.2.1 MONOMER SYNTHESIS  | 99        |
| 4.2.2 POLYMERS SYNTHESIS AND CHARACTERISATION  | 101       |
| 4.2.3 POLYMERS OPTICAL PROPERTIES  | 103       |
| 4.2.4 POLYMERS ELECTROCHEMICAL PROPERTIES  | 106       |
| 4.2.5 POLYMERS THERMAL PROPERTIES  | 107       |
| 4.2.6 POLYMERS STRUCTURE PROPERTIES  | 108       |
| 4.3 CONCLUSION   | 109       |

|  |            |
|--|------------|
| <b>4.4 REFERENCES</b>  | <b>111</b> |
| <b><u>CHAPTER V CONCLUSION AND FUTURE WORK</u></b>   | <b>113</b> |
| <b>5.1 CONCLUSION</b>  | <b>114</b> |
| <b>5.2 FUTURE WORK</b>   | <b>117</b> |
| <b>5.3 REFERENCES</b>  | <b>119</b> |
| <b><u>CHAPTER VI EXPERIMENTAL</u></b>  | <b>120</b> |
| <b>6.1 MATERIALS AND SOLVENTS</b>  | <b>121</b> |
| <b>6.2 ANALYTICAL TECHNIQUES</b>   | <b>121</b> |
| <b><u>6.3 PREPARATION OF MONOMERS</u></b>  | <b>123</b> |
| <b>3-ETHYL-4-METHYL-2-AMINOTHIOPHENE-3,4-DICARBOXYLATE (1)</b>                                       | <b>123</b> |
| <b>THIOPHENE-3,4-DICARBOXYLIC ACID (2)</b>   | <b>123</b> |
| <b>3,4- THIOPHENE DICARBOXYLIC ANHYDRIDE (3)</b>   | <b>124</b> |
| <b>5-(4-BUTYLPHENYL)-THIENO[3,4-C]PYRROLE-4,6-DIONE (M1)</b>   | <b>124</b> |
| <b>5-OCTYL-4H-THIENO[3,4-C]PYRROLE-4,6(5H)-DIONE (M2)</b>  | <b>125</b> |
| <b>1-BROMO-4-N-OCTYLBENZENE (4)</b>  | <b>125</b> |
| <b>3-(4-OCTYLPHENYL) THIOPHENE (5)</b>   | <b>126</b> |
| <b>2-BROMO-3-(4-OCTYLPHENYL) THIOPHENE (6)</b>   | <b>127</b> |
| <b>2,5-DIBROMO-3-(4-OCTYLPHENYL) THIOPHENE (M3)</b>  | <b>127</b> |
| <b>4,4,5,5-TETRAMETHYL-2-(3-(4-OCTYLPHENYL)THIOPHENE-2-YL)-1,3,2-DIOXABOROLANE (7)</b>               | <b>128</b> |
| <b>5-OCTYL-1-(3-(4-OCTYLPHENYL)THIOPHEN-2-YL)-4H-THIENO[3,4-C]PYRROLE-4,6(5H)-DIONE (8)</b>          | <b>128</b> |
| <b>1-(5-BROMO-3-(4-OCTYLPHENYL)THIOPHEN-2-YL)-5-OCTYL-4H-THIENO[3,4-C]PYRROLE-4,6(5H)-DIONE (M4)</b> | <b>129</b> |
| <b>5,5'-DIBROMO-4,4'-BIS(4-OCTYLPHENYL)-2,2'-BITHIOPHENE (M5)</b>                                    | <b>130</b> |
| <b>3,3'-BIS(4-OCTYLPHENYL)-2,2'-BITHIOPHENE (9)</b>  | <b>131</b> |
| <b>5,5'-DIBROMO-3,3'-BIS(4-OCTYLPHENYL)-2,2'-BITHIOPHENE (M6)</b>                                    | <b>131</b> |
| <b>2-(2-(2-METHOXYETHOXY)ETHOXY)ETHYL)-4-METHYLBENZENESULFONATE (10)</b>                             | <b>132</b> |
| <b>1-BROMO-3,7-DIMETHYL OCTANE (11)</b>  | <b>132</b> |
| <b>2-(2-(2-(2-METHOXYETHOXY)ETHOXY)ETHYL)ISOINDOLINE-1,3-DIONE (12)</b>                              | <b>133</b> |
| <b>2-(3,7- DIMETHYL OCTYL)ISOINDOL-1,3-DIONE (13)</b>  | <b>134</b> |
| <b>2-(2-(2-METHOXYETHOXY)ETHOXY)ETHANAMINE (14)</b>  | <b>134</b> |
| <b>3,7-DIMETHYL-1- OCTYL AMINE (15)</b>  | <b>135</b> |

|  |            |
|--|------------|
| <b>5-(2-(2-(2-METHOXYETHOXY)ETHOXY)ETHYL)-4H-THIENO[3,4-C]PYRROLE-4,6(5H)-DIONE (M7)</b>   | <b>135</b> |
| <b>5-(3,7-DIMETHYLOCTYL)-4H-THIENO[3,4-C]PYRROLE-4,6(5H)-DIONE (M8)</b>  | <b>136</b> |
| <b>2,7-DIBROMO-9,9-BIS(2-(2-(2-METHOXYETHOXY)ETHOXY)ETHYL)-9H-FLUORENE (16)</b>  | <b>136</b> |
| <b>2,7-DIBROMO-9,9-DIOCTYL-9H-FLUORENE (17)</b>  | <b>137</b> |
| <b>2,2'-(9,9-BIS(2-(2-(2-METHOXYETHOXY)ETHOXY)ETHYL)-9H-FLUORENE-2,7-DIYL)DITHIOPHENE (18)</b>   | <b>138</b> |
| <b>2,2'-(9,9-DIOCTYL-9H-FLUORENE-2,7-DIYL)DITHIOPHENE (19)</b>   | <b>138</b> |
| <b>5,5'-(9,9-BIS(2-(2-(2-METHOXYETHOXY)ETHOXY)ETHYL)-9H-FLUORENE-2,7-DIYL) BIS(2-BROMOTHIOPHENE) (M9)</b>  | <b>139</b> |
| <b>5,5'-(9,9-DIOCTYL-9H-FLUORENE-2,7-DIYL)BIS(2-BROMOTHIOPHENE) (M10)</b>  | <b>140</b> |
| <b>3-(BROMOMETHYL)THIOPHENE (20)</b>   | <b>140</b> |
| <b>3-((2-(2-METHOXYETHOXY)ETHOXY)METHYL)THIOPHENE (21)</b>   | <b>141</b> |
| <b>2,5-DIBROMO-3-((2-(2-METHOXYETHOXY)ETHOXY)METHYL)THIOPHENE (M11)</b>  | <b>141</b> |
| <br>   |            |
| <b><u>6.4 PREPARATION OF POLYMERS</u></b>  | <b>142</b> |
| <b>POLY(3-(4-N-OCTYLPHENYL)THIOPHENE-ALT-5-(4-BUTYLPHENYL)-THEINO-[3,4-C]PYRROLE-4,6-DIONE) (RIR-PT<sub>OP</sub>-TPD<sub>BP</sub>)</b>   | <b>142</b> |
| <b>POLY(3-(4-N-OCTYLPHENYL)THIOPHENE-ALT-5-(OCTYL)-THEINO-[3,4-C]PYRROLE-4,6-DIONE) (RIR-PT<sub>OP</sub>-TPD<sub>O</sub>)</b>  | <b>143</b> |
| <b>POLY(3-(4-N-OCTYLPHENYL)THIOPHENE-ALT-5-(OCTYL)-THEINO-[3,4-C]PYRROLE-4,6-DIONE) (RR-PT<sub>OP</sub>-TPD<sub>O</sub>)</b>   | <b>143</b> |
| <b>POLY(4,4'-BIS(4-OCTYLPHENYL)-2,2'-BITHIOPHENE-ALT-5-(OCTYL)-THEINO-[3,4-C]PYRROLE-4,6-DIONE) (PBT<sub>OP</sub>-TPD<sub>O</sub>[TT])</b>   | <b>144</b> |
| <b>POLY(3,3'-BIS(4-OCTYLPHENYL)-2,2'-BITHIOPHENE-ALT-5-(OCTYL)-THEINO-[3,4-C]PYRROLE-4,6-DIONE) (PBT<sub>OP</sub>-TPD<sub>O</sub>[HH])</b>   | <b>144</b> |
| <b>POLY(5-(9,9-BIS(2-(2-(2-METHOXYETHOXY)ETHOXY)ETHYL)-7-(THIOPHENE-2-YL)-9H-FLUORENE-2-YL)THIOPHENE-2-YL)-ALT-5-(2-(2-(2-METHOXYETHOXY)ETHOXY)ETHYL)-THIENO[3,4-C]PYRROLE-4,6-DIONE) (PF<sub>OXY</sub>DT-TPD<sub>OXY</sub>)</b> | <b>145</b> |
| <b>POLY(5-(9,9-BIS(2-(2-(2-METHOXYETHOXY)ETHOXY)ETHYL)-7-(THIOPHENE-2-YL)-9H-FLUORENE-2-YL)THIOPHENE-2-YL)-ALT-5-(3,7-DIMETHYLOCTYL)-THEINO-[3,4-C]PYRROLE-4,6-DIONE) (PF<sub>OXY</sub>DT-TPD<sub>DMO</sub>)</b>                 | <b>145</b> |
| <b>POLY(5-(9,9-DIOCTYL-7-(THIOPHENE-2-YL)-9H-FLUORENE-2-YL)THIOPHENE-2-YL)-ALT-5-(2-(2-(2-METHOXYETHOXY)ETHOXY)ETHYL)-THIENO[3,4-C]PYRROLE-4,6-DIONE) (PF<sub>O</sub>DT-TPD<sub>OXY</sub>)</b>                                   | <b>146</b> |

|  |     |
|--|-----|
| POLY(5-(9,9-DIOCTYL-7-(THIOPHENE-2-YL)-9H-FLUORENE-2-YL)THIOPHENE-2-YL)-ALT-5-<br>(-(3,7-DIMETHYLOCTYL))-THIENO-[3,4-C]PYRROLE-4,6-DIONE)(PF <sub>0</sub> DT-TPD <sub>DMO</sub> )      | 147 |
| POLY((3-((2-(2-METHOXYETHOXY)ETHOXY)METHYL)THIOPHENE-2,5-DIYL)-ALT-5-(3,7-<br>DIMETHYLOCTYL)-THIENO [3,4-C] PYRROLE-4,6-DIONE) (PT <sub>OXY</sub> -TPD <sub>DMO</sub> )                | 147 |
| POLY((3-((2-(2-METHOXYETHOXY)ETHOXY)METHYL)THIOPHENE-2,5-DIYL)-ALT-5-[2-[2-(2-<br>METHOXYETHOXY)ETHOXY]ETHYL]-THIENO[3,4-C]PYRROLE-4,6-DIONE) (PT <sub>OXY</sub> -TPD <sub>OXY</sub> ) | 148 |
| POLY((3-(2-OCTYLDODECYL)THIOPHENE-2,5-DIYL)-ALT-5-(3,7-DIMETHYLOCTYL) THIENO[3,<br>4-C]PYRROLE-4,6-DIONE) (PT <sub>ODD</sub> -TPD <sub>DMO</sub> )                                     | 148 |
| 6.5 REFERENCES   | 150 |
| <u>CHAPTER VII SUPPLEMENTARY INFORMATION</u>   | 152 |

>>

## TABLE OF Figures

|   |    |
|---|----|
| 1. 1. Chemical structures of an enormous breakthrough in conjugated polymers.   | 3  |
| 1. 2. Illustration of some important polymers incorporated in various electric applications.  | 3  |
| 1. 3. The formation of a $\pi$ -bond in conjugated polymers.  | 4  |
| 1. 4. Trans-poly (acetylene).   | 4  |
| 1. 5. Illustration of the energy gap for conjugated polymers.   | 5  |
| 1. 6. The identical geometric patterns of polyacetylene.  | 6  |
| 1. 7. The potential energy of degenerate trans-poly(acetylene).   | 7  |
| 1. 8. The structure of a neutral soliton in polyacetylene.  | 7  |
| 1. 9. Schematic representation of the band structure of a neutral, a positively charged and a negatively charged soliton on trans-poly(acetylene).    | 7  |
| 1. 10. The chemical structures of the aromatic form and quinoid form of a thieno[3,4-c]pyrrole-4,6-dione based polymer.                               | 8  |
| 1. 11. Schematic representation of band structures of positively and negatively charged polaron and bipolaron in non-degenerate ground state polymer. | 9  |
| 1. 12. The basic structure of organic field effect transistor.  | 10 |
| 1. 13. The basic structure of polymeric light-emitting diodes.  | 11 |
| 1. 14. Working principle of polymeric light-emitting diodes.  | 12 |
| 1. 15. Working principle of the conversion of sunlight into an electric current in a single layer.  | 13 |
| 1. 16. Working principle of the conversion of sunlight into an electric current in bulk heterojunction cells.   | 13 |
| 1. 17. Schematic structure of a single-layer solar cell.  | 14 |
| 1. 18. Schematic structure of a two-layer solar cell.   | 15 |
| 1. 19. Schematic structure of a bulk heterojunction cell (left) and polymer donor and fullerene derivative acceptors (right).                         | 16 |
| 1. 20. Illustration of Suzuki cross-coupling mechanism.   | 18 |
| 1. 21. The suggested mechanism of direct arylation cross-coupling.  | 19 |
| 1. 22. Current-voltage curves of a typical PV in the dark and under illumination.   | 20 |
| 1. 23. (a) Schematic diagram of donor-acceptor energy levels. (b) <b>PDTSTPD</b> . (c) <b>PBTTPD</b> .  | 23 |
| 1. 24. Chemical structures of a) bithiophene-TPD and b) BDT-TPD adopting various side chains.   | 25 |
| 1. 25. Chemical structures of a) fluorene-benzothiadiazole and b) DPP3T adopting various lengths of polar side chains.                                | 26 |
| 1. 26. Three possible connections on 3-alkylthiophene repeat units.   | 27 |



|  |    |
|--|----|
| 1. 27. The suggested explanation for the dipole moment of TPD-thiophene in the excited state.  | 29 |
| 1. 28. Polymer structures of <b>PTB2</b> , <b>PTB7</b> , <b>PTBF2</b> and <b>PBB3</b> with local dipole moment and PCE values.   | 30 |
| 1. 29. Polymer structures of <b>PID-C8</b> , <b>PPB-C8</b> , <b>PBT-C8</b> and <b>PBT-O8</b> with values of local dipole moments of a) single repeat unit and b) two repeat units and PCE.   | 31 |
| 1. 30. Polymer structures of poly alkylated TPD containing oligothiophenes.  | 34 |
| 1. 31. Polymer structures of poly alkylated TPD containing fused electron donors.  | 36 |
| 1. 32. Polymer structures of alkylated fluorene based copolymers.  | 38 |
| 1. 33. Polymer structure of <b>[RIR] PT<sub>OP</sub>-TPD<sub>BP</sub></b> , <b>[RIR] PT<sub>OP</sub>-TPD<sub>O</sub></b> , <b>[RR] PT<sub>OP</sub>-TPD<sub>O</sub></b> , <b>[T-T] PT<sub>2OP</sub>-TPD<sub>O</sub></b> and <b>[H-H] PT<sub>2OP</sub>-TPD<sub>O</sub></b> . | 41 |
| 1. 34. Polymer structure of <b>PF<sub>OXY</sub>DT-TPD<sub>OXY</sub></b> , <b>PF<sub>OXY</sub>DT-TPD<sub>DMO</sub></b> , <b>PF<sub>O</sub>DT-TPD<sub>OXY</sub></b> and <b>PF<sub>O</sub>DT-TPD<sub>DMO</sub></b> .  | 42 |
| 1. 35. Polymer structure of <b>PT<sub>OXY</sub>-TPD<sub>OXY</sub></b> , <b>PT<sub>OXY</sub>-TPD<sub>DMO</sub></b> and <b>PT<sub>ODD</sub>-TPD<sub>DMO</sub></b> .  | 42 |
| 2.1. Polymer structure of <b>[RIR] PT<sub>OP</sub>-TPD<sub>BP</sub></b> , <b>[RIR] PT<sub>OP</sub>-TPD<sub>O</sub></b> , <b>[RR] PT<sub>OP</sub>-TPD<sub>O</sub></b> , <b>[T-T] PT<sub>2OP</sub>-TPD<sub>O</sub></b> , and <b>[H-H] PT<sub>2OP</sub>-TPD<sub>O</sub></b> . | 54 |
| 2.2. Assumed dipole moment vector of a) <b>[RR] PT<sub>OP</sub>-TPD<sub>O</sub></b> ; b) <b>[RIR] PT<sub>OP</sub>-TPD<sub>O</sub></b> .  | 55 |
| 2.3. <sup>1</sup> H NMR spectrum of <b>M1</b> in CDCl <sub>3</sub> .   | 58 |
| 2.4. <sup>1</sup> H NMR spectrum of <b>M2</b> in CDCl <sub>3</sub> .   | 58 |
| 2.5. <sup>1</sup> H NMR spectrum of <b>M3</b> in CDCl <sub>3</sub> .   | 60 |
| 2.6. <sup>1</sup> H NMR spectrum of <b>M4</b> in CDCl <sub>3</sub> .   | 61 |
| 2.7. <sup>1</sup> H NMR spectrum of <b>M5</b> in CDCl <sub>3</sub> .   | 63 |
| 2.8. <sup>1</sup> H NMR spectrum of <b>M6</b> in CDCl <sub>3</sub> .   | 64 |
| 2.9. Optical absorption spectra of the TPD-based copolymers in: (a) chloroform solution; (b) thin films.   | 67 |
| 2.10. Cyclic voltammograms (top) and energy level diagram (bottom) of the TPD-based copolymers and PCBM.   | 68 |
| 2.11. TGA curve of TPD-based copolymers.   | 69 |
| 2.12. 2D image of the molecular organisation of the polymers.  | 70 |
| 2.13. Powder X-ray diffraction patterns of TPD-based copolymers.   | 71 |
| 3.1. Polymer structures of <b>PF<sub>OXY</sub>DT-TPD<sub>OXY</sub></b> , <b>PF<sub>OXY</sub>DT-TPD<sub>DMO</sub></b> , <b>PF<sub>O</sub>DT-TPD<sub>OXY</sub></b> , and <b>PF<sub>O</sub>DT-TPD<sub>DMO</sub></b> .   | 78 |
| 3.2. <sup>1</sup> H NMR spectrum of <b>M7</b> in CDCl <sub>3</sub> .   | 81 |
| 3.3. <sup>1</sup> H NMR spectrum of <b>M8</b> in C <sub>2</sub> D <sub>6</sub> OS.   | 82 |
| 3.4. <sup>1</sup> H NMR spectrum of <b>M9</b> in CDCl <sub>3</sub> .   | 83 |

|   |     |
|---|-----|
| 3.5. $^1\text{H}$ NMR spectrum of <b>M10</b> in $\text{CDCl}_3$ .   | 84  |
| 3.6. Normalized optical absorption spectra of <b>PF<sub>OXY</sub>DT-TPD<sub>OXY</sub></b> , <b>PF<sub>OXY</sub>DT-TPD<sub>DMO</sub></b> , <b>PF<sub>O</sub>DT-TPD<sub>OXY</sub></b> , and <b>PF<sub>O</sub>DT-TPD<sub>DMO</sub></b> in (a) chloroform solution and (b) as thin films. | 87  |
| 3.7. Cyclic voltammograms (top) and energy level diagram (bottom) of <b>PF<sub>OXY</sub>DT-TPD<sub>OXY</sub></b> , <b>PF<sub>OXY</sub>DT-TPD<sub>DMO</sub></b> , <b>PF<sub>O</sub>DT-TPD<sub>OXY</sub></b> , <b>PF<sub>O</sub>DT-TPD<sub>DMO</sub></b> , and PCBM.                    | 88  |
| 3.8. TGA curves of <b>PF<sub>OXY</sub>DT-TPD<sub>OXY</sub></b> , <b>PF<sub>OXY</sub>DT-TPD<sub>DMO</sub></b> , <b>PF<sub>O</sub>DT-TPD<sub>OXY</sub></b> , and <b>PF<sub>O</sub>DT-TPD<sub>DMO</sub></b> .  | 90  |
| 3.9. XRD patterns of <b>PF<sub>OXY</sub>DT-TPD<sub>OXY</sub></b> and <b>PF<sub>O</sub>DT-TPD<sub>DMO</sub></b> (left) and <b>PF<sub>OXY</sub>DT-TPD<sub>DMO</sub></b> and <b>PF<sub>O</sub>DT-TPD<sub>OXY</sub></b> (right)   | 90  |
| 4.1. Polymer structures of <b>PT<sub>OXY</sub>-TPD<sub>OXY</sub></b> , <b>PT<sub>OXY</sub>-TPD<sub>DMO</sub></b> , and <b>PT<sub>ODD</sub>-TPD<sub>DMO</sub></b> .  | 98  |
| 4.2. $^1\text{H}$ NMR spectrum of <b>M11</b> in $\text{CDCl}_3$   | 100 |
| 4.3. $^1\text{H}$ NMR spectrum of <b>M12</b> in $\text{CDCl}_3$ .   | 101 |
| 4.4. Normalised optical absorption spectra of <b>PT<sub>OXY</sub>-TPD<sub>OXY</sub></b> , <b>PT<sub>OXY</sub>-TPD<sub>DMO</sub></b> , and <b>PT<sub>ODD</sub>-TPD<sub>DMO</sub></b> in (a) chloroform solution and (b) thin films.  | 103 |
| 4.5. Normalised optical absorption spectra of (a) <b>PT<sub>OXY</sub>-TPD<sub>OXY</sub></b> and (b) <b>PT<sub>OXY</sub>-TPD<sub>DMO</sub></b> in different solutions.   | 104 |
| 4.6. Normalized optical absorption spectra of (a) <b>PT<sub>OXY</sub>-TPD<sub>OXY</sub></b> and (b) <b>PT<sub>OXY</sub>-TPD<sub>DMO</sub></b> cast from different solutions.  | 105 |
| 4.7. Cyclic voltammograms of (a) <b>PT<sub>OXY</sub>-TPD<sub>OXY</sub></b> and <b>PT<sub>OXY</sub>-TPD<sub>DMO</sub></b> , (b) <b>PT<sub>ODD</sub>-TPD<sub>DMO</sub></b> , and (c) energy levels diagram of all the respective polymers and PCBM.                                     | 107 |
| 4.8. TGA curve of <b>PT<sub>OXY</sub>-TPD<sub>OXY</sub></b> and <b>PT<sub>OXY</sub>-TPD<sub>DMO</sub></b> .   | 108 |
| 4.9. Powder XRD patterns of <b>PT<sub>OXY</sub>-TPD<sub>OXY</sub></b> and <b>PT<sub>OXY</sub>-TPD<sub>DMO</sub></b> .   | 109 |
| <b>S 1.</b> $^1\text{H}$ NMR spectrum of <b>RIR-PBT<sub>OP</sub>-TPD<sub>BP</sub></b> in $\text{C}_2\text{D}_2\text{Cl}_4$ at 100 °C.   | 153 |
| <b>S 2.</b> $^1\text{H}$ NMR spectrum of <b>RIR-PBT<sub>OP</sub>-TPD<sub>O</sub></b> in $\text{C}_2\text{D}_2\text{Cl}_4$ at 100 °C.  | 153 |
| <b>S 3.</b> $^1\text{H}$ NMR spectrum of <b>RR-PBT<sub>OP</sub>-TPD<sub>O</sub></b> in $\text{C}_2\text{D}_2\text{Cl}_4$ at 100 °C.   | 154 |
| <b>S 4.</b> $^1\text{H}$ NMR spectrum of <b>TT-PBT<sub>OP</sub>-TPD<sub>O</sub></b> in $\text{C}_2\text{D}_2\text{Cl}_4$ at 100 °C.   | 154 |
| <b>S 5.</b> $^1\text{H}$ NMR spectrum of <b>HH-PBT<sub>OP</sub>-TPD<sub>O</sub></b> in $\text{C}_2\text{D}_2\text{Cl}_4$ at 100 °C.   | 155 |
| <b>S 6.</b> $^1\text{H}$ NMR spectrum of <b>PF<sub>OXY</sub>DT-TPD<sub>OXY</sub></b> in $\text{C}_2\text{D}_2\text{Cl}_4$ at 100 °C.  | 155 |
| <b>S 7.</b> $^1\text{H}$ NMR spectrum of <b>PF<sub>OXY</sub>DT-TPD<sub>DMO</sub></b> in $\text{C}_2\text{D}_2\text{Cl}_4$ at 100 °C.  | 156 |
| <b>S 8.</b> $^1\text{H}$ NMR spectrum of <b>PF<sub>O</sub>DT-TPD<sub>OXY</sub></b> in $\text{C}_2\text{D}_2\text{Cl}_4$ at 100 °C.  | 156 |
| <b>S 9.</b> $^1\text{H}$ NMR spectrum of <b>PF<sub>O</sub>DT-TPD<sub>DMO</sub></b> in $\text{C}_2\text{D}_2\text{Cl}_4$ at 100 °C.  | 157 |
| <b>S 10.</b> $^1\text{H}$ NMR spectrum of <b>PT<sub>OXY</sub>-TPD<sub>DMO</sub></b> in $\text{C}_2\text{D}_2\text{Cl}_4$ at 100 °C.   | 157 |
| <b>S 11.</b> $^1\text{H}$ NMR spectrum of <b>PT<sub>OXY</sub>-TPD<sub>OXY</sub></b> in $\text{C}_2\text{D}_2\text{Cl}_4$ at 100 °C.   | 158 |
| <b>S 12.</b> $^1\text{H}$ NMR spectrum of <b>PT<sub>ODD</sub>-TPD<sub>DMO</sub></b> in $\text{CDCl}_3$ at 25 °C.  | 158 |

- S 13.** Particles size analysis of **PT<sub>OXY</sub>-TPD<sub>DMO</sub>** with DLS in CHCl<sub>3</sub> solution. **159**
- S 14.** Particles size analysis of **PT<sub>OXY</sub>-TPD<sub>DMO</sub>** with DLS in TCE solution. **159**

>>  
**TABLE OF SCHEMES**

|   |    |
|---|----|
| 2. 1. i) DMF, Et <sub>3</sub> N, 50 °C; ii)(a) THF, <i>t</i> -BuONO, 90 °C;(b) 2M NaOH, 95 °C; iii) Ac <sub>2</sub> O, 110 °C; iv)(a) THF, R-NH <sub>2</sub> , 55 °C;(b) SOCl <sub>2</sub> , 55 °C.   | 55 |
| 2. 2. The chemical mechanism of formation of 3-ethyl-4-methyl-2-amino thiophene-3,4-dicarboxylate.  | 56 |
| 2. 3. The brief chemical mechanism of 3,4-thiophene dicarboxylic anhydride.   | 57 |
| 2. 4. The chemical mechanism of <b>M1</b> and <b>M2</b> .   | 57 |
| 2. 5. i)(a) THF, <i>n</i> -BuLi, Br-C <sub>8</sub> H <sub>17</sub> ; ii)(a) THF, NaHCO <sub>3</sub> Pd(OAc) <sub>2</sub> , P( <i>o</i> -tol) <sub>3</sub> ; iii) CHCl <sub>3</sub> /AcOH, NBS; iv) same to (iii), 60°C;v) Et <sub>2</sub> O, <i>n</i> -BuLi, <sup>i</sup> PrOB(pin); vi)(1) THF, PdCl <sub>2</sub> (MeCN) <sub>2</sub> , P( <i>o</i> -anisyl) <sub>3</sub> , Cs <sub>2</sub> CO <sub>3</sub> , PivOH; (2) same to (iii); vii) DMSO, AgNO <sub>3</sub> , KF, PdCl <sub>2</sub> ( benzonitrile) <sub>2</sub> ; viii)(1) Toluene, compound (7), K <sub>2</sub> CO <sub>3</sub> , Aliquat 336, Pd(PPh <sub>3</sub> ) <sub>4</sub> ; (2) same to (iv). | 59 |
| 2. 6. Illustration of dehydrogenative homocoupling mechanism for <b>M5</b> .  | 62 |
| 3. 1. Synthesis of <b>M7</b> and <b>M8</b> .  | 79 |
| 3. 2. Proposed mechanism for the synthesis of (12).   | 80 |
| 3. 3. Proposed mechanism for the synthesis of (13).   | 80 |
| 3. 4. Proposed mechanism for the synthesis of (14) and (15).  | 81 |
| 3. 5. Synthesis routes for <b>M9</b> and <b>M10</b> .   | 82 |
| 4. 1. Synthesis routes for <b>M11</b> .   | 99 |
| 4. 2. Proposed mechanism for the synthesis of 3-((2-(2-methoxyethoxy)ethoxy)methyl)thiophene (21).  | 99 |

>>  
**TABLE OF TABLES**

|   |     |
|---|-----|
| 1. 1. $E_g$ (opt), electrochemical properties, photovoltaic properties and hole mobility of poly alkylated TPD containing oligothiophene.   | 34  |
| 1. 2. $E_g$ (opt), electrochemical properties and photovoltaic properties of poly alkylated TPD containing fused electron donors.   | 36  |
| 1. 3. $E_g$ (opt), electrochemical properties and photovoltaic properties of alkylated fluorene-based copolymers.   | 39  |
| 2.1. (a) Molecular, optical, and (b) electrochemical data for [RIR] $PT_{OP}$ -TPD <sub>BP</sub> , [RIR] $PT_{OP}$ -TPD <sub>O</sub> , [RR] $PT_{OP}$ -TPD <sub>O</sub> , [T-T] $PT2_{OP}$ -TPD <sub>O</sub> , and [H-H] $PT2_{OP}$ -TPD <sub>O</sub> . | 65  |
| 2.2. Molecular structure data and thermal characteristic of TPD-based copolymers.   | 71  |
| 3.1. (a) Molecular, optical, and (b) electrochemical data for $PF_{OXY}DT$ -TPD <sub>OXY</sub> , $PF_{OXY}DT$ -TPD <sub>DMO</sub> , $PF_{O}DT$ -TPD <sub>OXY</sub> , and $PF_{O}DT$ -TPD <sub>DMO</sub> .   | 85  |
| 3. 2. Molecular structural data of fluorene-based copolymers.   | 91  |
| 4.1. (a) Molecular, optical, and (b) electrochemical data for $PT_{OXY}$ -TPD <sub>OXY</sub> , $PT_{OXY}$ -TPD <sub>DMO</sub> and $PT_{ODD}$ -TPD <sub>DMO</sub> .  | 102 |
| 4. 2. Molecular structural data of $PT_{OXY}$ -TPD <sub>OXY</sub> and $PT_{OXY}$ -TPD <sub>DMO</sub> .  | 109 |

>>  
**GLOSSARY OF ABBREVIATIONS  
AND TERMS**



|   |  |
|---|--|
| Aceton-d <sub>6</sub>                         | Deuterated Aceton (NMR)                  |
| AgNO <sub>3</sub>                             | Silver nitrate                           |
| Ar  | Argon gas                                |
| a.u.  | Arbitrary units                          |
| BHJ   | Bulk Heterojunction                      |
| br  | Broad peak (NMR)                         |
| CB  | Conduction Band                          |
| Cs <sub>2</sub> CO <sub>3</sub>               | Cesium carbonate                         |
| CH <sub>3</sub> OH                            | Methanol                                 |
| CHCl <sub>3</sub>                             | Chloroform                               |
| CDCl <sub>3</sub> -d <sub>1</sub>             | Deuterated Chloroform (NMR)              |
| C <sub>2</sub> D <sub>2</sub> Cl <sub>4</sub> | Deuterated 1,1,2,2-Tetrachlorethan (NMR) |
| CV  | Cyclic Voltammetry                       |
| D-A   | Donor-Acceptor                           |
| DCM   | Dichloromethane                          |
| DMSO-d <sub>6</sub>                           | Deuterated dimethyl sulfoxide (NMR)      |
| DMSO  | Dimethyl Sulfoxide                       |
| DMF   | N,N-dimethylformamide                    |
| DP  | Degree of Polymerization                 |
| d   | Doublet (NMR)                            |
| dd  | Doublet of doublet (NMR)                 |
| E <sub>g</sub> (opt)                          | Optical band gap                         |
| E <sub>g</sub> (elec)                         | Electrochemical band gap                 |
| EA (EtOAc)                                    | Ethyl acetate                            |
| Et <sub>2</sub> O                             | Diethyl ether                            |
| Et <sub>3</sub> N                             | Triethylamine                            |
| EI  | Electron Ionization (MS)                 |
| eV  | Electron volt                            |

|                 |  |
|-----------------|--|
| FET             | Field Effect Transistor                                    |
| FF              | Fill Factor  |
| GPC             | Gel Permeation Chromatography                              |
| HCl             | Hydrochloric acid  |
| HOMO            | Highest Occupied Molecular Orbital                         |
| Hz              | Hertz (NMR)  |
| ICT             | Intra-molecular Charge Transfer                            |
| ITO             | Indium Tin Oxide   |
| <i>J</i>        | Coupling constant (NMR)                                    |
| $J_{sc}$        | Short circuit current                                      |
| J-V             | Current-Voltage  |
| $K_2CO_3$       | Potassium carbonate  |
| LUMO            | Lowest Unoccupied Molecular orbital                        |
| LEDs            | Light Emitting Diodes                                      |
| $\lambda_{max}$ | Maximum absorption wavelength                              |
| MALDI-TOF       | Matrix-assisted laser desorption/ionisation-Time of flight |
| m/z             | Mass to charge ratio (MS)                                  |
| MS              | Mass spectrometry  |
| $MgSO_4$        | Magnesium sulphate   |
| $M_n$           | Number Average Molecular Weight                            |
| $M_w$           | Weight Average Molecular Weight                            |
| m               | Multiplet (NMR)  |
| M.p             | Melting Point  |
| NMR             | Nuclear Magnetic Resonance                                 |
| NBS             | <i>N</i> -Bromosuccinide                                   |
| <i>n</i> -BuLi  | <i>n</i> -Butyl lithium                                    |
| $NaHCO_3$       | Sodium bicarbonate   |
| $NaCO_3$        | Sodium carbonate   |
| OPV             | Organic Photovoltaic                                       |
| OSC             | Organic Solar Cell   |
| PA              | Polyacetylene  |
| PANI            | Polyaniline  |
| PCE             | Power Conversion Efficiency                                |

|   |  |
|---|--|
| PCBM  | Phenyl-C <sub>x</sub> -butyric acid methyl ester       |
| PDI   | Polydispersity Index                                   |
| PEDOT:PSS   | Poly(3,4-ethylenedioxythiophene):Polystyrene sulfonate |
| PivOH   | Pivalic acid   |
| ppm   | Part per million                                       |
| pent  | Pentet (NMR)   |
| PPy   | Polypyrrole  |
| PT  | Poly(thiophene)  |
| P( <i>o</i> -tol) <sub>3</sub>                                | Tri-ortho-tolyl phosphine                              |
| P(C <sub>6</sub> H <sub>4</sub> - <i>o</i> -OMe) <sub>3</sub> | Tris(ortho-methoxyphenyl)phosphine                     |
| PPh <sub>3</sub>  | Triphenyl phosphine                                    |
| Pd(PPh <sub>3</sub> ) <sub>2</sub> Cl <sub>2</sub>            | Bis(triphenylphosphine)palladium(II)dichloride         |
| Pd(PPh <sub>3</sub> ) <sub>4</sub>                            | Tetrakis(triphenylphosphine)palladium(0)               |
| Pd(OAc) <sub>2</sub>  | Palladium(II)acetate                                   |
| Pd <sub>2</sub> (dba) <sub>3</sub>                            | Tris(dibenzylideneacetone)palladium(0)                 |
| qui   | quintet (NMR)  |
| s   | singlet (NMR)  |
| se  | sextet (NMR)   |
| SOCl <sub>2</sub>   | thionyl chloride                                       |
| <i>t</i> -BuONO   | Tert-butyl nitrite                                     |
| <i>T</i> <sub>d</sub>   | Decomposition temperature (TGA)                        |
| TGA   | Thermal Gravimetric Analysis                           |
| TLC   | Thin Layer Chromatography                              |
| THF   | Tetrahydrofuran  |
| TCE   | 1,1,2,2-tetrachloroethane                              |
| t   | triplet (NMR)  |
| TPD   | Thieno[3,4- <i>c</i> ]pyrrole-4,6-dione                |
| UV-vis  | Ultraviolet-visible spectroscopy                       |
| V <sub>oc</sub>   | Open circuit voltage                                   |
| XRD   | X-ray diffraction                                      |

**>>CHAPTER I  
INTRODUCTION**

## 1.1 Introduction

The threat of global warming and high oil prices are creating a worldwide demand for carbon-free energy solutions such as solar cells. The energy that comes from sunlight is a significant renewable resource and one of few sources that provide enough energy to fulfil our current and future power requirements. Solar energy is environmentally friendly and can play a part in developing global energy needs. In addition, the negative influences of atmospheric emissions on the environment can be reduced by using photovoltaic (PV) technology, in which sunlight is directly absorbed to provide plentiful energy. This technique has been intensively investigated in organic solar cells (OSC) to increase the efficiency of solar energy conversion. Indeed, PV has been successfully used in the most popular class of polymer solar cell (PSC) devices, known as bulk-heterojunction (BHJ), which has been recorded as the best OSC device developed to date.<sup>1,2</sup> This concept is based on silicon technology that has developed over the last 20 years and that still dominates the highly commercial solar market. Although silicon is too expensive to use in solar cell devices, there are numerous alternatives that would be reasonably inexpensive. Organic solar energy also has several advantages such as low thermal budget processes, which make the devices mechanically flexible, extremely lightweight and of low cost to fabricate. Another key advantage of conjugated polymers is that the molecular design can easily be tuned to receive better physical and optoelectronic properties, leading to ultimate performance in organic PV applications. Indeed, the latter is required to make good headway towards commercialisation.<sup>3,4,5,6</sup>

## 1.2 Background and development of conductive polymers

In the past, it was strongly believed that conduction of electricity would only be achieved via inorganic compounds and metals and that organic composites functioned as insulators.<sup>7</sup> In the mid-nineteenth century, the formation of polyaniline (PANI) (**Figure 1.1-a**) as the electrochemical oxidation product of aniline in acidic media was investigated by Dr Letheby, who observed that the product was dark blue in an oxidised state but colourless in a reduced state.<sup>8,9</sup> In 1963, Bolto et al. developed an iodine-doped polypyrrole (**PPy**) (**Figure**

**1.1-b)** with a conductivity of 1 S/cm.<sup>10</sup> As a result, the previous phenomenon was no longer acceptable. In 1974, Shirakawa and Ito synthesised the well-defined conjugated polymer poly(acetylene) (PA) (**Figure 1.1-c**) in the form of a thin film by a fortunate accident.<sup>11,12</sup> Although poly(acetylene) was first synthesised by Natta et al. in 1958, this polymer did not receive much attention from scientists. In the late 1970s,<sup>13</sup> Heeger et al. reported that halogen-doped poly(acetylene)s are electrically conductive,<sup>14,15</sup> —a discovery for which they received the Noble Prize for Chemistry in 2000.

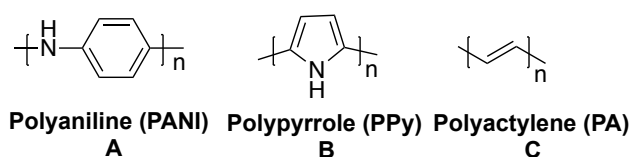


**Figure 1. 1.** Chemical structures of an enormous breakthrough in conjugated polymers.

In the last two decades, many new organic semiconductors (see **Figure 1.2**) have been extensively investigated, developed and incorporated into a variety of applications, such as polymer solar cells (PSCs),<sup>16,17</sup> polymer light-emitting diodes (PLEDs)<sup>18,19</sup> and organic field effect transistors (OFET)<sup>20,21</sup>. In addition, the scope of research in semiconducting materials has become one of the most interesting and interdisciplinary areas in science and technology, leading people who work in the industry to join academic researchers in designing and enhancing the properties of organic semiconductors.

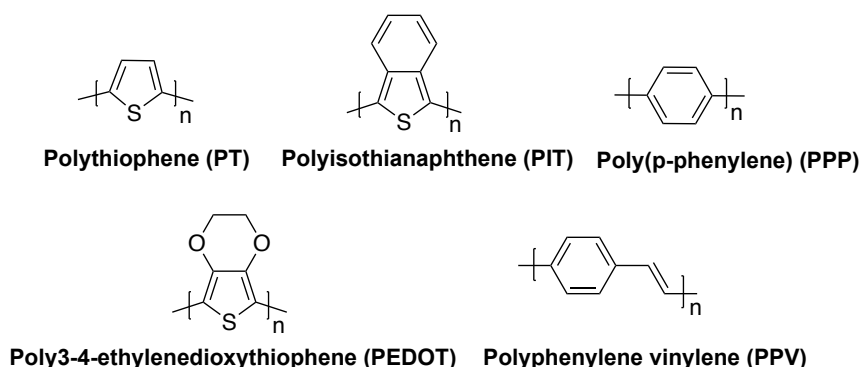


**Figure 1. 2.** Illustration of some important polymers incorporated in various electric applications.

### 1.3 $\pi$ - Conjugated polymers and semiconductor properties

Organic macromolecules composed of alternating single and double bonds along the backbone are known as conjugated polymers. Carbon atoms coupled with heteroatoms (such as nitrogen, oxygen and sulphur) that provide a continuous overlapping of their  $p$ -orbitals are also conjugated polymers. Conjugated conducting polymers are primarily the result of the electron in the  $p_z$ -orbital of each  $sp^2$ -hybridised carbon atom interacting with the neighbouring  $p_z$  electrons to form a  $\pi$ -bond over the backbone chain. These  $\pi$ -electrons are of a delocalised nature as they have the capacity to move from one bond to the other where the double bond overlaps along the single bond. The image below, **Figure 1.3**, clearly depicts the chemical formula of a  $\pi$ -bond.

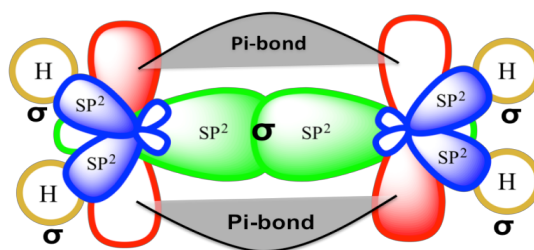


**Figure 1. 3.** The formation of a  $\pi$ -bond in conjugated polymers.

Polyacetylene (PA) is one of the simplest examples of conjugated polymers. In the middle of the twentieth century, Natta et al.<sup>22</sup> reported PA as being an intractable black powder. This original concept played an important role for many conjugated polymers. PA consists of alternating single and double bonds, resulting in an unequal carbon-carbon (C-C) bond length, **Figure 1.4**, known as the Peierls distortion, which leads to a significant gap between the bottom of the conduction band (CB) and the top of the valence (known as the band gap, or  $E_g$ ).

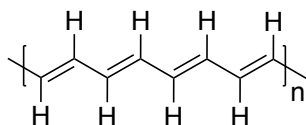


**Figure 1. 4.** Trans-poly (acetylene).

An energy gap can also be defined as the difference between the lowest unoccupied molecular orbital (LUMO), which refers to  $\pi^*$ -bonding, and the highest occupied molecular orbital (HOMO), which refers to  $\pi$ -bonding. The  $E_g$  is generally high in a single molecule. In a conjugated polymer, however, the gap decreases as more orbitals are added due to the polymer chain during increasing polymerisation. Therefore, the energy levels merge and form energy bands (see **Figure 1.5**).<sup>22,23,24</sup>

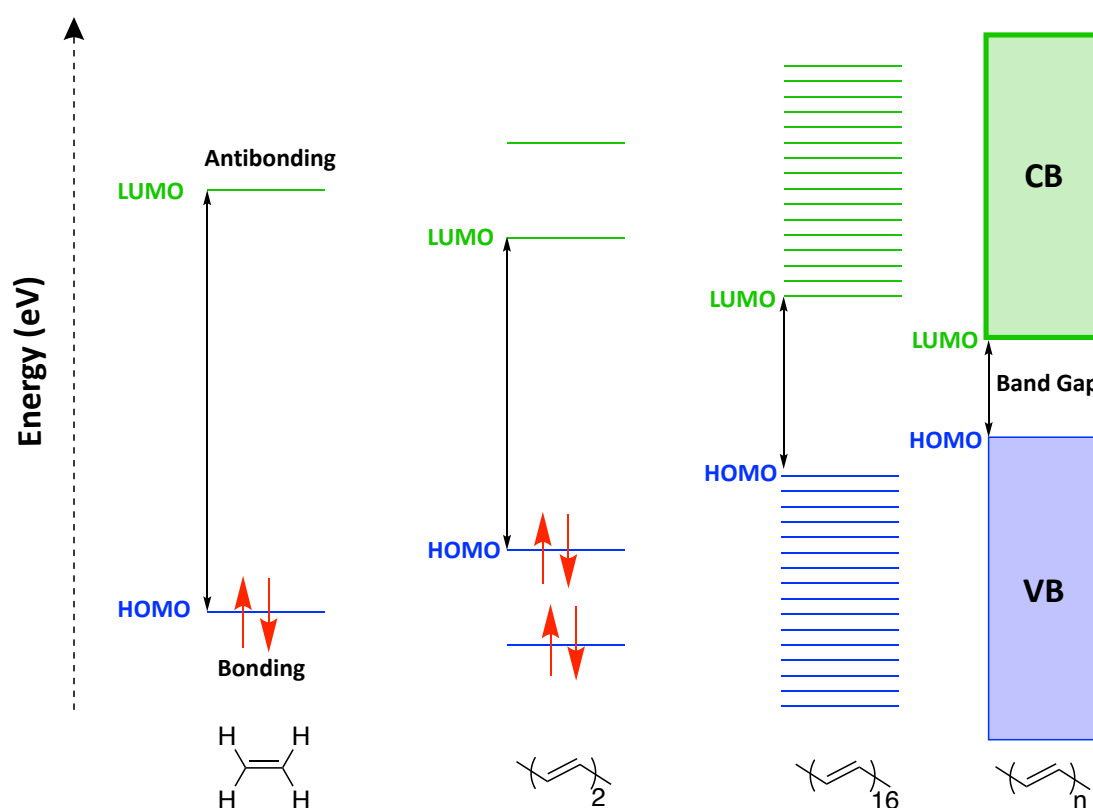


**Figure 1. 5.** Illustration of the energy gap for conjugated polymers.

In other words, as the unlimited extension of a  $\pi$ -conjugated length is formed, a narrow  $E_g$  is achieved, causing a bathochromic shift in the absorption band (a longer wavelength), leading to the absorbance of more photons, promoting a light-harvesting property. In addition, this gap is determined by the conductive and electronic properties of those polymers, so control of the HOMO and LUMO gap by structural modification is extremely significant in the design of low-energy gap polymers.<sup>25</sup>



## 1.4 Electronic conduction in semiconductor polymers

Delocalisation of  $\pi$ -electron bonding over the entire polymer backbone makes the polymer act as an effective electronic conductor if the bond length of all carbon-carbons is uniform—that is, if the  $\pi$ -electrons are fully delocalised. This means that no  $E_g$  separation would occur because the electrons can move freely within the materials, producing a progressive closure of the  $E_g$ , like as in a metal. However, this system is unstable, leading carbon-carbon groups to move towards each other with respect to Peierls' transition. As a consequence, the electrons of semiconductor polymers are not completely delocalised, and the structure forms alternating long (single) and short (double) bonds, resulting in unequal carbon-carbon (C-C) bond lengths, lowering the energy of the system (making it more stable).<sup>26,27</sup>

Therefore, the simplest basic structure and most conjugated polymer is *trans*-poly(acetylene), which has alternating bonds (short and long bonds). These form two patterns of PA: pattern A (double bond indicating to the left) and pattern B (double bonds indicating to the right) (see **Figure 1.6**). Both patterns are of identical geometry with identical energy, which creates a degenerate ground state,<sup>27</sup> as shown in **Figure 1.7**.

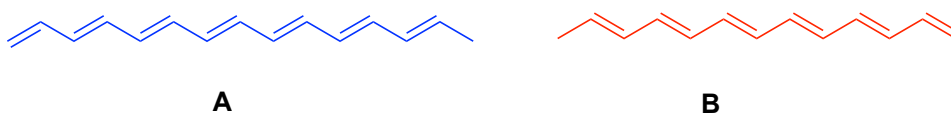


**Figure 1. 6.** The identical geometric patterns of polyacetylene.

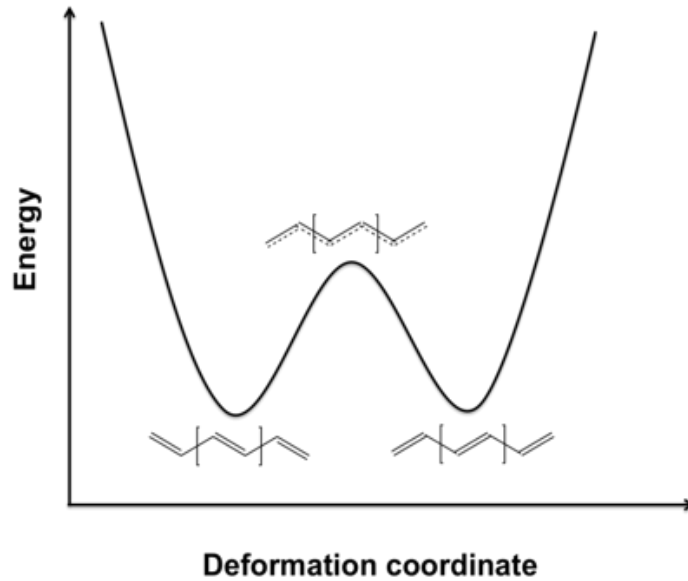


**Figure 1. 7.** The potential energy of degenerate trans-poly(acetylene).

When the two patterns coexist as a piece of chain, the bond ends with a mismatch, resulting in one unpaired  $\pi$  electron (in a non-bonding state). This effect is called soliton (see **Figure 1.8**). The non-bonding  $\pi$  electron and the geometric symmetry of the structure means a new localised energy level will be midway between the valence band and the conduction band. As a result, the charged soliton could exist in three possible types: neutral (one unpaired electron) in which the spin =  $\frac{1}{2}$ , negatively charged (two-paired electron) or positively charged in which the spin = 0 upon doping (see **Figure 1.9**).<sup>28</sup>

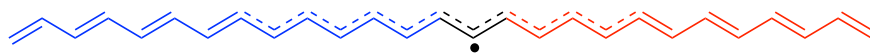


**Figure 1. 8.** The structure of a neutral soliton in polyacetylene.

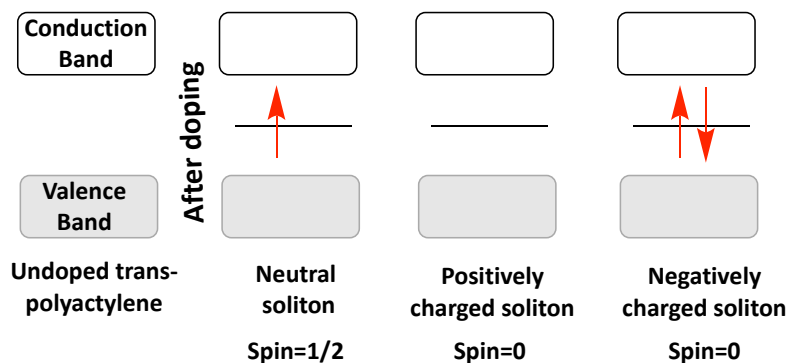


**Figure 1. 9.** Schematic representation of the band structure of a neutral, a positively charged and a negatively charged soliton on trans-poly(acetylene).

However, for polymers with non-degenerate states, two states of different energies are observed, indicating two asymmetric structures. These two structures are referred to as *aromatic* in the ground state and as *quinoid* in the excited state, as the latter conformation has a higher energy than the aromatic conformation (see **Figure 1.10**). As a result, the quinoid form is unstable and the system continuously seeks to change to the most stable aromatic form. Stability occurs when these two asymmetric materials are isolated. This result or defect is termed a *polaron*, and it generates two new localised electronic states within the energy gap. Analogous to a charged soliton, the polaron charge can be negative, neutral or positive. In some cases, two identical charges can be associated with a non-degenerate state polymer chain to form a *bipolaron*, which is energetically more favourable than the formation of two singly charged polarons (see **Figure 1.11**).<sup>28,29,30</sup> From this point of view, the semiconductor materials will provide fair electrical conductivities by only oxidising or reducing agents (doping agents). In other words, the weak semiconductors or insulators can be converted to conductors through doping.<sup>31</sup>

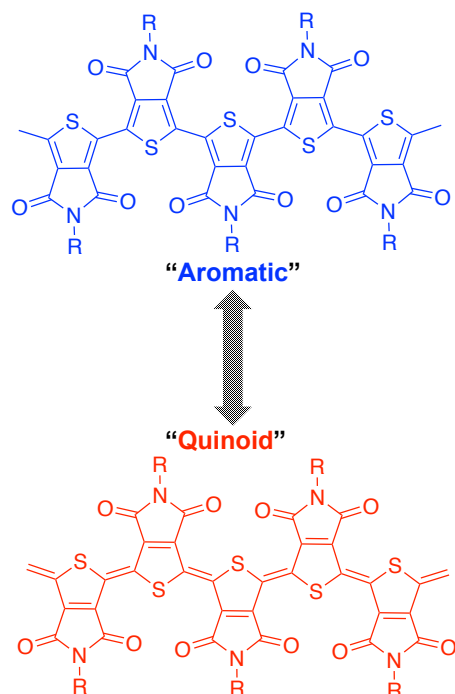


**Figure 1. 10.** The chemical structures of the aromatic form and quinoid form of a thieno[3,4-c]pyrrole-4,6-dione based polymer.

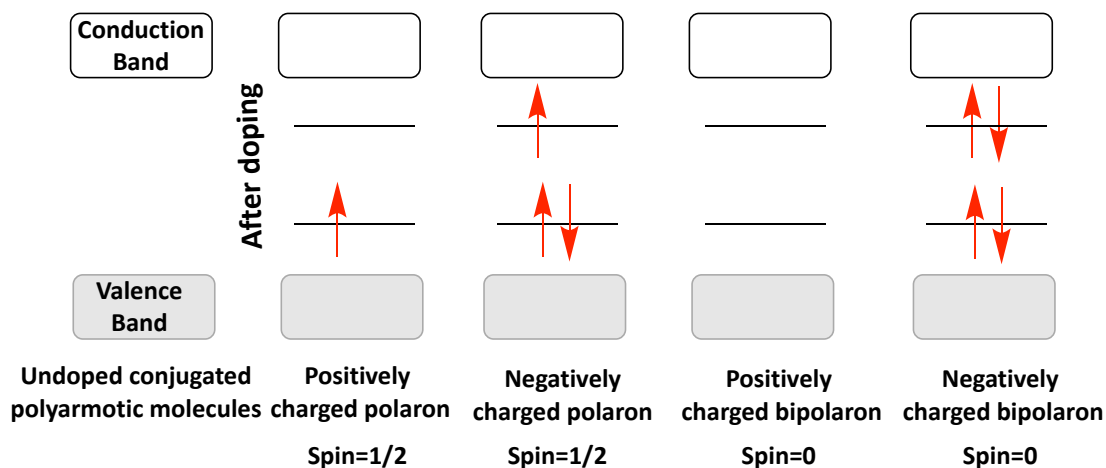


**Figure 1. 11.** Schematic representation of band structures of positively and negatively charged polaron and bipolaron in non-degenerate ground state polymer.

## 1.5 Applications of conjugated systems in organic electronic and photonic devices

The capacity to generate electron and transporting charges in semiconducting materials with  $\pi$ -electrons along the (hetero) aromatic backbone chain has been extremely attractive to many academic and industrial researchers. As attention for this approach grew in this area, the era of semiconducting polymers began.<sup>32</sup> It was realised that the unique optical and semiconducting properties of conjugated polymers could be utilised in a variety of organic electronic and photonic devices, such as PSCs,<sup>33,34</sup> PLEDs,<sup>35,36</sup> sensors,<sup>37,38</sup> laser photoconductors,<sup>39</sup> OFETs<sup>40,41,42</sup> and electrochromic applications<sup>43</sup>.

The following paragraphs will briefly describe three interesting semiconductor device applications. PSCs will be used to describe this research area in depth, and the basic idea of the operation of a PV cell will be explained.

### 1.5.1 Organic field effect transistors (OFETs)

FETs are semiconductor devices that switch electrical signals.<sup>44</sup> The fundamental concept of the FET was initially suggested by Lilienfeld in the early 1930s.<sup>45</sup> Since then, different types of FETs have been fabricated on the basis of silicon, such as the metal-oxide-semiconductor and metal-insulator-semiconductor (which can be considered the first generation semiconductor). Although the first demonstration of the silicon FET has now evolved to use

more attractive technology, a new technological development that can provide a similar influence would be required to replace silicon transistors. Organic semiconductors for the OFETs have an enormous potential to achieve a high device performance. In 1987, Koezuka et al. reported the first OFET, which was based on the electrochemical polymerisation of thiophene molecules.<sup>46,47</sup>

The OFET is composed of three fundamental components (drain, source and gate), an organic semiconducting layer and a dielectric layer, as shown in **Figure 1.12**.<sup>48</sup> In this electronic equipment, the current flows between the source (S) and the drain (D) electrodes. To control this flow, two independent biases apply to this device: one located between the source and the drain ( $V_{SD}$ ) and one located between the source and the gate (G) ( $V_{SG}$ ); the number of charge carriers in the FET channel is controlled by the latter bias. Consequently, if the  $V_{SG}$  is equal to zero voltage, the charge carrier density will be of very low conductance or no current will flow at all. In other words, the device is turned off. However, if the  $V_{SG}$  is greater than zero, a high charge carrier density will be observed, meaning that the device is turned on.<sup>32</sup>

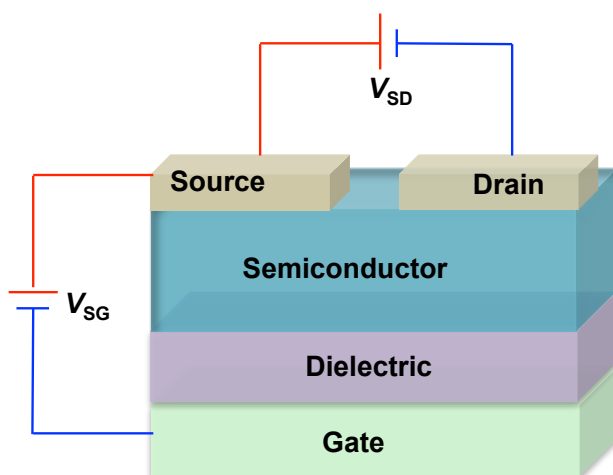


**Figure 1. 12.** The basic structure of organic field effect transistor.

### 1.5.2 Polymer light-emitting diodes (PLEDs)

Electroluminescence, in LEDs, is a light emission process that occurs within a wide range of semiconductor materials. The first LEDs were based on organic molecular crystals, as these have electroluminescent properties, and date back to the early 1960s.<sup>49,50</sup> However, Tang and Vanslyke demonstrated the

significant step of electroluminescence efficiency via thin film organic LEDs in 1987.<sup>51</sup> Three years later, Burroughes et al. reported the first semiconducting polymer-based LEDs (PLEDs) via the use of polyphenylene vinylene.<sup>52,53</sup> This discovery aroused intense interest, and much consequent research has contributed to developing this field.

PLEDs are composed of a thin polymer film layer sandwiched between two electrodes: the anode and the cathode. The anode generally uses a highly transparent material, such as indium tin oxide (ITO), which allows generation of the light within the diode and then emission of that light from the device. The cathode is a metal, such as aluminium (Al), barium (Ba) or calcium (Ca) and is placed on top of the emitting polymer layer. The basic structure of PLEDs is depicted in **Figure 1.13**.

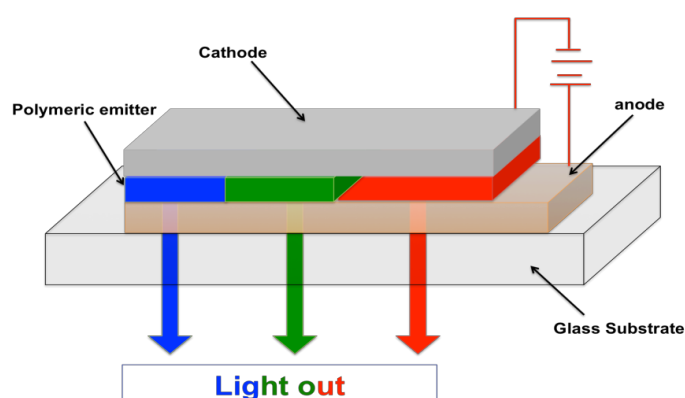


**Figure 1. 13.** The basic structure of polymeric light-emitting diodes.

Once the external voltage is applied to the device, holes are injected from the anode into the hole-transporting layer, and electrons are injected from the cathode into the electron-transporting layer. The holes and electrons then travel towards opposite electrodes where they meet each other in the emissive polymer layer, forming bound electron-hole pairs (excitons). This recombination releases energy that results in emitting photons (light emission). The working principle of PLEDs is demonstrated in **Figure 1.14**.<sup>54,55</sup>

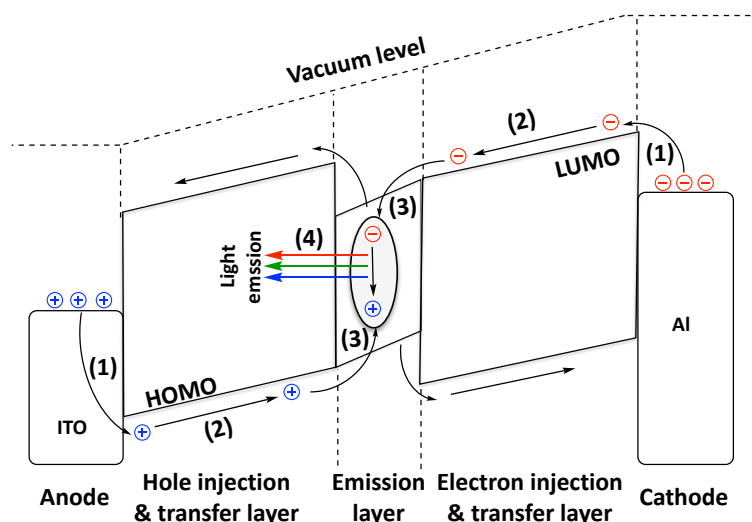


**Figure 1. 14.** Working principle of polymeric light-emitting diodes.

### 1.5.3 Organic solar cells (OSCs)

#### 1.5.3.1 Basic operation of photovoltaic cells

In an organic PV cell, three main steps convert the light into an electric current. First, in the excited state, the organic active layer absorbs a photon, leading to the formation of an electron-hole pair (known as an exciton). Second, this electron-hole pair is then dissociated, and free charges are formed. Finally, the electrons are transferred to the cathode and the holes are moved to the anode to provide a direct current for the consumer load<sup>23</sup> (see **Figure 1.15**). An electrical field is required to achieve the second step (separation of the electron-hole pair). This field can be provided by either a donor-acceptor interface or the different work functions of the electrodes.<sup>5</sup>

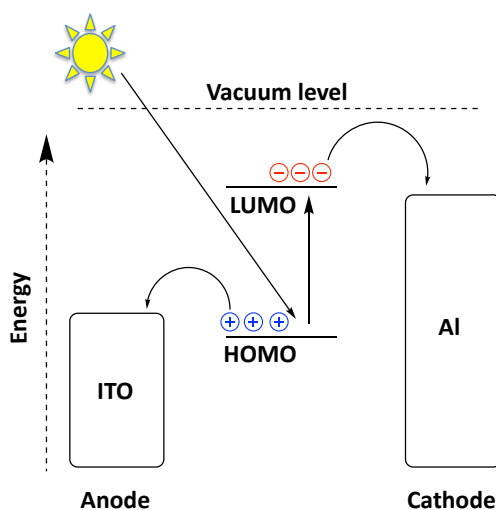


**Figure 1. 15.** Working principle of the conversion of sunlight into an electric current in a single layer.

In contrast, donor and acceptor materials in bulk heterojunction (BHJ) cells are in contact at the heterojunction interface. The active layer directly leads to the formation of an exciton system by the absorption of a photon. This exciton is split into two charges: a hole and an electron. If the donor's LUMO is sufficiently higher than the acceptor's LUMO, the electron will transfer from the former to the latter (see **Figure 1.16**).

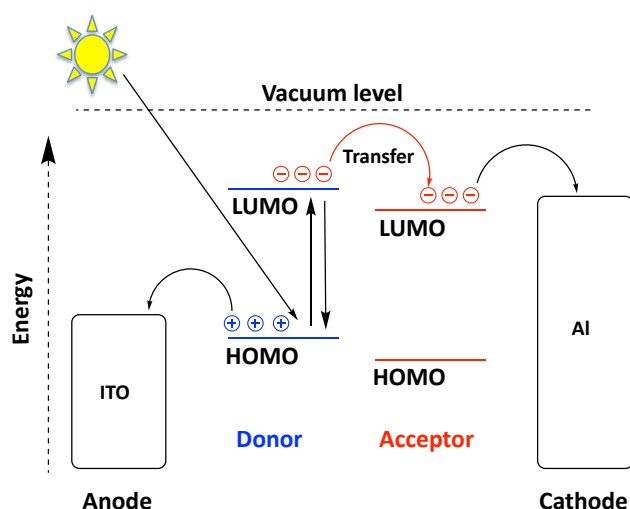


**Figure 1. 16.** Working principle of the conversion of sunlight into an electric current in bulk heterojunction cells.

### 1.5.3.2 Device architectures

#### 1.5.3.2.1 Single-layer device

The first device structure of an organic PV is an organic layer that lies between two electrodes. An anode with a high work function is commonly a transparent conductive oxide, such as ITO, which is an effective material for an anode. Conversely, a cathode with a low work function is commonly a layer of metal, such as Ca, Al or magnesium (Mg). These materials are located between the active layer (semiconducting layer) and the glass substrate (see **Figure 1.17**). The difference between the work functions of these two conductors provides an electric field that assists in the separation of the charge carrier by driving the holes towards the anode while the electrons are driven towards the cathode.<sup>56,57</sup> This type of device records very low power conversion efficiency (less than 0.1%) due to the short exciton diffusion length, which is around 1-10nm, and leads to a recombination of the hole and



electron instead of driving towards the electrodes. In such a device, the efficiency is limited by the exciton diffusion. However, this issue has been solved with the addition of a new layer.<sup>58,59</sup>

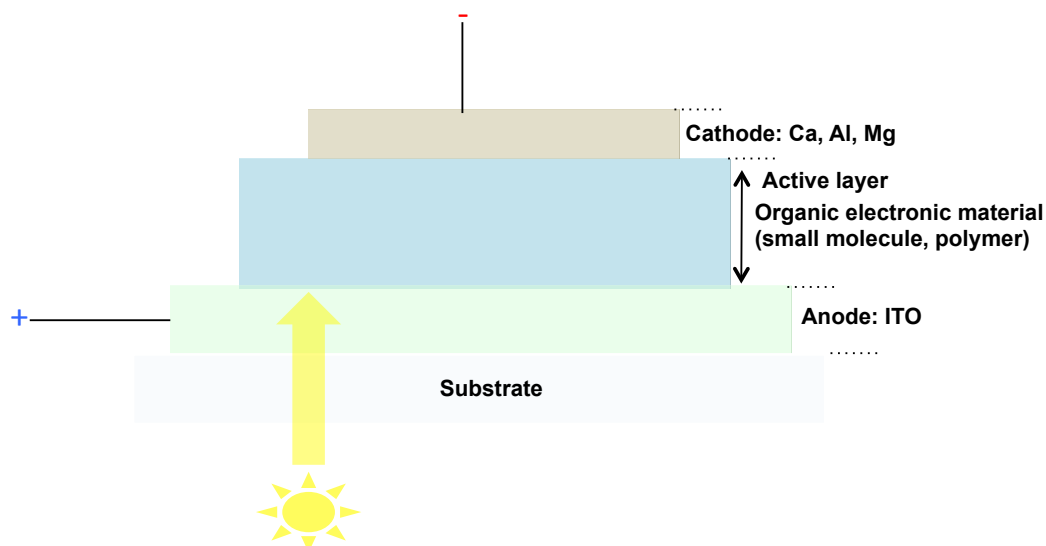


**Figure 1. 17.** Schematic structure of a single-layer solar cell.

#### 1.5.3.2.2 Bi-layer heterojunction

Tang et al.<sup>59</sup> have reported a power conversion efficiency of around 1% in two-layer PV cells. This two-layer device was created using copper phthalocyanine as the donor and a perylene tetracarboxylic dianhydride as the acceptor. The system also consists of two materials that are exposed to different frontier orbital levels (the donor HOMO and the acceptor LUMO). As the ionisation potential of the donor is low and the electron affinity of the acceptor is high, the result is an electrostatic force that can separate the exciton pair into free charges (see **Figure 1.18**).

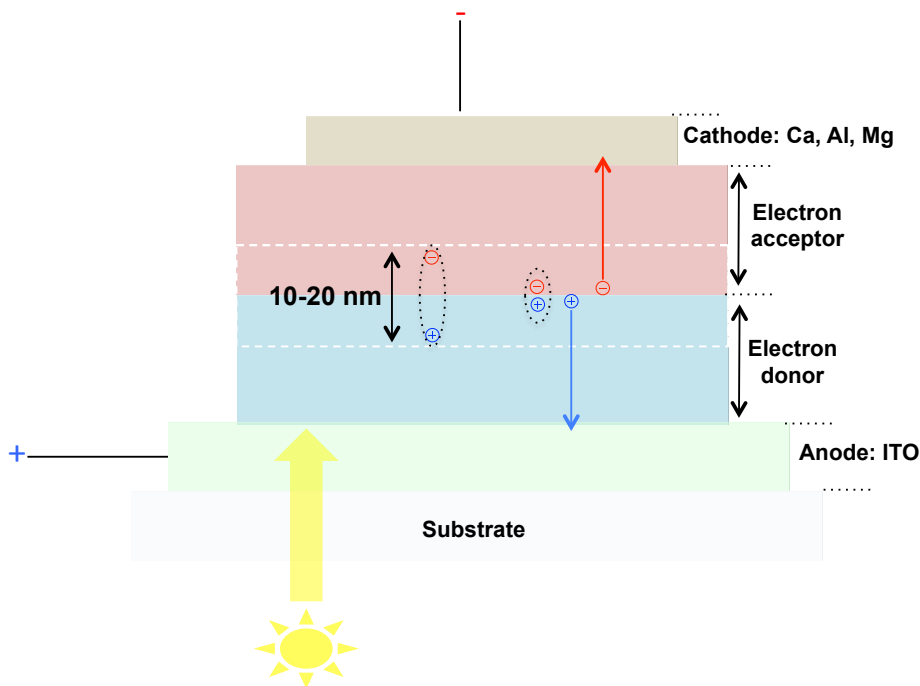


**Figure 1. 18.** Schematic structure of a two-layer solar cell.

The bi-layer device played an important role in achieving many advantages over a single-layer cell in which the exciton is split at the interface and the holes and electrons travel away from each other in the opposite direction (cathode and anode) based on charges. This dual-layer can prevent them from recombining with each other. However, the exciton is formed within a small distance (10-20 nm) of the interface. Thus, some of the excitons do reach the interface, resulting in the loss of absorbed photons. This issue leads to low quantum efficiency.<sup>59,33,60</sup> The power conversion efficiency observed by Jiangeng Xue et al. was around 4.2 % for copper phthalocyanine/C<sub>60</sub>.<sup>61</sup>

### 1.5.3.2.3 Bulk heterojunction

In the early 1990s, a new concept of photoactive devices was introduced to promote and explain the low exciton diffusion length in polymer solar cells and the desired thickness for an adequate absorption of sunlight.<sup>62</sup> This device is called the BHJ solar cell<sup>63</sup> and was devised by Heeger et al.<sup>62,64</sup> The principle idea of this device is that the polymer donor and fullerene acceptor derivative (PC<sub>61</sub>BM or PC<sub>71</sub>BM, see **Figure 1.19**) are mixed together in an active layer using different fullerene loading dissolved in different solvents to be processed by alternative processing methods (e.g. roll to roll and spin coating)

to provide a much better compatibility between them and to form bicontinuous phase separations and morphology with a limited length scale of phase separation, unlike in bi-layer devices in which the mixing at both polymer donor/PCBM acceptor interface is not possible (see **Figure 1.19**). As a result, the phase separations between polymer donor/PCBM acceptor are no longer planar within the active layer. As they blend in a bulk volume, each polymer donor-PCBM acceptor interface separates into a small distance of around 10-20nm, which is less than the exciton diffusion length. All electron-hole pairs will be separated within their lifetime, so recombination will be reduced.<sup>23,60</sup> Although excitons can be separated efficiently over the solar cell, some of them remain difficult to dissociate due to strong Coulomb-bound charge carrier pairs, resulting in an increase of disorder in polymeric semiconductors. However, the performance advantages of the BHJ device exceed the drawbacks.<sup>63</sup> The best power conversion efficiency that has been achieved by this device was recorded as being higher than 8%.<sup>65,66,67</sup>

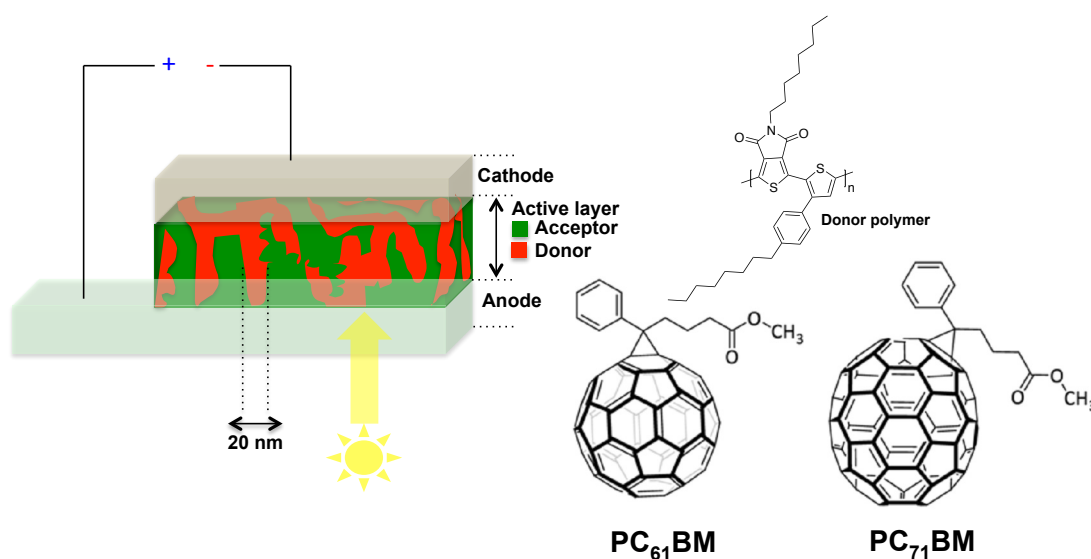


**Figure 1. 19.** Schematic structure of a bulk heterojunction cell (left) and polymer donor and fullerene derivative acceptors (right).

## 1.6 Synthesis of conjugated polymers

Numerous routes have been discovered for the preparation of various conjugated polymers, such as oxidative self-polymerisation, condensation polymerisation and transition-metal-catalysed cross-coupling polymerisation. However, the final technique has received the most attention since it

facilitates many functional groups. This thesis discusses the most popular technique (Suzuki) as well as direct arylation couplings.

### 1.6.1 Suzuki coupling

Suzuki coupling polymerisation is the palladium-catalysed cross-coupling of arylboronic ester/acid derivatives and aryl halides in the presence of a base to produce the carbon-carbon bonds of biaryl compounds. This method has been widely used in the preparation of a broad range of polymeric materials owing to its higher tolerance of broad functional groups and its higher stability in natural environments as well as its less toxic reagent compared to the other arylmetallic reagents, including arylstannanes and arylzinc.<sup>68-71</sup> However, it is believed that this type of cross-coupling has some drawbacks, including its limitation to aryl bromides and iodides due to the aryl chloride reactions being slow when used for coupling. Furthermore, unwanted byproducts, such as homocoupling products or coupling products of phosphine-bound aryl, are often produced during the polymerisation reaction. Despite all disadvantages, the oxygen-free conditions can reduce the rate of homocoupling products, and using a bulky phosphine ligand can assist in preventing the unwanted ligand-related side products in the biaryl synthesis, resulting in good to excellent yields of the obtained products.<sup>69,72,73</sup>

This type of synthesis mainly follows three fundamental intermediate mechanisms to complete the catalytic cycle of the Suzuki reaction to end up with the products (**Figure 1.20**). First, the oxidative addition in which aryl halides react with the palladium catalyst (two groups added to a metal) forms arylpalladium halide, **Intermediate I**, causing the oxidation state of palladium to switch from Pd (0) to Pd (II). Kinetically, this intermediate is often considered to be the rate-limiting step in the catalytic cycle<sup>74</sup>. Second, **Intermediate II** is followed by the anion species of the base-attacking palladium and exchanging the halogen groups. Under the presence of the same base, arylboronic ester/acid derivatives are activated to encourage the reaction with **Intermediate II** in the transmetallation process to afford **Intermediate III**, followed by reductive elimination to afford the desired product and regenerate the catalyst.<sup>74,75</sup>

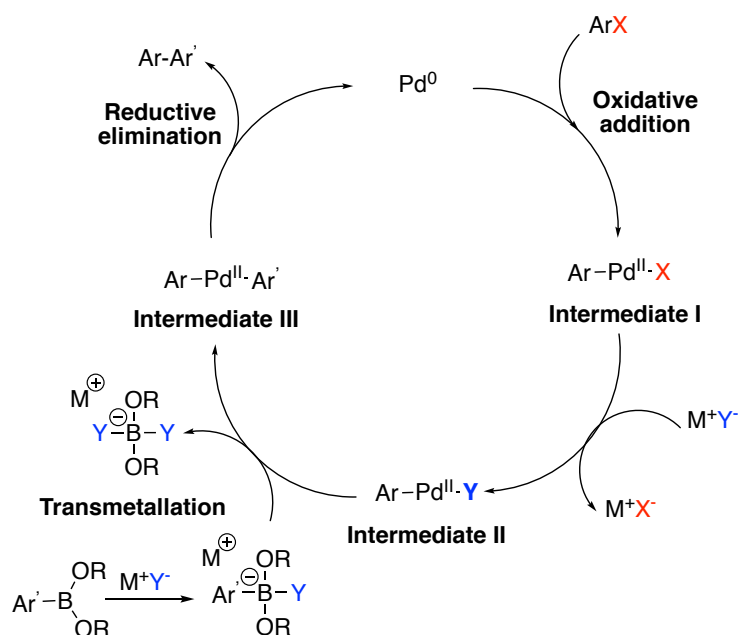


**Figure 1. 20.** Illustration of Suzuki cross-coupling mechanism.

### 1.6.2 Direct(hetero)aromatic arylation coupling

Using a metal-catalyst, direct C-H heteroarylation polycondensation has recently received great attention from numerous polymer chemists, as it has been used in the synthesis of a wide range of  $\pi$ -conjugated organic polymers. In contrast to traditional methods, such as Stille and Suzuki cross-coupling reactions, direct arylation is more environmentally friendly when constructing a new C-C bond. Its economic processes reduce the formation of unwanted chemical waste and byproducts and eliminates the use of toxic organometallic reagents.<sup>76,77,78,79</sup> Scientifically, this alternative polymerisation method can be carried out in the presence of palladium catalysts, a base such as caesium carbonate ( $\text{Cs}_2\text{CO}_3$ ) or potassium carbonate ( $\text{K}_2\text{CO}_3$ ) and a carboxylate source such as pivalic acid (trimethyl acetic acid),<sup>76,80,81</sup> in which the monomers have two different functional groups: unreactive arenes and aryl halide.

The suggested mechanism of this type of coupling is shown in **Figure 1.21**. In this mechanism, the pre-reduction of a palladium (II) complex is activated to become a palladium (0) complex, followed by an oxidative addition in which the aryl bromide ( $\text{Ar-Br}$ ) is incorporated into the palladium (0) to form

**Intermediate I** and generate the palladium (II) compound. Following, the pivalate anion interacts with the palladium intermediate and exchanges bromine ligand to form **Intermediate II**. Subsequently, deprotonation of aryl substrate (**Ar-H**) takes place, forming **Intermediate III** via a concerted metalation-deprotonation (CMD) transition state. Finally, pivalic acid detaches and assists the reductive elimination step to form Aryl-Aryl products and regenerate the catalyst.<sup>82-84</sup>

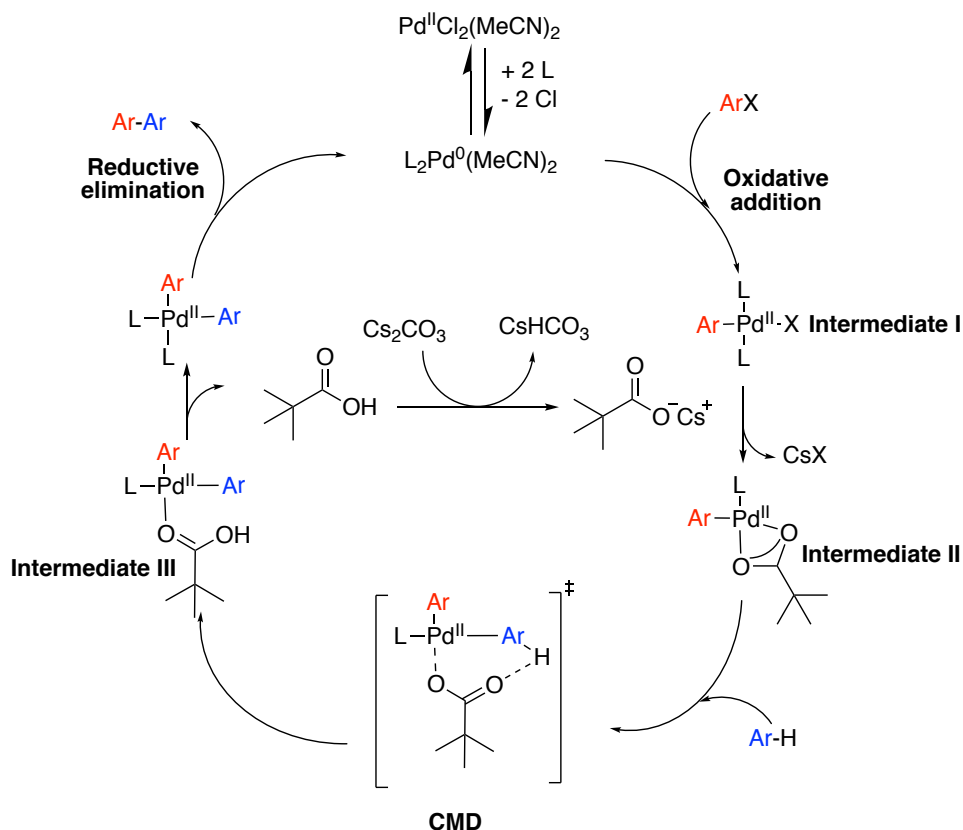


**Figure 1. 21.** The suggested mechanism of direct arylation cross-coupling.

## 1.7 Characteristics of a solar cell

The characterisation of a typical PV device is depicted in **Figure 1.22**. The cell performance is generally characterised by J-V curves representing the relationship between the electric current flowing through an electronic device and the voltage across the terminals of the device in the dark (blue line) and under illumination (red line). Under dark conditions, the J-V curve passes across the source with no potential, so no current flows. In a certain stage, the device works as p-n junction diode as a result of the sign of the forward voltage and current through the device and consequently the power is positive

which simply points out that the current is flowing into the positive terminal and out of the negative terminal (from anode to cathode in a closed circuit). This process leads to have charge carriers losing energy, which must be gained by the device. Under illumination conditions, the p-n junction diode converts to solar cell as a result of photoexcitation in donor conjugated polymers following by exciton dissociation at the D/A interface, the electron then transferred to cathode, which simply points to the reverse current that is flowing into the negative terminal and out of positive terminal (from cathode to anode in a closed circuit), resulting in J-V curve shifts down as shown in **Figure 1.22**. Thus, the energy of light absorbed generates charge carriers, which flow through the device and out in an external circuit.

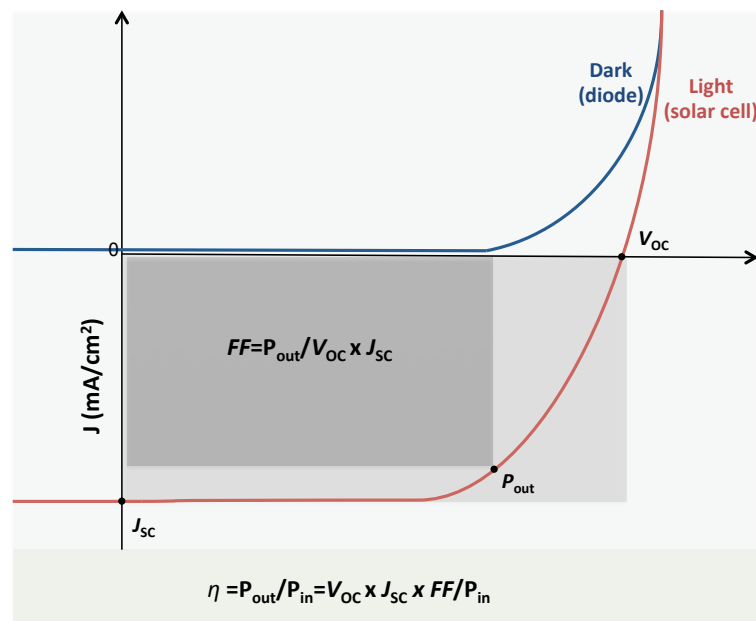


**Figure 1. 22.** Current-voltage curves of a typical PV in the dark and under illumination.

Efficiency is one of the main parameters for solar cells. The power conversion efficiency ( $\eta$ ) of those cells is determined as the maximum reaching ratio of power output ( $P_{out}$ ) to the power input ( $P_{in}$ ). Three factors play an active role in power conversion efficiency: open-circuit voltage ( $V_{oc}$ ), short-circuit current ( $J_{sc}$ ) and the fill factor (FF).

$V_{oc}$  is defined as the maximum voltage that can be observed in a PV cell when the cells terminals are not connected to any load in a circuit and there is

no current flowing between the terminals. This factor essentially depends on the selected material to be used in the active layer and the difference between the HOMO level of the donor (D) and the LUMO level of the acceptor (A). However,  $V_{oc}$  could also be impacted by the recombination process, which cannot be fully avoided, leading to a decrease in the maximum  $V_{oc}$ .<sup>57,85,86</sup>

A  $J_{sc}$  is defined as the maximum current that can be gained in a PV device when the devices terminals are connected to a load resistance where the current passes through the path of the lowest resistance and nearly zero potential difference. This  $J_{sc}$  characteristic relies on the number of photons absorbed from the light<sup>87</sup> and depends on the active layer thickness, as organic semiconductor materials have low motilities and will therefore limit the layer thickness of PV devices. Moreover, charge carrier mobility plays an active role in improving the short-circuit current<sup>23,87</sup>.

The FF is defined as the ratio of the maximum effectiveness of the power output of a PV cell to its theoretical power output when voltage and current are both at their maximum limits. The FF determines the performance of the solar cells,<sup>56</sup> which is also determined by the amount of generated charge carrier that essentially reaches the electrodes. In fact, the FF relies on the competition between the charge carrier recombination and the transfer process.

Most critical for the design of material combinations intensively studied for efficient OSC is the control of a multiparameter problem. This can be achieved by choosing a convenient combination of donor and acceptor materials and by controlling the absorption properties and material composition, which can play an important role in  $V_{oc}$ ,  $J_{sc}$  and FF.<sup>60,87</sup>

## **1.8 Structure-property relationships of conjugated polymers**

### **1.8.1 Molecular energy levels of the polymer solar cells**

Tuning the positions of the highest occupied molecular orbital (HOMO) and the lowest unoccupied molecular orbital (LUMO) of donor-acceptor



conjugated polymers is the essential approach to enhance the energy-conversion performance in bulk heterojunction (BHJ) solar cells. The utility of this approach facilitates the reduction of the energy gap of the conjugated polymers by either raising the HOMO level or lowering the LUMO level. This is to capture most of photon portions from the blue to the red end of the solar spectrum since the high photon flux density of solar spectra is dominated within the red visible region (longer wavelengths and shorter energy).<sup>88</sup> However, more factors need to be considered far beyond the optical absorption property (**Figure 1.23-a**). After photoexcitation of the polymer, excitons diffuse to the polymer donor and fullerene acceptor interface to dissociate into free charge carriers. The charge dissociation process is originally driven by the energy difference between the LUMO levels of polymer donor and fullerene acceptor; the polymer donor with a LUMO energy level closest to 0.3 eV is energetically favourable in overcoming the exciton binding energy.<sup>89, 90</sup> For example, the conjugated polymer **PDTSTPD**—based on thieno[3,4-*c*]pyrrole-4,6-dione (TPD) as the acceptor and dithieno[3,2-*b*:2',3'-*d*]silole (DTS) as the donor—has the potential to provide an energy offset of 0.4 eV (LUMO = -3.9 eV) with an efficiency up to 7.3%<sup>91</sup> (**Figure 1.23-b**). Furthermore, the relationship of HOMO-LUMO energy levels between the polymer donor and the fullerene acceptor is linearly reflected in the open circuit voltage ( $V_{OC}$ ) of BHJ solar cells. Lowering the HOMO energy level of the polymer would theoretically promote  $V_{OC}$  factor.<sup>92</sup> In 2010, Wei et al. prepared the best polymer solar cells based on TPD and bithiophene materials **PBTTPD** with the  $V_{OC}$  as high as 0.92 V (HOMO = -5.6 eV) and the PCE as high as 7.3%<sup>93</sup> (**Figure 1.23-c**). On this basis, controlling both energy levels of the polymer donor is necessary to compromise all the above features within photovoltaic materials for better photovoltaic performance.

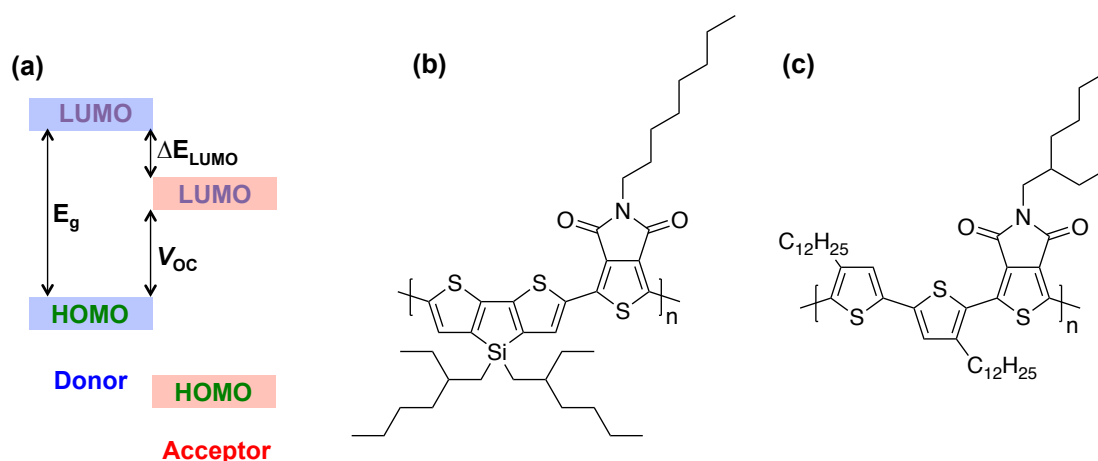


**Figure 1. 23.** (a) Schematic diagram of donor-acceptor energy levels.  
(b) **PDTSTPD.** (c) **PBTPD.**

### 1.8.2 Side chains: Outside the context of solubility

The presence of side chains on the backbone of semiconductor materials provides great potential to take advantage of replacing inorganic semiconductor materials in the manufacturing process of optoelectronic devices with a low cost. The utility of this approach in the field of organic optoelectronic materials is highly important since the nature of side chains engaged into the conjugated polymer properties in their solid state, which in turn reflects in the optoelectronic properties. The vast majority of donor-acceptor conjugated polymers pends alkyl, alkoxy or oligo (ethylene glycol) side chains for a purpose beyond the physical property of solubility.

To better understand the influence of the side chain, Wei et al.<sup>94</sup>, Facchetti et al.<sup>95</sup>, Heeger et al.<sup>96</sup> and McCulloch et al.<sup>97</sup> have published a series of TPD-bithiophene-based copolymers with various side chains (**Figure 1.24-a**). Wei et al. was able to prepare **P1a** featuring 2-ethylhexyl substitutions on the TPD backbone while the dodecyl side chain grafted 3,3'-bithiophenes in which  $M_n = 9.7$  kDa and PDI = 1.4. **P1a** has an energy band gap of 1.82 eV and a  $V_{OC}$  of 0.95 V because of strong intermolecular interactions between polymer chains and deep HOMO energy levels (-5.56 eV), respectively. Two years later, Heeger et al. changed the solubilising group on TPD to 1-octylonyl and copolymerised with the same alkyl-substituted bithiophene, affording **P1b** with a high molecular weight ( $M_n = 41$  kDa, PDI = 2.3). They observed that the HOMO level of **P1b** decreased by 0.1 eV (-5.66 eV) and the  $V_{OC}$  value was

0.90 V, resulting in a power conversion efficiency (PCE) of 1.90%, which is two and a half times smaller than that of **P1a** (PCE = 4.7%) due to the lack of miscibility between **P1b** and PCBM, unlike with **P1a**.

Furthermore, the same properties of the HOMO energy level and optical band gap of **P1a** was observed for **P1c** when the TPD backbone utilised linear dodecyl substitution.<sup>95</sup> However, the lamellar spacing of the thin film **P1c** (28.41 Å) increased by ~2.4 Å more than that of **P1a** (26 Å) because of the steric effect resulting from the long alkyl chains in **P1c**. When comparing **P1c** with **P1b**, **P1c** exhibits a higher hole mobility ( $6.9 \times 10^{-3} \text{ cm}^2 \text{V}^{-1} \text{s}^{-1}$ ) than **P1b** ( $4.3 \times 10^{-3} \text{ cm}^2 \text{V}^{-1} \text{s}^{-1}$ ), which is attributed to the reduction of any distortion of bonds in pyrrolidone moiety, thereby promoting the interaction between the TPD carbonyl (O) and its neighbouring bithiophenes' sulphur atom, resulting in greater  $\pi$ -delocalisation. Similar results have been observed when McCulloch et al. shortened the alkyl chain substitutions on both units (**P1d**) leading to even greater polymer packing (~22 Å) compared to **P1a** and **P1c**.

Replacing the alkyl-substituted TPD with the alkoxy substitutes has also been investigated by Yang et al.<sup>98</sup> However, they used the most donor candidate, 4,8-bis(alkoxy)benzo[1,2-*b*:4,5-*b'*]-dithiophene (BDT), with various side chain lengths functionalised TPD moiety (**Figure 1.24-b**). As a result, only the octyloxy-substituted TPD (**P2a**) afforded a PCE of 8.22%, which is morphologically favourable and more efficient than those reported either with different alkoxy lengths of **P2b-e**<sup>98</sup> or the alkyl-substituted TPD **P2f-h**<sup>99</sup>.

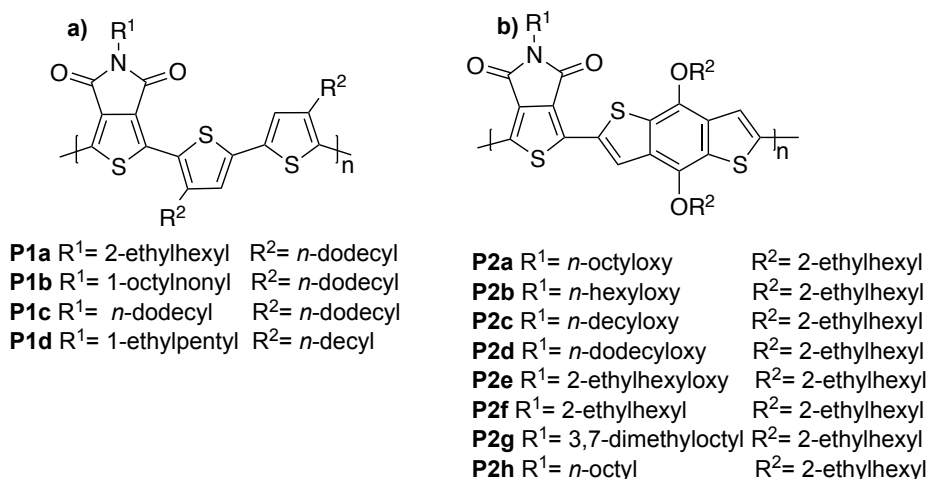


**Figure 1. 24.** Chemical structures of a) bithiophene-TPD and b) BDT-TPD adopting various side chains.

In researching how to improve polymer packing and exciton dissociation after photoexcitation for better photovoltaic performance, Wang et al.<sup>100,101</sup> incorporated different flexible oligo (ethylene glycol) (OEG) side chain lengths on polymer backbones. In 2015, they synthesised four conjugated copolymers (**P3a-d**), including fluorene and dithiophenes, as donors and 2,1,3-benzothiadiazole (BT) as an acceptor moiety (**Figure 1.25-a**). They found that the introduction of the OEG side chains on fluorene moiety decreased the  $\pi$ - $\pi$  stacking distance from 0.44 nm for the full hydrophobic copolymer **P3a** to 0.41 nm for **P3b-d**, resulting in higher hole mobility for **P3b-c** and smaller band gap for **P3b-d**.

However, increasing the length of the OEG substitutions (**P3b-d**) led to a reduction in the molecular ordering as well as in the value of  $V_{oc}$  (the  $V_{oc}$  is largely related to HOMO levels), therefore the PCE diminished from 4.04% to 1.30%<sup>100</sup>. After a year, similar responses were observed when the same group introduced branched OEG with various side chain lengths on a diketopyrrolopyrrole (DPP) unit flanking dithiophene moiety (**Figure 1.25-b**) (**P4a-d**). In addition, the dielectric constant ( $\epsilon_r$ ) increased from 2.1 for **P4a** to 5.8 for **P4b**, which should in turn facilitate the reduction of exciton binding energy for efficient charge separation to achieve high PCE. However, among them, **P4c** recorded the highest PCE (5.37%), ascribed to a good match of the surface energy of the two materials **P4c** (35.27 mJm<sup>-2</sup>)<sup>101</sup> and PC<sub>71</sub>BM

(34.2 mJm<sup>-2</sup>), thus minimising the required energy for good blend morphology with a large interfacial area.<sup>102</sup>

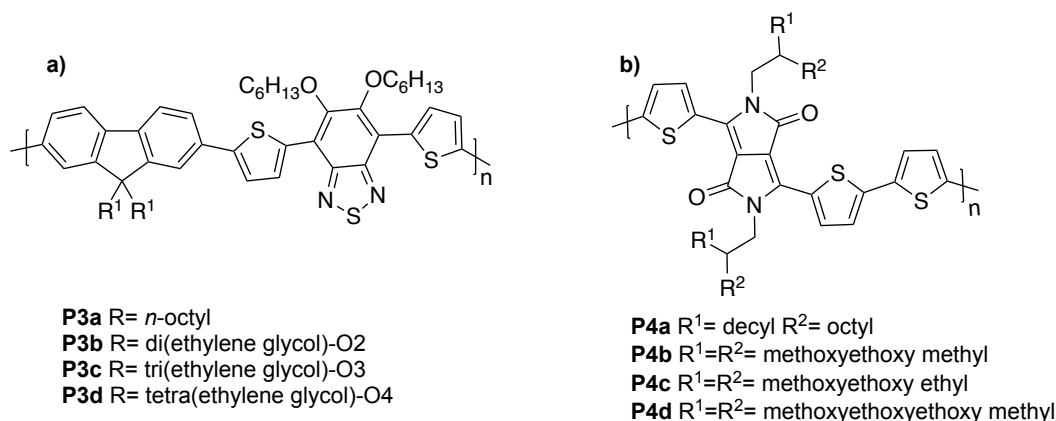


**Figure 1. 25.** Chemical structures of a) fluorene-benzothiadiazole and b) DPP3T adopting various lengths of polar side chains.

### 1.8.3 Regioregularity of the polymers

Conjugated polymers with high charge carrier mobility are essential for better device performance.<sup>103</sup> Thus, one of the underlying themes to achieve this obligation originally relied on improving the structural ordering in semiconductor polymers<sup>104,105</sup> because it would also effectively facilitate the molecular packing with lamellar structure to promote charge carrier transport along the backbone of a polymer chain and through the  $\pi$ -stacking.<sup>105, 106</sup> As a result, many efforts have been dedicated to studying the influence of Poly(3-hexylthiophene) (P3HT) regioregularity on its optoelectronic and photovoltaic properties<sup>107-111</sup>.

**Figure 1.26** shows three possible attachments of side chains positioned at both C4 and C3, at only C3 and at only C4 on a coupling of two 3-alkylthiophene rings, in which the first possible attachment presents head-to-tail coupling (HT), the second presents head-to-head coupling (HH) and the third presents tail-to-tail coupling (TT). P3AT combined with a mixture of three possible couplings is referred to as irregular and has a regiodefect HH configuration that causes a sterically driven distortion of thiophene backbones, resulting in a high loss of coplanarity. On the other hand, regioregular HT coupling can energetically facilitate a coplanar conformation.<sup>112</sup>

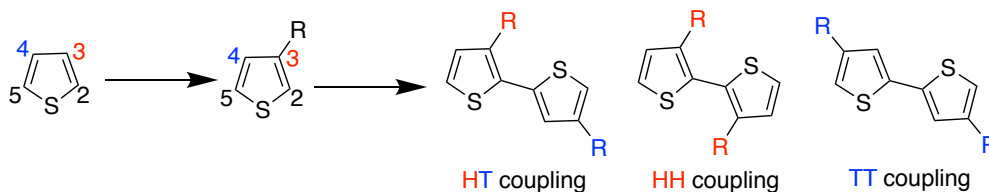


**Figure 1. 26.** Three possible connections on 3-alkylthiophene repeat units.

It is clear that these structural differences in regioregularity patterns can dramatically affect the approach of the molecular packing of conjugated polymers for desirable  $\pi$ - $\pi$  interaction. Kim et al.<sup>103</sup> showed that as regioregularity of HT configuration is raised from 90.7% to 95.2%, the performance of P3HT:PCBM solar cells increases from ~1% to ~4%. This positive result is clearly attributed to better  $\pi$ - $\pi$  stacking within the material, which in turn enhances optical absorption and charge carrier transport properties.

Recently, Chandrasekaran et al. conducted a study on Poly(3-hexylthiophene) (P3HT) and PCBM blend and found that the hole mobility of a 100% HT configuration (DF-P3HT) is  $1.41 \times 10^{-2} \text{ cm}^2 \text{ V}^{-1} \text{ s}^{-1}$ , which is more than two and a half orders of magnitude higher than that of a 92% HT configuration (rr-P3HT), because of the enhancement of interchain packing order and the crystallinity of the conjugated polymer chain<sup>113</sup>, resulting in overall improvement of PCE of DF-P3HT compared to rr-P3HT<sup>114</sup>.

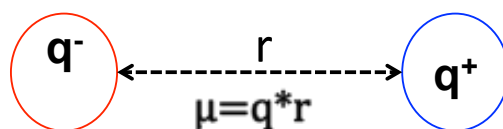
However, it should be noted that increasing the level of structural ordering in P3HT is not always the case for achieving a high level of PCE. Indeed, devices containing 86%, 90% and 96% HT configuration blends have reflected that, with lower RR, the device is thermally stable as a result of the reduction of driven force for polymer crystallisation upon annealing at  $150^\circ\text{C}$ <sup>115</sup>. Furthermore, a high degree of regioregularity of P3HT potentially facilitates the formation of crystalline domains that are larger than the exciton diffusion length, causing exciton relaxation and recombination losses.<sup>116</sup> A high bimolecular recombination has also been observed in a DF-P3HT blend as a result of high charge transport, creating significant opportunity for free

charge carriers to meet each other and recombine bimolecularly before collecting at electrodes.<sup>114</sup>

These results provide understanding of how differences in the molecular packing of regioregularity is extended to charge mobility and the performance of a photovoltaic device, which would conclude that the preferred form of P3HT for optoelectronic applications should be at a level of regioregularity that could minimise all different loss mechanisms.

#### 1.8.4 Electric dipole moments

A system of two opposite charges (positive and negative) that are separated by a distance  $r$ , resulting in the creation of a dipole moment,  $\mu$ .



In this illustration,  $q$  is the magnitude of the separated charges and  $r$  is the distance between them. In a molecule with polar atoms, the different electronegativities would lead to polar bonds, resulting in overall dipole moments for the molecule.<sup>117</sup> This electric dipole moment is measured in a unit called Debye (D); one Debye is equal to approximately  $3.33 \times 10^{-30}$  C\*M. In addition, the general orientation of a polar molecule determines the overall dipole moment of that polarised molecule. On this basis, if the geometry of molecules is entirely asymmetric, then the polarities will cancel each other out and there will be no dipoles, unlike with symmetric geometry which leads to low or high dipole moments (**Figure 1.27**). As a result, the total sum of dipole moments in functional groups of a molecule leads to a dielectric constant.<sup>118,</sup>

119

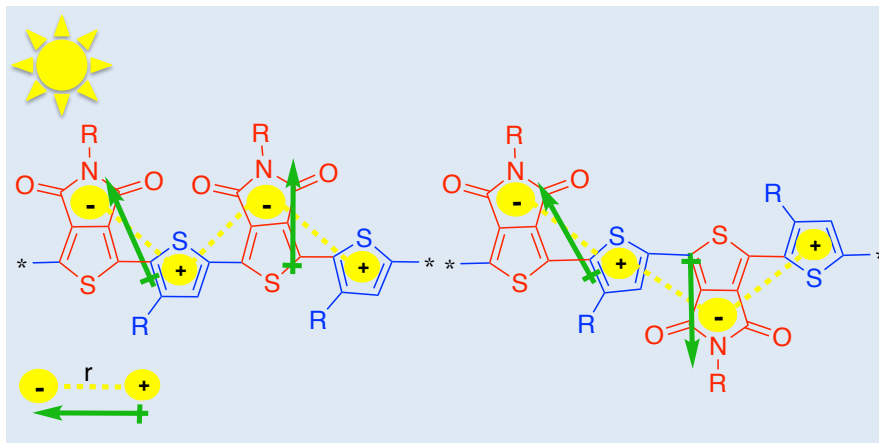


**Figure 1. 27.** The suggested explanation for the dipole moment of TPD-thiophene in the excited state.

From this aspect, it should be highlighted that organic semiconductors have a low dielectric constant due to a strong coulomb attraction between an electron and a hole. In order for an electron to move farther away from its tightly bound hole, a strong, polarisable conjugated polymer must develop the exciton dissociation.<sup>120</sup> Therefore, increasing the internal dipole moment along the polymer backbone can assist in reducing the exciton binding energy, thus improving the photovoltaic properties.

To promote this phenomenon, Yu et al. recently prepared a set of conjugated polymers and found that there is an obvious relationship between the performance of OPV (PCE) and the local dipole moment. In the cases of **PTB2** and **PTB7**, as shown in **Figure 1.28**, the polymers exhibit a large difference in dipole moments ( $\Delta\mu_{ge}$ ) between the ground ( $\mu_g$ ) and excited states ( $\mu_e$ ). They become highly polarised in an excited state, thereby facilitating the charge separation. High power conversion efficiencies (more than 5%) were observed in **PTB2** and **PTB7**, unlike in **PTBF2** and **PBB3**. This difference was caused by the presence of two adjacent TT opposite to each other in the case of **PBB3** and two opposite faces of fluorine atoms in **PTBF2**, resulting in a relatively small dipole moment.<sup>121</sup>



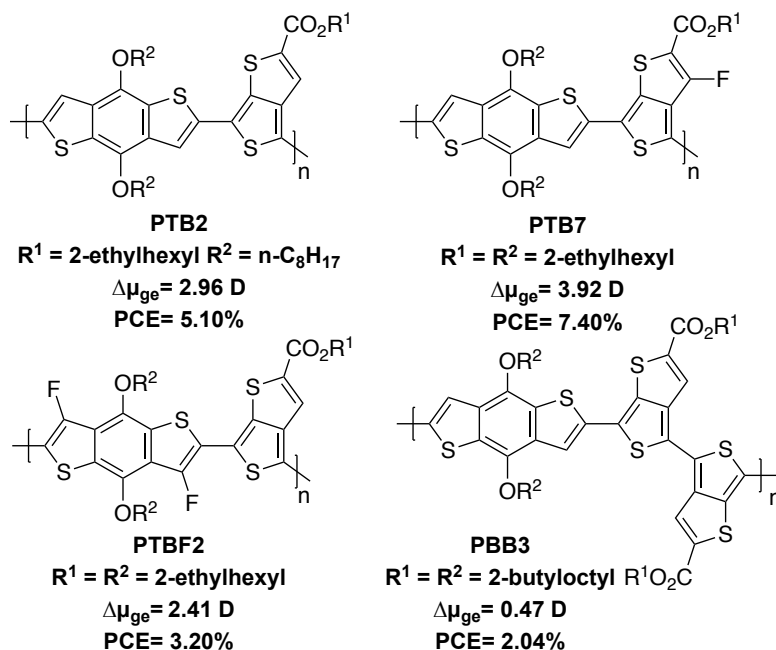


**Figure 1. 28.** Polymer structures of **PTB2**, **PTB7**, **PTBF2** and **PBB3** with local dipole moment and PCE values.

However, the linear relationship between PCE and  $\Delta\mu_{ge}$  appears to be limited to some degree. A study based on 3-oxothieno[3,4-d]isothiazole-1,1-dioxide (TID) and thieno[3,4-c]pyrrole-4,6-dione (TPD) as acceptor moieties represented a large  $\Delta\mu_{ge}$  and a low PCE for **PID-C8** and **PPB-C8**<sup>122</sup> (**Figure 1.29-a**). Recently, Yang et al.<sup>98</sup> proved Yu's hypothesis regarding thieno[3,4-*b*]thiophene motif<sup>121</sup> by preparing **PBT-O8** and the same polymer discussed above (**PPB-C8**) **PBT-C8** for comparison (**Figure 1.29-b**). Depending upon the dipole moment calculation of two repeat units, they found that when the alkyl substitution is replaced with an octyloxy side chain, the  $\Delta\mu_{ge}$  is increased to 14.11 D, thereby encouraging exciton dissociation and resulting in a high PCE of 8.22% for **PBT-O8**.<sup>98</sup> As a result, compromising the  $\Delta\mu_{ge}$  value of conjugated polymers is required to reach a high PCE value.

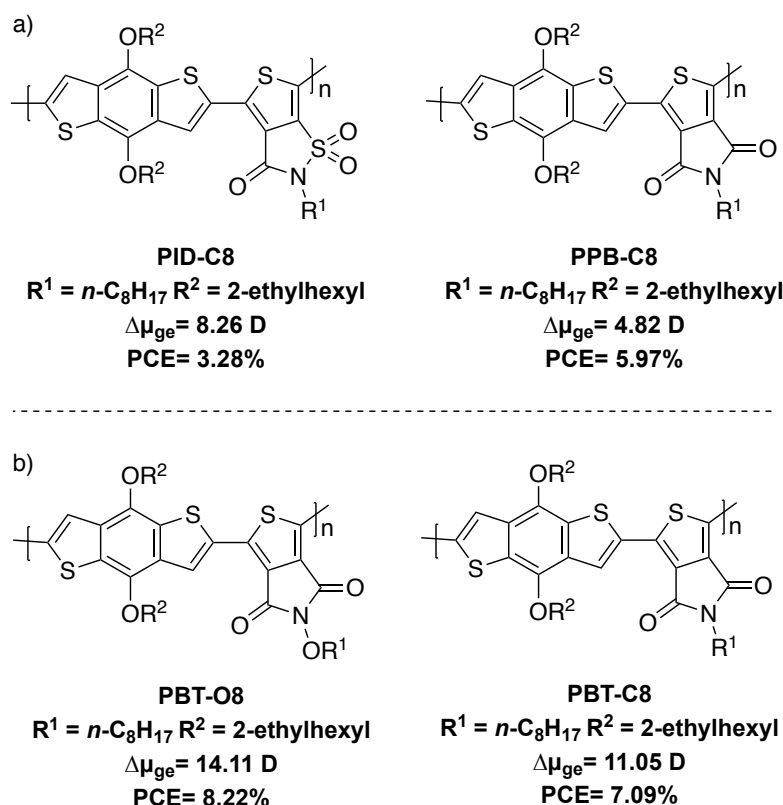


**Figure 1. 29.** Polymer structures of **PID-C8**, **PPB-C8**, **PBT-C8** and **PBT-O8** with values of local dipole moments of a) single repeat unit and b) two repeat units and PCE.

## 1.9 Low band gap-based donor-acceptor copolymers

### 1.9.1 Poly(thieno[3,4-c]pyrrole-4,6-dione) containing electron-donating moieties

Recently, thieno[3,4-c]pyrrole-4,6-dione [TPD] became a favourable electron-withdrawing unit in the design of low bandgap donor-acceptor copolymers for highly efficient optoelectronic devices.<sup>95,123,124</sup> In 1997, this unit was initially synthesised by Zhang and Tour and utilised for an alternating donor/acceptor (D/A) system that had an imide in preference to a dinitro acceptor unit.<sup>125</sup> A while later, Pomerantz and Bjørnholm et al.<sup>126,127</sup> studied the TPD structure and found that the most stable conformation of homopolymers of TPD is the coplanar structure. This structure has favourable electrostatic oxygen-sulphur interactions and efficient chain packing, which could be favourable for  $\pi$ -electron delocalisation within conjugated systems.

However, this acceptor did not receive much attention until 2010 when the utility of the TPD copolymers became more highlighted. It was used for the first time in bulk heterojunction solar cells by Leclerc et al.,<sup>124</sup> Frechet et al.,<sup>99</sup> Jen et al.,<sup>128</sup> and Xie et al.<sup>129</sup> simultaneously. As a result, this acceptor has become a promising building block for developing new, low-energy gap conjugated polymers for photovoltaic cells and charge carrier mobility for organic thin film transistors (OTFT)<sup>130</sup> since the quinoidal form of the TPD backbone (thiophene-maleimide) is able to gain some stabilisation resonance energy in the excited state, which effectively reduces the band gap of polymers when combined into a D/A system.<sup>128,131</sup> The deficient nature of this building block also lowers the HOMO energy levels, ensuring device stability towards air oxidation and maximising the open circuit voltage towards 1.0 V.<sup>128</sup>

Since the nitrogen atom of TPD moiety can be easily functionalised by a large number of substituents, Leclerc et al.<sup>131</sup> prepared a series of TPD homopolymers bearing branched alkyl chains (**P1a-b**, **Figure 1.30**) via direct arylation polymerisation, taking into consideration that most of the previous preparations featuring linear alkyl chains limited the material's solubility and processability. The solubility of **P1a-b** was significantly improved as a result of a higher average molecular weight ( $M_n$ ) (21-23 kDa) compared to polymers with linear alkyl substituents with  $M_n$  up to 4.7 kDa.<sup>95,127,132</sup> Comparison of the optical band gap ( $E_g$ ) of **P1a** and **P1b** featuring the branched substituents on C2 and C1, respectively, showed that the significant reduction of bandwidth realized in that branched far from the backbone **P1a** ( $E_g = 1.9$ ), allowing much more flexibility and further UV-vis absorption to red shift in solid state with more ordered conformation. Only **P1a** was electronically investigated, which had a HOMO level of -6.1 eV and a LUMO level of -4.3 eV (**Table 1.1**), which is deeper by about 1.0 eV with respect to P3HT.<sup>131</sup>

When the branched alkyl-substituted TPD coupled with free thiophene by Stille coupling (**P2a**, **Figure 1.30**), the optical band gap and the HOMO level were further reduced to 1.74 eV and -5.73 eV, respectively, with a hole mobility ( $\mu_h$ ) of  $2.5 \times 10^{-4} \text{ cm}^2 \text{ V}^{-1} \text{ s}^{-1}$ <sup>95</sup>. This positive observation motivated

Facchetti et al. to synthesise a series of TPD coupling several substituted thiophenes in order to increase the conjugation length and tune the electronic properties. When the TPD was coupled with T-T bi(dodecyl) or bi(tetradecyl) bithiophenes (**P3a** and **P3b**, respectively, **Figure 1.30**), the optical band gap and electronic properties were almost the same ( $\sim 0.01$  eV difference, **Table 1.1**); however, **P3b** had a greater  $M_n$  (14.0 kDa vs. 7.3 kDa) and reflected a higher degree of crystallinity, resulting in a higher hole mobility ( $0.175 \text{ cm}^2 \text{ v}^{-1} \text{ s}^{-1}$  vs.  $3.5 \times 10^{-3}$ ) than **P3a**.<sup>95</sup>

Prior to this work, Wei et al. were able to prepare **P3c** (see **Figure 1.30**) bearing a branched alkyl chain on TPD (2-ethylhexyl) and studied the photovoltaic (PV) properties. As a result, device blending of a **P3c**:PC<sub>61</sub>BM chloroform (CF) solution showed a promising PCE of 4.7% with a  $V_{oc}$  of 0.95 V, a short circuit current ( $J_{sc}$ ) of  $8.02 \text{ mA cm}^{-2}$  and a fill factor (FF) of 62 (**Table 1.1**).<sup>94</sup>

Similar work and better results have been recently obtained by Zhou et al., utilising the same substitution on the TPD moiety of **P2a** to prepare **P2a\*** and **P3d** (**Figure 1.30**) for PV and OTFT studies. The OTFT study revealed better performance for **P2a\*** in comparison with **P2a**, which was attributed to better hole injection from the electrode to the HOMOs. PV cells based on active layer and spun-cast from **P2a\***:PC<sub>71</sub>BM (1:1 w/w ratio) CF with 2% diiodooctane (DIO) demonstrated a low PCE of 0.35% with a  $V_{oc}$  of 0.59 V, a  $J_{sc}$  of  $1.75 \text{ mA cm}^{-2}$  and an FF of 33.4. On the other hand, the higher  $M_n$  (17.3 kDa vs. 9.7 kDa) of **P3d** and further treatment on the **P3d**:PC<sub>71</sub>BM (1:2 w/w ratio) active layer reduced the PCBM domain size by 2% DIO, reflecting greater PCE for **P3d** of about 5.66% (**Table 1.1**), which is an order of magnitude higher than **P3c** although **P3d** contains the bulkier side chain along the polymer backbone.<sup>133</sup>

Following the first studies on the copolymers **P3a-b**, further additions of thiophenes resulting in HT configuration **P4** (see **Figure 1.30**) did not dramatically change the optical band gap; however, it did increase the HOMO

energy level to -5.42 eV and reduce the degree of crystallinity, leading to lower  $\mu_h$  ( $0.136 \text{ cm}^2\text{V}^{-1}\text{s}^{-1}$ ) compared to **P3b** (Table 1.1).<sup>95</sup>

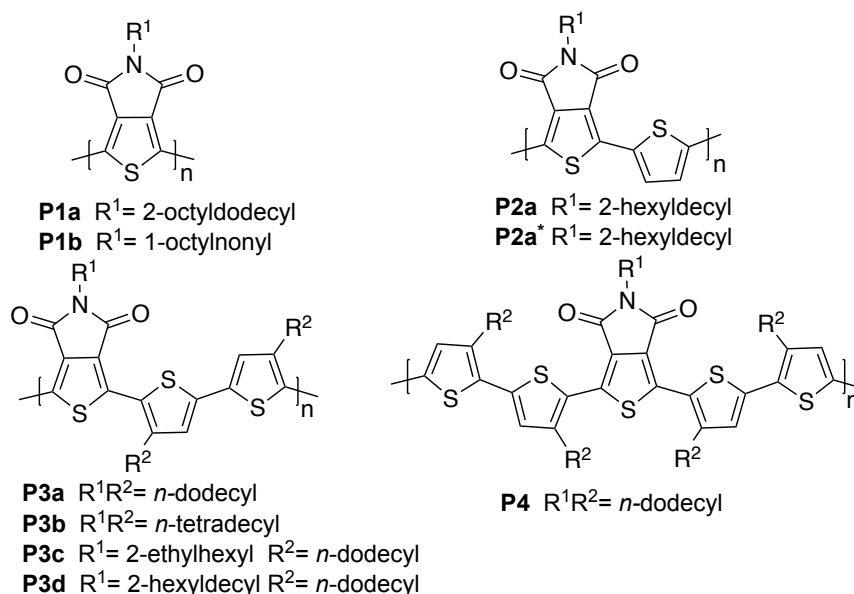


**Figure 1. 30.** Polymer structures of poly alkylated TPD containing oligothiophenes.

**Table 1. 1.**  $E_g$  (opt), electrochemical properties, photovoltaic properties and hole mobility of poly alkylated TPD containing oligothiophene.

| Polymer | $E_g^{\text{optical}}$ (eV) | HOMO (eV) | LUMO (eV)          | $V_{\text{OC}}$ (V) | $J_{\text{SC}}$ ( $\text{mA cm}^{-2}$ ) | FF   | PCE (%)             | $\mu_h$ ( $\text{cm}^2\text{V}^{-1}\text{s}^{-1}$ ) <sup>b</sup> | Ref |
|---------|-----------------------------|-----------|--------------------|---------------------|---|------|---------------------|--|-----|
| P1a     | 1.90                        | -6.10     | -4.3               | -                   | -                                       | -    | -                   | -  | 131 |
| P1b     | 2.2                         | -         | -                  | -                   | -                                       | -    | -                   | -  | 131 |
| P2a     | 1.74                        | -5.73     | -3.27              | -                   | -                                       | -    | -                   | $2.5 \times 10^{-4}$   | 95  |
| P2a*    | 1.73                        | -5.67     | -3.94 <sup>a</sup> | 0.59                | 1.75                                    | 33.4 | 0.35 <sup>c,f</sup> | $2.8 \times 10^{-3}$   | 133 |
| P3a     | 1.80                        | -5.53     | -3.73 <sup>a</sup> | -                   | -                                       | -    | -                   | $3.5 \times 10^{-3}$   | 95  |
| P3b     | 1.79                        | -5.54     | -3.75 <sup>a</sup> | -                   | -                                       | -    | -                   | 0.175  | 95  |
| P3c     | 1.82                        | -5.56     | -3.10              | 0.95                | 8.02                                    | 62   | 4.7 <sup>d,t</sup>  | -  | 94  |
| P3d     | 1.82                        | -5.47     | -3.65 <sup>a</sup> | 0.90                | 8.92                                    | 70.7 | 5.66 <sup>e,f</sup> | $6.2 \times 10^{-3}$   | 133 |
| P4      | 1.82                        | -5.42     | -3.60 <sup>a</sup> | -                   | -                                       | -    | -                   | 0.136  | 95  |

<sup>a</sup>calculated according to  $\text{LUMO} = E_g^{\text{optical}} + \text{HOMO}$ . <sup>b</sup>TFT measurements.

<sup>c</sup>Polymer:PC<sub>71</sub>BCM (1:1 wt:wt). <sup>d</sup>Polymer:PC<sub>61</sub>BCM (1:1.5 wt:wt).

<sup>e</sup>Polymer:PC<sub>71</sub>BCM (1:2 wt:wt). <sup>f</sup>spin-coated from CF solution.

In order to further tune the electronic properties and capture more photons from the solar spectra, Leclerc et al.<sup>134</sup> added BDT unit facing thiophene spacers to the TPD based donor-acceptor conjugated system **P5a-f** (Figure 1.31) and observed that  $E_g$  energetically localised between 1.65 and 1.95 eV, with a HOMO level ranging from -5.49 to -5.73 eV and a LUMO level ranging from -3.70 to -3.83 eV. However, these polymers revealed poor PCE extending from 0.2 to 3.9% at **P5a-f**:PC<sub>61</sub>BM=1:2 (w/w ratio) as a result of low

FF (**Table 1.2**). Meanwhile, when substituted dithiophenes were completely replaced with BDT, **P6a-c** (see **Figure 1.31**), the HOMO levels ranged from -5.32 to -5.56 eV<sup>98, 99, 124, 128, 135</sup> and the LUMO level ranged from -3.40 to -3.75 eV<sup>124, 128, 135</sup> (see **Table 1.2**). In particular, **P6a**:PC<sub>71</sub>BM (1:1.5 w/w ratio) cast from chlorobenzene (CB) with 5% 1-chloronaphthalene (CN) exhibited the best photovoltaic performance (a PCE of 8.50%) compared to **P6b** (7.50%)<sup>136</sup> and **P6c** (8.22%)<sup>98</sup> (**Table 1.2**). It appears as though each methylene in the solubilising side chain attached to the TPD is responsible for increasing the insulating ratio against the active conjugation backbone<sup>136</sup> and causing different morphology surfaces.

In 2011, Ding and co-worker<sup>137</sup>, Watson and co-worker<sup>138</sup>, Leclerc and co-worker<sup>91</sup>, and Reynolds and co-worker<sup>139, 140</sup> initially studied the replacement of the fused electron donor BDT with cyclopenta[2,1-*b*;3,4-*b*]dithiophene (CPDT) using different atom bridges (**P7a-c**) (**Figure 1.31**). For example, **P7a** revealed an  $E_g$  of 1.59 eV and HOMO and a LUMO levels of -5.29 and -3.63 eV, respectively. When **P7a** was blended with PC<sub>71</sub>BM in a 1:2 (w/w) ratio cast from 1,2-dichlorobenzene (*o*-DCB) with 4.2% DIO, a PCE of 6.41% with a  $V_{oc}$  of 0.75 V, a  $J_{sc}$  of 14.1 mA cm<sup>-2</sup> and an FF of 60.7 were achieved. Recently, Reynolds et al.<sup>141</sup> applied **P7b-c**:PC<sub>71</sub>BM (1:1.5 w/w ratio) cast from CB with 5% DIO solution on organic photovoltaics and observed a very impressive PCE of 7.4% for **P7b** with a  $V_{oc}$  of 0.91 V, a  $J_{sc}$  of 12.2 mA cm<sup>-2</sup> and an FF of 72. The PCE was 8.0% for **P7c**, with a  $V_{oc}$  of 0.87 V, a  $J_{sc}$  of 13.6 mA cm<sup>-2</sup> and an FF of 70 (**Table 1.2**). They found that C-Ge and C-Si bonds were longer than C-C bonds, keeping the insulating substitutions far away from the thiophene, thereby leading to better conformations, stacking and device performance.<sup>141</sup>

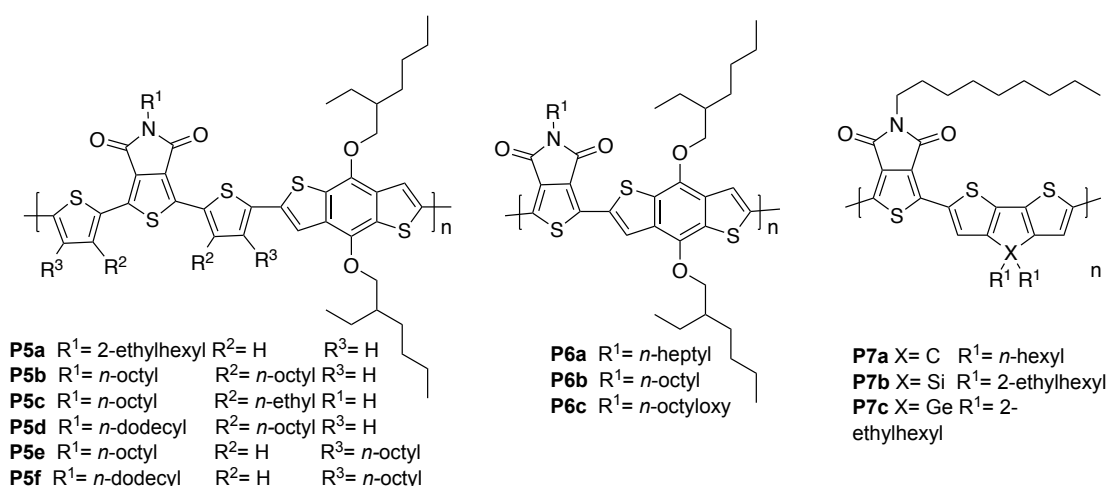


**Figure 1. 31.** Polymer structures of poly alkylated TPD containing fused electron donors.

**Table 1. 2.**  $E_g(\text{opt})$ , electrochemical properties and photovoltaic properties of poly alkylated TPD containing fused electron donors.

| Polymer | $E_g^{\text{optical}}$ (eV) | HOMO (eV)   | LUMO (eV)          | $V_{\text{OC}}$ (V) | $J_{\text{SC}}$ (mA cm <sup>-2</sup> ) | FF   | PCE (%)             | Ref                 |
|---------|-----------------------------|-------------|--------------------|---------------------|--|------|---------------------|---------------------|
| P5a     | 1.65                        | -5.49       | -3.70              | 0.76                | 2.9                                    | 43   | 0.95 <sup>b,e</sup> | 134                 |
| P5b     | 1.86                        | -5.56       | -3.70              | 0.89                | 7.6                                    | 57   | 3.9 <sup>b,t</sup>  | 134                 |
| P5c     | 1.76                        | -5.54       | -3.78              | 0.76                | 9.0                                    | 51   | 3.5 <sup>b,e</sup>  | 134                 |
| P5d     | 1.86                        | -5.56       | -3.70              | 0.87                | 7.2                                    | 58   | 3.6 <sup>b,f</sup>  | 134                 |
| P5e     | 1.83                        | -5.66       | -3.83              | 0.66                | 1.2                                    | 26   | 0.2 <sup>b,t</sup>  | 134                 |
| P5f     | 1.95                        | -5.73       | -3.78              | 0.92                | 2.3                                    | 34   | 0.7 <sup>b,t</sup>  | 134                 |
| P6a     | 1.75                        | -5.32       | -3.57 <sup>a</sup> | 0.97                | 12.60                                  | 70   | 8.50 <sup>c,g</sup> | 135,136             |
| P6b     | 1.81                        | -(5.4-5.56) | -(3.4-3.75)        | 0.93                | 12.50                                  | 65   | 7.50 <sup>c,g</sup> | 124,99,128, 135,136 |
| P6c     | 1.80                        | -5.42       | -3.62 <sup>a</sup> | 0.94                | 14.35                                  | 60.2 | 8.22 <sup>c,g</sup> | 98                  |
| P7a     | 1.59                        | -5.29       | -3.63              | 0.75                | 14.1                                   | 60.7 | 6.41 <sup>d,e</sup> | 137                 |
| P7b     | 1.71                        | -5.67       | -3.53              | 0.91                | 12.2                                   | 72   | 7.4 <sup>c,g</sup>  | 141                 |
| P7c     | 1.69                        | -5.60       | -3.61              | 0.87                | 13.6                                   | 70   | 8.22 <sup>c,g</sup> | 141                 |

<sup>a</sup>Calculated according to  $\text{LUMO} = E_g^{\text{optical}} + \text{HOMO}$ . <sup>b</sup>Polymer:PC<sub>61</sub>BCM (1:2 wt:wt).

<sup>c</sup>Polymer:PC<sub>71</sub>BCM (1:1.5 wt:wt). <sup>d</sup>Polymer:PC<sub>71</sub>BCM (1:2 wt:wt). <sup>e</sup>Spin-coated from *o*-DCB solution. <sup>f</sup>Spin-coated from CF solution. <sup>g</sup>Spin-coated from CB solution

### 1.9.2 Poly(fluorene) containing electron-accepting moieties

Polyfluorenes (PFOs) have received remarkable attention as the most promising class of semiconductor materials in the active layer of optoelectronic applications due to their unique optoelectronic properties and capability to modulate chemically. PFOs and their derivatives are rigidly planar molecules that generally exhibit rather large optical band gaps (3.0±0.10 eV) and deep-lying HOMO levels ranging from -5.55 eV to -5.80 eV<sup>142</sup>, making them more physically and chemically resistant to both photo-

degradation and thermal oxidation under illumination and high temperature operation of the optoelectronic device. Easy functionalisation along the fluorene backbone with fewer steric substituents at the bridge C<sub>9</sub>-site and highly regioselective coupling at the C<sub>2</sub>,C<sub>7</sub>-sites allows for enhanced molecular solubility of the backbone, controlling interchain interactions and extending the effective delocalisation length to further improve charge transport. A high absorption coefficient, good hole transporting properties and excellent thermal and environmental stability of polyfluorene derivatives have originally driven this class of material to be extensively utilised in the field of solid-state lighting (SSL).<sup>36,143</sup> Meanwhile, PFOs became a favourable electron-donating unit for photovoltaic devices with the theoretical expectation of high open-circuit voltages; however, their wide band gap restricts the coverage across the solar spectrum. This restriction can be overcome by copolymerising an electron-accepting moiety into the main polyfluorene chain to tune the band gap and the energy levels.<sup>88, 144</sup>

Indeed, a further reduction of the optical bandwidth of PFOs is achieved by contributing bithiophene to the main chain system in **P8** (2.41 eV), as shown in **Figure 1.32**. However, the HOMO level rose up to -5.50 eV, which is ~0.05-0.3 eV higher than that of homo-PFOs and ~0.34 eV lower than that of P3HT (-5.16 eV)<sup>95</sup>. As a result, when **P8** was blended with PC<sub>61</sub>BM in a 1:2 (w/w) ratio cast from tetrachlorobenzene (TCB), a PCE of 2.14% was observed with a V<sub>oc</sub> of 0.99 V, a J<sub>sc</sub> of 4.24 mA cm<sup>-2</sup> and an FF of 51 (**Table 1.3**).<sup>145</sup>

Placing a large common electron acceptor, Benzothiadiazole (BT), in between bithiophene (**P9**, **Figure 1.32**) has been extensively studied<sup>88</sup> in order to enrich the performance of the push-pull concept, thereby enhancing the electronic properties for superior BHJ device outcomes. Accordingly, Iraqi et al.<sup>146</sup> were able to prepare **P9** with Suzuki coupling, resulting in a high M<sub>n</sub> (78.4 kDa), a nearly ideal HOMO level of -5.44 eV and a smaller band gap by ~0.43 eV in comparison to **P8**. This ideal HOMO level resulted in a high V<sub>oc</sub> of 1.02 V when the device's active layer **P9**:PC<sub>71</sub>BM (1:4 w/w ratio) was spin-coated from a CB solution, recording the best device performance of **P9** until



now (**Table 1.3**). Once the insulating component was introduced on bithiophene and removed from the BT backbone (**P10**, **Figure 1.32**), the  $M_n$  was higher than that of **P9** (175 kDa vs. 78.4 kDa), and the HOMO level shifted down to -5.60 eV, whereby promoting a high value of  $V_{oc}$  (**Table 1.3**).<sup>147</sup> Nevertheless, the PCE was nearly analogous to **P8** and varied from 4.94% for **P9** to 2.2% for **P10** at **P10**:PC<sub>71</sub>BM=1:3 (w/w) ratio for **P10**.

On the other hand, what result would be expected if a BT unit was replaced with a TPD unit has been addressed by only two journal papers. Like **P9** and **P10**, Hashimoto group<sup>148</sup> and Tian group<sup>149</sup> synthesised **P11** and **P12** (**Figure 1.32**), indicating that the electron-accepting ability of the TPD unit had a negligible effect on the HOMO level compared to the BT unit, which were -5.59 eV and -5.66 eV, respectively, and which might also be explained by poor co-planarity and poor delocalisation of the HOMO levels of the corresponding copolymers, resulting in wide optical band gaps (**Table 1.3**). A BHJ solar cell based on **P11**:PC<sub>71</sub>BM (1:2 w/w ratio) and spin-coated from *o*-DCB demonstrated a low PCE of 1.06%, which is more than four orders of magnitude higher than that of **P12** and lower than that of **P9** (see **Table 1.3**). It is worth noting that the performance of the BHJ device of **P12** provides a higher  $V_{oc}$  (about 1.01 V) and a lower  $J_{sc}$  (0.62 mA cm<sup>-2</sup>) compared to **P11** due to its downward shift of the HOMO levels and its weak match to the solar radiation, respectively. Besides, poor morphology is responsible for the device performance reflection.

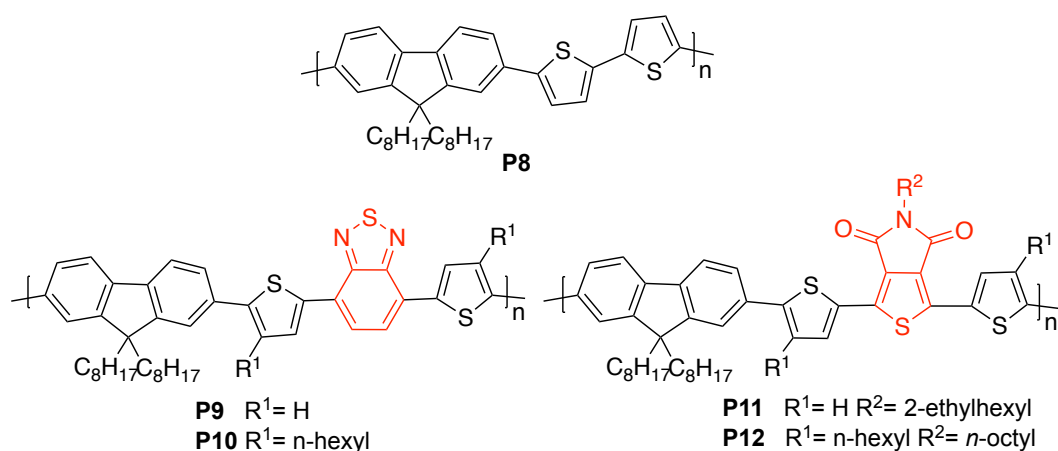


**Figure 1. 32.** Polymer structures of alkylated fluorene based copolymers.

**Table 1. 3.**  $E_g$ (opt), electrochemical properties and photovoltaic properties of alkylated fluorene-based copolymers.

| Polymer | $E_g^{\text{optical}}$<br>(eV) | HOMO<br>(eV) | LUMO<br>(eV)       | $V_{\text{OC}}$<br>(V) | $J_{\text{SC}}$<br>(mA cm <sup>-2</sup> ) | FF    | PCE<br>(%)          | Ref |
|---------|--------------------------------|--------------|--------------------|------------------------|---|-------|---------------------|-----|
| P8      | 2.41                           | -5.50        | -3.10              | 0.99                   | 4.24                                      | 51    | 2.14 <sup>b,f</sup> | 145 |
| P9      | 1.98                           | -5.44        | -3.32              | 1.02                   | 10.22                                     | 47.57 | 4.94 <sup>c,g</sup> | 146 |
| P10     | 1.97                           | -5.60        | -3.63 <sup>a</sup> | 1.06                   | 4.9                                       | 41    | 2.2 <sup>d,h</sup>  | 147 |
| P11     | 2.14                           | -5.59        | -3.49              | 0.82                   | 3.05                                      | 43    | 1.06 <sup>e,i</sup> | 148 |
| P12     | 2.30                           | -5.66        | -3.66              | 1.01                   | 0.62                                      | 35    | 0.22 <sup>e,i</sup> | 149 |

<sup>a</sup>Calculated according to  $\text{LUMO} = E_g^{\text{optical}} + \text{HOMO}$ . <sup>b</sup>Polymer:PC<sub>61</sub>BCM (1:2 wt:wt).

<sup>c</sup>Polymer:PC<sub>71</sub>BCM (1:4 wt:wt). <sup>d</sup>Polymer:PC<sub>71</sub>BCM (1:3 wt:wt). <sup>e</sup>Polymer:PC<sub>71</sub>BCM

(1:2 wt:wt). <sup>f</sup>Spin-coated from TCB solution. <sup>g</sup>Spin-coated from CB solution. <sup>h</sup>Spin-

coated from CF solution. <sup>i</sup>Spin-coated from *o*-DCB solution.

## 1.10 Aims of the work

The synthesis and design of low-bandgap conjugated copolymers are of growing interest in the realm of electronic applications due to their potential to enhance charge transfer rates along the polymer chain, which can promote their use in optical and electronic devices. In the case of solar energy, it is highly important to design and select suitable electron donors (D) and acceptors (A) to increase the optical absorption of photons with energy higher than that of the band gap.

The primary objective of this work is to synthesise a series of new types of conjugated copolymers based on an alkylated thieno[3,4-c]pyrrole-4,6-dione (TPD) as the main electron-transport material, in which the TPD moiety is relatively simple, symmetric, rigidly fused and planar in structure and exhibits a strong electron-withdrawing effect that can decrease HOMO and LUMO energy levels.<sup>123,124</sup> Thus, this study will couple the acceptor TPD with various hole-transporting materials through an eco-friendly coupling approach (direct arylation) to develop the performance properties of the resultant copolymers for application in electronic devices. Prior to polymerisation, all the monomers will initially be subjected to characterisation by nuclear magnetic resonance (NMR), mass spectrometry (MS) and elemental analysis. After the polymerisation, the characterisation and photophysical properties of the target copolymers will then be studied by <sup>1</sup>H NMR, gel permeation chromatography (GPC), UV-visible absorption spectroscopy, Cyclic voltammetry (CV), thermal gravimetric analysis (TGA) and powder x-ray diffraction (PXRD).

Chapter II will study the effect of thienyl-TPD regioregularity on the chemical and physical properties of the resulting polymers. Many literature studies strongly assert that optical and electronic properties are linearly responsive to the polymer packing.<sup>103, 150</sup> For OPV solar cells, the exciton dissociation at the BHJ polymer/fullerene interfaces is still low and considered as the main limiting factor to obtaining efficient performance. Accordingly, the orientation of polymer chains is physically responsible for the magnitude of their dipole moments. Different pattern fashions of a number of thiophenes (including

conjugated side chain (phenyl ring), which should effectively act as tools to control polymer chain orientation) will be coupled with substituted TPD units (**Figure 1.33**) in order to study the structural variation on their electrochemical properties, optical and thermal properties and their solid-state packing. OPV studies will ultimately be undertaken on these materials. The expected outcomes of these different studies should serve to rationalise the substitution pattern on thiophene polymers to provide materials with high overall dipole moment. This in turn should hopefully provide materials with high power conversion efficiencies in OPV devices.

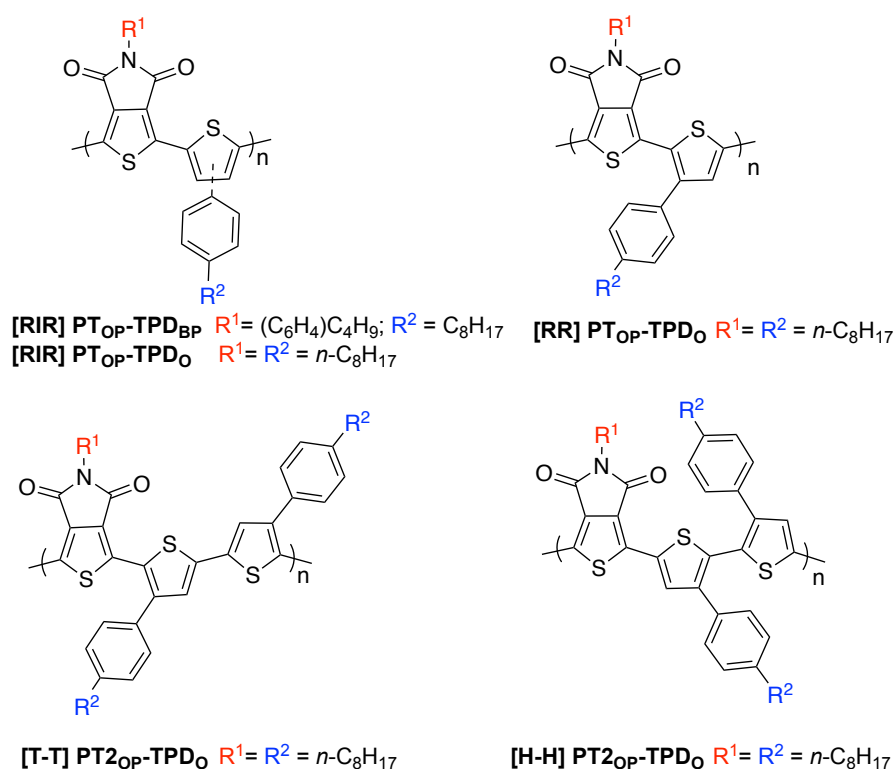


**Figure 1. 33.** Polymer structure of **[RIR] PT<sub>OP</sub>-TPD<sub>BP</sub>** , **[RIR] PT<sub>OP</sub>-TPD<sub>O</sub>**, **[RR] PT<sub>OP</sub>-TPD<sub>O</sub>**, **[T-T] PT<sub>2OP</sub>-TPD<sub>O</sub>** and **[H-H] PT<sub>2OP</sub>-TPD<sub>O</sub>**.

As side chains would affect optoelectronic properties, chapter III and chapter IV examine the extent of the influence of hydrophilic tri(ethylene glycol) (TEG) side chains as a replacement for alkyl side chains in conjugated polymers on the chemical and physical properties. Previous work has been motivated to utilise the less steric hydrophilic chains on a series of conjugated polymers based on a fluorene unit<sup>100</sup> or a diketopyrrolopyrrole unit<sup>101</sup>. As a result, it was found that replacing hydrophobic chains with flexible hydrophilic chains strongly facilitates the polymer chain interactions<sup>100,101</sup> and the dielectric

constant for fast charge separation in BHJ solar cells.<sup>101</sup> To the best of our knowledge, the utility of this approach onto a TPD acceptor unit has not been reported for PSC in the literature yet. It will be interesting to evaluate the capability of TEG chains to affect the resulting polymer properties. Chapter III will focus on introducing TEG and branched alkyl side chains onto TPD moiety. This moiety will be copolymerised with a fluorene unit featuring TEG and straight alkyl side chains and facing thiophene spacers at 2,7-positions (see **Figure 1.34**). Like chapter III, chapter IV will study the replacement of the entire donor backbone with thiophene containing TEG and branched chains and favouring random walk (see **Figure 1.35**).

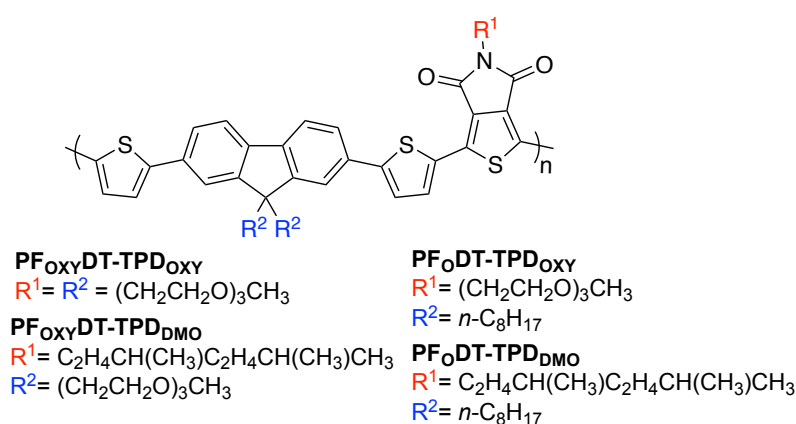


**Figure 1. 34.** Polymer structure of **PF<sub>OXY</sub>DT-TPD<sub>OXY</sub>**, **PF<sub>OXY</sub>DT-TPD<sub>DMO</sub>**, **PF<sub>O</sub>DT-TPD<sub>OXY</sub>** and **PF<sub>O</sub>DT-TPD<sub>DMO</sub>**.

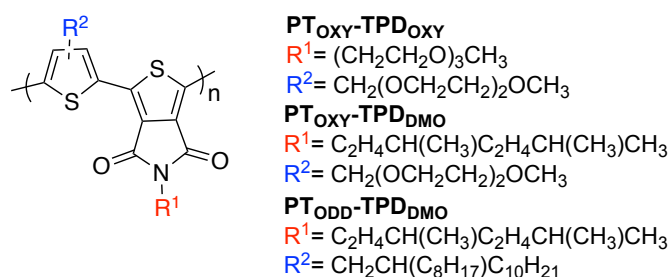


**Figure 1. 35.** Polymer structure of **PT<sub>OXY</sub>-TPD<sub>OXY</sub>**, **PT<sub>OXY</sub>-TPD<sub>DMO</sub>** and **PT<sub>ODD</sub>-TPD<sub>DMO</sub>**.

## 1.11 References

1. M. C. Scharber and N. S. Sariciftci, *Progress in Polymer Science*, 2013, **38**, 1929-1940.
2. C. J. Brabec, N. S. Sariciftci and J. C. Hummelen, *Advanced Functional Materials*, 2001, **11**, 15-26.
3. R. Koepppe, O. Bossart, G. Calzaferri and N. Sariciftci, *Solar Energy Materials and Solar Cells*, 2007, **91**, 986-995.
4. B. A. Gregg and M. C. Hanna, *Journal of Applied Physics*, 2003, **93**, 3605-3614.
5. H. Spanggaard and F. C. Krebs, *Solar Energy Materials and Solar Cells*, 2004, **83**, 125-146.
6. J.-L. Brédas, J. E. Norton, J. Cornil and V. Coropceanu, *Accounts of Chemical Research*, 2009, **42**, 1691.
7. M. Korzhov, R. Shikler and D. Andelman, *Physics World*, 2008, **21**, 29-33.
8. H. Letheby, *Journal of the Chemical Society*, 1862, **15**, 161-163.
9. G. Inzelt, *Conducting Polymers: a New Era in Electrochemistry*, 2008, 265-267.
10. B. A. Bolto, R. McNeill and D. E. Weiss, *Australian Journal of Chemistry*, 1963, **16**, 1090-1103.
11. T. Ito, Shirakawa, H. and S. Ikeda, *Journal of Polymer Science Part A: Polymer Chemistry*, 1974, **12**, 11-20.
12. H. Shirakawa, *Angewandte Chemie-International Edition*, 2001, **40**, 2574-2580.
13. G. Natta, Mazzanti, G., & Corradini, P., *Atti della Accademia Nazionale dei Lincei. Classe di Scienze Fisiche, Matematiche e Naturali. Rendiconti Lincei*, 1958, **3**.
14. C. K. Chiang, C. R. Fincher, Y. W. Park, A. J. Heeger, H. Shirakawa, E. J. Louis, S. C. Gau and A. G. Macdiarmid, *Physical Review Letters*, 1977, **39**, 1098-1101.
15. C. K. Chiang, M. A. Druy, S. C. Gau, A. J. Heeger, E. J. Louis, A. G. Macdiarmid, Y. W. Park and H. Shirakawa, *Journal of the American Chemical Society*, 1978, **100**, 1013-1015.
16. L. Huo, T. Liu, X. Sun, Y. Cai, A. J. Heeger and Y. Sun, *Advanced Materials*, 2015, **27**, 2938-2944.
17. J.-S. Wu, S.-W. Cheng, Y.-J. Cheng and C.-S. Hsu, *Chemical Society Reviews*, 2015, **44**, 1113-1154.
18. L. Zhang, Z. Liu, X. Zhang, J. Chen and Y. Cao, *Journal of Inorganic and Organometallic Polymers and Materials*, 2015, **25**, 64-72.
19. C. L. Ho, & Wong, W. Y., *Organometallics and Related Molecules for Energy Conversion*, Springer-Verlag Berlin Heidelberg, 2015.
20. A. Facchetti, *Chemistry of Materials*, 2011, **23**, 733-758.
21. I. Osaka, *Polymer Journal*, 2015, **47**, 18-25.

22. W. J. Feast, J. Tsibouklis, K. L. Pouwer, L. Groenendaal and E. W. Meijer, *Polymer*, 1996, **37**, 5017-5047.
23. H. Hoppe and N. S. Sariciftci, *Journal of Materials Research*, 2004, **19**, 1924-1945.
24. U. Salzner, J. B. Lagowski, P. G. Pickup and R. A. Poirier, *Synthetic Metals*, 1998, **96**, 177-189.
25. A. Ajayaghosh, *Chemical Society Reviews*, 2003, **32**, 181-191.
26. S. Mahajan, & Kimerling, L. C., *Concise Encyclopedia of Semiconducting Materials & Related Technologies*, Elsevier, Amsterdam, 2013.
27. M. C. Petty, Bryce, M. R., & Bloor, D, *An Introduction to Molecular Electronics*, Oxford University Press, London, 1995.
28. D. Bloor and B. Movaghar, *Iee Proceedings-I Communications Speech and Vision*, 1983, **130**, 225-232.
29. J. L. Bredas and G. B. Street, *Accounts of Chemical Research*, 1985, **18**, 309-315.
30. A. K. Bakhshi and G. Bhalla, *Journal of Scientific & Industrial Research*, 2004, **63**, 715-728.
31. P. Kar, *Doping in Conjugated Polymers*, 2013, 1-156.
32. B. de Boer and A. Facchetti, *Polymer Reviews*, 2008, **48**, 423-431.
33. K. M. Coakley and M. D. McGehee, *Chemistry of Materials*, 2004, **16**, 4533-4542.
34. G. G. Wallace, P. C. Dastoor, D. L. Officer and C. O. Too, *Chemical Innovation*, 2000, **30**, 15-22.
35. J. Kovac, L. Peternai and O. Lengyel, *Thin Solid Films*, 2003, **433**, 22-26.
36. M. T. Bernius, M. Inbasekaran, J. O'Brien and W. S. Wu, *Advanced Materials*, 2000, **12**, 1737-1750.
37. L. H. Chen, D. W. McBranch, H. L. Wang, R. Helgeson, F. Wudl and D. G. Whitten, *Proceedings of the National Academy of Sciences of the United States of America*, 1999, **96**, 12287-12292.
38. L. Torsi, G. M. Farinola, F. Marinelli, M. C. Tanese, O. H. Omar, L. Valli, F. Babudri, F. Palmisano, P. G. Zambonin and F. Naso, *Nature Materials*, 2008, **7**, 412-417.
39. G. Yu, J. Wang, J. McElvain and A. J. Heeger, *Advanced Materials*, 1998, **10**, 1431-1434.
40. A. Facchetti, *Materials Today*, 2007, **10**, 28-37.
41. A. R. Murphy and J. M. J. Frechet, *Chemical Reviews*, 2007, **107**, 1066-1096.
42. G. Horowitz, *Advanced Materials*, 1998, **10**, 365-377.
43. R. J. Mortimer, *Chemical Society Reviews*, 1997, **26**, 147-156.
44. J. Mei, Y. Diao, A. L. Appleton, L. Fang and Z. Bao, *Journal of the American Chemical Society*, 2013, **135**, 6724-6746.

45. J. E. Lilienfeld, U.S. Patent No 1745175, 1930.
46. H. Koezuka, A. Tsumura and T. Ando, *Synthetic Metals*, 1987, **18**, 699-704.
47. A. Tsumura, H. Koezuka and T. Ando, *Synthetic Metals*, 1988, **25**, 11-23.
48. A. Facchetti, M. H. Yoon and T. J. Marks, *Advanced Materials*, 2005, **17**, 1705-1725.
49. M. Pope, P. Magnante and H. P. Kallmann, *Journal of Chemical Physics*, 1963, **38**, 2042-2043.
50. W. Helfrich and Schneide.Wg, *Physical Review Letters*, 1965, **14**, 229-&.
51. C. W. Tang and S. A. Vanslyke, *Applied Physics Letters*, 1987, **51**, 913-915.
52. D. Braun and A. J. Heeger, *Applied Physics Letters*, 1991, **58**, 1982-1984.
53. J. H. Burroughes, D. D. C. Bradley, A. R. Brown, R. N. Marks, K. Mackay, R. H. Friend, P. L. Burn and A. B. Holmes, *Nature*, 1990, **347**, 539-541.
54. X.-Y. Deng, *International Journal of Molecular Sciences*, 2011, **12**, 1575-1594.
55. W. Bruetting, J. Frischeisen, T. D. Schmidt, B. J. Scholz and C. Mayr, *Physica Status Solidi a-Applications and Materials Science*, 2013, **210**, 44-65.
56. M. D. McGhee and M. A. Topinka, *Nature Materials*, 2006, **5**, 675-676.
57. T. L. Benanti and D. Venkataraman, *Photosynthesis Research*, 2006, **87**, 73-81.
58. S. Karg, W. Riess, V. Dyakonov and M. Schwoerer, *Synthetic Metals*, 1993, **54**, 427-433.
59. C. W. Tang, *Applied Physics letters*, 1986, **48**, 183-185.
60. S. Guenes, H. Neugebauer and N. S. Sariciftci, *Chemical Reviews*, 2007, **107**, 1324-1338.
61. J. G. Xue, S. Uchida, B. P. Rand and S. R. Forrest, *Applied Physics Letters*, 2004, **84**, 3013-3015.
62. G. Yu, J. Gao, J. C. Hummelen, F. Wudl and A. J. Heeger, *Science*, 1995, **270**, 1789-1791.
63. C. Deibel and V. Dyakonov, *Reports on Progress in Physics*, 2010, **73**.
64. G. Yu and A. J. Heeger, *Journal of Applied Physics*, 1995, **78**, 4510-4515.
65. Y.-W. Su, S.-C. Lan and K.-H. Wei, *Materials Today*, 2012, **15**, 554-562.
66. J. You, C.-C. Chen, Z. Hong, K. Yoshimura, K. Ohya, R. Xu, S. Ye, J. Gao, G. Li and Y. Yang, *Advanced Materials*, 2013, **25**, 3973-3978.



67. A. R. b. M. Yusoff, D. Kim, H. P. Kim, F. K. Shneider, W. J. da Silva and J. Jang, *Energy & Environmental Science*, 2015, **8**, 303-316.
68. L. A. Wang, Y. H. Zhang, L. F. Liu and Y. G. Wang, *Journal of Organic Chemistry*, 2006, **71**, 1284-1287.
69. S. Kotha, K. Lahiri and D. Kashinath, *Tetrahedron*, 2002, **58**, 9633-9695.
70. J. Hassan, M. Sevignon, C. Gozzi, E. Schulz and M. Lemaire, *Chemical Reviews*, 2002, **102**, 1359-1470.
71. C. M. So and F. Y. Kwong, *Chemical Society Reviews*, 2011, **40**, 4963-4972.
72. S. Kotha, K. Lahiri and D. Kashinath, *Tetrahedron*, 2002, **58**, 9633-9695.
73. M. G. Hu, Z. An, W. Du, J. Li and A. A. Gao, *Chinese Journal of Chemistry*, 2007, **25**, 1183-1186.
74. N. Miyaura and A. Suzuki, *Chemical Reviews*, 1995, **95**, 2457-2483.
75. C. Amatore, A. Jutand and G. Le Duc, *Chemistry-a European Journal*, 2011, **17**, 2492-2503.
76. K. Wang and M. Wang, *Current Organic Chemistry*, 2013, **17**, 999-1012.
77. D. J. Schipper and K. Fagnou, *Chemistry of Materials*, 2011, **23**, 1594-1600.
78. A. Facchetti, L. Vaccaro and A. Marrocchi, *Angewandte Chemie-International Edition*, 2012, **51**, 3520-3523.
79. K. Okamoto, J. Zhang, J. B. Housekeeper, S. R. Marder and C. K. Luscombe, *Macromolecules*, 2013, **46**, 8059-8078.
80. M. Wakioka, N. Ichihara, Y. Kitano and F. Ozawa, *Macromolecules*, 2014, **47**, 626-631.
81. D. Alberico, M. E. Scott and M. Lautens, *Chemical Reviews*, 2007, **107**, 174-238.
82. S.-Y. Chang, P.-H. Lin and C.-Y. Liu, *RSC Advances*, 2014, **4**, 35868-35878.
83. S. I. Gorelsky, D. Lapointe and K. Fagnou, *Journal of Organic Chemistry*, 2012, **77**, 658-668.
84. L. G. Mercier and M. Leclerc, *Accounts of Chemical Research*, 2013, **46**, 1597-1605.
85. W. J. Potscavage, Jr., A. Sharma and B. Kippelen, *Accounts of Chemical Research*, 2009, **42**, 1758-1767.
86. H. Kiess and W. Rehwald, *Solar Energy Materials and Solar Cells*, 1995, **38**, 45-55.
87. A. Mishra and P. Baeuerle, *Angewandte Chemie-International Edition*, 2012, **51**, 2020-2067.
88. Y. Cheng, S. Yang and C. S. Hsu, *Chemical Reviews*, 2009, **109**, 5868-5923.

89. L. J. A. Koster, V. D. Mihailetschi and P. W. M. Blom, *Applied Physics Letters*, 2006, **88**, 093511.
90. J. Bredas, J. Norton, J. Cornil and V. Coropceanu, *Accounts of Chemical Research*, 2009, **42**, 1691-1699.
91. T. Y. Chu, J. Lu, S. Beaupré, Y. Zhang, J. R. Pouliot, S. Wakim, J. Zhou, M. Leclerc, Z. Li, J. Ding and Y. Tao, *Journal of the American Chemical Society*, 2011, **133**, 4250-4253.
92. N. K. Elumalai and A. Uddin, *Energy & Environmental Science*, 2016, **9**, 391-410.
93. M. S. Su, C. Y. Kuo, M. C. Yuan, U. S. Jeng, C. J. Su and K. H. Wei, *Advanced Materials*, 2011, **23**, 3315-3319.
94. M.-C. Yuan, M.-Y. Chiu, S.-P. Liu, C.-M. Chen and K.-H. Wei, *Macromolecules*, 2010, **43**, 6936-6938.
95. X. Guo, R. P. Ortiz, Y. Zheng, M. G. Kim, S. Zhang, Y. Hu, G. Lu, A. Facchetti and T. J. Marks, *Journal of the American Chemical Society*, 2011, **133**, 13685-13697.
96. J. Jo, A. Pron, P. Berrouard, W. L. Leong, J. D. Yuen, J. S. Moon, M. Leclerc and A. J. Heeger, *Advanced Energy Materials*, 2012, **2**, 1397-1403.
97. J. W. Rumer, C. K. L. Hor, I. Meager, C. P. Yau, Z. Huang, C. B. Nielsen, S. E. Watkins, H. Bronstein and I. McCulloch, *Journal of Organic Semiconductors*, 2013, **1**, 30-35.
98. D. Q. Zhu, Q. Q. Zhu, C. T. Gu, D. Ouyang, M. Qiu, X. C. Bao and R. Q. Yang, *Macromolecules*, 2016, **49**, 5788-5795.
99. C. Piliago, T. W. Holcombe, J. D. Douglas, C. H. Woo, P. M. Beaujuge and J. M. J. Fréchet, *Journal of the American Chemical Society*, 2010, **132**, 7595-7597.
100. B. Meng, H. Song, X. Chen, Z. Xie, J. Liu and L. Wang, *Macromolecules*, 2015, **48**, 4357-4363.
101. X. Chen, Z. Zhang, Z. Ding, J. Liu and L. Wang, *Angewandte Chemie-International Edition*, 2016, **55**, 10376-10380.
102. J. Lee, M. Kim, B. Kang, S. B. Jo, H. G. Kim, J. Shin and K. Cho, *Advanced Energy Materials*, 2014, **4**, 1400087.
103. K. Youngkyoo, C. Steffan, M. T. Sachetan, A. C. Stelios, N. Jenny, R. D. James, D. C. B. Donal, G. Mark, M. Iain, H. Chang-Sik and R. Moonhor, *Nature Materials*, 2006, **5**, 197.
104. L. A. Perez, P. Zalar, L. Ying, K. Schmidt, M. F. Toney, T. Q. Nguyen, G. C. Bazan and E. J. Kramer, *Macromolecules*, 2014, **47**, 1403-1410.
105. Z. Bao, A. Dodabalapur and A. Lovinger, *Applied Physics Letters*, 1996, **69**, 4108-4110.
106. M. L. Chabinyc, M. F. Toney, R. J. Kline, I. McCulloch and M. Heeney, *Journal of the American Chemical Society*, 2007, **129**, 3226-3237.

107. R. Mauer, M. Kastler and F. Laquai, *Advanced Functional Materials*, 2010, **20**, 2085-2092.
108. G. Li, V. Shrotriya, Y. Yao, J. S. Huang and Y. Yang, *Journal of Materials Chemistry*, 2007, **17**, 3126-3140.
109. D. Venkataraman, S. Yurt, B. H. Venkatraman and N. Gavvalapalli, *Journal of Physical Chemistry Letters*, 2010, **1**, 947-958.
110. G. Dennler, M. C. Scharber and C. J. Brabec, *Advanced Materials*, 2009, **21**, 1323-1338.
111. H. Zhou, L. Yang and W. You, *Macromolecules*, 2012, **45**, 607-632.
112. R. D. McCullough, *Advanced Materials*, 1998, **10**, 93-116.
113. N. Chandrasekaran, E. Gann, N. Jain, A. Kumar, S. Gopinathan, A. Sadhanala, R. H. Friend, C. R. McNeill and D. Kabra, *ACS Applied Materials & Interfaces*, 2016, **8**, 20243-20250.
114. N. Chandrasekaran, A. C. Y. Liu, A. Kumar, C. R. McNeill and D. Kabra, *Journal of Physics D: Applied Physics*, 2018, **51**, 015501.
115. C. H. Woo, B. C. Thompson, B. J. Kim, M. F. Toney and J. M. J. Fréchet, *Journal of the American Chemical Society*, 2008, **130**, 16324-16329.
116. Y. Tamai, H. Ohkita, H. Benten and S. Ito, *Journal of Physical Chemistry Letters*, 2015, **6**, 3417-3428.
117. D. R. E. Whitten. Kenneth W, Peck. Larry M, Stanley. George G., *Chemistry*, Cengage Learning, Brooks/Cole: USA, 9th edition edn., 2010.
118. B. R. S. Tro. Nivaldo J, Bularzik. Joseph H, Cleaver. William M., *Chemistry: A Molecular Approach*, Pearson Education, London: Prentice Hall, 1st edition edn., 2006.
119. S. A. G. Housecroft. Catherine E, *Inorganic Chemistry*, Pearson Education Harlow: Prentice Hall, 3rd edition edn., 2008.
120. B. C. Thompson and J. M. J. Fréchet, *Angewandte Chemie-International Edition*, 2008, **47**, 58-77.
121. B. Carsten, J. M. Szarko, H. J. Son, W. Wang, L. Y. Lu, F. He, B. S. Rolczynski, S. J. Lou, L. X. Chen and L. P. Yu, *Journal of the American Chemical Society*, 2011, **133**, 20468-20475.
122. T. Xu, L. Y. Lu, T. Y. Zheng, J. M. Szarko, A. Schneider, L. X. Chen and L. P. Yu, *Advanced Functional Materials*, 2014, **24**, 3432-3437.
123. J.-H. Kim, J. B. Park, I. H. Jung, A. C. Grimsdale, S. C. Yoon, H. Yang and D.-H. Hwang, *Energy & Environmental Science*, 2015, **8**, 2352-2356.
124. Y. Zou, A. Najari, P. Berrouard, S. Beaupre, B. R. Aich, Y. Tao and M. Leclerc, *Journal of the American Chemical Society*, 2010, **132**, 5330-5331.
125. Q. T. Zhang and J. M. Tour, *Journal of the American Chemical Society*, 1997, **119**, 5065-5066.

126. M. Pomerantz, *Tetrahedron Letters*, 2003, **44**, 1563-1565.
127. C. B. Nielsen and T. Bjornholm, *Organic Letters*, 2004, **6**, 3381-3384.
128. Y. Zhang, S. K. Hau, H. L. Yip, Y. Sun, O. Acton and A. K. Y. Jen, *Chemistry of Materials*, 2010, **22**, 2696-2698.
129. G. B. Zhang, Y. Y. Fu, Q. Zhang and Z. Y. Xie, *Chemical Communications*, 2010, **46**, 4997-4999.
130. P. Berrouard, A. Najari, A. Pron, D. Gendron, P. O. Morin, J. R. Pouliot, J. Veilleux and M. Leclerc, *Angewandte Chemie-International Edition*, 2012, **51**, 2068-2071.
131. P. Berrouard, S. Dufresne, A. Pron, J. Veilleux and M. Leclerc, *Journal of Organic Chemistry*, 2012, **77**, 8167-8173.
132. M. Pomerantz and A. S. Amarasekara, *Synthetic Metals*, 2003, **135**, 257-258.
133. N. J. Zhou, X. G. Guo, R. P. Ortiz, T. Harschneck, E. F. Manley, S. J. Lou, P. E. Hartnett, X. G. Yu, N. E. Horwitz, P. M. Burrezo, T. J. Aldrich, J. T. L. Navarrete, M. R. Wasielewski, L. X. Chen, R. P. H. Chang, A. Facchetti and T. J. Marks, *Journal of the American Chemical Society*, 2015, **137**, 12565-12579.
134. A. Najari, S. Beaupre, P. Berrouard, Y. P. Zou, J. R. Pouliot, C. Lepage-Perusse and M. Leclerc, *Advanced Functional Materials*, 2011, **21**, 718-728.
135. X. Q. Chen, X. Yao, X. Xiang, L. Liang, W. Shao, F. G. Zhao, Z. Q. Lu, W. W. Wang, J. J. Lic and W. S. Li, *Journal of Materials Chemistry A*, 2016, **4**, 9286-9292.
136. C. Cabanetos, A. El Labban, J. A. Bartelt, J. D. Douglas, W. R. Mateker, J. M. J. Frechet, M. D. McGehee and P. M. Beaujuge, *Journal of the American Chemical Society*, 2013, **135**, 4656-4659.
137. Z. Li, S. W. Tsang, X. M. Du, L. Scoles, G. Robertson, Y. G. Zhang, F. Toll, Y. Tao, J. P. Lu and J. F. Ding, *Advanced Functional Materials*, 2011, **21**, 3331-3336.
138. X. Guo, H. Xin, F. S. Kim, A. D. T. Liyanage, S. A. Jenekhe and M. D. Watson, *Macromolecules*, 2011, **44**, 269-277.
139. C. M. Amb, S. Chen, K. R. Graham, J. Subbiah, C. E. Small, F. So and J. R. Reynolds, *Journal of the American Chemical Society*, 2011, **133**, 10062-10065.
140. C. E. Small, S. Chen, J. Subbiah, C. M. Amb, S. W. Tsang, T. H. Lai, J. R. Reynolds and F. So, *Nature Photonics*, 2012, **6**, 115-120.
141. C. K. Lo, B. R. Gautam, P. Selter, Z. L. Zheng, S. D. Oosterhout, I. Constantinou, R. Knitsch, R. M. W. Wolfe, X. P. Yi, J. L. Bredas, F. So, M. F. Toney, V. Coropceanu, M. R. Hansen, K. Gundogdu and J. R. Reynolds, *Chemistry of Materials*, 2018, **30**, 2995-3009.
142. L. S. Liao, M. K. Fung, C. S. Lee, S. T. Lee, M. Inbasekaran, E. P. Woo and W. W. Wu, *Applied Physics Letters*, 2000, **76**, 3582-3584.

143. U. Scherf and E. J. W. List, *Advanced Materials*, 2002, **14**, 477-487.
144. S. L. C. Hsu, Y. C. Lin, R. F. Lee, C. Sivakumar, J. S. Chen and W. Y. Chou, *Journal of Polymer Science Part A: Polymer Chemistry*, 2009, **47**, 5336-5343.
145. J. H. Huang, C. Y. Yang, Z. Y. Ho, D. Kekuda, M. C. Wu, F. C. Chien, P. L. Chen, C. W. Chu and K. C. Ho, *Organic Electronics*, 2009, **10**, 27-33.
146. A. A. B. Alghamdi, D. C. Watters, H. N. Yi, S. Al-Faifi, M. S. Almeataq, D. Coles, J. Kingsley, D. G. Lidzey and A. Iraqi, *Journal of Materials Chemistry A*, 2013, **1**, 5165-5171.
147. W. W. Li, R. P. Qin, Y. Zhou, M. Andersson, F. H. Li, C. Zhang, B. S. Li, Z. P. Liu, Z. S. Bo and F. L. Zhang, *Polymer*, 2010, **51**, 3031-3038.
148. E. J. Zhou, J. Z. Cong, K. Tajima, C. H. Yang and K. Hashimoto, *Journal of Physical Chemistry C*, 2012, **116**, 2608-2614.
149. S. P. Wen, W. D. Cheng, P. F. Li, S. Y. Yao, B. Xu, H. Li, Y. J. Gao, Z. L. Wang and W. J. Tian, *Journal of Polymer Science Part A: Polymer Chemistry*, 2012, **50**, 3758-3766.
150. S. Varghese and S. Das, *Journal of Physical Chemistry Letters*, 2011, **2**, 863-873.

>>

**CHAPTER II**  
**EFFECTS OF REGIOREGULARITY**  
**OF THIENYL-TPD POLYMERS**  
**ON THE OPTICAL AND**  
**ELECTRONIC PROPERTIES**

## 2.1 Introduction

Development of new organic semiconductors has focused on the design and synthesis of low band gap polymers for organic photovoltaic devices.<sup>1-3</sup> Consequently, several common strategies have been developed and determined to be very effective on the polymers' properties. These strategies include (i) introducing a structure containing the 'push-pull' or 'donor-acceptor' (D-A) design concept into the polymer backbone in which the band gap is effectively reduced by simultaneously lowering the donor's HOMO and raising the acceptor's LUMO<sup>4</sup>; (ii) synthesizing a planar-fused ring in order to stabilize the quinoid conformation<sup>5</sup> and increase the electron delocalization and interchain interaction, leading to a significant enhancement of charge mobility<sup>6, 7</sup>; and (iii) incorporating conjugated side chains on the backbone that can significantly influence not only the polymer solubility and stability<sup>3</sup>, but also the molecular packing and charge transport characteristics.<sup>5</sup>

Importantly, one of the most essential photophysical processes in an organic bulk heterojunction photovoltaic device's blend system is the exciton dissociation at the donor/acceptor interface generating free charge carriers.<sup>8</sup> However, this phenomenon is very inefficient due to low dielectric constant of organic semiconductor materials producing a strong coulomb attraction between an electron and a hole pair.<sup>9</sup> In light of this, several experimental and theoretical studies demonstrated that there is a linear correlation between the change in ground ( $\mu_g$ ) and excited states ( $\mu_e$ ) dipole moment of repeating units of conjugated polymer and PCE that could develop into efficient charge separation.<sup>10-12</sup>

Yu et al<sup>10</sup> investigated the effect of the net dipole moment on photovoltaic performance for PTB series of polymers based on thieno[3,4-*b*] thiophene (TT) as acceptor and benzodithiophene (BDT) as donor and deduced the possible rationalization of strong correlation between dipole change and PCE. However, a further study based on 3-oxothieno[3,4-*d*]isothiazole-1,1-dioxide (TID) and thieno [3,4-*c*]pyrrole-4,6-dione (TPD) as acceptor moieties found that further increasing the dipole moment ( $\mu_{ge}$ ) value tends to lower PCE. As a

result, optimizing the dipole moment ( $\mu_{ge}$ ) values of conjugated polymers is required to reach high PCE values.<sup>13</sup>

Further, efficient charge transport through the active layer must be taken into consideration to help charges travel easily from one molecule to another and not to become trapped or scattered.<sup>14</sup> Therefore, controlling both the molecular conformations and microstructure of the solid is vital in order to yield a desired set of properties for optoelectronic function.<sup>15, 16</sup> In light of this concept, numerous systematic studies have been conducted to evaluate the effect regio-regularity has on the polymer's properties. The most popular study in this case is poly (3-alkylthiophene) (P3AT), which has three possible configurations, head-to-tail (**H-T**), head-to-head (**H-H**) or tail-to-tail (**T-T**). Of these configurations, pure **H-T** coupling, which has smaller steric interactions between nearby substituents resulting in high level of polymer crystallinity, provides a strong influence on photovoltaic performance. This influence can be ascribed to strong interchain aggregation and high charge carrier motility.<sup>17, 18</sup>

On the contrary, P3AT with low regio-regularity shows a significant number of defect configurations, including a mixture of three connections tending to bring about the amorphous state.<sup>19</sup> Conversely, poly(4,4'-dialkyl-2,2'-bithiophenes) and poly(3,3'-dialkyl-2,2'-bithiophenes) show remarkable structural features compared to the more classical P3AT, although they have the same stoichiometry. These two P3AT provide high level of chain regularity as compared to P3AT and no coupling defects have been spectroscopically observed. However, the closeness of neighbouring alkyl chains, with respect to poly(3,3'-dialkyl-2,2'-bithiophenes), leads to lower delocalization along polymer backbone due to the torsional bond of thiophenes that arises from undesirable steric interaction between the alkyl chains.<sup>20, 21</sup>

In our research, we primarily focused on alternative candidates of thieno[3,4-*b*] thiophene with thieno[3,4-*c*]pyrrole-4,6-dione (TPD) unit due to its symmetry, compact planar structure<sup>22</sup> and smaller resonance energy which should, in principle, reduce its steric interaction and bond length alternation.<sup>23</sup>



TPD containing D-A copolymers have a relatively low HOMO and LUMO gap when incorporated into various donor components due to their excellent electron withdrawing nature.<sup>22, 24-26</sup> This feature makes the system prone to enhancing intra-molecular charge transfer along the polymer backbone and inter-molecular charge transfer between coplanar polymer chains.<sup>23, 27, 28</sup> Such properties make TPD more attractive in the OPV research community. To this end, we prepared TPD-based alternating copolymers containing thiophene and bithiophene electron donating units in a fashion similar to those of P3HTs via direct arylation polymerization named as follows **[RIR] PT<sub>OP</sub>-TPD<sub>BP</sub>**, **[RIR] PT<sub>OP</sub>-TPD<sub>O</sub>**, **[RR] PT<sub>OP</sub>-TPD<sub>O</sub>**, **[T-T] PT<sub>2OP</sub>-TPD<sub>O</sub>**, and **[H-H] PT<sub>2OP</sub>-TPD<sub>O</sub>** (See **Figure 2.1**). In these copolymers, the phenyl ring is introduced onto the polythiophene backbone, which leads to extending the conjugation length and activating the thiophene ring in a manner more efficient than an alkyl side chain to produce high molecular weight polymers.<sup>29, 30</sup>

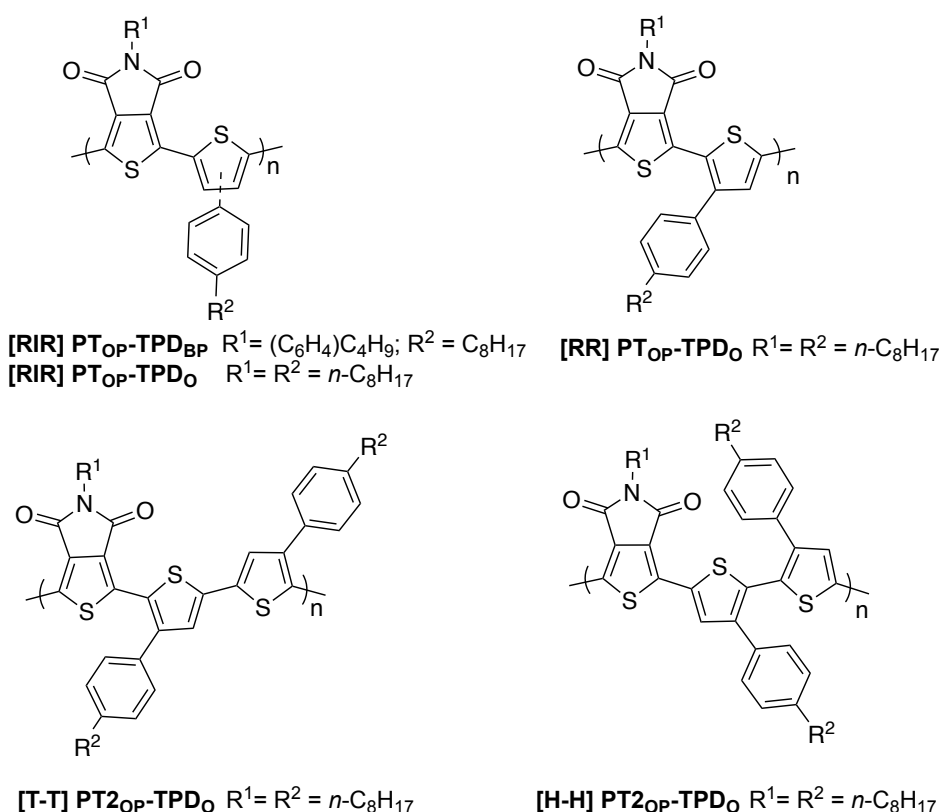


**Figure 2.1.** Polymer structure of **[RIR] PT<sub>OP</sub>-TPD<sub>BP</sub>**, **[RIR] PT<sub>OP</sub>-TPD<sub>O</sub>**, **[RR] PT<sub>OP</sub>-TPD<sub>O</sub>**, **[T-T] PT<sub>2OP</sub>-TPD<sub>O</sub>**, and **[H-H] PT<sub>2OP</sub>-TPD<sub>O</sub>**.

It could be argued that both regioregular [RR] PT<sub>OP</sub>-TPD<sub>O</sub> and regio-irregular [RIR] PT<sub>OP</sub>-TPD<sub>O</sub> might have a similar orientation and alignment of their dipole moment stimulated effectively by the introduction of the bulky group (phenyl ring) and by attractive (thienyl) S---O (carbonyl) interactions as shown in **Figure 2.2**. This interaction should, in theory, decrease the exciton binding energy and promote exciton dissociation resulting in better OPV performance. The properties of this series of polymers together with studies of their electronic and optical properties are outlined below.

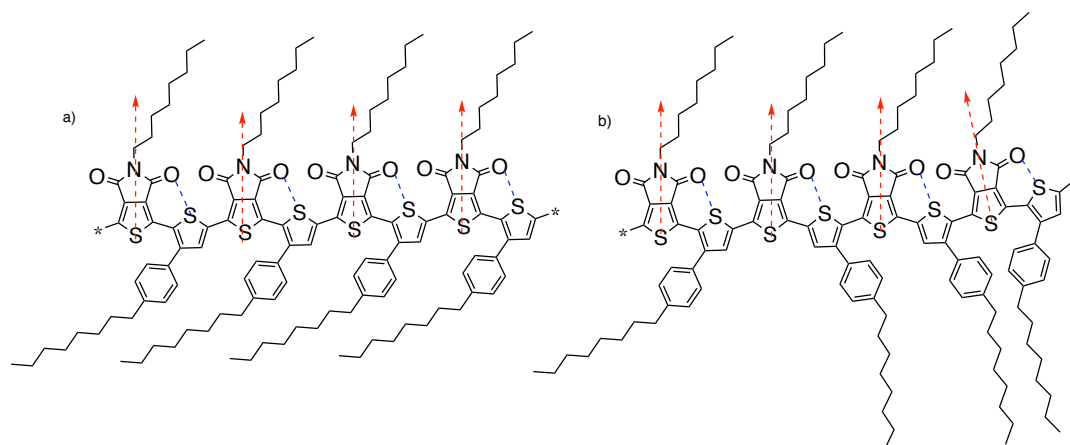
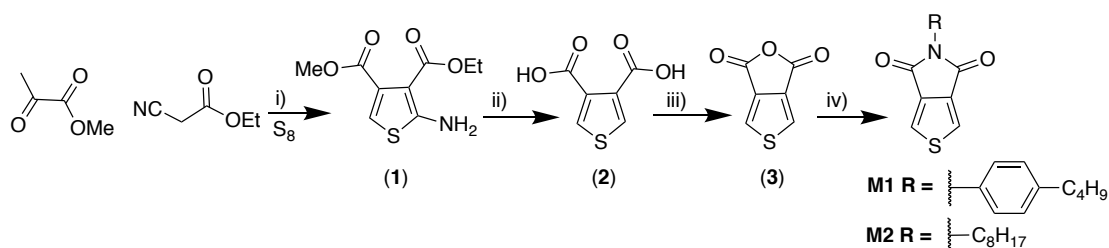


**Figure 2.2.** Assumed dipole moment vector of a) [RR] PT<sub>OP</sub>-TPD<sub>O</sub>; b) [RIR] PT<sub>OP</sub>-TPD<sub>O</sub>.

## 2.2 Results and Discussions

### 2.2.1 Monomer synthesis

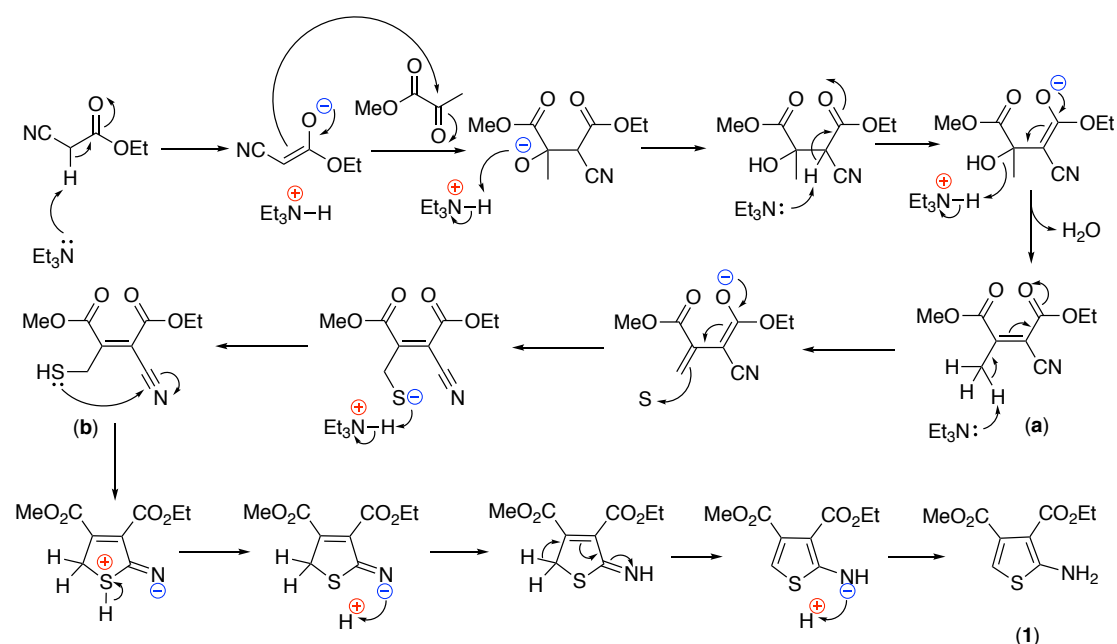
The TPD units (**M1** and **M2**) were prepared following a procedure reported in the literature<sup>24, 31</sup> as shown in **Scheme 2.1**.



**Scheme 2.1.** i) DMF, Et<sub>3</sub>N, 50 °C; ii)(a) THF, *t*-BuONO, 90 °C;(b) 2M NaOH, 95 °C; iii) Ac<sub>2</sub>O, 110 °C; iv)(a) THF, R-NH<sub>2</sub>, 55 °C;(b) SOCl<sub>2</sub>, 55 °C.

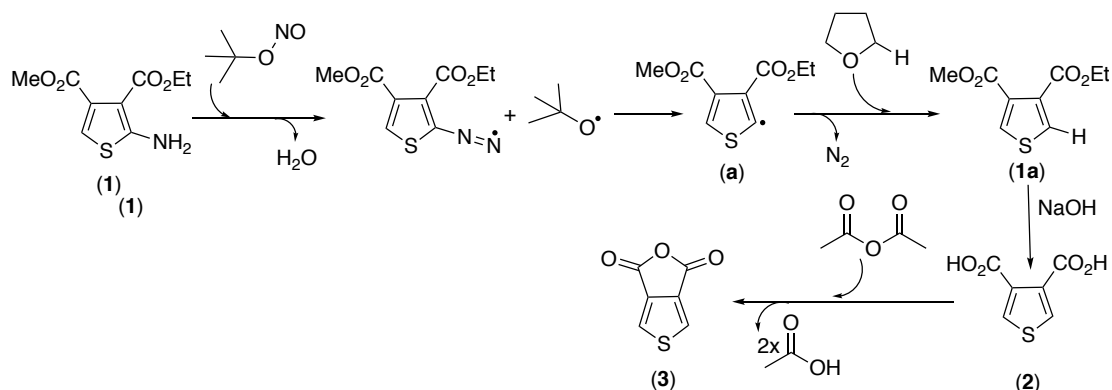
The reaction to form intermediate (**1**) is through the condensation of an active methylene unit (ethyl cyanoacetate) with a carbonyl compound (methyl pyruvate) using a strong base (trimethylamine) to facilitate deprotonation to

$\alpha,\beta$ -unsaturated nitrile, followed by a dehydration reaction to form the stable intermediate **(a)**. This reaction sequence is thus called Knoevenagel–Cope condensation. The subsequent addition of a sulphur element mechanism is not yet completely understood, but it is thought that the final ring closure process occurs via an intermolecular nucleophilic attack of a sulphur anion on the proton of the conjugated acid yielding the reactive ylidene-sulfur intermediate which re-attacks on the cyano group **(b)**, leading to the formation of the desired product **(1)** <sup>32,33</sup> (see **Scheme 2.2**).



**Scheme 2.2.** The chemical mechanism of formation of 3-ethyl-4-methyl-2-amino thiophene-3,4-dicarboxylate.

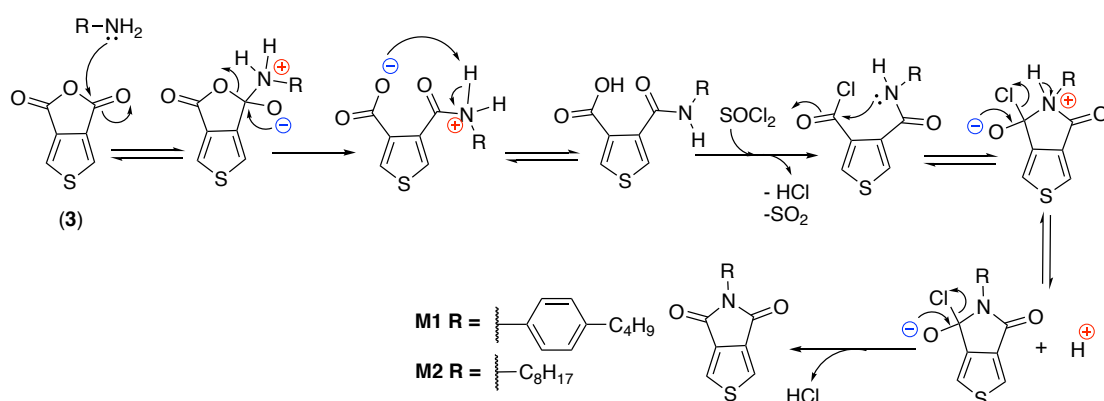
The next intermediate involved two treatment steps. The first step included the modification of the Sandmeyer protocol using *t*-BuONO to deaminate the aromatic amino group of compound **(1)** and produce two electrically uncharged radicals, followed by releasing nitrogen gas. As the free aryl radical formed **(a)**, the hydrogen of the polar organic solvent, with THF as the hydrogen donor, can be then abstracted to re-bond with **(a)**, forming the compound **(1a)**. The next step, then, was to hydrolyse the esters into carboxylic acid in the presence of a diluted base, followed by an aqueous acid workup to afford **(2)**. Following this, compound **(2)** condensed using acetic anhydride, which serves as a dehydrating reagent, to initiate intramolecular ring closure and acetic acid to form compound **(3)** as shown in **Scheme 2.3**.



**Scheme 2.3.** The brief chemical mechanism of 3,4-thiophene dicarboxylic anhydride.

The last step involving the preparation of TPD acceptor monomers (**M1** and **M2**) uses a primary amine, 4-butylaniline or *n*-octylamine, and thionyl chloride to convert the anhydride group, compound (**3**), into imides to promote their solubility and accepting functionality.

In this reaction, the nucleophilic electron pair, on the primary amine molecule, attacks the acetic anhydride's carbonyl. The  $\text{SOCl}_2$  is then free to attack the carboxylic acid and convert it into an acid chloride to expel the good leaving group ( $\text{Cl}^-$ ) and re-react with amine to produce the imide **M1** and **M2** as shown in **Scheme 2.4**.



**Scheme 2.4.** The chemical mechanism of **M1** and **M2**.

The chemical structure of these two monomers (**M1** and **M2**) was proven via NMR as shown in **Figure 2.3** and **2.4**, as a single peak at a range of 7.97-7.82 ppm corresponded to the proton attached to TPD in both monomers.

Further, a peak at 7.30 ppm with multiplet pattern reflected the hydrogens attached to the phenyl ring at the second and third positions. The upfield peaks resonate below 3.70 ppm in general belong to the protons placed on the alkyl chains.

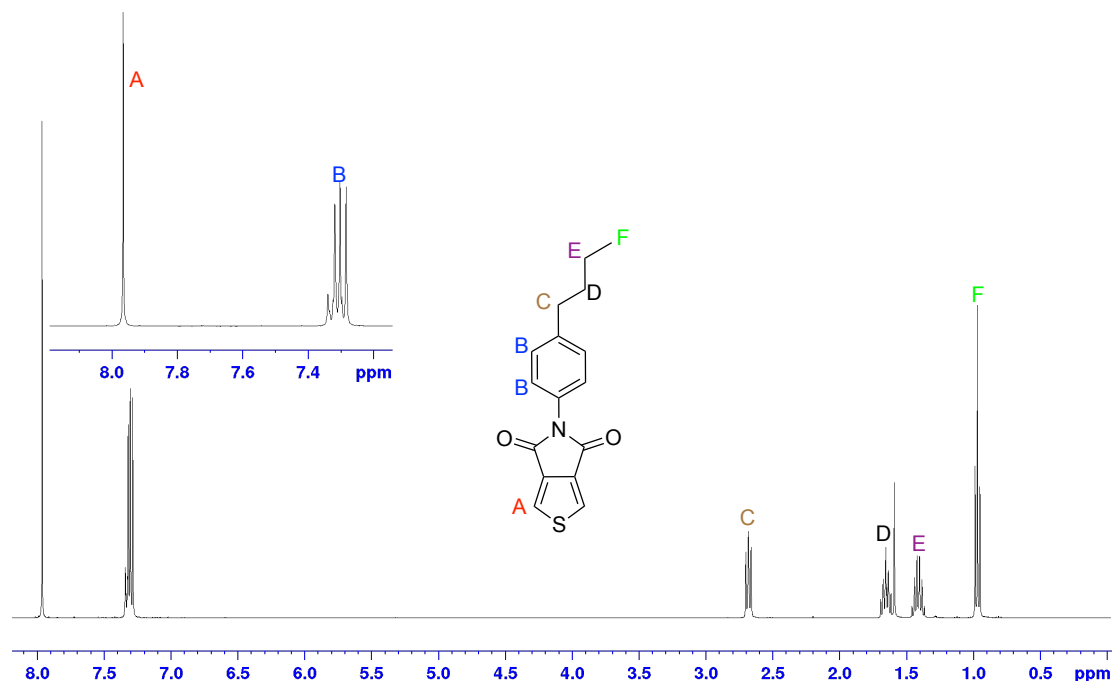


**Figure 2.3.**  $^1\text{H}$  NMR spectrum of **M1** in  $\text{CDCl}_3$ .

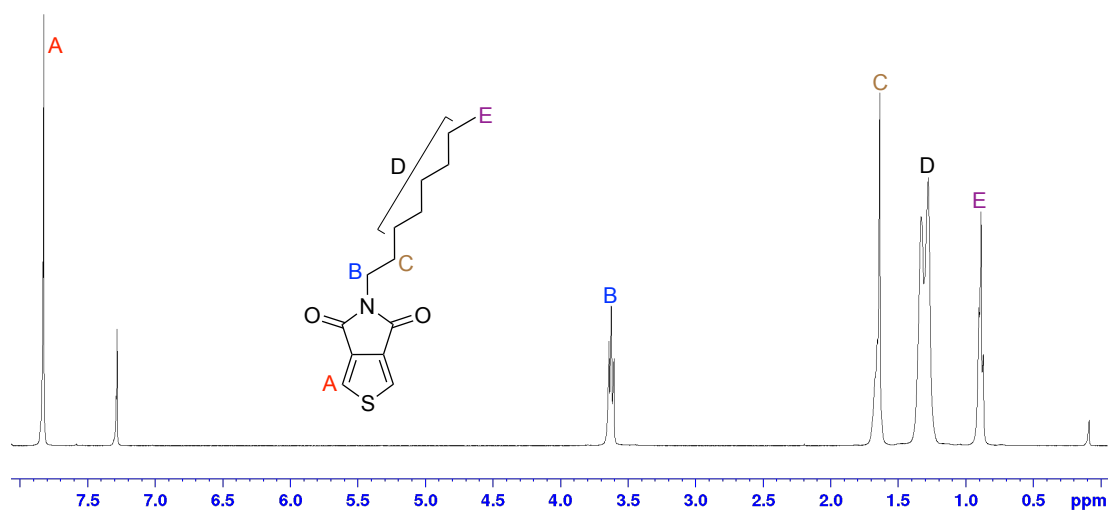
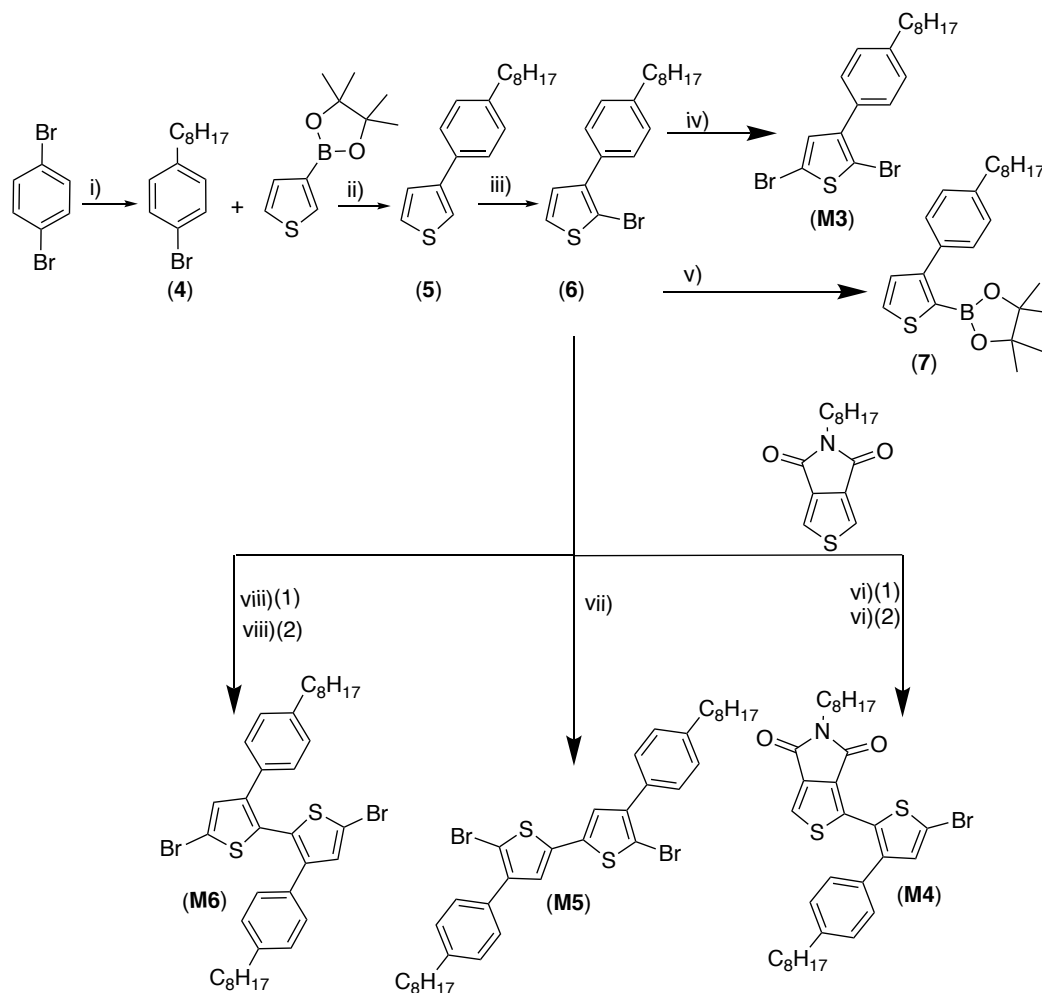


**Figure 2.4.**  $^1\text{H}$  NMR spectrum of **M2** in  $\text{CDCl}_3$ .

The synthetic methods for the preparation of 2,5-dibromo-3-(4-octylphenyl)thiophene (**M3**), 1-(5-bromo-3-(4-octylphenyl)thiophen-2-yl)-5-

octyl- 4H-thieno[3,4-c]pyrrole-4,6(5H)-dione (**M4**), 5,5'-dibromo- 4,4'-bis(4-octylphenyl)-2,2'- bithiophenes (**M5**), 5,5'-dibromo- 3,3'-bis(4-octylphenyl)-2,2'- bithiophenes (**M6**) are illustrated below in **Scheme 2.5**. The experimental procedures are described in more sufficient details in Methods section.



**Scheme 2.5.** i)(a) THF, *n*-BuLi, Br-C<sub>8</sub>H<sub>17</sub>; ii)(a) THF, NaHCO<sub>3</sub>Pd(OAc)<sub>2</sub>, P(*o*-tol)<sub>3</sub>; iii) CHCl<sub>3</sub>/AcOH, NBS; iv) same to (iii), 60°C; v) Et<sub>2</sub>O, *n*-BuLi, <sup>i</sup>PrOB(pin); vi)(1) THF, PdCl<sub>2</sub>(MeCN)<sub>2</sub>, P(*o*-anisyl)<sub>3</sub>, Cs<sub>2</sub>CO<sub>3</sub>, PivOH; (2) same to (iii); vii) DMSO, AgNO<sub>3</sub>, KF, PdCl<sub>2</sub>(benzonitrile)<sub>2</sub>; viii)(1) Toluene, compound (7), K<sub>2</sub>CO<sub>3</sub>, Aliquat 336, Pd(PPh<sub>3</sub>)<sub>4</sub>; (2) same to (iv).

Compound (**4**) is formed using a well-known mechanism called bromine-lithium exchange, in which a bromine atom is replaced by a lithium atom as a reactive intermediate. Then, phenyl anion attacks 1-bromooctane to form a C-C bond and releases LiBr. Then, this product was reacted with 3-(4,4,5,5-tetramethyl)-1,3,2-dioxaborolan-2-yl)thiophene to form compound (**5**) through Suzuki-Miyaura reaction (Chapter I, **Figure 1.20**).

Intermediate (**5**) was then treated with the electrophilic reagent N-Bromosuccinimide (NBS) in a 1:1 ratio in glacial acetic acid and chloroform, in order to convert thiophene into (**6**) and (**M3**), with 1 and 2 equivalents of the bromine source in high yield.

The purity of (**M3**) was proven by  $^1\text{H}$  NMR spectra as shown in **Figure 2.5**. Two peaks at 7.25 and 7.43 ppm corresponded to the phenyl ring protons with doublet splitting patterns for each, while the thiophene ring proton appears as a single peak at 7.03. The latter split indicated that the bromine atom allocated at 2, 5-C of thiophene. The chemical shifts of protons bounded to aliphatic chain are recorded below 2.70 ppm.

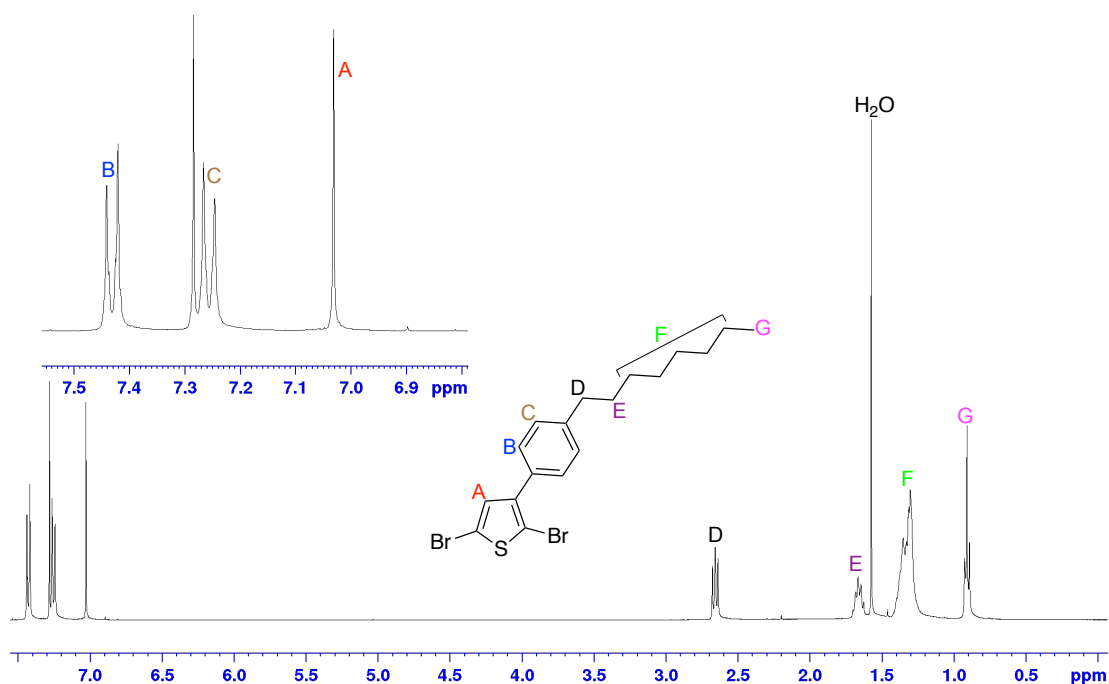


**Figure 2.5.**  $^1\text{H}$  NMR spectrum of **M3** in  $\text{CDCl}_3$ .

The preparation of the next monomer started from monobrominated thiophene (**6**), which was first coupled with TPD (**M2**) acceptor by direct arylation reaction, generating a dimer-monomer (Thiophene-TPD) using a palladium/phosphine catalytic system, caesium carbonate as base, and pivalic acid as carboxylate source.<sup>34</sup> The general mechanism of this type of coupling has been described in chapter I, **Figure 1.21**.

This dimer product (Thiophene-TPD) was then brominated following the same procedure used for compound (**M3**) to afford, at the end, 1-(5-bromo-3-(4-octylphenyl)thiophen-2-yl)-5-octyl-4H-thieno[3,4-c]pyrrole-4,6(5H)-dione (**M4**). The structure of this brominated dimer (**M4**) was confirmed by  $^1\text{H}$  NMR as shown in **Figure 2.6**, as single peaks at 7.54 and 7.07 ppm corresponded to the proton attached to TPD acceptor and thiophene donor, respectively. Also, a peak at a range of 7.26-7.18 ppm with multiplet pattern mirrored the hydrogen bounded to the phenyl ring at the second and third positions. The more shielded protons that resonate below 3.70 ppm belong to the alkyl chains on both units.

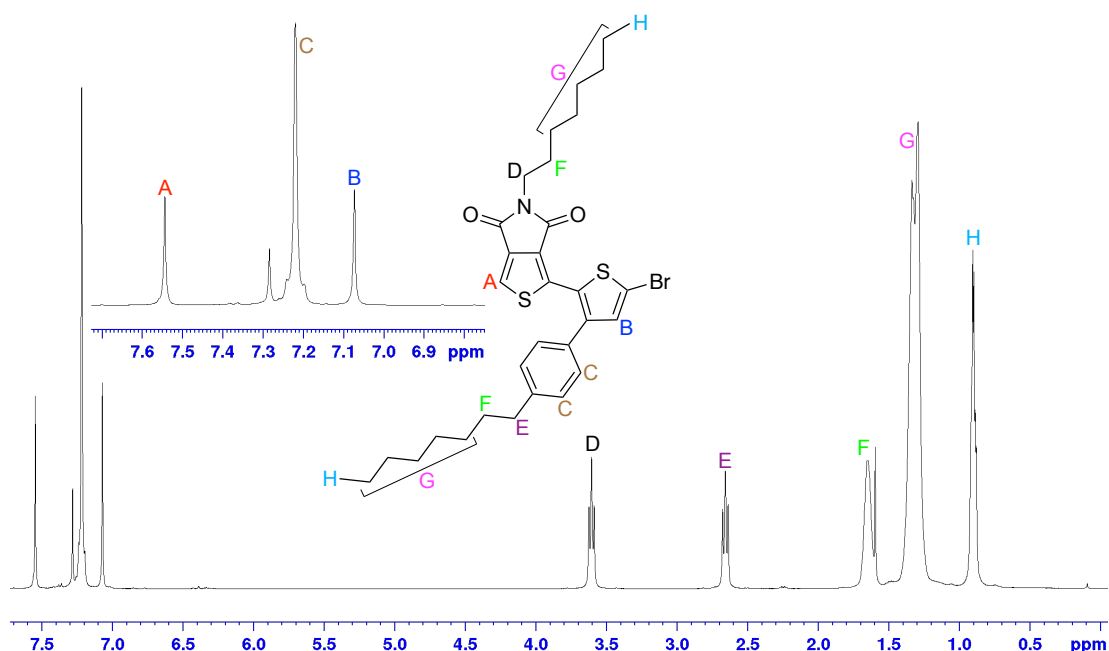
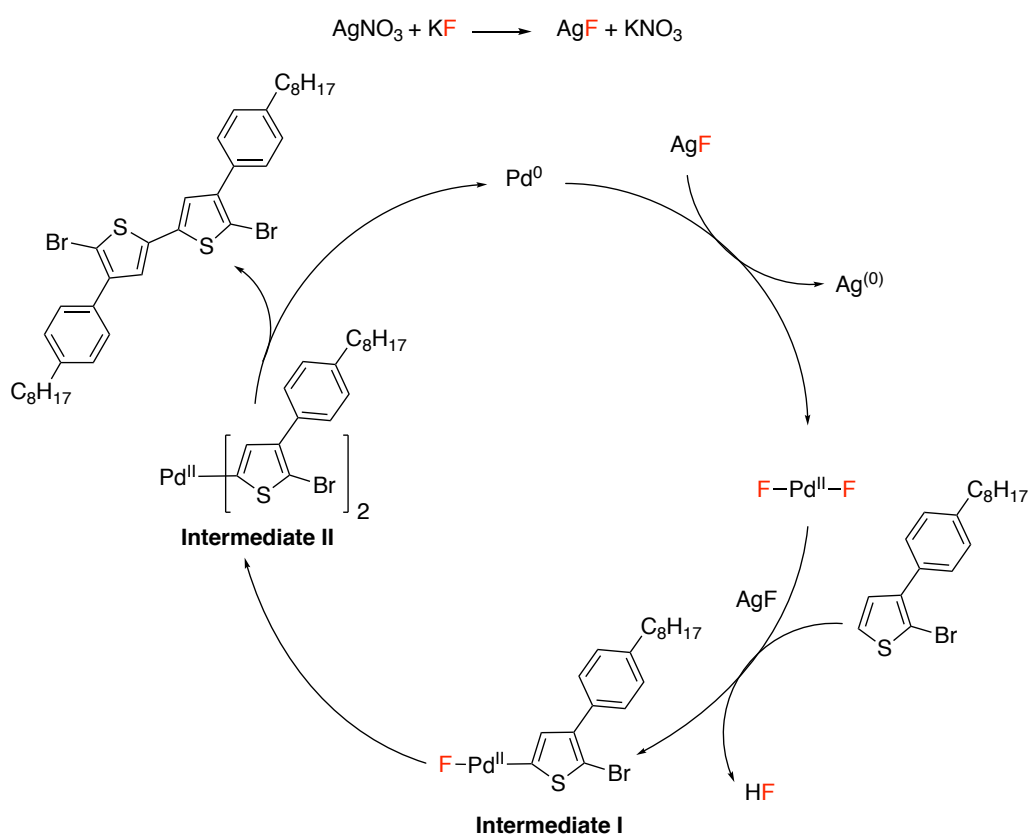


**Figure 2.6.**  $^1\text{H}$  NMR spectrum of **M4** in  $\text{CDCl}_3$ .

The next monomer, 5,5'-dibromo-4,4'-bis(4-octylphenyl)-2,2'-bithiophene (**M5**), was prepared through homocoupling of 2-bromo-3-(4-octylphenyl)thiophene (**6**) (**Scheme 2.5**) through C-H bond activation at alpha position whereas the carbon-bromine bond remains intact. This reaction took place in the presence of a palladium (II) catalyst and a combination of silver (I) nitrate and potassium fluoride system as an activator to produce the desired coupling product (**M5**) in a yield of 28%. This poor yield could be caused by small portions of the silver (I) nitrate and potassium fluoride mixture, which, in



turn, form AgF reagent in situ, as this reagent might degrade by light or heat during the reaction.<sup>36</sup> The mechanism of this reaction proceeds as shown in **Scheme 2.6**, as first Pd (0) interacts with an oxidizing agent (AgF) to generate Pd(II)F<sub>2</sub>. Subsequently, electrophilic metallation with thiophene and a promoter AgF forms **intermediate I**. This process proceeds twice to form **intermediate II**, followed by a reductive elimination, which, in turn, releases the homocoupling product from palladium.<sup>37-39</sup>



**Scheme 2.6.** Illustration of dehydrogenative homocoupling mechanism for **M5**.

This Tail-to-Tail thiophene monomer (**M5**) was successfully prepared and proven by <sup>1</sup>H NMR as shown in **Figure 2.7**. Two peaks at 7.28 and 7.50 ppm represented about four protons each assigned to the phenyl ring whereas the two protons that are bound on thiophene backbone peaked at 7.07 ppm.

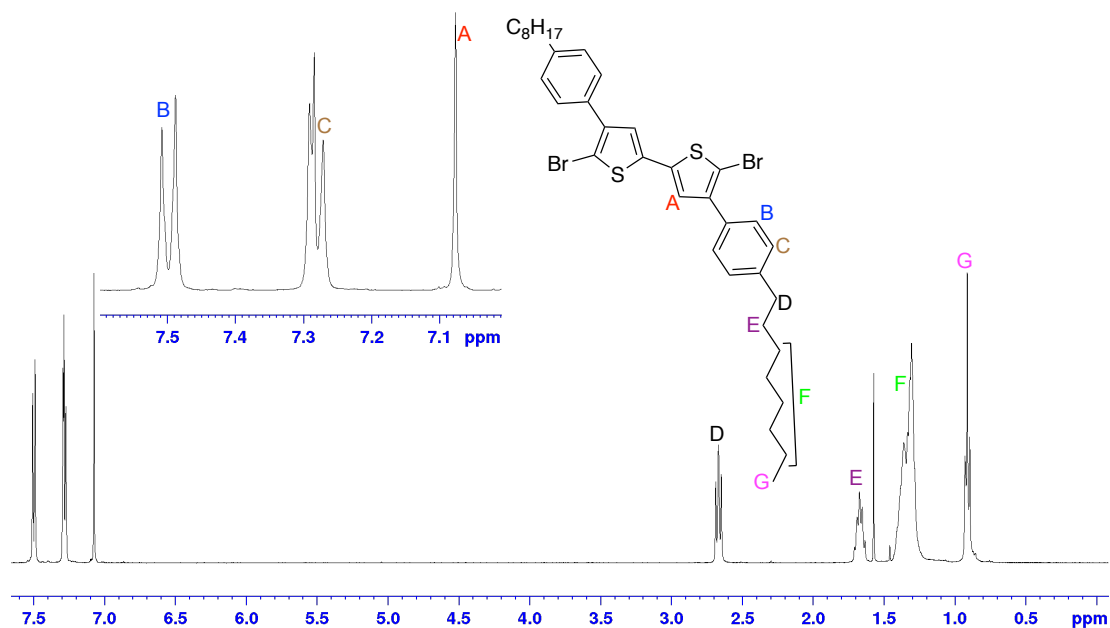


**Figure 2.7.**  $^1\text{H}$  NMR spectrum of **M5** in  $\text{CDCl}_3$ .

The preparation of the head-to-head monomer, 5,5'-dibromo- 3,3'-bis(4-octylphenyl)-2,2'- bithiophene (**M6**), has been accomplished using the Suzuki-Miyaura cross-coupling reaction of 4,4,5,5-tetramethyl-2-(3-(4-octylphenyl)thiophene-2-yl)-1,3,2 dioxaborolane (**7**) and 2-bromo-3-(4-octylphenyl)thiophene (**6**). This type of reaction follows similar mechanism that has been explained for the compound (**5**). The corresponding **Head-to-Head** dimerization product was then brominated to yield the desired dimer (**M6**). This dimer product was confirmed by  $^1\text{H}$  NMR, as described in **Figure 2.8**. This figure indicated that phenyl protons are more shielded than the ones in thiophene as compared to (**M5**) due to an electronegative atom (bromine) on thiophene backbone that is significantly removed from the valence electron density on carbon atoms in phenyl ring. This phenomenon is also applied to those protons bound in alkyl chains resonating at low frequency.

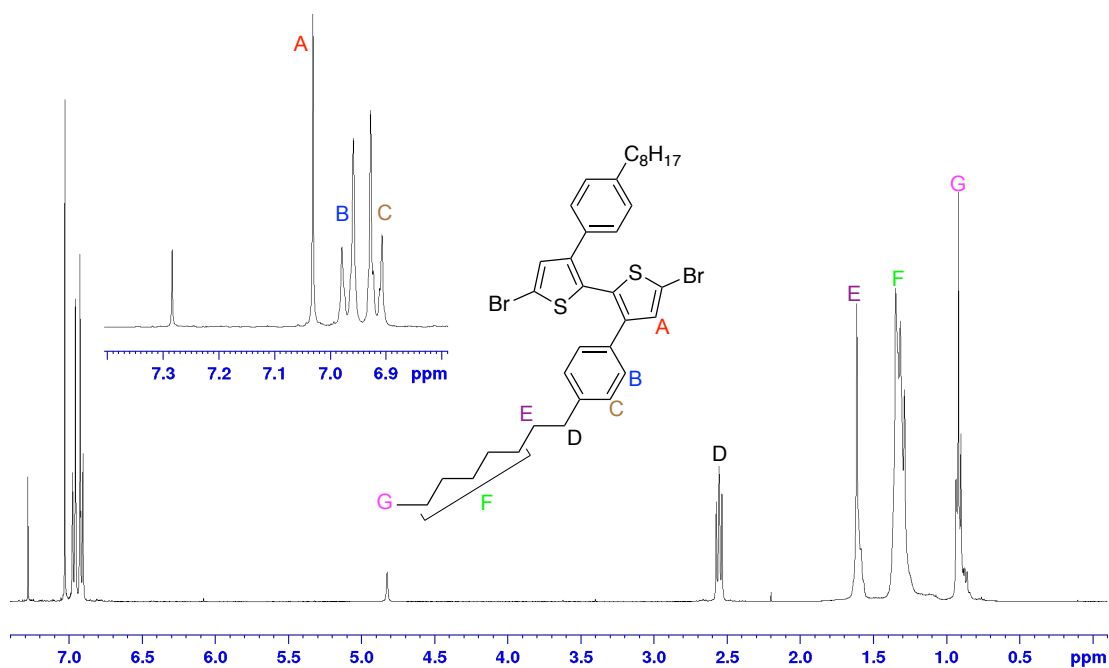


**Figure 2.8.**  $^1\text{H}$  NMR spectrum of **M6** in  $\text{CDCl}_3$ .

## 2.2.2 Polymers synthesis and characterisation

**Figure 2.1** describes the molecular structure of the donor-acceptor conjugated polymers. Five alternating copolymers were synthesized by the direct arylation polymerization to control molecular weights and minimize reaction time. The preparation conditions followed a similar procedure detailed previously in literature.<sup>40</sup> The polymerization was stopped after the polymer precipitated from the solution. All polymers were poured into methanol with vigorous stirring and purified *via* Soxhlet extraction using methanol, acetone, hexane, toluene, and chloroform in succession. The polymerization procedures are described in more details in the experimental section. The chemical structure of the synthesized copolymers was confirmed by  $^1\text{H}$  NMR and elemental analysis. In the  $^1\text{H}$  NMR spectrum of **[RIR] PT<sub>OP</sub>-TPD<sub>BP</sub>** and **[RIR] PT<sub>OP</sub>-TPD<sub>O</sub>** (Chapter VII, Figure S1 and S2), the characteristic peaks at 7.13-7.12 ppm are assigned to the hydrogen atom in the thiophene ring. The peak due to proton in  $-\text{CH}_2-$  linked to benzene ring is at 2.66 ppm. However, the proton chemical shift of the hydrogen atoms in the thiophene rings of **[RR] PT<sub>OP</sub>-TPD<sub>O</sub>**, **[T-T] PT<sub>2OP</sub>-TPD<sub>O</sub>** and **[H-H] PT<sub>2OP</sub>-TPD<sub>O</sub>** is downfield with respect to peaks resonated between 7.24-8.01 ppm, (see chapter VII, Figure S3, S4 and S5). The peak at 3.70-3.64 corresponded

to  $-\text{CH}_2-$  linked to the N atom. The peaks at 2.71-0.88 ppm assigned to the protons of the alkyl chains of all copolymers. The number-average molecular weight ( $M_n$ ) and polydispersity index (PDI) were estimated by gel permeation chromatography (GPC) based on polystyrene standards and the results are summarized in **Table 2.1-a**. The degree of polymerization was strongly affected with **[RIR] PT<sub>OP</sub>-TPD<sub>BP</sub>** resulting in a lower  $M_n$  (4.4 kDa) as compared to **[RIR] PT<sub>OP</sub>-TPD<sub>O</sub>** (19.8 kDa). It has been observed that long polymerization processes switch the polymer from a red to an orange colour. This behaviour may be attributed to poor stability of the phenyl group on TPD moiety at the high temperature during polymerizations, forcing the polymerization process to stop prior to precipitation, which, in turn, limited the ability to create long polymer chains. High regio-regular **[RR] PT<sub>OP</sub>-TPD<sub>O</sub>** is also reported and expected to have low  $M_n$  (2.7 kDa) due to the fact that increasing the degree of crystallinity reduces the solubility, thus decreasing the molecular weight of polymer. To obtain regio-regular polymer with high molecular weight, the introduction of another substituted thiophene unit in the backbone is required. Consequently, **[T-T] PT<sub>2OP</sub>-TPD<sub>O</sub>** and **[H-H] PT<sub>2OP</sub>-TPD<sub>O</sub>** exhibited higher  $M_n$  of 31.6 kDa and 10.5 kDa, with a PDI of 4.10 and 1.91, respectively.

**Table 2.1.** (a) Molecular, optical, and (b) electrochemical data for **[RIR] PT<sub>OP</sub>-TPD<sub>BP</sub>**, **[RIR] PT<sub>OP</sub>-TPD<sub>O</sub>**, **[RR] PT<sub>OP</sub>-TPD<sub>O</sub>**, **[T-T] PT<sub>2OP</sub>-TPD<sub>O</sub>**, and **[H-H] PT<sub>2OP</sub>-TPD<sub>O</sub>**.

(a)

| Polymer   | Molecular data <sup>c</sup> |       |      | Optical data                |         |                                  |
|---|-----------------------------|-------|------|-----------------------------|---------|----------------------------------|
|   | (kDa)                       |       |      | $\lambda_{\text{max}}$ (nm) |         | (eV)                             |
|   | $M_n$                       | $M_w$ | PDI  | Solution                    | Film    | $E_g^d$                          |
| <b>[RIR] PT<sub>OP</sub>-TPD<sub>BP</sub><sup>a</sup></b> | 4.4                         | 11.7  | 2.65 | 482                         | 531     | 1.83 ( $\pm 0.01$ ) <sup>g</sup> |
| <b>[RIR] PT<sub>OP</sub>-TPD<sub>O</sub><sup>a</sup></b>  | 19.8                        | 48.0  | 2.42 | 518                         | 551     | 1.87 ( $\pm 0.11$ ) <sup>g</sup> |
| <b>[RR] PT<sub>OP</sub>-TPD<sub>O</sub><sup>a</sup></b>   | 2.7                         | 3.6   | 1.32 | 525/629                     | 543/683 | 1.80 ( $\pm 0.01$ ) <sup>g</sup> |
| <b>[T-T] PT<sub>2OP</sub>-TPD<sub>O</sub><sup>b</sup></b> | 31.6                        | 129.0 | 4.10 | 502                         | 512     | 2.02 ( $\pm 0.02$ ) <sup>g</sup> |
| <b>[H-H] PT<sub>2OP</sub>-TPD<sub>O</sub><sup>b</sup></b> | 10.5                        | 20.0  | 1.91 | 459                         | 474     | 2.07 ( $\pm 0.01$ ) <sup>g</sup> |

(b)

| Polymer   | Electrochemical data |                   |                             |
|---|----------------------|-------------------|-----------------------------|
|   | (eV)                 |                   |                             |
|   | HOMO <sup>e</sup>    | LUMO <sup>e</sup> | E <sub>g</sub> <sup>f</sup> |
| <b>[RIR] PT<sub>OP</sub>-TPD<sub>BP</sub><sup>a</sup></b> | -5.36                | -3.36             | 2.00                        |
| <b>[RIR] PT<sub>OP</sub>-TPD<sub>O</sub><sup>a</sup></b>  | -5.53                | -3.32             | 2.21                        |
| <b>[RR] PT<sub>OP</sub>-TPD<sub>O</sub><sup>a</sup></b>   | -5.38                | -3.57             | 1.81                        |
| <b>[T-T] PT<sub>2OP</sub>-TPD<sub>O</sub><sup>b</sup></b> | -5.62                | -3.60             | 2.02                        |
| <b>[H-H] PT<sub>2OP</sub>-TPD<sub>O</sub><sup>b</sup></b> | -5.61                | -3.58             | 2.03                        |

<sup>a</sup>Collected in chloroform. <sup>b</sup>Collected in toluene. <sup>c</sup>GPC measurements in chloroform eluent. <sup>d</sup>Optical band gap estimated from the film onset. <sup>e</sup>HOMO/LUMO levels calculated from oxidation /reduction onset. <sup>f</sup>Electrochemical band gap. <sup>g</sup>Range error at the peak of the absorbance curve of a different extinction coefficient.

### 2.2.3 Polymers Optical Properties

The absorption spectra of the TPD-based copolymers were studied by UV-vis spectroscopy on both diluted solutions and on films and are shown in **Figure 2.9**. An overview of this study finding is given in the **Table 2.1-a**. From the data above, the ICT peaks for regio-irregular polymers **[RIR] PT<sub>OP</sub>-TPD<sub>BP</sub>** and **[RIR] PT<sub>OP</sub>-TPD<sub>O</sub>** were red shifted by 33 nm and 49 nm, respectively, from solution to solid state indicating that the linear side chain induced a better  $\pi$ -stacking of the polymer chains in the solid state. Nevertheless, the calculated  $E_g^{\text{opt}}$  is 0.04 eV larger than that of the bearing phenyl group on TPD moiety. In case of **[RR] PT<sub>OP</sub>-TPD<sub>O</sub>**, as compared to **[RIR] PT<sub>OP</sub>-TPD<sub>O</sub>**, a very small hypsochromic shift in solid state was observed in regio-regular polymer. This shift is caused by a low molecular weight. However, the strong intermolecular electronic interaction between the polymer chains is more pronounced for **[RR] PT<sub>OP</sub>-TPD<sub>O</sub>**, resulting in a broad vibronic shoulder at higher wavelengths. The origin of this absorption is attributed to the high ordered arrangement of this polymer with strong  $\pi$ - $\pi$  stacking between polymer backbones causing a much narrower band gap than those values stated for P3HT.<sup>41</sup> On the other hand, polymers that contain **[H-H] PT<sub>2OP</sub>-TPD<sub>O</sub>** and **[T-T] PT<sub>2OP</sub>-TPD<sub>O</sub>** linkages have absorption maximum ( $\lambda_{\text{max}}$ ) in the range from 474 to 512 nm in solid state, respectively. As a result, **T-T** coupling has the potential to maintain the planarity more efficiently than **H-H** coupling due to the reduced steric repulsion between alkyl chains. Consequently, the conjugation length in the

main chain of both models is strongly affected, and a large band gap obtained. Furthermore, by comparing the results above with polymers that were produced by Facchetti group<sup>42</sup>, one could conclude that incorporating of phenyl ring in polythiophene units increased the torsion angle between the phenyl ring and the thiophene, and between two consecutive head to head connections.

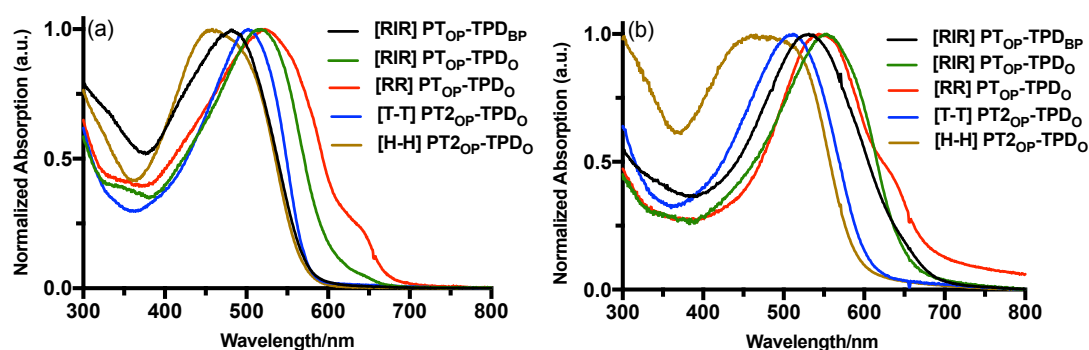


**Figure 2.9.** Optical absorption spectra of the TPD-based copolymers in: (a) chloroform solution; (b) thin films.

## 2.2.4 Polymers Electrochemical Properties

The energy levels of polymers were determined by cyclic voltammetry measurements as shown in **Figure 2.10** and summarized in **Table 2.1-b**. onsets of oxidation waves at 0.81 V and 0.64 V were observed for **[RIR] PT<sub>OP</sub>-TPD<sub>O</sub>** and **[RIR] PT<sub>OP</sub>-TPD<sub>BP</sub>**, which corresponded to HOMO energy levels at -5.53 eV and -5.36 eV, respectively. The results indicate that incorporation of phenyl ring on TPD moiety reduce the conjugation within the polymer backbone and decrease oxidation potential further than linear octyl side chain. Conceivably, this performance might be as well attributed to the lower molecular weight observed for **[RR] PT<sub>OP</sub>-TPD<sub>O</sub>**. Further comparison between **[RR] PT<sub>OP</sub>-TPD<sub>O</sub>** and **[RIR] PT<sub>OP</sub>-TPD<sub>O</sub>** shows that, although these two polymers have the same backbone structures, the oxidation onset for **[RIR] PT<sub>OP</sub>-TPD<sub>O</sub>** is more positive by 0.15 V and as a result has a deeper HOMO level. This result indicates that the impact of molecular weight values is less important than regioregularity of the polymer and despite the lower molecular weight of the regioregular polymer, its HOMO level is nevertheless deeper than that of the regioirregular polymer. This order phenomena also occurred in their LUMO levels, which exhibited the LUMO at -3.36 eV and

-3.32 eV for [RIR] PT<sub>OP</sub>-TPD<sub>BP</sub> and [RIR] PT<sub>OP</sub>-TPD<sub>O</sub>, respectively, while LUMOs with those of regio-regular [RR] PT<sub>OP</sub>-TPD<sub>O</sub>, [T-T] PT<sub>2OP</sub>-TPD<sub>O</sub>, and [H-H] PT<sub>2OP</sub>-TPD<sub>O</sub> estimated to be at -3.57 eV, -3.60 eV, and -3.58 eV. One can notice that all regio-regular polymers have low-lying LUMO, which is most likely due to their high planarity. Compared to [RR] PT<sub>OP</sub>-TPD<sub>O</sub>, T-T coupling and H-H coupling show deeper HOMO levels of approximately -5.62 eV and -5.61 eV, which should exhibit a high open circuit voltage ( $V_{OC}$ ) in device versus P3HT. It is important to note that the energy difference between the LUMO levels of all electron-donating conjugated polymers and PCBM is greater than 0.6 eV, which should resolve the strong exciton binding energy and facilitate the exciton separation significantly.

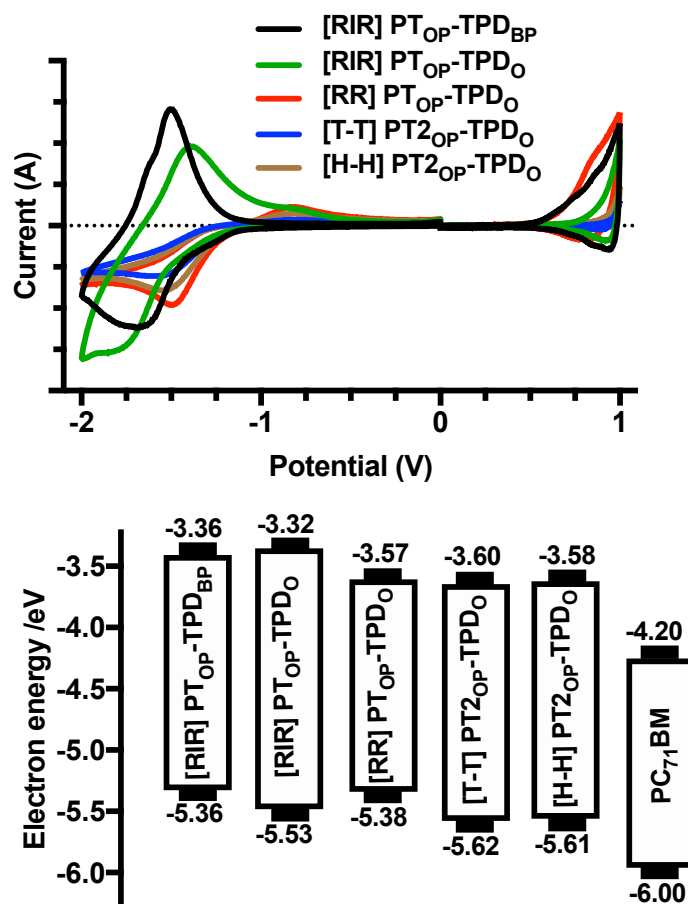


**Figure 2.10.** Cyclic voltammograms (top) and energy level diagram (bottom) of the TPD-based copolymers and PCBM.

## 2.2.5 Polymers Thermal Properties

The thermal behaviour of the TPD-based copolymers was evaluated by Thermogravimetric analysis (TGA) between room temperature and 800°C

under nitrogen atmosphere as shown in **Figure 2.11** and tabulated in **Table 2.2**. All polymers exhibit high thermal decomposition temperatures up to 473°C except for **[RIR] PT<sub>OP</sub>-TPD<sub>BP</sub>**. The first stage of the thermal behaviour started with **[RIR] PT<sub>OP</sub>-TPD<sub>BP</sub>** at 368°C. This poor behaviour, when compared with its family, is due to both short alkyl chain (butyl) and poor stability of the bulky group (phenyl ring) on imide moiety. However, the heat resistance capability of **[RIR] PT<sub>OP</sub>-TPD<sub>O</sub>** backbone increased to about ~20% (473°C). In a reverse manner, **[RR] PT<sub>OP</sub>-TPD<sub>O</sub>** exhibit degradation temperature of 465°C, which is unexpectedly less resistant to heat than **[RIR] PT<sub>OP</sub>-TPD<sub>O</sub>**, almost certainly owing to its low molecular weight. **[T-T] PT<sub>2OP</sub>-TPD<sub>O</sub>**, and **[H-H] PT<sub>2OP</sub>-TPD<sub>O</sub>** also decompose at lower temperature. It is speculated that the additional alkyl chain on the second thiophene backbone brought about some extra free volume resulting in low temperature thermal degradations (*T<sub>d</sub>*). All TGA studies concluded that all the synthesized conjugated polymers revealed good thermal stability for use in electronic devices

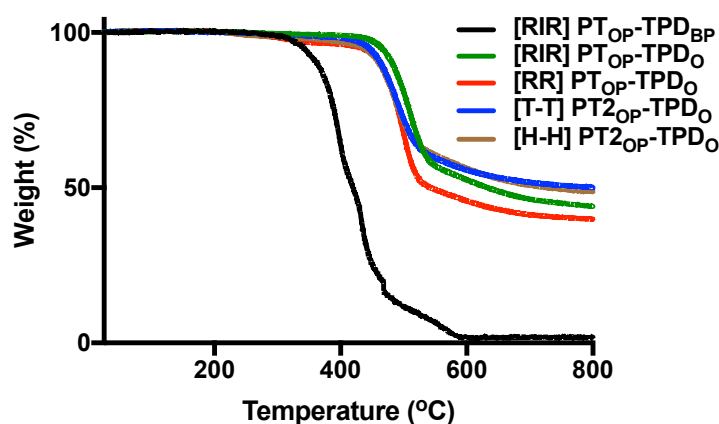


**Figure 2.11.** TGA curve of TPD-based copolymers.

## 2.2.6 Polymers Molecular structure

The investigation of the molecular organization of TPD-based copolymers was studied by powder X-ray diffraction in the solid state as shown in **Figure 2.13** and summarized in **Table 2.2**. **[RIR] PT<sub>OP</sub>-TPD<sub>BP</sub>** and **[RR] PT<sub>OP</sub>-TPD<sub>O</sub>** present weak peaks reflected at low angle 3.70° (23.85 Å) and 3.50° (25.21 Å), respectively, while no observable low angle reflection was obtained for **[RIR] PT<sub>OP</sub>-TPD<sub>O</sub>**, **[T-T] PT<sub>2OP</sub>-TPD<sub>O</sub>**, and **[H-H] PT<sub>2OP</sub>-TPD<sub>O</sub>**. These peaks



contributed to the lamellar stacking distance between the adjacent polymer chains (see **Figure 2.12**). The reduction of lamellar stacking distance of  $\sim 1.40$  Å for **[RIR] PT<sub>OP</sub>-TPD<sub>BP</sub>** might be ascribed to less steric hindrance for alkyl chains on imide moieties, better interchain interdigitation of conjugated and alkyl moieties, and high planarity along the polymer chains compared to **[RR] PT<sub>OP</sub>-TPD<sub>O</sub>**, leading to crystallization/lamellar aggregates between the polymer chains. Subsequently, **[RIR] PT<sub>OP</sub>-TPD<sub>BP</sub>** and **[RR] PT<sub>OP</sub>-TPD<sub>O</sub>** should provide decent charge motilities in comparison to the other polymers.

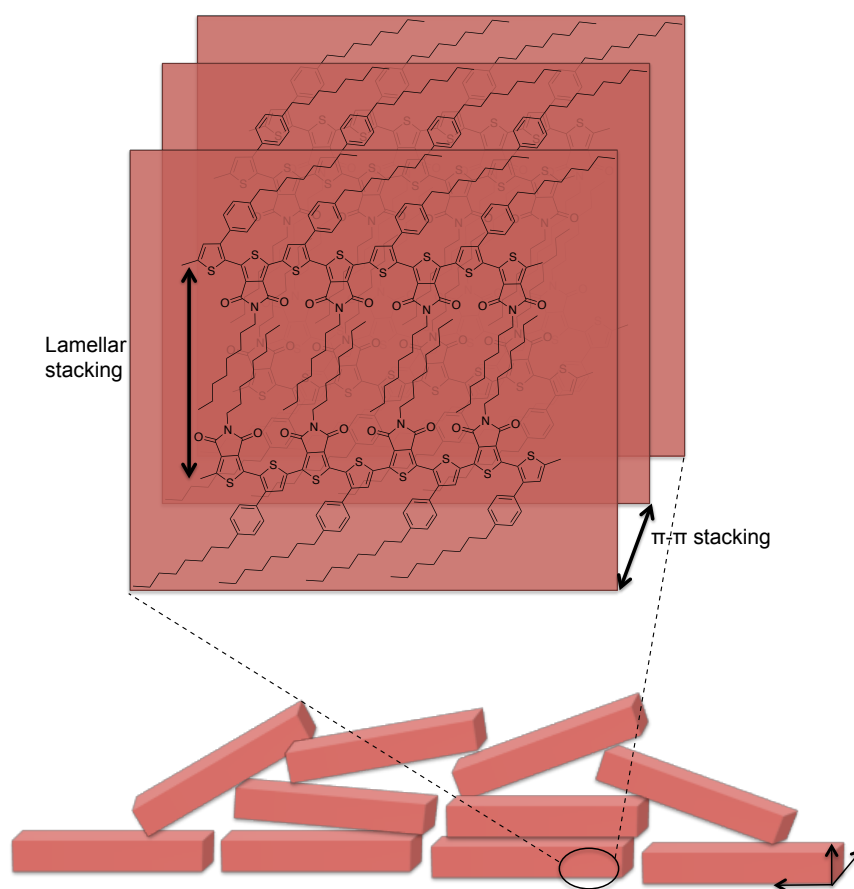


**Figure 2.12.** 2D image of the molecular organisation of the polymers.

Besides, **[RIR] PT<sub>OP</sub>-TPD<sub>BP</sub>**, **[RIR] PT<sub>OP</sub>-TPD<sub>O</sub>**, **[RR] PT<sub>OP</sub>-TPD<sub>O</sub>**, **[T-T] PT<sub>2OP</sub>-TPD<sub>O</sub>**, and **[H-H] PT<sub>2OP</sub>-TPD<sub>O</sub>** revealed peaks at wide angle reflection that contribute to  $\pi$ - $\pi$  stacking distance, (see **Figure 2.12**), of 3.48 Å, 4.21 Å, 4.41 Å, 4.40 Å, and 4.16 Å, respectively. The results of this study can conclude that **[RIR] PT<sub>OP</sub>-TPD<sub>BP</sub>** observed a better interaggregate interaction and interchain interdigitation as a result of the shortest  $\pi$ - $\pi$  and lamellar

distance. However, the nature of all the synthesized conjugated polymers tends to form amorphous domains larger than crystalline domains in solid state.

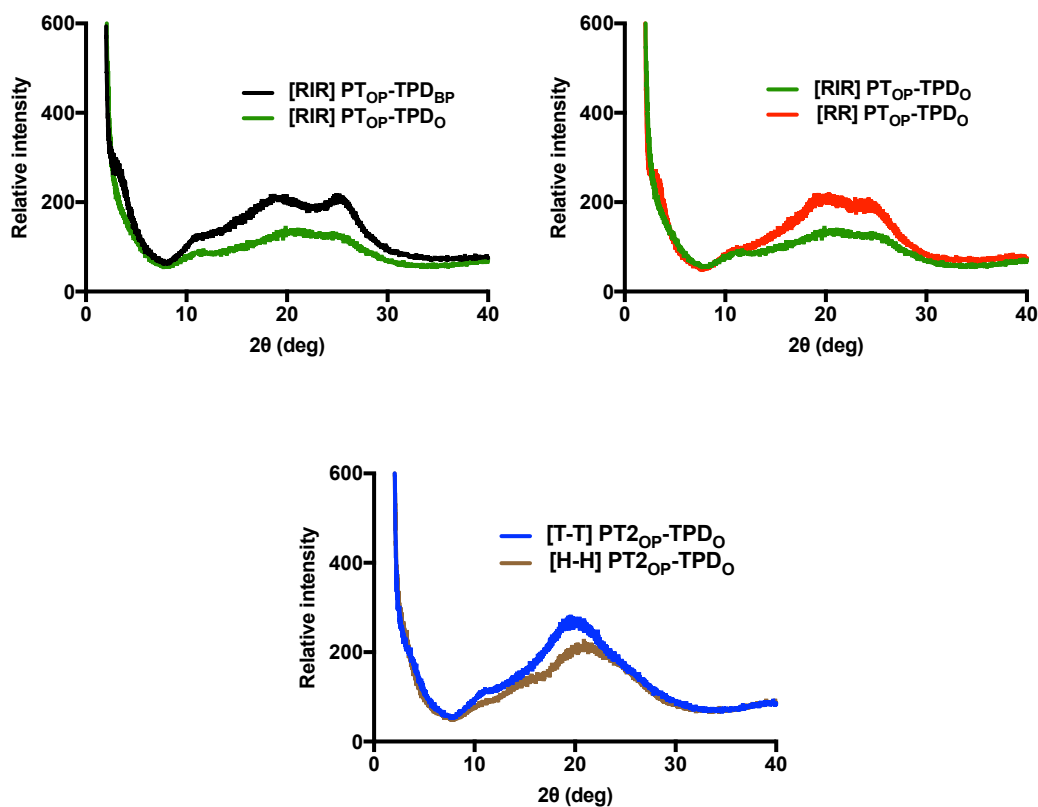


**Figure 2.12.** Powder X-ray diffraction patterns of TPD-based copolymers.

**Table 2.2.** Molecular structure data and thermal characteristic of TPD-based copolymers.

| Polymer                                   | $2\theta/\text{deg}$ | $d$         | $2\theta/\text{deg}$ | $d$         | $T_d$ |
|---|----------------------|-------------|----------------------|-------------|-------|
|   | spacing/Å(nm)        |             | spacing/Å(nm)        |             |       |
| [RIR] PT <sub>OP</sub> -TPD <sub>BP</sub> | 3.70                 | 23.85(2.38) | 25.58                | 3.48(~0.35) | 368   |
| [RIR] PT <sub>OP</sub> -TPD <sub>O</sub>  | -                    | -           | 21.08                | 4.21(0.42)  | 473   |
| [RR] PT <sub>OP</sub> -TPD <sub>O</sub>   | 3.50                 | 25.21(2.52) | 20.10                | 4.41(0.44)  | 465   |
| [T-T] PT <sub>2OP</sub> -TPD <sub>O</sub> | -                    | -           | 20.14                | 4.40(0.44)  | 454   |
| [H-H] PT <sub>2OP</sub> -TPD <sub>O</sub> | -                    | -           | 21.32                | 4.16(~0.42) | 453   |

### 2.3. Conclusions

A series of new donor-acceptor copolymer semiconductors based on thieno[3,4-c]pyrrole-4,6-dione (TPD) acceptor with butylphenyl (**BP**) and linear octyl (**O**) side groups, and thiophene (**T**) or bithiophene (**T2**) units as donor was prepared by direct arylation polymerization (DAP) to yield the following copolymers in a fashion similar to those of P3HTs, **[RIR] PT<sub>OP</sub>-TPD<sub>BP</sub>**, **[RIR] PT<sub>OP</sub>-TPD<sub>O</sub>**, **[RR] PT<sub>OP</sub>-TPD<sub>O</sub>**, **[T-T] PT<sub>2OP</sub>-TPD<sub>O</sub>**, and **[H-H] PT<sub>2OP</sub>-TPD<sub>O</sub>**. Incorporation of phenyl ring, particularly on imide moiety in **[RIR] PT<sub>OP</sub>-TPD<sub>BP</sub>**, was found to impede the ability to create long chains of polymer resulting in lower molecular weight and thermal property as compared to all synthesized copolymers except **[RR] PT<sub>OP</sub>-TPD<sub>O</sub>**. This polymer's poor molecular weight was largely due to its high crystalline property causing a much narrower band gap than those values stated for P3HT.<sup>41</sup> The lack of aggregation and crystallinity increased not only the opportunity to have an  $M_n$  over 10.5 kDa for **[RIR] PT<sub>OP</sub>-TPD<sub>O</sub>**, **[T-T] PT<sub>2OP</sub>-TPD<sub>O</sub>**, and **[H-H] PT<sub>2OP</sub>-TPD<sub>O</sub>** but also the optical band gap from 1.87-2.07 eV. The latter three copolymers show deeper HOMO levels in the range of 5.57-5.62 eV, which should lead to a high open circuit voltage ( $V_{oc}$ ) in OPV device versus P3HT. In addition to that, all regio-regular copolymers' LUMO results would facilitate to diminish the energy loss in the electron transfer from the copolymer to PCBM acceptor more efficiently than regio-random copolymers due to their medium LUMO offset. X-ray diffraction studies provided smaller crystalline domains within **[RIR] PT<sub>OP</sub>-TPD<sub>BP</sub>** with a lamellar distance of 23.85 Å that is 1.40 Å shorter than **[RR] PT<sub>OP</sub>-TPD<sub>O</sub>**. However, the nature of all polymers tends to form amorphous domains more than crystalline domains in solid state. The photovoltaic properties of this series of polymers will be investigated in collaboration with colleagues in the Physics Department. It will be extremely important to study the effect of the dipole moments of these polymers and consequences on the power conversion efficiency of these materials in bulk heterojunction solar cells.

## 2.4 References

1. J. Roncali, *Chemical Reviews*, 1997, **97**, 173-205.
2. C. Winder and N. S. Sariciftci, *Journal of Materials Chemistry*, 2004, **14**, 1077-1086.
3. Y. J. Cheng, S. H. Yang and C. S. Hsu, *Chemical Reviews*, 2009, **109**, 5868-5923.
4. A. P. Zoombelt, M. Fonrodona, M. G. R. Turbiez, M. M. Wienk and R. A. J. Janssen, *Journal of Materials Chemistry*, 2009, **19**, 5336-5342.
5. H. J. Wang, C. P. Chen and R. J. Jeng, *Materials*, 2014, **7**, 2411-2439.
6. Y. Y. Liang, Y. Wu, D. Q. Feng, S. T. Tsai, H. J. Son, G. Li and L. P. Yu, *Journal of the American Chemical Society*, 2009, **131**, 56-57.
7. E. W. Zhu, G. D. Ge, J. K. Shu, M. D. Yi, L. Y. Bian, J. F. Hai, J. S. Yu, Y. Liu, J. Zhou and W. H. Tang, *Journal of Materials Chemistry A*, 2014, **2**, 13580-13586.
8. M. Klein, S. Majumdar, P. Zassowski and W. Stampor, *Journal of Materials Chemistry C*, 2018, **6**, 482-490.
9. B. C. Thompson and J. M. J. Fréchet, *Angewandte Chemie-International Edition*, 2008, **47**, 58-77.
10. B. Carsten, J. M. Szarko, H. J. Son, W. Wang, L. Y. Lu, F. He, B. S. Rolczynski, S. J. Lou, L. X. Chen and L. P. Yu, *Journal of the American Chemical Society*, 2011, **133**, 20468-20475.
11. K. Kranthiraja, S. Kim, C. Lee, K. Gunasekar, V. G. Sree, B. Gautam, K. Gundogdu, S. H. Jin and B. J. Kim, *Advanced Functional Materials*, 2017, **27**, 1701256.
12. B. Carsten, J. M. Szarko, L. Y. Lu, H. J. Son, F. He, Y. Y. Botros, L. X. Chen and L. P. Yu, *Macromolecules*, 2012, **45**, 6390-6395.
13. T. Xu, L. Y. Lu, T. Y. Zheng, J. M. Szarko, A. Schneider, L. X. Chen and L. P. Yu, *Advanced Functional Materials*, 2014, **24**, 3432-3437.
14. V. Coropceanu, J. Cornil, D. Da Silva, Y. Olivier, R. Silbey and J. Bredas, *Chemical Reviews*, 2007, **107**, 926-952.
15. A. Facchetti, *Chemistry of Materials*, 2011, **23**, 733-758.
16. C. H. Duan, F. Huang and Y. Cao, *Journal of Materials Chemistry*, 2012, **22**, 10416-10434.
17. Y. Kim, S. Cook, S. M. Tuladhar, S. A. Choulis, J. Nelson, J. R. Durrant, D. D. C. Bradley, M. Giles, I. McCulloch, C. S. Ha and M. Ree, *Nature Materials*, 2006, **5**, 197-203.
18. S. Allard, M. Forster, B. Souharce, H. Thiem and U. Scherf, *Angewandte Chemie-International Edition*, 2008, **47**, 4070-4098.
19. L. Ying, F. Huang and G. C. Bazan, *Nature Communications*, 2017, **8**.
20. G. Louarn, J. Kruszka, S. Lefrant, M. Zagorska, I. Kulszewicz-Bayer and A. Proń, *Synthetic Metals*, 1993, **61**, 233-238.
21. M. Łapkowski, M. Zagórska, I. Kulszewicz-Bajer and A. Proń, *Journal of Electroanalytical Chemistry*, 1992, **341**, 151-163.

22. Y. Zou, A. Najari, P. Berrouard, S. Beaupre, B. R. Aich, Y. Tao and M. Leclerc, *Journal of the American Chemical Society*, 2010, **132**, 5330-5331.
23. X. G. Guo, H. Xin, F. S. Kim, A. D. T. Liyanage, S. A. Jenekhe and M. D. Watson, *Macromolecules*, 2011, **44**, 269-277.
24. P. Berrouard, S. Dufresne, A. Pron, J. Veilleux and M. Leclerc, *Journal of Organic Chemistry*, 2012, **77**, 8167-8173.
25. D. Q. Zhu, Q. Q. Zhu, C. T. Gu, D. Ouyang, M. Qiu, X. C. Bao and R. Q. Yang, *Macromolecules*, 2016, **49**, 5788-5795.
26. A. Pron, P. Berrouard and M. Leclerc, *Macromolecular Chemistry and Physics*, 2013, **214**, 7-16.
27. J. W. Rumer, C. K. L. Hor, I. Meager, C. P. Yau, Z. Huang, C. B. Nielsen, S. E. Watkins, H. Bronstein and I. McCulloch, *Journal of Organic Semiconductors*, 2013, **1**, 30-35.
28. C. L. Chochos and S. A. Choulis, *Progress in Polymer Science*, 2011, **36**, 1326-1414.
29. M. Andersson, D. Selse, M. Berggren, H. Jarvinen, T. Hjertberg, O. Inganas, O. Wennerstrom and J. Osterholm, *Macromolecules*, 1994, **27**, 6503-6506.
30. A. L. Ding, J. Pei, Y. H. Lai and W. Huang, *Journal of Materials Chemistry*, 2001, **11**, 3082-3086.
31. E. W. Zhu, B. Ni, B. F. Zhao, J. F. Hai, L. Y. Bian, H. B. Wu and W. H. Tang, *Macromolecular Chemistry and Physics*, 2014, **215**, 227-234.
32. Z. Puterova, A. Krutosikova and D. Vegh, *Arkivoc*, 2010, 209-246.
33. J. J. Li, *Gewald aminothiophene synthesis. In Name Reactions*, Springer International Publishing, Cham, 5th edn., 2014.
34. S. Y. Chang, P. H. Lin and C. Y. Liu, *RSC Advances*, 2014, **4**, 35868-35878.
35. L. G. Mercier and M. Leclerc, *Accounts of Chemical Research*, 2013, **46**, 1597-1605.
36. K. Kobayashi, A. Sugie, M. Takahashi, K. Masui and A. Mori, *Organic Letters*, 2005, **7**, 5083-5085.
37. S. H. Cho, J. Y. Kim, J. Kwak and S. Chang, *Chemical Society Reviews*, 2011, **40**, 5068-5083.
38. K. Masui, H. Ikegami and A. Mori, *Journal of the American Chemical Society*, 2004, **126**, 5074-5075.
39. S. L. You and J. B. Xia, *C-H Activation*, 2010, **292**, 165-194.
40. M. Wakioka, N. Ichihara, Y. Kitano and F. Ozawa, *Macromolecules*, 2014, **47**, 626-631.
41. A. Marrocchi, D. Lanari, A. Facchetti and L. Vaccaro, *Energy & Environmental Science*, 2012, **5**, 8457-8474.
42. X. G. Guo, R. P. Ortiz, Y. Zheng, M. G. Kim, S. M. Zhang, Y. Hu, G. Lu, A. Facchetti and T. J. Marks, *Journal of the American Chemical Society*, 2011, **133**, 13685-13697.

>>

**CHAPTER III**  
**EXAMINING THE EFFECT OF**  
**TRI (ETHYLENE GLYCOL) AS SIDE**  
**CHAIN OF CONJUGATED POLYMERS**  
**ON THEIR CHEMICAL AND PHYSICAL**  
**PROPERTIES**

### 3.1 Introduction

In recent decades, conjugated polymers have received much attention for application in flexible and low-cost optoelectronic devices, such as light-emitting diodes (OLEDs), field-effect transistors (OFETs), and photovoltaic cells (OPVs)<sup>1-3</sup> owing to their solution processability as compared to inorganic semiconductors; the higher processability results from the appendage of flexible side chains onto conjugated moieties.<sup>4, 5</sup> The selection of appropriate side chains is a key factor for balancing numerous considerations far beyond polymer solubility; these considerations include molecular packing, blend morphology of the polymer donor, and the device performance.<sup>6, 7</sup> Thus far, a multitude of efforts have been put in towards optimising the alkyl chain type, length, and branching point position for enhancing the performance of photonic devices.<sup>8, 9</sup>

Triethylene glycol (TEG) chains are well known for their hydrophilicity.<sup>10, 11</sup> They are often used to increase polymer solubility in water or polar organic solvents.<sup>12</sup> Accordingly, TEG chains have been introduced as side chains in conjugated polymers to promote the fabrication process with environmentally friendly solvents and to enhance the performance of OLED, OFET, and OPV devices<sup>13, 14</sup>. For instance, Hou et al.<sup>13</sup> reported an amphiphilic-conjugated polymer PBDTTT-TEG with a power conversion efficiency of 5.23%; it was processed with a polar non-halogenated solvent (e.g., *N*-methyl-2-pyrrolidone (NMP)), making this design more advantageous over its alkylated analogues. Besides, recent studies demonstrated that hydrophilic TEG chains are more flexible than hydrophobic chains<sup>15</sup>, which can effectively facilitate a close intermolecular  $\pi$ - $\pi$  stacking in the conjugated polymer backbone and improve the device performance. Wang et al.<sup>15</sup> investigated the effect of substitution on polyfluorenes and found that hydrophilic oligo(ethylene glycol) chains are more effective in enhancing intermolecular interactions than their alkylated counterparts, resulting in an increased hole mobility, red-shifted absorption spectra, and a low-energy bandgap. It was also reported that the OPV performance of isoindigo/DPP-based conjugated polymers was improved when alkyl side chains were replaced with oligo(ethylene glycol) chains.<sup>9, 16</sup>

Consequently, it can be concluded that the natural flexibility of hydrophilic oligo(ethylene glycol) chains is advantageous for their effect as replacements for alkyl side chains in conjugated polymers in photonic devices.

This new approach motivated us to construct a new donor-acceptor copolymer, using fluorene as the donor and 5-thieno[3,4-*c*]pyrrole-4,6-dione (TPD) as the acceptor with TEG side chains, and compare its optoelectronic properties and molecular packing with polymers containing alkyl side chains. Polyfluorenes are seen as the most promising class of conjugated polymers due to their thermal and environmental stability<sup>17</sup>, high absorption coefficients<sup>18</sup>, and easy functionalisation at the 9-positions.<sup>19</sup> Generally, polyfluorenes have a wide band gap (3.0 eV)<sup>20</sup> that would minimise their absorption coverage across the solar spectrum.<sup>21</sup> However, this issue can be overcome by incorporating an electron-accepting unit into the main polyfluorene chain to tune not only the band gap but also the energy levels.<sup>22</sup> Large common electron-accepting units, such as benzothiadiazole[BT]<sup>23</sup>, diketopyrrolopyrrole [DPP]<sup>24</sup>, quinoxaline [Qx]<sup>25</sup>, and theinopyrroledione [TPD]<sup>26</sup>, have been used to extend spectral coverage. In particular, TPD has been chosen in this study as its electron-deficient nature significantly deepens the highest-occupied molecular orbitals (HOMOs) of the resultant copolymers and enhances intramolecular charge transfer characteristics. Furthermore, the planarity of the TPD skeleton and its ability to be involved in hydrogen bonding promotes intermolecular interactions between polymer chains for efficient charge transport.<sup>27, 28</sup>

In this study, we synthesised and characterised a series of fluorene-TPD-based donor-acceptor conjugated copolymers, **PF<sub>OXY</sub>DT-TPD<sub>OXY</sub>**, **PF<sub>OXY</sub>DT-TPD<sub>DMO</sub>**, **PF<sub>O</sub>DT-TPD<sub>OXY</sub>**, and **PF<sub>O</sub>DT-TPD<sub>DMO</sub>** (see **Figure 3.1**), by direct arylation polymerisation. They share the same backbone architecture with different solubilising groups. Fluorene monomer is flanked on both side ends by unsubstituted thiophenes as spacer units to prevent steric interaction along the copolymer backbone. The results show that substituted TEGs on both units can facilitate  $\pi$ - $\pi$  stacking more effectively than TEGs substituted with either donor or acceptor moieties individually or by alkyl substitution on both



backbones. The preparation optical and electrochemical properties of these materials are presented in this chapter with an emphasis on the effect of ethylene glycol substituents on the properties of the resulting polymers.

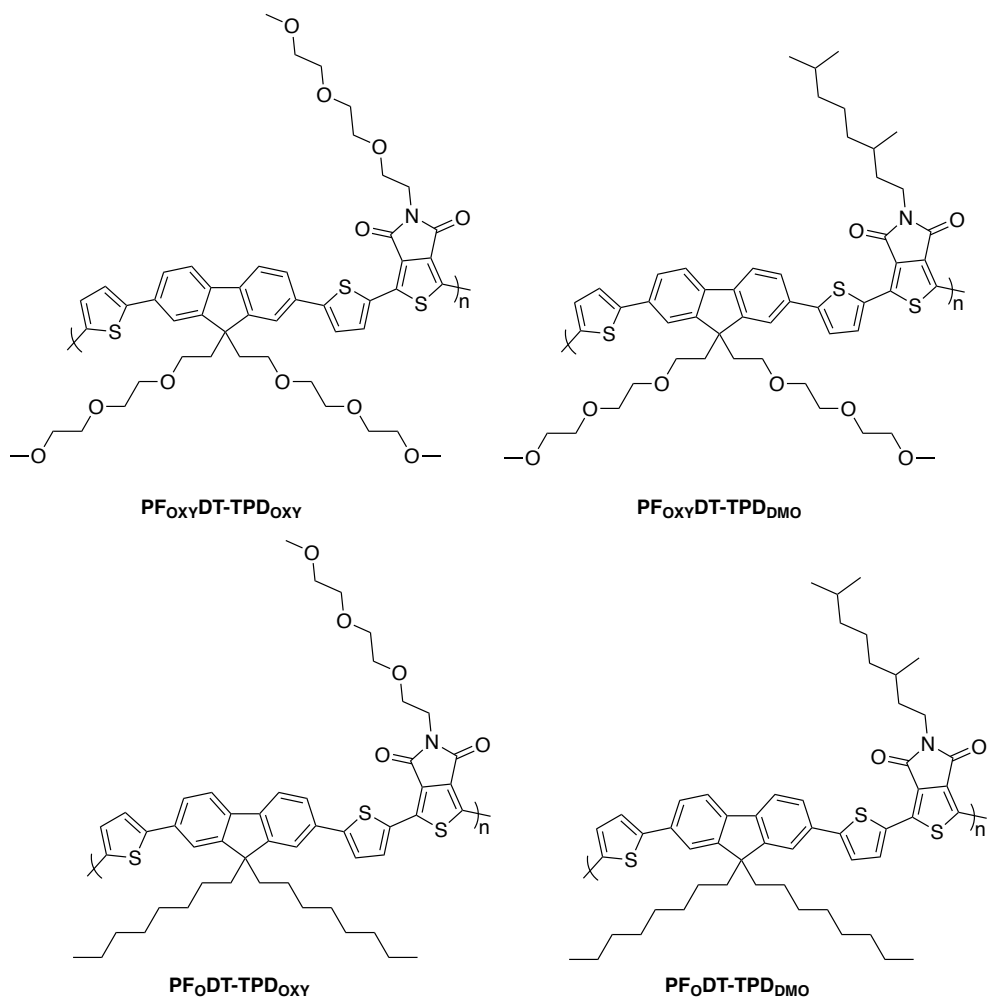
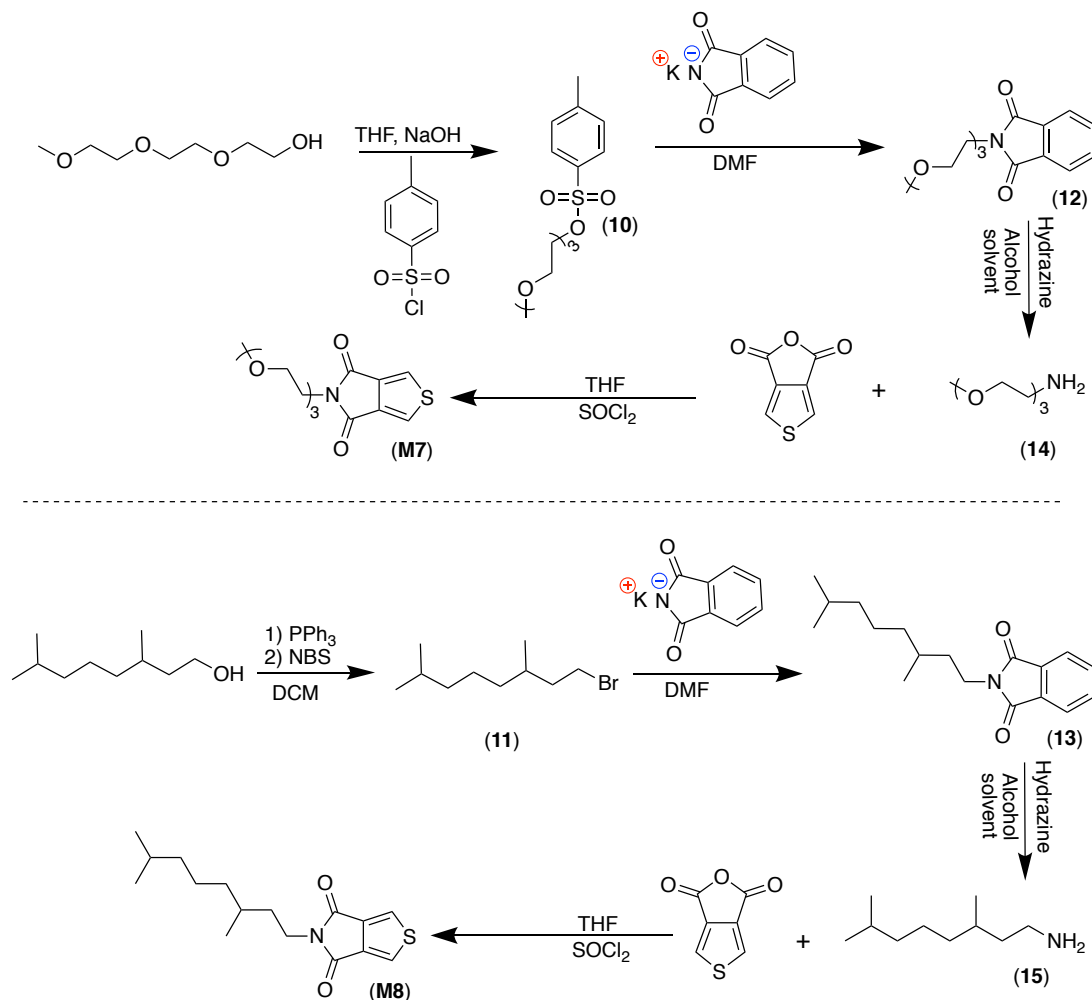


**Figure 3.1.** Polymer structures of **PF<sub>Oxy</sub>DT-TPD<sub>Oxy</sub>**, **PF<sub>Oxy</sub>DT-TPD<sub>DMO</sub>**, **PF<sub>O</sub>DT-TPD<sub>Oxy</sub>**, and **PF<sub>O</sub>DT-TPD<sub>DMO</sub>**.

## 3.2. Results and discussion

### 3.2.1 Monomer synthesis

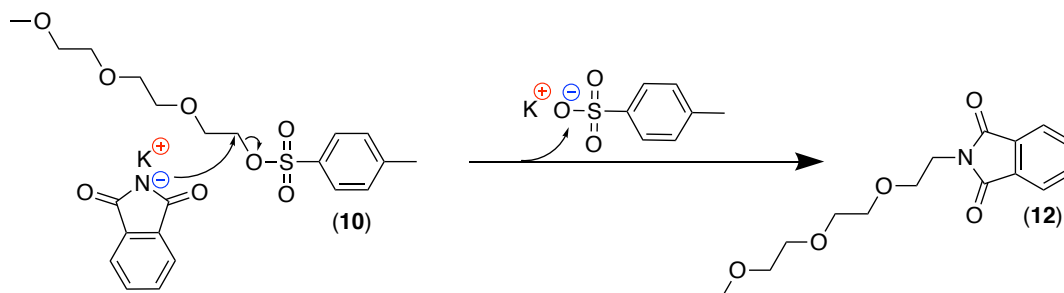
Two TPD derivatives, 5-(3,7-dimethyloctyl)-4*H*-thieno[3,4-*c*]pyrrole-4,6(5*H*)-dione (**M7**) and 5-(2-(2-(2-methoxyethoxy)ethoxy)ethyl)-4*H*-thieno[3,4-*c*]pyrrole-4,6(5*H*)-dione (**M8**) (**Scheme 3.1**) were required in this study. They were prepared in good yields, following the procedure used for **M1** and **M2** synthesis as described in Chapter II.



**Scheme 3.1.** Synthesis of **M7** and **M8**.

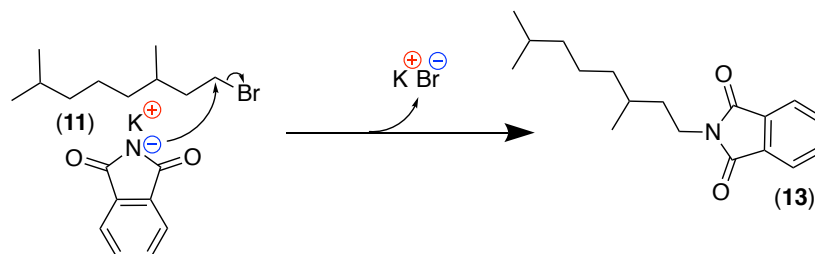
Amino functionalised triethylene glycol (**14**) and the dimethyl-octyl amine compound (**15**) were required in this reaction. Compound (**14**) was prepared starting from methyltriethyleneglycol. The alcohol functional group in this material was treated with NaOH producing sodium salt of triethylene glycol followed by nucleophilic substitution of p-toluenesulphonyl chloride affording compound (**10**). Subsequently, Gabriel synthesis of primary amine<sup>29</sup> was

conducted in which firstly triethylene glycol tosylate (**10**) were immersed in dimethylformamide (DMF) and potassium phthalimide. The nitrogen nucleophile in potassium phthalimide attacks TEG-tosylate yielding potassium tosylate and 2-(2-(2-(2-methoxyethoxy)ethoxy)ethyl)isoindoline-1,3-dione (**12**) (**Scheme 3.2**).



**Scheme 3.2.** Proposed mechanism for the synthesis of (**12**).

In case of compound (**15**), the preparation was started from 3,7-dimethyloctanol where the alcohol functional group was converted to halide using triphenylphosphine and NBS to yield compound (**11**). Then, compound (**11**) was treated by similar reagents used for compound (**12**) to afford compound (**13**) and potassium bromide as shown in **Scheme 3.3**.



**Scheme 3. 3.** Proposed mechanism for the synthesis of (**13**).

In a separate experiment with the same condition, the intermediate (**12**) or (**13**) is further heated in the presence of hydrazine. As shown in **Scheme 3.4**, the nucleophilic electron pair in hydrazine attacks one of N-phthalimide's carbonyls to form acryl hydrazine (**a**) and an amide group. A couple of intramolecular nucleophilic steps are involved in the formation of 2-(2-(2-methoxyethoxy)ethoxy)ethanamine (**14**) or 3,7-dimethyl-1-octyl amine (**15**) and phthalhydrazine (**b**) as the by-products. The production of these primary amines, which are utilized for making TPD acceptor monomers **M7** and **M8**, is explained in more detail in chapter II.



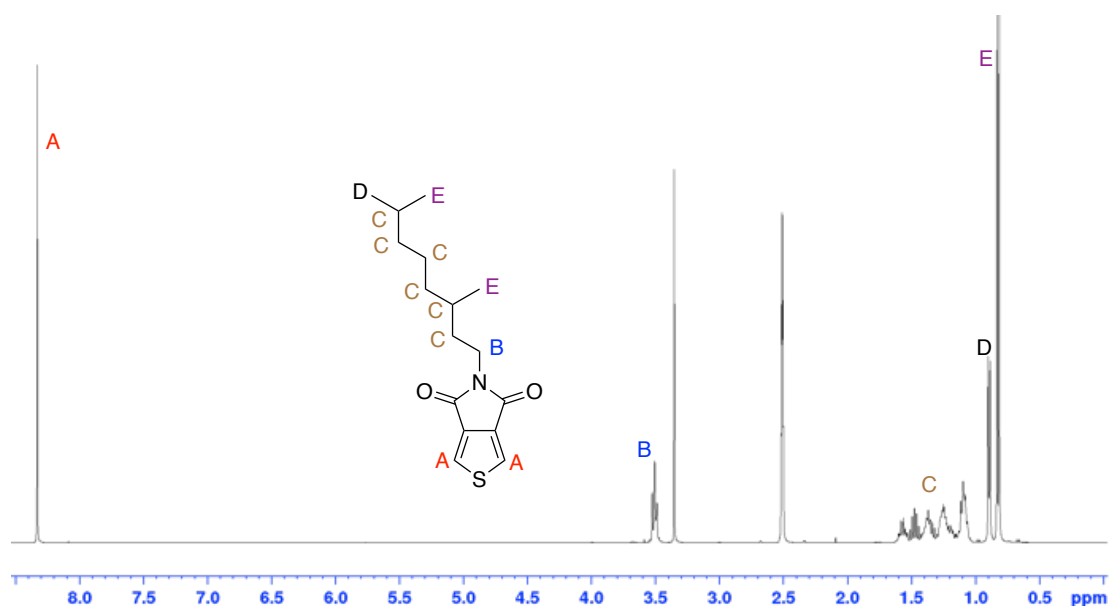
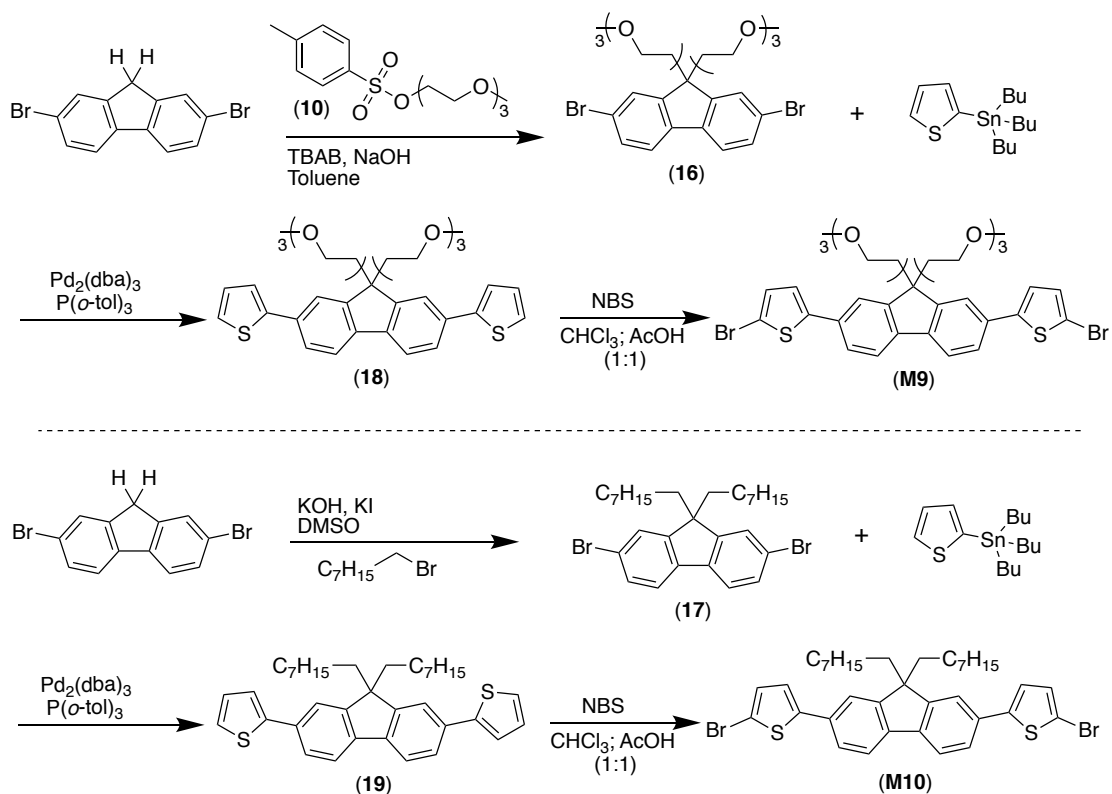


**Figure 3.3.**  $^1\text{H}$  NMR spectrum of **M8** in  $\text{C}_2\text{D}_6\text{OS}$ .

The other objective of this study is to prepare donor monomers to complete donor-acceptor polymer systems. Thus, the synthetic preparation of 5,5'-(9,9-bis(2-(2-(2-methoxyethoxy)ethoxy)ethyl)-9H-fluorene-2,7-diyl)bis(2-bromothiophene) (**M9**) and 5,5'-(9,9-dioctyl-9H-fluorene-2,7-diyl)bis(2-bromothiophene) (**M10**) are outlined in **Scheme 3.5**.



**Scheme 3.5.** Synthesis routes for **M9** and **M10**.

Briefly, these donor monomers were prepared from commercial 2,7-dibromofluorene to which TEG or alkyl moieties were attached to the fluorene units as side chains. The attachment process was carried out using sodium hydroxide in toluene to afford 2,7-dibromo-9,9-bis(2-(2-(2-methoxyethoxy)ethoxy)ethyl)-9H-fluorene (**16**) or potassium hydroxide in dimethylsulphoxide to produce 2,7-dibromo-9,9-di-n-octyl-9H-fluorene (**17**). Subsequently, the substituted fluorenes were flanked on the 2 and 7 positions by unsubstituted thiophene by Stille coupling to yield 2,2'-(9,9-bis(2-(2-(2-methoxyethoxy)ethoxy)ethyl)-9H-fluorene-2,7-diyl)dithiophene (**18**) and 2,2'-(9,9-di-n-octyl-9H-fluorene-2,7-diyl)dithiophene (**19**). Later, compounds (**18**) and (**19**) were brominated using *N*-bromosuccinimide (NBS) in chloroform and acetic acid to obtain the desired monomers, 5,5'-(9,9-bis(2-(2-(2-methoxyethoxy)ethoxy)ethyl)-9H-fluorene-2,7-diyl)bis(2-bromothiophene) (**M9**) and 5,5'-(9,9-dioctyl-9H-fluorene-2,7-diyl)bis(2-bromothiophene) (**M10**), respectively.

The chemical structure of the two donor monomers was evaluated by  $^1\text{H}$  NMR (**Figure 3.4** and **Figure 3.5**). Both the monomers showed almost similar spectra with respect to their aromatic protons, while the hydrophilic side chains resonated in the range of 3.50–2.45 ppm. Peaks below this range reflect hydrophobic side chains.

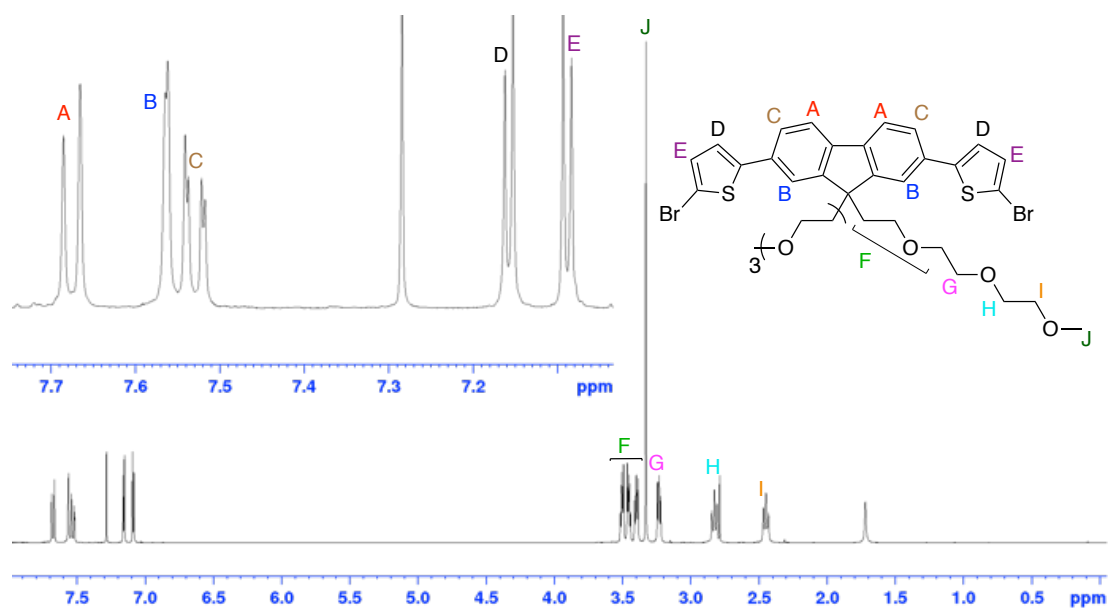


**Figure 3.4.**  $^1\text{H}$  NMR spectrum of **M9** in  $\text{CDCl}_3$ .

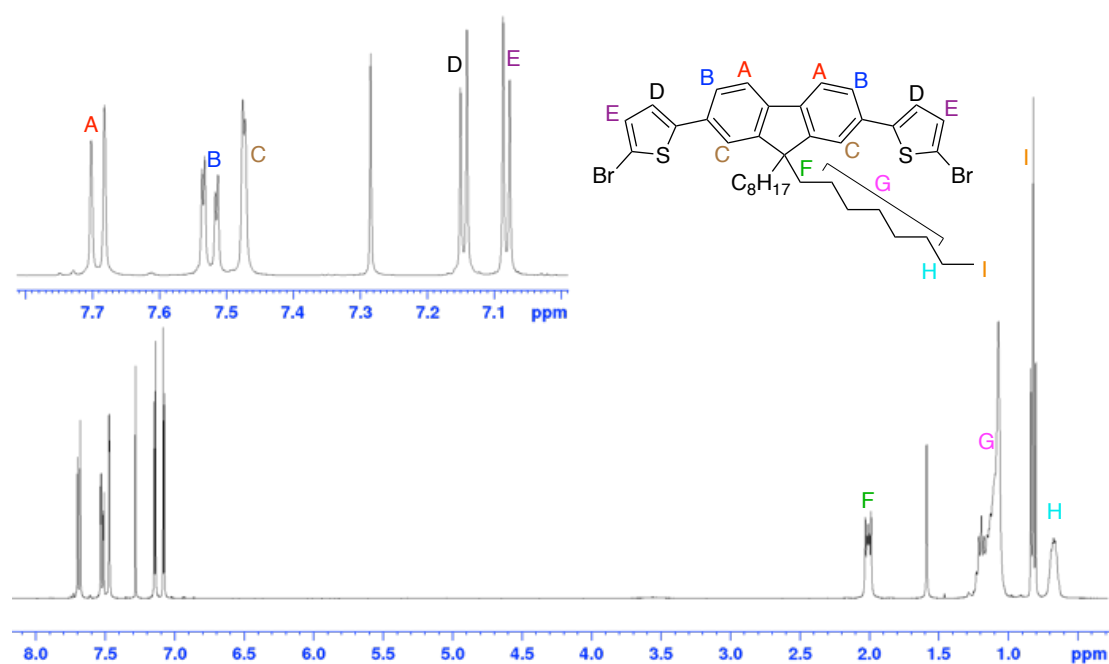


**Figure 3.5.**  $^1\text{H}$  NMR spectrum of **M10** in  $\text{CDCl}_3$ .

### 3.2.2 Polymers synthesis and characterisation

Four alternating copolymers based on fluorene-TPD with polar and nonpolar pendant groups on both units or one of the units were synthesised by direct arylation polymerisation using a palladium/phosphine catalytic system, caesium carbonate as the base, and pivalic acid as the carboxylate source for palladium to facilitate the cross-coupling reaction.<sup>30</sup> The polymerisation of **PF<sub>OXY</sub>DT-TPD<sub>OXY</sub>**, **PF<sub>OXY</sub>DT-TPD<sub>DMO</sub>**, **PF<sub>O</sub>DT-TPD<sub>OXY</sub>**, and **PF<sub>O</sub>DT-TPD<sub>DMO</sub>** was stopped after the copolymers precipitated from the solution. Subsequently, the precipitated copolymers were regained from the polymerisation vessel and purified by Soxhlet extraction using methanol, acetone, hexane, toluene, and chloroform in succession. The polymerisation approaches are described in detail in the experimental section. The chemical structure of the synthesized copolymers was confirmed by  $^1\text{H}$  NMR and elemental analysis. In the  $^1\text{H}$  NMR spectrum of **PF<sub>OXY</sub>DT-TPD<sub>OXY</sub>**, **PF<sub>OXY</sub>DT-TPD<sub>DMO</sub>**, **PF<sub>O</sub>DT-TPD<sub>OXY</sub>**, and **PF<sub>O</sub>DT-TPD<sub>DMO</sub>** (Chapter VII, Figure S6, S7, S8 and S9), the characteristic peaks at 8.13-8.11 and 7.48-7.45 ppm are assigned to the hydrogen atoms in the thiophene ring; The peaks at 7.85-7.68 ppm corresponded to the protons on the fluorene ring. The chemical shift from

3.97 to 2.52 is due to the protons of the polar side chains; the peaks below 2.52 ppm are due to the protons of non-polar side chains. High-temperature gel permeation chromatography (GPC) analysis was conducted to determine the molecular weights of the copolymers using 1,2,4-trichlorobenzene (TCB) as the eluent and a series of polystyrene standards as the calibration standards. The outcome of this analysis with respect to the copolymers is tabulated in **Table 3.1-a**. It can be observed that the polymers substituted with polar side chains (TEG) on both units displayed lower molecular weights compared to the polymers substituted with non-polar side chains (alkyl) onto a single or both units. Subsequently, one can note that the incorporation of flexible hydrophilic chains along the polymer backbone resulted in a marked propensity to form aggregates in TCB, which in turn limited the GPC capability, leading to an unreliable result for **PF<sub>OXY</sub>DT-TPD<sub>OXY</sub>**. However, the molecular weight results were well defined after TEG substitution onto polyfluorenes replaced with hydrophobic groups (Alkyl substituents). As a result, **PF<sub>O</sub>DT-TPD<sub>OXY</sub>** and **PF<sub>O</sub>DT-TPD<sub>DMO</sub>** exhibited  $M_n$  values of 46.6 kDa and 41.2 kDa, respectively, which are remarkably higher than that of **PF<sub>OXY</sub>DT-TPD<sub>DMO</sub>** (29.1 kDa). These results indicate that attaching non-polar chains to polyfluorene backbones disrupts  $\pi$ - $\pi$  stacking, leading to the formation of high-molecular weight materials.

**Table 3.1.** (a) Molecular, optical, and (b) electrochemical data for **PF<sub>OXY</sub>DT-TPD<sub>OXY</sub>**, **PF<sub>OXY</sub>DT-TPD<sub>DMO</sub>**, **PF<sub>O</sub>DT-TPD<sub>OXY</sub>**, and **PF<sub>O</sub>DT-TPD<sub>DMO</sub>**.

(a)

| Polymer  | Molecular data <sup>b</sup> |       |      | Optical data          |                       |                                 |
|--|-----------------------------|-------|------|-----------------------|-----------------------|---------------------------------|
|  | (kDa)                       |       |      | $\lambda_{max}$ (nm)  |                       | (eV)                            |
|  | $M_n$                       | $M_w$ | PDI  | Solution              | Film                  | $E_g^c$                         |
| <b>PF<sub>OXY</sub>DT-TPD<sub>OXY</sub></b> <sup>a</sup> | 4.0                         | 4.9   | 1.23 | 484 <sup>f</sup> /509 | 509 <sup>f</sup> /544 | 2.09 ( $\pm$ 0.08) <sup>g</sup> |
| <b>PF<sub>OXY</sub>DT-TPD<sub>DMO</sub></b> <sup>a</sup> | 29.1                        | 49.0  | 1.68 | 483 <sup>f</sup> /509 | 540 <sup>f</sup>      | 2.12 ( $\pm$ 0.03) <sup>g</sup> |
| <b>PF<sub>O</sub>DT-TPD<sub>OXY</sub></b> <sup>a</sup>   | 46.6                        | 102.9 | 2.21 | 500 <sup>f</sup> /533 | 502 <sup>f</sup> /539 | 2.11 ( $\pm$ 0.09) <sup>g</sup> |
| <b>PF<sub>O</sub>DT-TPD<sub>DMO</sub></b> <sup>a</sup>   | 41.2                        | 93.9  | 2.28 | 494 <sup>f</sup>      | 538 <sup>f</sup>      | 2.09 ( $\pm$ 0.03) <sup>g</sup> |



(b)

| Polymer  | Electrochemical data |                   |                             |
|--|----------------------|-------------------|-----------------------------|
|  | (eV)                 |                   |                             |
|  | HOMO <sup>d</sup>    | LUMO <sup>d</sup> | E <sub>g</sub> <sup>e</sup> |
| <b>PF<sub>OXY</sub>DT-TPD<sub>OXY</sub></b> <sup>a</sup> | -5.42                | -3.10             | 2.32                        |
| <b>PF<sub>OXY</sub>DT-TPD<sub>DMO</sub></b> <sup>a</sup> | -5.47                | -3.06             | 2.41                        |
| <b>PF<sub>O</sub>DT-TPD<sub>OXY</sub></b> <sup>a</sup>   | -5.45                | -3.04             | 2.41                        |
| <b>PF<sub>O</sub>DT-TPD<sub>DMO</sub></b> <sup>a</sup>   | -5.51                | -3.54             | 1.97                        |

<sup>a</sup>Collected in chloroform. <sup>b</sup>GPC measurements in 1,2,4-trichlorobenzene as the eluent. <sup>c</sup>Optical band gap estimated from the film onset. <sup>d</sup>HOMO/LUMO levels calculated from the oxidation/reduction onset. <sup>e</sup>Electrochemical band gap. <sup>f</sup>Wavelength of maximum absorbance. <sup>g</sup>Range error at the peak of the absorbance curve of a different extinction coefficient.

### 3.2.3 Polymers optical properties

The optical properties of the synthesised copolymers were investigated by UV-vis absorption spectroscopy in chloroform solutions and thin films (see **Figure 3.6**). The optical properties of **PF<sub>OXY</sub>DT-TPD<sub>OXY</sub>**, **PF<sub>OXY</sub>DT-TPD<sub>DMO</sub>**, **PF<sub>O</sub>DT-TPD<sub>OXY</sub>**, and **PF<sub>O</sub>DT-TPD<sub>DMO</sub>** are listed in **Table 3.1-a**. All the copolymers displayed nearly similar absorption spectra in the solution form due to their identical main backbone architecture. In particular, **PF<sub>OXY</sub>DT-TPD<sub>OXY</sub>** and **PF<sub>OXY</sub>DT-TPD<sub>DMO</sub>** showed a distinct shoulder at 509 nm reflecting their aggregation behaviour in solution. We attempted to observe this behaviour in dilute solutions of tetrahydrofuran (THF); a further redshift in their absorption spectra was observed compared to their spectra in chloroform, proving that there is aggregation within the polymer chains. Thus, it can be conceived that this phenomenon is caused by the hydrophilic groups grafted on polyfluorenes. Compared to the solutions, the absorption spectra of copolymer thin films are red-shifted by 60, 57, 2, and 44 nm for **PF<sub>OXY</sub>DT-TPD<sub>OXY</sub>**, **PF<sub>OXY</sub>DT-TPD<sub>DMO</sub>**, **PF<sub>O</sub>DT-TPD<sub>OXY</sub>**, and **PF<sub>O</sub>DT-TPD<sub>DMO</sub>**, respectively, owing to the strong  $\pi$ - $\pi$  stacking interactions between coplanar molecules in the solid state. **PF<sub>OXY</sub>DT-TPD<sub>OXY</sub>** showed a more pronounced vibronic structure at 509 nm and 544 nm, while **PF<sub>O</sub>DT-TPD<sub>OXY</sub>** displayed a vibronic shoulder at 539 nm, which indicates the strongest interchain interaction among all the synthesised copolymers. It is possible to attribute the strong interchain interactions of **PF<sub>OXY</sub>DT-TPD<sub>OXY</sub>** to the small  $\pi$ - $\pi$  stacking

distance between some chains within this copolymer compared to other copolymers.

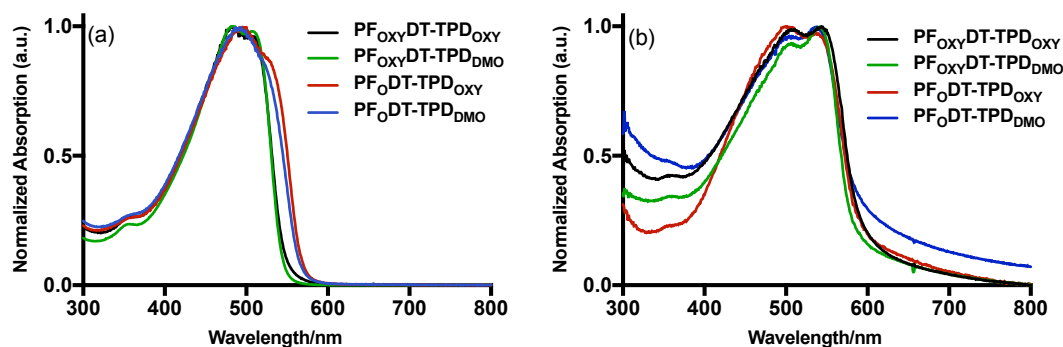


**Figure 3.6.** Normalized optical absorption spectra of **PF<sub>OXY</sub>DT-TPD<sub>OXY</sub>**, **PF<sub>OXY</sub>DT-TPD<sub>DMO</sub>**, **PF<sub>0</sub>DT-TPD<sub>OXY</sub>**, and **PF<sub>0</sub>DT-TPD<sub>DMO</sub>** in (a) chloroform solution and (b) as thin films.

The optical band gaps of **PF<sub>OXY</sub>DT-TPD<sub>OXY</sub>**, **PF<sub>OXY</sub>DT-TPD<sub>DMO</sub>**, **PF<sub>0</sub>DT-TPD<sub>OXY</sub>**, and **PF<sub>0</sub>DT-TPD<sub>DMO</sub>** were determined to be 2.09, 2.12, 2.11, and 2.09 eV, respectively. Although **PF<sub>OXY</sub>DT-TPD<sub>OXY</sub>** has the most red-shifted absorption band, the spectral onset of the absorption edge of the **PF<sub>0</sub>DT-TPD<sub>DMO</sub>** thin film shifted towards longer wavelengths resulting in an optical band gap similar to that of **PF<sub>OXY</sub>DT-TPD<sub>OXY</sub>**. These results are comparable to those reported by Wang et al.<sup>15</sup> on polyfluorene donors with the same alkyl chains, indicating that the nature of flexible TEG groups does not influence the optical properties significantly.

Furthermore, **PF<sub>OXY</sub>DT-TPD<sub>OXY</sub>** and **PF<sub>0</sub>DT-TPD<sub>OXY</sub>** exhibit the highest molar extinction coefficients of 49105 and 52625 M<sup>-1</sup> cm<sup>-1</sup>, respectively, when compared to their respective analogues, **PF<sub>OXY</sub>DT-TPD<sub>DMO</sub>** (28188 M<sup>-1</sup> cm<sup>-1</sup>) and **PF<sub>0</sub>DT-TPD<sub>DMO</sub>** (42748 M<sup>-1</sup> cm<sup>-1</sup>). Such high absorption coefficients are likely due to the extent of electron delocalisation in their molecules.

### 3.2.4 Polymers electrochemical properties

The electrochemical properties of the four copolymers were determined by cyclic voltammetry, as summarized in **Table 3.1-b**. **Figure 3.7** represents the cyclic voltammograms of all four-copolymer films on a platinum-working electrode with a solution of 0.1 M of Bu<sub>4</sub>NClO<sub>4</sub> in acetonitrile as the electrolyte and Ag/AgNO<sub>3</sub> as the reference electrode. The HOMO and LUMO values

were estimated from the oxidation and reduction onsets, respectively. In the anodic scan, the HOMO energy levels were estimated to be 5.42, 5.47, 5.45, and 5.51 eV for **PF<sub>OXY</sub>DT-TPD<sub>OXY</sub>**, **PF<sub>OXY</sub>DT-TPD<sub>DMO</sub>**, **PF<sub>O</sub>DT-TPD<sub>OXY</sub>**, and **PF<sub>O</sub>DT-TPD<sub>DMO</sub>**, respectively. In the cathodic scan, the LUMO energy levels were determined to be 3.10, 3.06, 3.04, and 3.54 eV for **PF<sub>OXY</sub>DT-TPD<sub>OXY</sub>**, **PF<sub>OXY</sub>DT-TPD<sub>DMO</sub>**, **PF<sub>O</sub>DT-TPD<sub>OXY</sub>**, and **PF<sub>O</sub>DT-TPD<sub>DMO</sub>**, respectively. Compared to **PF<sub>O</sub>DT-TPD<sub>DMO</sub>**, **PF<sub>OXY</sub>DT-TPD<sub>OXY</sub>** possesses low-lying LUMO and HOMO levels, resulting in a large band gap due to the substituent effects in  $\pi$ - $\pi$  stacking interactions. This phenomenon also contributed to changes in the energy levels of the rest of the copolymers, **PF<sub>OXY</sub>DT-TPD<sub>DMO</sub>** and **PF<sub>O</sub>DT-TPD<sub>OXY</sub>**.

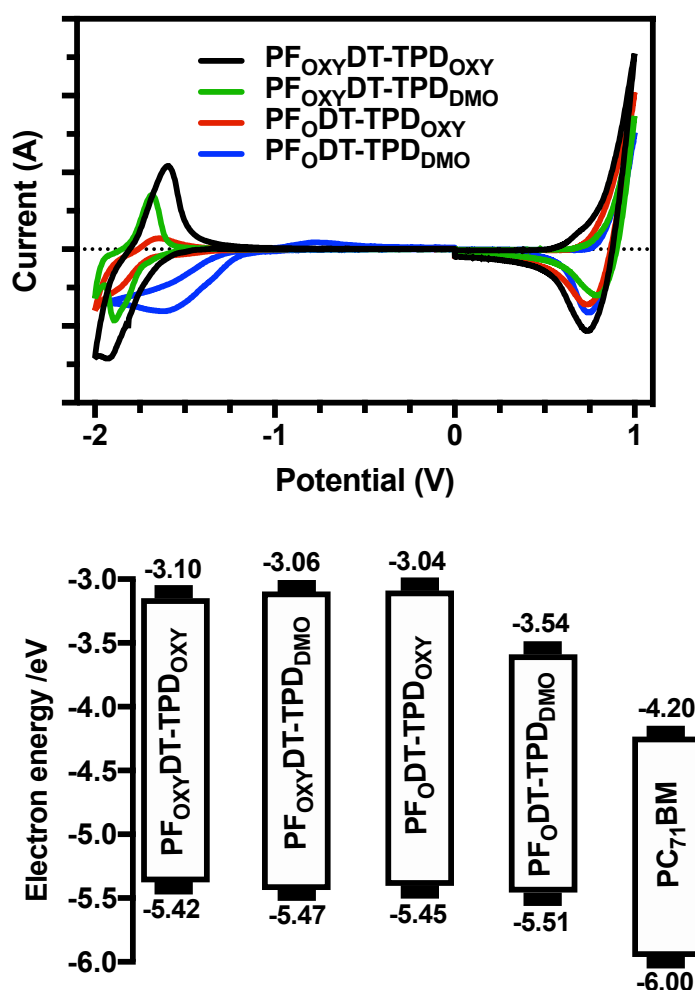


**Figure 3.7.** Cyclic voltammograms (top) and energy level diagram (bottom) of **PF<sub>OXY</sub>DT-TPD<sub>OXY</sub>**, **PF<sub>OXY</sub>DT-TPD<sub>DMO</sub>**, **PF<sub>O</sub>DT-TPD<sub>OXY</sub>**, **PF<sub>O</sub>DT-TPD<sub>DMO</sub>**, and PCBM.

Generally, higher substitution of flexible TEG side chains onto polymer backbones pushes the HOMO upwards and the LUMO downwards, leading to a small band gap; the absence of such substitution in **PF<sub>0</sub>DT-TPD<sub>DMO</sub>** leads to a band gap much smaller than that of other copolymers (see the energy level diagram in **Figure 3.7**). The electrochemical properties are almost consistent with those reported for **PFDTOBT-O<sub>x</sub>**<sup>15</sup>, except in the case of **PF<sub>0</sub>DT-TPD<sub>DMO</sub>**, in which case there was a conflict in the thin-film absorption spectra. It is worth noting that the LUMO energy levels of all electron-donating conjugated copolymers are highly capable of driving the electrons towards the electron acceptor, PCBM, which renders all four polymers synthesised in this study efficient donor materials for OPV devices.

### 3.2.5 Polymers thermal properties

The thermal stabilities of the four copolymers were studied by thermogravimetric analysis (TGA) in the temperature range of room temperature to 800 °C in a nitrogen atmosphere (see **Figure 3.8**). All the copolymers showed good thermal stability with their thermal decomposition temperatures ( $T_d$ ) higher than 410 °C. **PF<sub>OXY</sub>DT-TPD<sub>OXY</sub>** completely degraded at 421 °C, whereas **PF<sub>OXY</sub>DT-TPD<sub>DMO</sub>**, **PF<sub>0</sub>DT-TPD<sub>OXY</sub>**, and **PF<sub>0</sub>DT-TPD<sub>DMO</sub>** started degrading at 410, 426, and 440 °C, respectively with ~50% weight loss. It can be seen in the figure that an enhanced thermal stability was achieved in polymers containing nonpolar groups on their backbones as the large octyl and 3,7-dimethyloctyl chains are less volatile than TEG chains. However, the large size of the pendant group can simultaneously bring about some extra free volume in the polymer and thus reduce its thermal stability, as in the case of **PF<sub>OXY</sub>DT-TPD<sub>DMO</sub>**.

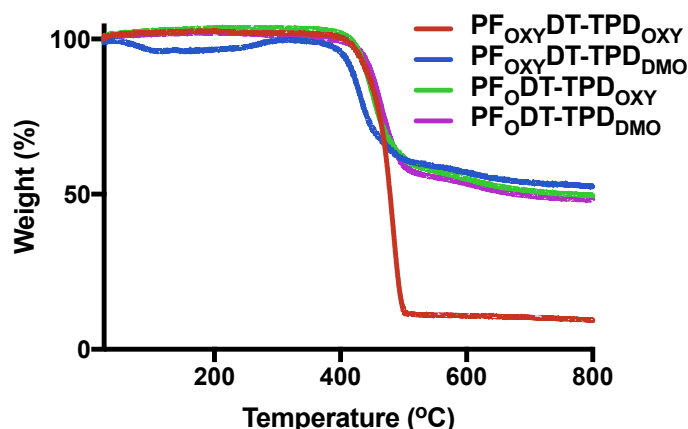


**Figure 3.8.** TGA curves of  $\text{PF}_{\text{OXY}}\text{DT-TPD}_{\text{OXY}}$ ,  $\text{PF}_{\text{OXY}}\text{DT-TPD}_{\text{DMO}}$ ,  $\text{PF}_{\text{O}}\text{DT-TPD}_{\text{OXY}}$ , and  $\text{PF}_{\text{O}}\text{DT-TPD}_{\text{DMO}}$ .

### 3.2.6 Polymers molecular structure

The powder x-ray diffraction (XRD) patterns of  $\text{PF}_{\text{OXY}}\text{DT-TPD}_{\text{OXY}}$ ,  $\text{PF}_{\text{OXY}}\text{DT-TPD}_{\text{DMO}}$ ,  $\text{PF}_{\text{O}}\text{DT-TPD}_{\text{OXY}}$ , and  $\text{PF}_{\text{O}}\text{DT-TPD}_{\text{DMO}}$  were recorded to investigate the effect of side chains on their solid-state organisation. As shown in **Figure 3.9**, all four polymers showed no diffraction peaks that could be assigned to lamellar stacking in the low angle region ( $2^\circ$ – $10^\circ$ ), indicating that although the flexibility of the hydrophilic groups caused little steric hindrance, their length probably prevented the formation of interdigitated phases in the solid-state.

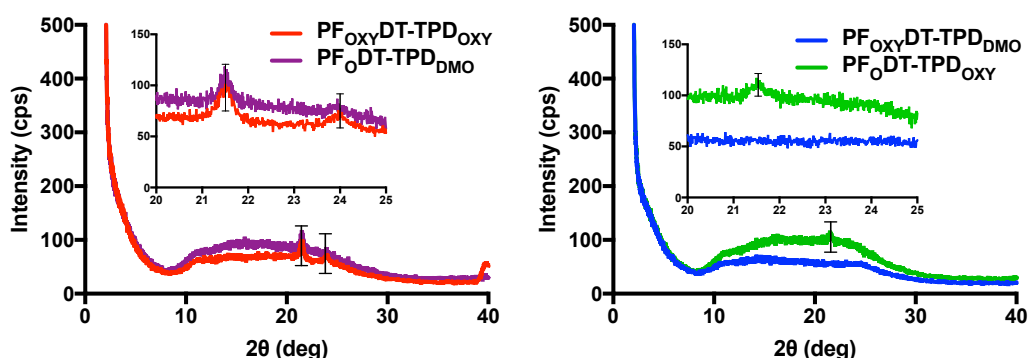


**Figure 3.9.** XRD patterns of  $\text{PF}_{\text{OXY}}\text{DT-TPD}_{\text{OXY}}$  and  $\text{PF}_{\text{O}}\text{DT-TPD}_{\text{DMO}}$  (left) and  $\text{PF}_{\text{OXY}}\text{DT-TPD}_{\text{DMO}}$  and  $\text{PF}_{\text{O}}\text{DT-TPD}_{\text{OXY}}$  (right)

However, the XRD scans revealed peaks of Bragg reflections in the wide-angle region. The first reflection peak, which presumably represents the majority of the interlayer chains, is located at nearly the same position ( $21.55^\circ$ ) in the XRD patterns of  $\text{PF}_{\text{OXY}}\text{DT-TPD}_{\text{OXY}}$ ,  $\text{PF}_{\text{O}}\text{DT-TPD}_{\text{OXY}}$ , and  $\text{PF}_{\text{O}}\text{DT-}$

**TPD<sub>DMO</sub>**; this corresponds to a  $\pi$ - $\pi$  stacking distance of 4.12 Å (see **Table 3.2**). In the case of **PF<sub>OXY</sub>DT-TPD<sub>DMO</sub>**, the absence of interchain interactions between the chains might be attributed to the large size of the side chain. Interestingly, **PF<sub>O</sub>DT-TPD<sub>DMO</sub>** exhibits a second peak at  $2\theta = 23.95^\circ$  (3.71 Å), while **PF<sub>OXY</sub>DT-TPD<sub>OXY</sub>** exhibits a second peak at  $2\theta = 24.05^\circ$  (3.70 Å) (see **Table 3.2**). As a result, when compared to alkyl side chains, TEG side chains on **PF<sub>OXY</sub>DT-TPD<sub>OXY</sub>** lead to the formation of a more ordered structure owing to a close  $\pi$ - $\pi$  stacking of the conjugated polymer backbone; this is because TEG is more flexible and induces less steric hindrance in interchain packing.

**Table 3. 2.** Molecular structural data of fluorene-based copolymers.

| Polymer                                     | $2\theta/^\circ$ | $d$              |            |
|---|------------------|------------------|------------|
|   |                  | $2\theta/^\circ$ | $d$        |
|   |                  | spacing/ Å(nm)   |            |
| <b>PF<sub>OXY</sub>DT-TPD<sub>OXY</sub></b> | 21.55            | 4.12(4.1)        | 3.70(0.37) |
| <b>PF<sub>OXY</sub>DT-TPD<sub>DMO</sub></b> | -                | -                | -          |
| <b>PF<sub>O</sub>DT-TPD<sub>OXY</sub></b>   | 21.55            | 4.12(4.1)        | -          |
| <b>PF<sub>O</sub>DT-TPD<sub>DMO</sub></b>   | 21.55            | 4.12(4.1)        | 3.71(0.37) |

### 3.3 Conclusion

By direct arylation polymerisation, four alternating copolymers based on fluorene-TPD with polar and nonpolar pendant groups on both units or on one of the units were successfully prepared; this is the first time that such polymers are being reported. The incorporation of flexible hydrophilic chains along the polymer backbone resulted in a marked propensity to form aggregates in TCB, which in turn limited GPC measurement accuracy, leading to an unreliable result for **PF<sub>OXY</sub>DT-TPD<sub>OXY</sub>**. This aggregation behaviour is also observed in UV-vis absorption spectroscopy in  $\text{CHCl}_3$  and THF solutions for **PF<sub>OXY</sub>DT-TPD<sub>OXY</sub>** and **PF<sub>OXY</sub>DT-TPD<sub>DMO</sub>**. The molecular weight results, however, were well defined after TEG substituents onto polyfluorenes were replaced with hydrophobic groups in **PF<sub>O</sub>DT-TPD<sub>DMO</sub>** and **PF<sub>O</sub>DT-TPD<sub>OXY</sub>**, which are much higher than **PF<sub>OXY</sub>DT-TPD<sub>DMO</sub>**. The optical spectra of polymer thin films showed two absorption bands, which indicated a pronounced vibronic structure for **PF<sub>OXY</sub>DT-TPD<sub>OXY</sub>**. This, in turn, indicates a highly

crystalline arrangement within the polymer. These results are consistent with the results of XRD analysis. Although the majority of interlayer chains of all the polymers observed by XRD analysis are located at the same angle, **PF<sub>OXY</sub>DT-TPD<sub>OXY</sub>** exhibited another intense peak and a slightly smaller  $\pi$ - $\pi$  stacking distance than **PF<sub>O</sub>DT-TPD<sub>DMO</sub>**. Furthermore, the electrochemical results suggest that the band gaps of those polymers substituted with TEG side chains are larger than those of polymers fully substituted with alkyl side chains (**PF<sub>O</sub>DT-TPD<sub>DMO</sub>**). This observation is attributed to the influence of TEG substitution in decreasing the LUMO and HOMO levels. The LUMOs are still high enough to transfer the electrons of the prepared conjugated polymers to the most widely used electron acceptor, PCBM. This work would open up new avenues for researchers to use such molecules on the side chains of conjugated polymers, such as oligo(propylene glycol) (OPG), to design new alternating donor-acceptor conjugated polymer materials for OPV devices with less toxicity and optimal performance.

### 3.4 References

1. G. Yu, J. Gao, J. C. Hummelen, F. Wudl and A. J. Heeger, *Science*, 1995, **270**, 1789-1791.
2. Z. Yi, S. Wang and Y. Liu, *Advanced Materials*, 2015, **27**, 3589-3606.
3. X. Guo, M. Baumgarten and K. Müllen, *Progress in Polymer Science*, 2013, **38**, 1832-1908.
4. T. Lei, J. Y. Wang and J. Pei, *Chemistry of Materials*, 2014, **26**, 594-603.
5. R. Kim, B. Kang, D. H. Sin, H. H. Choi, S.-K. Kwon, Y.-H. Kim and K. Cho, *Chemical Communications*, 2015, **51**, 1524-1527.
6. J. Mei and Z. Bao, *Chemistry of Materials*, 2014, **26**, 604-615.
7. B. Kang, R. Kim, S. B. Lee, S.-K. Kwon, Y.-H. Kim and K. Cho, *Journal of the American Chemical Society*, 2016, **138**, 3679.
8. K. Kranthiraja, K. Gunasekar, N. Chakravarthi, M. Song, J. H. Moon, J. Y. Lee, I.-N. Kang and S.-H. Jin, *Dyes and Pigments*, 2015, **123**, 100-111.
9. X. Chen, Z. Zhang, J. Liu and L. Wang, *Polymer Chemistry*, 2017, **8**, 5496-5503.
10. W.-S. Li, Y. Yamamoto, T. Fukushima, A. Saeki, S. Seki, S. Tagawa, H. Masunaga, S. Sasaki, M. Takata and T. Aida, *Journal of the American Chemical Society*, 2008, **130**, 8886.
11. X. Zhang, Z. Chen and F. Würthner, *Journal of the American Chemical Society*, 2007, **129**, 4886-4887.
12. M. Shao, Y. He, K. Hong, C. Rouleau, D. Geohegan and K. Xiao, *Polymer Chemistry*, 2013, **4**, 5270-5274.
13. Y. Chen, S. Zhang, Y. Wu and J. Hou, *Advanced Materials*, 2014, **26**, 2744-2749.
14. C. Kanimozhi, N. Yaacobi-Gross, K. W. Chou, A. Amassian, T. D. Anthopoulos and S. Patil, *Journal of the American Chemical Society*, 2012, **134**, 16532.
15. B. Meng, H. Song, X. Chen, Z. Xie, J. Liu and L. Wang, *Macromolecules*, 2015, **48**, 4357-4363.
16. X. Chen, Z. Zhang, Z. Ding, J. Liu and L. Wang, *Angewandte Chemie-International Edition*, 2016, **55**, 10376-10380.
17. Y. Cheng, S. Yang and C. S. Hsu, *Chemical Reviews*, 2009, **109**, 5868-5923.
18. S. L. C. Hsu, Y. C. Lin, R. F. Lee, C. Sivakumar, J. S. Chen and W. Y. Chou, *Journal of Polymer Science Part A: Polymer Chemistry*, 2009, **47**, 5336-5343.
19. Q. Jiang, S. Zhen, D. Mo, K. Lin, S. Ming, Z. Wang, C. Liu, J. Xu, Y. Yao, X. Duan, D. Zhu and H. Shi, *Journal of Polymer Science Part A: Polymer Chemistry*, 2016, **54**, 325-334.



20. L. S. Liao, M. K. Fung, C. S. Lee, S. T. Lee, M. Inbasekaran, E. P. Woo and W. W. Wu, *Applied Physics Letters*, 2000, **76**, 3582-3584.
21. Y. J. Cheng, S. H. Yang and C. S. Hsu, *Chemical Reviews*, 2009, **109**, 5868-5923.
22. L. Zhou, X. Bao, Q. Liu, J. Yu, Y. Chen, R. Yang and M. Sun, *Journal of Applied Polymer Science*, 2014, **131**, 40478.
23. O. Inganäs, M. Svensson, F. Zhang, A. Gadisa, N. K. Persson, X. Wang and M. R. Andersson, *Materials Science & Processing*, 2004, **79**, 31-35.
24. E. Zhou, C. Yang, K. Hashimoto, S. Yamakawa and K. Tajima, *Chemistry of Materials*, 2009, **21**, 4055-4061.
25. F. Zhang, W. Mammo, L. M. Andersson, S. Admassie, M. R. Andersson and O. Inganäs, *Advanced Materials*, 2006, **18**, 2169-2173.
26. W. Wang, L. Liang, M. Zhou, M. Sun, S. Yan and Q. Ling, *Macromolecular Research*, 2015, **23**, 30-37.
27. J. W. Rumer, C. K. L. Hor, I. Meager, C. P. Yau, Z. Huang, C. B. Nielsen, S. E. Watkins, H. Bronstein and I. McCulloch, *Journal of Organic Semiconductors*, 2013, **1**, 30-35.
28. X. Guo, H. Xin, F. S. Kim, A. D. T. Liyanage, S. A. Jenekhe and M. D. Watson, *Macromolecules*, 2011, **44**, 269-277.
29. W. G. Nigh, *Journal of Chemical Education*, 1975, **52**, 670-671.
30. S. Y. Chang, P. H. Lin and C. Y. Liu, *RSC Advances*, 2014, **4**, 35868-35878.

>>

**CHAPTER IV**  
**EFFECTS OF TRIETHYLENE GLYCOL**  
**SUBSTITUTION PATTERN ON THE PROPERTIES**  
**OF THIENYL/THIENO-PYRROLE ALTERNATING**  
**COPOLYMERS**

## 4.1. Introduction

Since their discovery in the mid-1970s, organic semiconductor polymers have become useful materials for scientific and industrial communities to use in optoelectronic devices<sup>1, 2</sup>—such as light emitting diodes (OLEDs)<sup>3, 4</sup>, field effect transistor (OFETs)<sup>5, 6</sup>, polymer solar cells (PSCs)<sup>3, 7</sup>, and organic-inorganic hybrid perovskite solar cells (HPSCs)<sup>8</sup>—because this class of materials is inexpensive to manufacture and easily solution-processed into thin, flexible films through printing methods<sup>2, 9</sup> (e.g. roll-to-roll, inkjet, spin coating). In the case of organic solar cells, the essential element of a cell is the photovoltaic active layer, which is made of a mixture of electron-rich conjugated polymers and electron-deficient fullerene derivatives, typically [6,6]-phenyl-C<sub>71</sub>-butyric acid methyl ester (PC<sub>71</sub>BM) or [6,6]-phenyl-C<sub>61</sub>-butyric acid methyl ester (PC<sub>61</sub>BM).<sup>10</sup> The device's performance relies largely on this complex design<sup>11</sup>, in which the excitons (bound electron and hole pairs) are generated from a donor polymer, separated into free carriers at the donor-acceptor interface, and then transported to electrodes, producing photocurrent. However, the high value of exciton binding energy, which results from low dielectric constants of organic semiconductor polymers ( $\epsilon_r \approx 2-4$ ), leads to low efficiency of exciton dissociation and low power conversion efficiency.<sup>12</sup> Furthermore, the energy of frontier molecular energy levels of conjugated polymers is of great importance in developing efficient exciton separation as modifying the highest occupied molecular orbital (HOMO) and the lowest unoccupied molecular orbital (LUMO) energy levels to decrease the HOMO-LUMO gap will decrease the energy level offset for the HOMO or LUMO between the donor-acceptor materials and diminish the driving force for exciton separation, providing poor device efficiency.<sup>13-15</sup>

In order to achieve a high power conversion efficiency in organic solar cells, increasing the dielectric constant of conjugated polymers is required to overcome the exciton binding energy for fast charge separation<sup>12</sup>; this boost minimises the charge recombination process, which enables the fabrication of PSC devices with a thicker active layer for better photon harvesting, thereby improving the device's performance.<sup>3, 12</sup> Another approach to achieve efficient performance is to optimise the HOMO/LUMO energy level positions of the

donor polymers and the acceptors to reduce the energy offset without losing any photo-generated voltage.<sup>16, 17</sup> Further efficiency improvements include the modification of chemical functional groups on the backbone of the polymer chains to tune the solubility, molecular packing, and morphology.<sup>6, 15, 18, 19</sup>

To capture the above-mentioned properties in donor-acceptor moieties, polarisable oligo ethylene glycol (OEG) side chains are effective in enhancing the dielectric constant of organic semiconductor polymers. They are easily functionalised on the polymer backbones and are more flexible than alkyl chains, favouring not only a close intermolecular  $\pi$ - $\pi$  stacking between the polymer backbones for better polymer charge carrier mobility, but also easy reorientations of the dipole moments, which increase the dielectric constant.<sup>7, 12, 20</sup> OEG moieties are known for their solubility in more hydrophilic solvents (e.g. water and alcohol), allowing the resulting polymers to process with less of an environmental impact on device production.<sup>21</sup>

In 2006, Breselge et al. introduced the hydrophilic substitution OEG on a poly(p-phenylene vinylene) (PPV) and found that the value of the dielectric constant ( $\epsilon_r = 5.5$ ) increased almost two times higher than MDMO-PPV ( $\epsilon_r = 3$ ). However, the output performance of the solar cell was poor due to the BHJ morphology issue.<sup>22</sup> Recently, Wang et al. investigated the consequences of OEG on polyfluorenes and indicated that OEG side chains reduced the  $\pi$ - $\pi$  stacking distance toward 0.41 nm, which is lower than their alkylated counterparts, resulting in a low LUMO energy level, an increased hole mobility, a red-shifted absorption spectrum, and a low-energy bandgap.<sup>7</sup> A year later, the same group built a new polymer series of PDPP3T-O<sub>x</sub> with branched OEG side chains. The glycoated polymers shortened the  $\pi$ - $\pi$  stacking distance of the polymer backbone from 0.38 nm to 0.36 nm, reduced the optical bandgap, and increased the dielectric constant, which outperformed the alkylated PDPP3T-C<sub>20</sub>.<sup>3</sup> Therefore, the swiftness and flexibility of hydrophilic OEG substitutions make them favourable replacements for alkyl substitutions in donor-acceptor conjugated polymers within optoelectronic devices.

To validate these concepts, we designed a new series of alternating donor-acceptor conjugated polymers comprising thienyl units and thieno-pyrrole dione units, T-TPD copolymers, which contain triethylene glycol substituents on thiophene and 5-thieno[3,4-c]pyrrole-4,6-dione moieties for poly((3-((2-(2-methoxyethoxy)ethoxy)methyl)thiophene)-2,5-diyl-*alt*-5-(2-(2-(2-methoxyethoxy)ethoxy)ethyl)-4*H*-thieno[3,4-c]pyrrole-4,6(5*H*)-dione) [**PT<sub>OXY</sub>-TPD<sub>OXY</sub>**]; and only thiophene moiety for poly((3-((2-(2-methoxyethoxy)ethoxy)methyl)thiophene)-2,5-diyl-*alt*-5-(3,7-dimethyloctyl)-4*H*-thieno[3,4-c]pyrrole-4,6(5*H*)-dione) [**PT<sub>OXY</sub>-TPD<sub>DMO</sub>**]. For comparison purposes, polymer with alkyl side chains on both units has been included to afford poly((3-(2-octyldodecyl)thiophene)-2,5-diyl-*alt*-5-(3,7-dimethyloctyl)-4*H*-thieno[3,4-c]pyrrole-4,6(5*H*)-dione) [**PT<sub>ODD</sub>-TPD<sub>DMO</sub>**] (see **Figure 4.1**). We present in this chapter our studies on the properties and characterisation of these polymers and the effect of the hydrophilic substitutions on the photophysical and the electrochemical properties of the synthesised copolymers, as well as their impact on the intermolecular distance along the  $\pi$ - $\pi$  stacking.

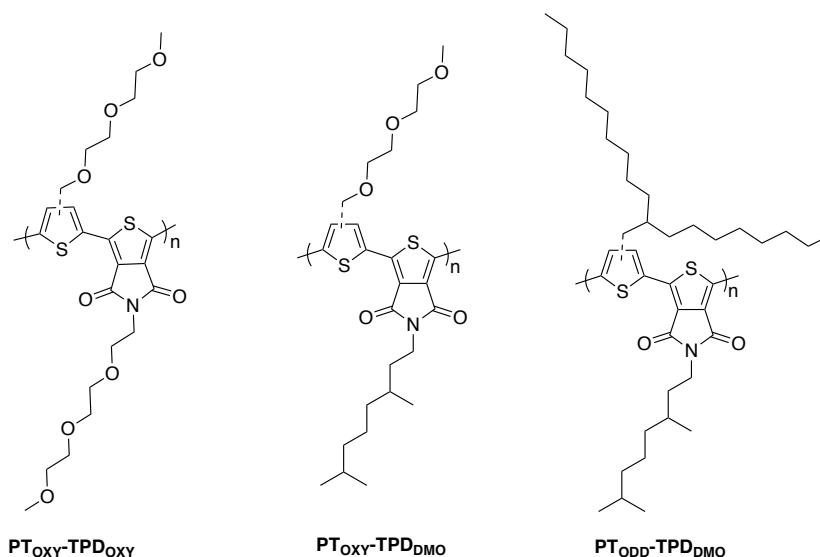
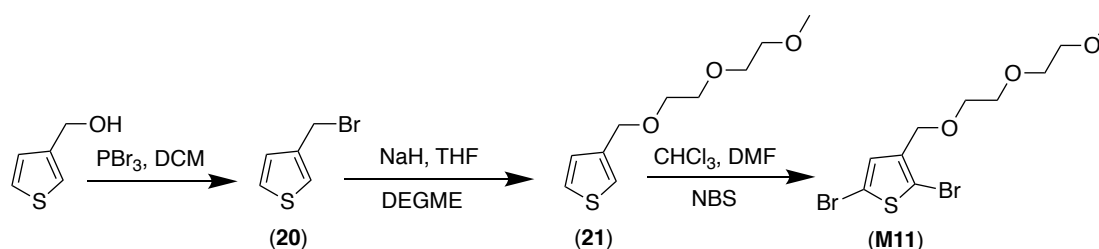


**Figure 4.1.** Polymer structures of **PT<sub>OXY</sub>-TPD<sub>OXY</sub>**, **PT<sub>OXY</sub>-TPD<sub>DMO</sub>**, and **PT<sub>ODD</sub>-TPD<sub>DMO</sub>**.

## 4.2 Results and Discussion

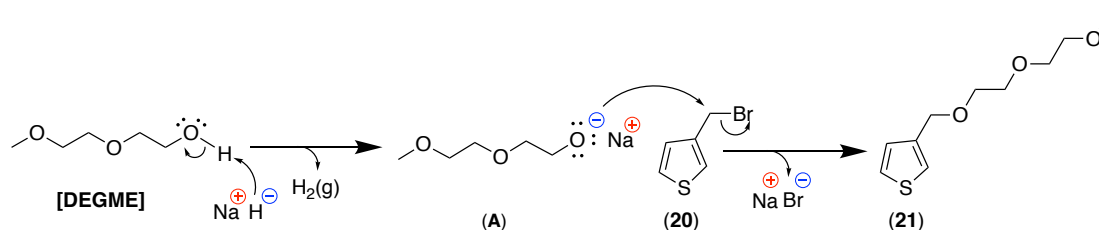
### 4.2.1 Monomer synthesis

TPD derivatives 5-(3,7-dimethyloctyl)-4*H*-thieno[3,4-*c*]pyrrole-4,6(5*H*)-dione (**M7**) and 5-(2-(2-(2-methoxyethoxy)ethoxy)ethyl)-4*H*-thieno[3,4-*c*]pyrrole-4,6(5*H*)-dione (**M8**) were already described in Chapters II and III. The synthetic steps of 3-((2-(2-methoxyethoxy)ethoxy)methyl)thiophene (**M11**) is depicted in **Scheme 4.1**. 3-(2-octyldodecyl)thiophene (**M12**) was synthesized by the Iraqi group.



**Scheme 4.1.** Synthesis routes for **M11**.

**M11** was prepared from commercial 3-thiophenemethanol, which was first converted to 3-(bromomethyl)thiophene (**20**) using phosphorus tribromide. The resulting product (**20**) underwent the Williamson reaction, employing sodium hydride as the base with diethylene glycol monomethyl ether (DEGME) to deprotonate the alcohol and produce a conjugate base anion ( $\text{RO}^-$ ) (**A**) which acts as the nucleophile and attacks 3-(bromomethyl)thiophene (**20**), to yield 3-((2-(2-methoxyethoxy)ethoxy)methyl)thiophene (**21**), as described in **Scheme 4.2**.



**Scheme 4.2.** Proposed mechanism for the synthesis of 3-((2-(2-methoxyethoxy)ethoxy)methyl)thiophene (**21**).

Compound (**21**) was brominated in chloroform using *N*-bromosuccinimide (NBS) in DMF to obtain the desired monomer, 2,5-dibromo-3-((2-(2-methoxyethoxy)ethoxy)methyl)thiophene (**M11**).

$^1\text{H}$  NMR spectroscopy was used to confirm the chemical structures of **M11** and **M12**. As shown in **Figure 4.2**, two singlet peaks at 7.00 ppm and 4.45 ppm corresponded with the proton attached to the thiophene ring and the first hydrogen proton of the TEG moieties bonded to the thiophene ring system. The peaks between 3.69 ppm and 3.41 ppm reflected the rest of the TEG moieties. On the other hand, **Figure 4.3** of **M12** showed a singlet peak resonated at 6.76 ppm, which corresponded to the single thiophene's hydrogen proton, and peaks with different patterns resonated separately at different frequencies below 3.5 ppm, which accounted for the octyldodecyl side chain.

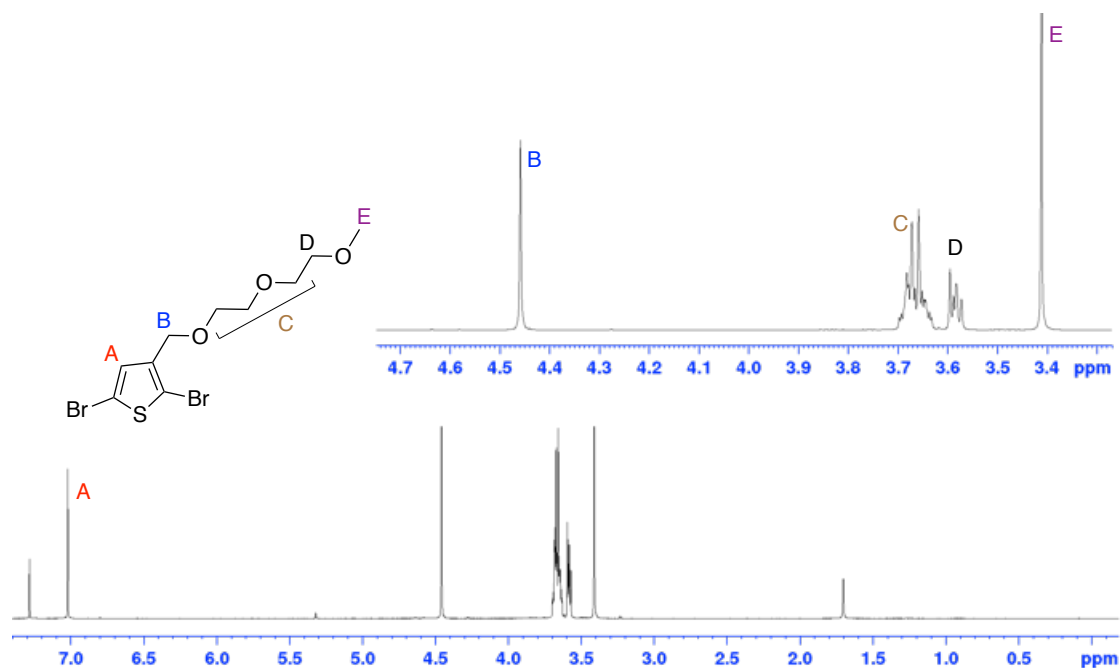


**Figure 4.2.**  $^1\text{H}$  NMR spectrum of **M11** in  $\text{CDCl}_3$

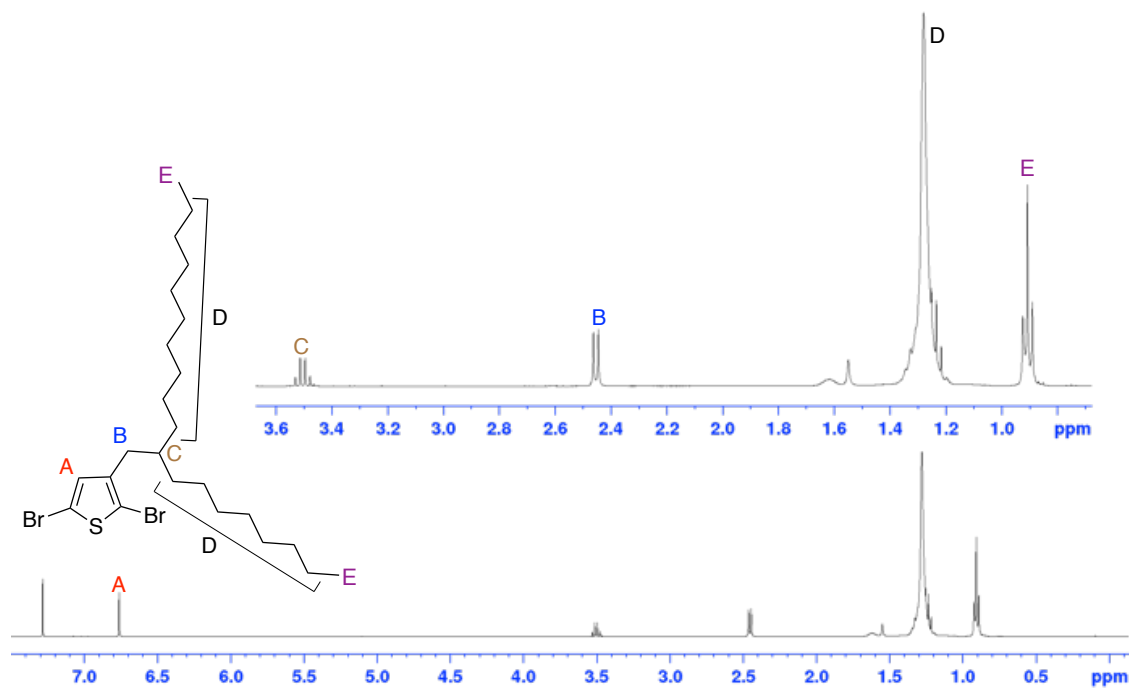


**Figure 4.3.**  $^1\text{H}$  NMR spectrum of **M12** in  $\text{CDCl}_3$ .

#### 4.2.2 Polymers synthesis and characterisation

**Figure 4.1** shows the molecular structure of the conjugated polymers **PT<sub>OXY</sub>-TPD<sub>OXY</sub>**, **PT<sub>OXY</sub>-TPD<sub>DMO</sub>**, and **PT<sub>ODD</sub>-TPD<sub>DMO</sub>**. The three alternating conjugated copolymers of thiophene and theino[3,4-*c*]pyrrole-4,6-dione were synthesised through palladium-catalysed direct (hetero)arylation polymerisation with a reaction time of four hours and a procedure similar to a literature procedure.<sup>23</sup> After that, all the polymers were isolated using a Soxhlet extraction using acetone, hexane, and chloroform in succession. Solvents like methanol were avoided in this extraction, since hot methanol can remove the desired amphiphilic polymers, as well as unreacted monomers and catalyst residues. For example, in this project, the total yield of pure **PT<sub>OXY</sub>-TPD<sub>OXY</sub>** after further purification, reduced to 51%. Further details of the polymer preparation are provided in the experimental section. The chemical structures of the three polymers were confirmed by  $^1\text{H}$  NMR and elemental analysis. In the  $^1\text{H}$  NMR spectrum of **PT<sub>OXY</sub>-TPD<sub>OXY</sub>**, **PT<sub>OXY</sub>-TPD<sub>DMO</sub>** and **PT<sub>ODD</sub>-TPD<sub>DMO</sub>** (Chapter VII, Figure S10, S11 and S12), the characteristic peaks at 8.08-7.94 ppm are assigned to the hydrogen atom in the thiophene ring. The peak due to proton in  $-\text{OCH}_2-$  linked to thiophene ring is at 4.75-



4.74 ppm. The chemical shift from 3.89 to 3.31 is due to the protons of the polar side chains; the peaks below 3.31 ppm are due to the protons of non-polar side chains. The molecular weights of the three polymers were investigated through high temperature gel permeation chromatography (GPC) analysis, using 1,2,4-trichlorobenzene (TCB) as the eluent and a series of monodisperse polystyrene standards as the calibration standards. As listed in **Table 4.1-a**, **PT<sub>OXY</sub>-TPD<sub>OXY</sub>** revealed a  $M_n$  of 1.6 kDa, while **PT<sub>OXY</sub>-TPD<sub>DMO</sub>** had a  $M_n$  of 29.4 kDa. This low molecular weight is apparently due to the strong influence of the polar nature of **PT<sub>OXY</sub>-TPD<sub>OXY</sub>**, which reduces the solubility in various solvents (e.g. chloroform, THF, CB, and TCB) and prefers to form aggregates in the resulting solutions. On the other hand, **PT<sub>ODD</sub>-TPD<sub>DMO</sub>** has a relatively high  $M_n$  of 13.3 kDa compared to **PT<sub>OXY</sub>-TPD<sub>OXY</sub>** as a result of the  $\pi$ - $\pi$  stacking disruptions caused by the branched alkyl side chains on **PT<sub>ODD</sub>-TPD<sub>DMO</sub>**.

**Table 4.1.** (a) Molecular, optical, and (b) electrochemical data for **PT<sub>OXY</sub>-TPD<sub>OXY</sub>**, **PT<sub>OXY</sub>-TPD<sub>DMO</sub>** and **PT<sub>ODD</sub>-TPD<sub>DMO</sub>**.

(a)

| Polymer   | Molecular data <sup>b</sup> |       |      | Optical data          |                       |                                  |
|---|-----------------------------|-------|------|-----------------------|-----------------------|----------------------------------|
|   | (kDa)                       |       |      | $\lambda_{\max}$ (nm) |                       | (eV)                             |
|   | $M_n$                       | $M_w$ | PDI  | Solution              | Film                  | $E_g^c$                          |
| <b>PT<sub>OXY</sub>-TPD<sub>OXY</sub><sup>a</sup></b> | 1.6                         | 1.7   | 1.06 | 483 <sup>f</sup>      | 565 <sup>f</sup> /604 | 1.86 ( $\pm 0.02$ ) <sup>g</sup> |
| <b>PT<sub>OXY</sub>-TPD<sub>DMO</sub><sup>a</sup></b> | 29.4                        | 48.1  | 1.64 | 496 <sup>f</sup> /585 | 575 <sup>f</sup> /610 | 1.84 ( $\pm 0.05$ ) <sup>g</sup> |
| <b>PT<sub>ODD</sub>-TPD<sub>DMO</sub><sup>a</sup></b> | 13.3                        | 18.0  | 1.35 | 465 <sup>f</sup>      | 512 <sup>f</sup>      | 1.95 ( $\pm 0.01$ ) <sup>g</sup> |

(b)

| Polymer   | Electrochemical data |                   |         |
|---|----------------------|-------------------|---------|
|   | (eV)                 |                   |         |
|   | HOMO <sup>d</sup>    | LUMO <sup>d</sup> | $E_g^e$ |
| <b>PT<sub>OXY</sub>-TPD<sub>OXY</sub><sup>a</sup></b> | -5.41                | -3.65             | 1.76    |
| <b>PT<sub>OXY</sub>-TPD<sub>DMO</sub><sup>a</sup></b> | -5.40                | -3.45             | 1.95    |
| <b>PT<sub>ODD</sub>-TPD<sub>DMO</sub><sup>a</sup></b> | -5.42                | -3.56             | 1.86    |

<sup>a</sup>Collected in chloroform. <sup>b</sup>GPC measurements in 1,2,4-trichlorobenzene as the eluent. <sup>c</sup>Optical band gap estimated from the film onset. <sup>d</sup>HOMO/LUMO levels calculated from the oxidation/reduction onset. <sup>e</sup>Electrochemical band gap. <sup>f</sup>Wavelength of maximum absorbance. <sup>g</sup>Range error at the peak of the absorbance curve of a different extinction coefficient.

### 4.2.3 Polymers optical properties

Figure 4.4 shows the normalised UV-vis absorption spectra of the three polymers in dilute chloroform solution and in films. Table 4.1-a summarises their optical properties. In the solution, all the polymers showed a broad absorption ranging from 465 nm to 496 nm, attributed to an intramolecular charge transfer (ICT) between the thiophene-based donor units and the TPD-based acceptor units. The absorption shoulder peak at 585 nm in **PT<sub>OXY</sub>-TPD<sub>DMO</sub>** is explained by the aggregation of the polymer. Upon dynamic light scattering measurements, particles of a diameter of  $\sim 2 \mu\text{m}$  were observed in the chloroform solution, indicating that this polymer formed a colloidal mixture rather than a true solution

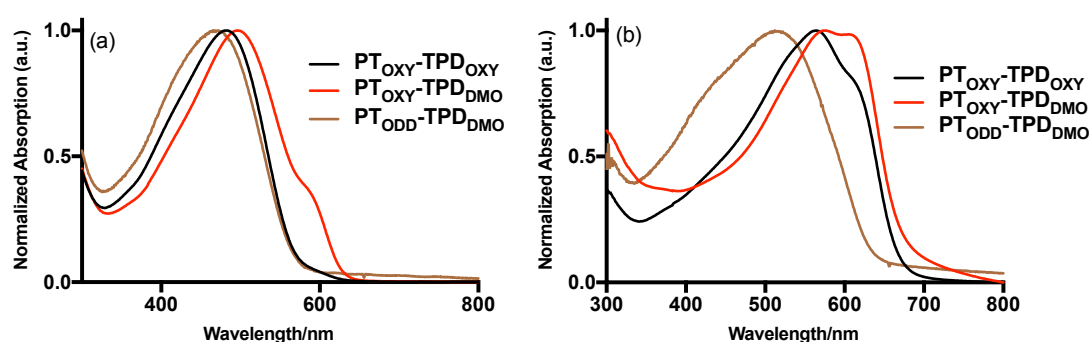
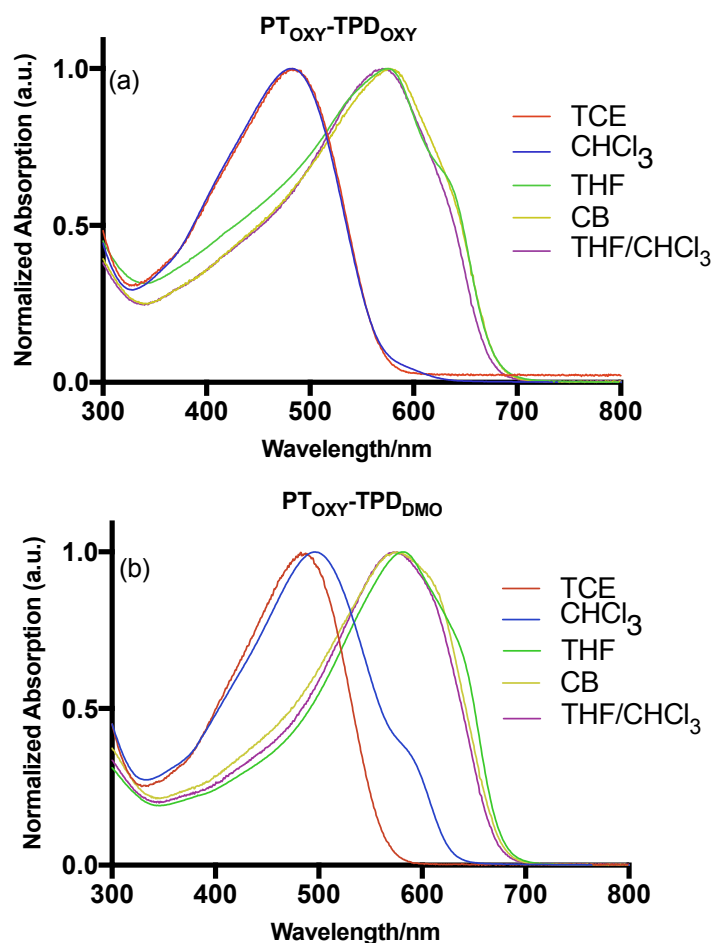


Figure 4.4. Normalised optical absorption spectra of **PT<sub>OXY</sub>-TPD<sub>OXY</sub>**, **PT<sub>OXY</sub>-TPD<sub>DMO</sub>**, and **PT<sub>ODD</sub>-TPD<sub>DMO</sub>** in (a) chloroform solution and (b) thin films.

The aggregation phenomenon of the polymers was further studied using solvents of different polarities. The absorption shape of **PT<sub>OXY</sub>-TPD<sub>OXY</sub>** and **PT<sub>OXY</sub>-TPD<sub>DMO</sub>** in THF, chlorobenzene (CB), or a mixture of THF/chloroform (50%/50% v/v) solutions provided similar spectra to their films (see Figure 4.5), indicating that the polymer molecules tend to form aggregates of colloidal particles. Nevertheless, the absorption shape of **PT<sub>OXY</sub>-TPD<sub>OXY</sub>** and **PT<sub>OXY</sub>-TPD<sub>DMO</sub>** in 1,1,2,2-TCE solutions exhibited a clear difference from solution to film as a result of the solubilising power of this solvent in the aggregation. DLC measurements detected particles in the TCE solution with a diameter of  $\sim 1 \mu\text{m}$ , however, which suggests that **PT<sub>OXY</sub>-TPD<sub>DMO</sub>** still prefers to aggregate due to hydrophilic substitutions on the polymer backbones.



**Figure 4.5.** Normalised optical absorption spectra of (a)  $\text{PT}_{\text{OXY}}\text{-TPD}_{\text{OXY}}$  and (b)  $\text{PT}_{\text{OXY}}\text{-TPD}_{\text{DMO}}$  in different solutions.

**Figure 4.4** shows that the absorption spectrum of the polymer thin films cast from the chloroform are red shifted by 82 nm, 79 nm, and 56 nm for  $\text{PT}_{\text{OXY}}\text{-TPD}_{\text{OXY}}$ ,  $\text{PT}_{\text{OXY}}\text{-TPD}_{\text{DMO}}$ , and  $\text{PT}_{\text{ODD}}\text{-TPD}_{\text{DMO}}$ , respectively, presumably due to strong non-covalent interactions (e.g.  $\pi$ -stacking) between the polymer chains in the solid state. The optical band gaps ( $E_g$  eV) of the polymers were estimated from film onset absorptions; they were 1.86 eV, 1.84 eV, and 1.95 eV for  $\text{PT}_{\text{OXY}}\text{-TPD}_{\text{OXY}}$ ,  $\text{PT}_{\text{OXY}}\text{-TPD}_{\text{DMO}}$ , and  $\text{PT}_{\text{ODD}}\text{-TPD}_{\text{DMO}}$ , respectively. This strong red shift and small band gap of  $\text{PT}_{\text{OXY}}\text{-TPD}_{\text{DMO}}$  are likely due to the coplanarity of polymer backbone with longer conjugation length.  $\text{PT}_{\text{OXY}}\text{-TPD}_{\text{DMO}}$  displayed a more pronounced distinct shoulder at 610 nm, while the vibronic shoulder of  $\text{PT}_{\text{OXY}}\text{-TPD}_{\text{OXY}}$  showed at 604 nm. Although this observation might indicate a strong interchain interaction for  $\text{PT}_{\text{OXY}}\text{-TPD}_{\text{OXY}}$  and  $\text{PT}_{\text{OXY}}\text{-TPD}_{\text{DMO}}$ , it is also possible that the shoulder in non-uniform thin film absorption, particularly of  $\text{PT}_{\text{OXY}}\text{-TPD}_{\text{DMO}}$ , is a result of film made of solution

containing particle aggregates. The thin films of  $\text{PT}_{\text{OXY}}\text{-TPD}_{\text{OXY}}$  and  $\text{PT}_{\text{OXY}}\text{-TPD}_{\text{DMO}}$  that cast from different solvents, as shown in **Figure 4.6**, are further studied.  $\text{PT}_{\text{OXY}}\text{-TPD}_{\text{DMO}}$  thin films revealed that different shoulder shapes of the absorption spectrum are due to a number of aggregate particles does not completely dissolve to form a true solution, which results in the formation of different absorptions. This cause would slightly apply to  $\text{PT}_{\text{OXY}}\text{-TPD}_{\text{OXY}}$ , especially to that casts from THF solvent as a result of its solution already having aggregation (see **Figure 4.6** (a)). Besides to aggregate particles within the polymers,  $\text{PT}_{\text{OXY}}\text{-TPD}_{\text{OXY}}$  and  $\text{PT}_{\text{OXY}}\text{-TPD}_{\text{DMO}}$  would probably reflect some crystallisation in the resulting thin film spectrum. This feature would not apply to  $\text{PT}_{\text{ODD}}\text{-TPD}_{\text{DMO}}$  due to the strong steric hindrance of branched alkyl chains along the backbone, which increases the backbone torsion, inducing a blue shift of the absorption spectrum and a wide band gap (see **Figure 4.4** (b)).

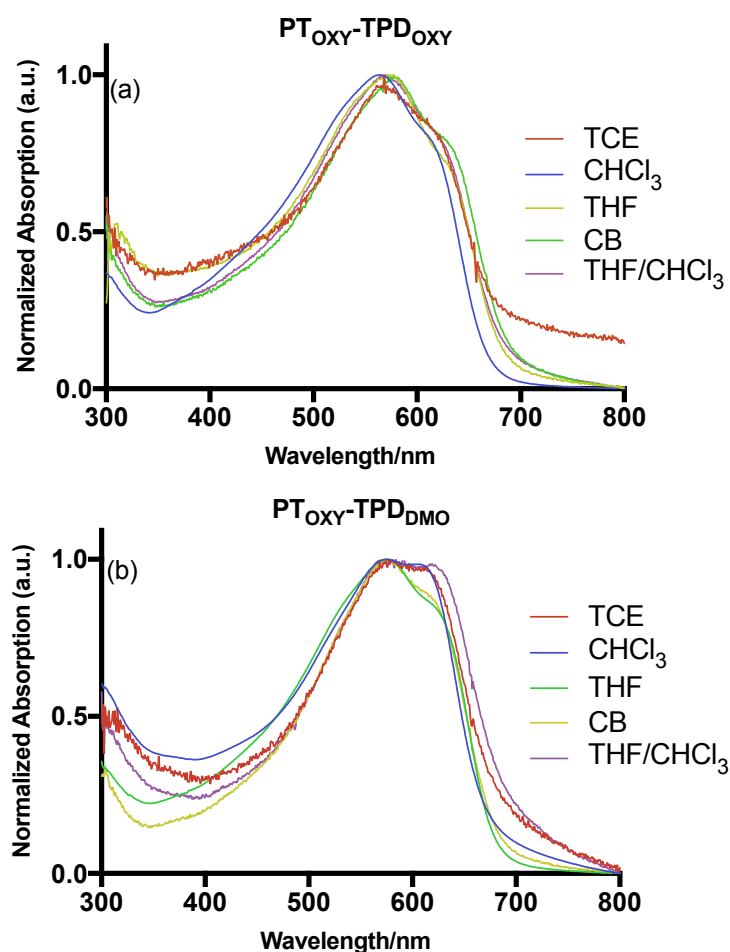


**Figure 4.6.** Normalized optical absorption spectra of (a)  $\text{PT}_{\text{OXY}}\text{-TPD}_{\text{OXY}}$  and (b)  $\text{PT}_{\text{OXY}}\text{-TPD}_{\text{DMO}}$  cast from different solutions.

#### 4.2.4 Polymers electrochemical properties

The electrochemical features of the three polymers were studied through cyclic voltammetry (CV) to determine the energy levels of their HOMO and LUMO, as shown in **Figure 4.7a-b**. The diagram in **Figure 4.7c** presents the position of the frontier molecular orbital of all three polymers' HOMO and LUMO levels according to their onset potential of the oxidation waves and reduction waves. The results are also summarised in **Table 4.1-b**. The HOMO energy levels of **PT<sub>OXY</sub>-TPD<sub>OXY</sub>**, **PT<sub>OXY</sub>-TPD<sub>DMO</sub>** and **PT<sub>ODD</sub>-TPD<sub>DMO</sub>** (-5.41 eV, -5.40 eV, and -5.42 eV, respectively) had only ~0.02 eV difference between them due to their identical backbones, regardless of the substitutions. Meanwhile, the LUMO energy levels of all the polymers were reduced from -3.45 eV to -3.65 eV when the substitutions of alkyl side chains were replaced with full flexible glycol chains on the same backbones. The position of the LUMO level of **PT<sub>OXY</sub>-TPD<sub>DMO</sub>** also upshifted, compared to **PT<sub>OXY</sub>-TPD<sub>OXY</sub>** and **PT<sub>ODD</sub>-TPD<sub>DMO</sub>**, possibly due to the injection barriers at the electrode and polymer contact interface, resulting in a large band gap. Compared to **PT<sub>ODD</sub>-TPD<sub>DMO</sub>**, **PT<sub>OXY</sub>-TPD<sub>OXY</sub>** with triethylene glycol (TEG) on both the donor and acceptor units demonstrated a great decrease in LUMO level while retaining an almost constant HOMO level, leading to smaller band gap. This is mainly attributed to the extended coplanar polymer backbone—a result of high flexible TEG side chains that caused a strong compact  $\pi$ - $\pi$  stacking in their backbones. The HOMO levels of the three polymers indicates a high air stability of these materials towards oxidative degradation, while the electron donating conjugated polymers' LUMO findings provide a sufficient driving force for transferring electrons towards the electron acceptor, PCBM.

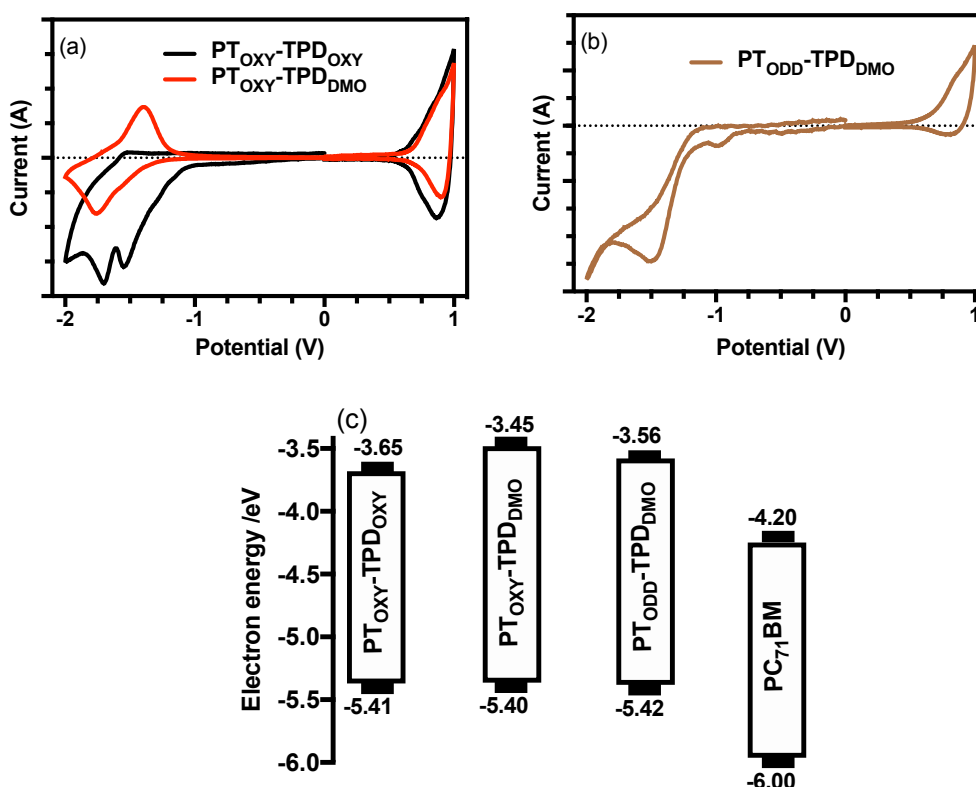


**Figure 4.7.** Cyclic voltammograms of (a) **PT<sub>OXY</sub>-TPD<sub>OXY</sub>** and **PT<sub>OXY</sub>-TPD<sub>DMO</sub>**, (b) **PT<sub>ODD</sub>-TPD<sub>DMO</sub>**, and (c) energy levels diagram of all the respective polymers and PCBM.

#### 4.2.5 Polymers thermal properties

As the operational lifetime of polymer solar cells (PSCs) is linearly correlated to the thermal stability of the active layer materials; therefore, a high temperature ( $T_d$ ) to thermal degradation of the conjugated polymer is required. The thermal stability value of two synthesized polymers, **PT<sub>OXY</sub>-TPD<sub>OXY</sub>** and **PT<sub>OXY</sub>-TPD<sub>DMO</sub>**, was measured by thermogravimetric analysis in a range from room temperature to 800 °C in inert atmosphere. **Figure 4.8** shows that all the polymers have good thermal stability—~ 340 °C for **PT<sub>OXY</sub>-TPD<sub>OXY</sub>** and ~370 °C for **PT<sub>OXY</sub>-TPD<sub>DMO</sub>**—with ~ 45-40% total weight loss, possibly corresponding to the degradation of the substitution chains. The degradation of **PT<sub>OXY</sub>-TPD<sub>DMO</sub>** involved two degradation steps, reflecting the loss of hydrophilic side chains in the first stage and then the hydrophobic side chains afterwards. The findings show that all the synthesized conjugated polymers could potentially be used in PSCs with long time durability.

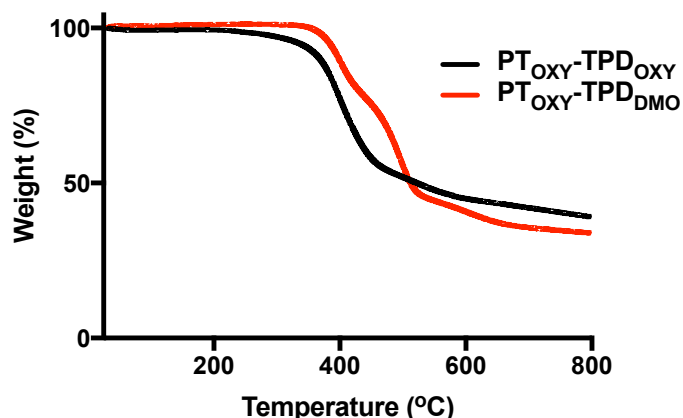


**Figure 4.8.** TGA curve of  $\text{PT}_{\text{OXY}}\text{-TPD}_{\text{OXY}}$  and  $\text{PT}_{\text{OXY}}\text{-TPD}_{\text{DMO}}$ .

#### 4.2.6 Polymers structure properties

To examine the effect of the substitution of the polymers with different substituents on the molecular organization of the resulting polymers in the solid state, powder X-ray diffraction (PXRD) analyses were conducted (see **Figure 4.9**). The reflected angle and  $d$  spacing values are tabulated in **Table 4.2**. The alternating copolymers,  $\text{PT}_{\text{OXY}}\text{-TPD}_{\text{OXY}}$  and  $\text{PT}_{\text{OXY}}\text{-TPD}_{\text{DMO}}$ , showed no sign of lamella stacking at low angle diffraction ( $2^{\circ}$ - $10^{\circ}$ ), indicating that the inherent nature of all the copolymers generally forms amorphous domains in their solid state. This lack of crystalline features in the copolymers might be attributed to the absence of the thin film deposition technique and the resultant steric hindrance of the side chains, particularly with  $\text{PT}_{\text{OXY}}\text{-TPD}_{\text{DMO}}$ . However, major reflection peaks were observed at  $24.75^{\circ}$  (corresponding to a distance of  $\sim 0.36$  nm) for  $\text{PT}_{\text{OXY}}\text{-TPD}_{\text{OXY}}$  and around  $21.66^{\circ}$  and  $24.07^{\circ}$  ( $\sim 0.37$ - $0.41$  nm) for  $\text{PT}_{\text{OXY}}\text{-TPD}_{\text{DMO}}$ , which relates to a  $\pi$ - $\pi$  stacking distance between co-planar alkyl chains. These reflection values are nearly similar to those reported for PDPP3T- $\text{O}_x$  and the other alternating copolymers.<sup>3, 6, 7</sup>

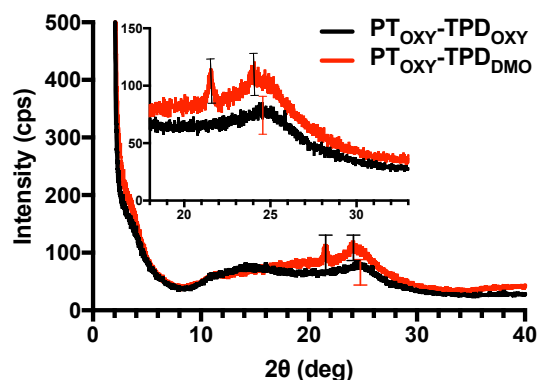


**Figure 4.9.** Powder XRD patterns of **PT<sub>OXY</sub>-TPD<sub>OXY</sub>** and **PT<sub>OXY</sub>-TPD<sub>DMO</sub>**.

Compared to **PT<sub>OXY</sub>-TPD<sub>DMO</sub>**, **PT<sub>OXY</sub>-TPD<sub>OXY</sub>** displays the smallest  $\pi$ -stacking distance due to having less sterically hindering triethylene glycol (TEG) side chain pendants onto thieno[3,4-c]pyrrole-4,6-dione than **PT<sub>OXY</sub>-TPD<sub>DMO</sub>** which has bulky branched alkyl side chains on the same unit. Furthermore, **PT<sub>OXY</sub>-TPD<sub>DMO</sub>** shows a slightly sharp reflection peak at 21.66°, which represents on interlayer distance between chains of 0.41 nm, in addition to a reflection peak at 24.07° with an inter-chain spacing of 0.37 nm. The results conclude that as more hydrophilic side chains are grafted onto the polymer backbone, a closer  $\pi$ -stacking of the conjugated polymer backbone is observed.

**Table 4. 2.** Molecular structural data of **PT<sub>OXY</sub>-TPD<sub>OXY</sub>** and **PT<sub>OXY</sub>-TPD<sub>DMO</sub>**.

| Polymer                                   | $2\theta/^\circ$ | $d$ spacing/nm | $2\theta/^\circ$ | $d$ spacing/nm |
|---|------------------|----------------|------------------|----------------|
| <b>PT<sub>OXY</sub>-TPD<sub>OXY</sub></b> | -                | -              | 24.75            | 0.36           |
| <b>PT<sub>OXY</sub>-TPD<sub>DMO</sub></b> | 21.66            | 0.41           | 24.07            | 0.37           |

### 4.3 Conclusion

A series of donor-acceptor alternating copolymers with varying number of triethylene glycol (**OXY**) chains, 3,7-dimethyloctane (**DMO**) chains, and 2-octyldodecyl (**ODD**) chains on thiophene and thieno[3,4-c]pyrrole-4,6-dione as pendant groups were prepared to afford **PT<sub>OXY</sub>-TPD<sub>OXY</sub>**, **PT<sub>OXY</sub>-TPD<sub>DMO</sub>**, and **PT<sub>ODD</sub>-TPD<sub>DMO</sub>** in order to study the effect of substitution on their optoelectronic properties, thermal stability, and molecular packing. The GPC results indicate that introducing hydrophilic side chains along conjugated



polymer chains in **PT<sub>OXY</sub>-TPD<sub>OXY</sub>** led to the formation of insoluble aggregates within tetrachlorobenzene (TCB) solution, which impeded the solubility of the polymer and presented problems in the GPC measurements to determine its molecular weight. However, this problem was seemingly limited for **PT<sub>OXY</sub>-TPD<sub>DMO</sub>**, and **PT<sub>ODD</sub>-TPD<sub>DMO</sub>** in the TCB solution, where the hydrophilic chains were replaced with hydrophobic ones; the solubility of the two polymers was much improved which lead to relatively high molecular weight polymers. Investigation of the optical properties of **PT<sub>OXY</sub>-TPD<sub>OXY</sub>** and **PT<sub>OXY</sub>-TPD<sub>DMO</sub>** in various solutions shows that these polymers in CB, THF, and a mixture of THF/CHCl<sub>3</sub> solutions provide similar spectra to their films, indicating that polymer chains tend to form aggregates that begin as part of a packing of solid particles. Meanwhile, the optical spectra of these polymers in TCE and CHCl<sub>3</sub> solutions provide a clear difference from solution to film where the large difference is observed in **PT<sub>OXY</sub>-TPD<sub>DMO</sub>** in TCE solution, unlike in **PT<sub>OXY</sub>-TPD<sub>OXY</sub>**, indicating that the polymer solubility decreased when the hydrophilic substituents grafted on TPD units. The absorption spectra of **PT<sub>OXY</sub>-TPD<sub>OXY</sub>** and **PT<sub>OXY</sub>-TPD<sub>DMO</sub>** films are significantly red-shifted compared to the **PT<sub>ODD</sub>-TPD<sub>DMO</sub>** film, resulting in a smaller band gap of 1.86 eV and 1.84 eV for **PT<sub>OXY</sub>-TPD<sub>OXY</sub>** and **PT<sub>OXY</sub>-TPD<sub>DMO</sub>**, respectively, due to having more coplanar polymer backbones as compared to **PT<sub>ODD</sub>-TPD<sub>DMO</sub>**. The oxidation potential of all three polymers was almost the same while the reduction potential was more positive for **PT<sub>OXY</sub>-TPD<sub>OXY</sub>** as a result of high flexible TEG side chains that caused a strong compact  $\pi$ - $\pi$  stacking in their backbones. Replacing the alkyl chain in **PT<sub>OXY</sub>-TPD<sub>DMO</sub>** with the less sterically TEG chain in **PT<sub>OXY</sub>-TPD<sub>OXY</sub>** decreased the  $\pi$ - $\pi$  stacking distance between the polymer backbones in its solid state from 0.37 to 0.36 nm. Based on these findings, the new approach toward conjugated polymers with TEG side chains provides materials that could potentially provide higher power conversion efficiencies than analogous polymers with alkyl substituents. The photovoltaic properties of these materials are to be investigated in collaboration with colleagues in the Physics Department.

## 4.4 References

1. Z. T. Zhang, M. Liao, H. Q. Lou, Y. J. Hu, X. M. Sun and H. S. Peng, *Advanced Materials*, 2018, **30**, 1704261.
2. I. Ohnishi, K. Hashimoto and K. Tajima, *Royal Society Open Science*, 2018, **5**, 172025.
3. X. X. Chen, Z. J. Zhang, Z. C. Ding, J. Liu and L. X. Wang, *Angewandte Chemie-International Edition*, 2016, **55**, 10376-10380.
4. J. Liu, Q. G. Zhou, Y. X. Cheng, Y. H. Geng, L. X. Wang, D. G. Ma, X. B. Jing and F. S. Wang, *Advanced Materials*, 2005, **17**, 2974-2978.
5. C. Kanimozhi, N. Yaacobi-Gross, E. K. Burnett, A. L. Briseno, T. D. Anthopoulos, U. Salzner and S. Patil, *Physical Chemistry Chemical Physics*, 2014, **16**, 17253-17265.
6. R. Kim, B. Kang, D. H. Sin, H. H. Choi, S. K. Kwon, Y. H. Kim and K. Cho, *Chemical Communications*, 2015, **51**, 1524-1527.
7. B. Meng, H. Song, X. Chen, Z. Xie, J. Liu and L. Wang, *Macromolecules*, 2015, **48**, 4357-4363.
8. F. L. Cai, J. L. Cai, L. Y. Yang, W. Li, R. S. Gurney, H. N. Yi, A. Iraqi, D. Liu and T. Wang, *Nano Energy*, 2018, **45**, 28-36.
9. H. S. Peng, X. M. Sun, W. Weng and X. Fang, *Polymer Materials for Energy and Electronic Applications*, 2017, 9-61.
10. R. H. Lee, L. C. Yang, J. Y. Wu and R. J. Jeng, *RSC Advances*, 2017, **7**, 1016-1025.
11. H. J. Son, W. Wang, T. Xu, Y. Y. Liang, Y. E. Wu, G. Li and L. P. Yu, *Journal of the American Chemical Society*, 2011, **133**, 1885-1894.
12. J. Brebels, E. Douvogianni, D. Devisscher, R. T. Eachambadi, J. Manca, L. Lutsen, D. Vanderzande, J. C. Hummelen and W. Maes, *Journal of Materials Chemistry C*, 2018, **6**, 500-511.
13. V. N. Viswanathan, A. D. Rao, U. K. Pandey, A. V. Kesavan and P. C. Ramamurthy, *Beilstein Journal of Organic Chemistry*, 2017, **13**, 863-873.
14. J. Q. Zhang, L. Y. Zhu and Z. X. Wei, *Small Methods*, 2017, **1**, 1700258.
15. J. Brebels, J. V. Manca, L. Lutsen, D. Vanderzande and W. Maes, *Journal of Materials Chemistry A*, 2017, **5**, 24037-24050.
16. N. A. Ran, J. A. Love, M. C. Heiber, X. C. Jiao, M. P. Hughes, A. Karki, M. Wang, V. V. Brus, H. Wang, D. Neher, H. Ade, G. C. Bazan and T. Q. Nguyen, *Advanced Energy Materials*, 2018, **8**, 1701073.
17. M. Olguin, L. Basurto, R. R. Zope and T. Baruah, *ArXiv Preprint ArXiv*, 2013.
18. Y. Huang, E. Kramer, A. Heeger and G. Bazan, *Chemical Reviews*, 2014, **114**, 7006-7043.

19. L. J. Lindgren, F. Zhang, M. Andersson, S. Barrau, S. Hellström, W. Mammon, E. Perzpn, O. Inganäs and M. R. Andersson, *Chemistry of Materials*, 2009, **21**, 3491-3502.
20. S. Torabi, F. Jahani, I. Van Severen, C. Kanimozhi, S. Patil, R. W. A. Havenith, R. C. Chiechi, L. Lutsen, D. J. M. Vanderzande, T. J. Cleij, J. C. Hummelen and L. J. A. Koster, *Advanced Functional Materials*, 2015, **25**, 150-157.
21. M. Shao, Y. J. He, K. L. Hong, C. M. Rouleau, D. B. Geohegan and K. Xiao, *Polymer Chemistry*, 2013, **4**, 5270-5274.
22. M. Bresselge, I. Van Severen, L. Lutsen, P. Adriaensens, J. Manca, D. Vanderzande and T. Cleij, *Thin Solid Films*, 2006, **511**, 328-332.
23. M. Wakioka, N. Ichihara, Y. Kitano and F. Ozawa, *Macromolecules*, 2014, **47**, 626-631.

>>

**CHAPTER V  
CONCLUSION AND  
FUTURE WORK**

## 5.1 Conclusion

The essential aim of this thesis was to synthesise and characterise a new series of soluble low bandgap (LBG) conjugated copolymers that contain alternating units of various electron-donating capabilities with electron acceptor units for application in electronic devices. Generally, the properties of a large number of conjugated polymers, in literature, can be tuned by modification of the molecular structure, including chain regioregularity and side chain substituents, to realize efficient optoelectronic performance. For OPV devices, the use of TPD-based copolymers in the active layer led to a PCE of up to 9.21%.<sup>1</sup> Therefore, increased efforts to design new generations of polymer solar cells particularly using polymers where TPD is the electron acceptor units in the push-pull conjugated system have been undertaken. As a result, the research presented in this thesis covers a wide range of strategies, including polymer regioregularity and side chain engineering involved with TPD-based copolymers. Thus, the second chapter of the thesis focused on studying different fashions of thiophene regioregularity that coupled with a TPD unit. The third chapter studied the nature of side chain types on polymer properties. The fourth chapter combined the two aspects of chapters II and III. The outcome of the research studies discussed in each chapter is summarized individually in the forthcoming paragraphs.

Chapter II involved the preparation of a series of new donor-acceptor copolymer semiconductors based on thieno[3,4-c]pyrrole-4,6-dione (TPD) acceptor with butylphenyl (**BP**) and linear octyl (**O**) side groups, and thiophene (**T**) or bithiophene (**T2**) units as donor was prepared by direct arylation polymerization (DAP) to yield the following copolymers in a fashion similar to those of P3HTs, **[RIR] PT<sub>OP</sub>-TPD<sub>BP</sub>**, **[RIR] PT<sub>OP</sub>-TPD<sub>O</sub>**, **[RR] PT<sub>OP</sub>-TPD<sub>O</sub>**, **[T-T] PT<sub>2OP</sub>-TPD<sub>O</sub>**, and **[H-H] PT<sub>2OP</sub>-TPD<sub>O</sub>**. Incorporation of phenyl ring, particularly on imide moiety in **[RIR] PT<sub>OP</sub>-TPD<sub>BP</sub>**, was found to impede the ability to create long chains of polymer resulting in lower molecular weight and thermal property as compared to all synthesized copolymers except **[RR] PT<sub>OP</sub>-TPD<sub>O</sub>**. This polymer's poor molecular weight was largely due to its high crystalline property causing a much narrower band gap than those values

stated for P3HT.<sup>2</sup> The lack of aggregation and crystallinity increased not only the opportunity to have an  $M_n$  over 10.5 kDa for **[RIR] PT<sub>OP</sub>-TPD<sub>O</sub>**, **[T-T] PT<sub>2OP</sub>-TPD<sub>O</sub>**, and **[H-H] PT<sub>2OP</sub>-TPD<sub>O</sub>** but also the optical band gap from 1.87-2.07 eV. The latter three copolymers show deeper HOMO levels in the range of 5.57-5.62 eV, which should lead to a high open circuit voltage ( $V_{oc}$ ) in OPV device versus P3HT. In addition to that, all regio-regular copolymers' LUMO results would facilitate to diminish the energy loss in the electron transfer from the copolymer to PCBM acceptor more efficiently than regio-random copolymers due to their medium LUMO offset. X-ray diffraction studies provided smaller crystalline domains within **[RIR] PT<sub>OP</sub>-TPD<sub>BP</sub>** with a lamellar distance of 23.85 Å that is 1.40 Å shorter than **[RR] PT<sub>OP</sub>-TPD<sub>O</sub>**. However, the nature of all polymers tends to form amorphous domains more than crystalline domains in solid state. The photovoltaic properties of this series of polymers will be investigated in collaboration with colleagues in the Physics Department. It will be extremely important to study the effect of the dipole moments of these polymers and consequences on the power conversion efficiency of these materials in bulk heterojunction solar cells.

Chapter III examined the effect of hydrophilic/hydrophobic substitution pattern on dithienylfluorene-*alt*-thienopyrroledione alternating copolymers; this is the first time that such polymers are being reported. The incorporation of flexible hydrophilic chains along the polymer backbone resulted in a marked propensity to form a solution containing particle aggregates in TCB, which in turn limited GPC measurement accuracy, leading to an unreliable result for **PF<sub>OXY</sub>DT-TPD<sub>OXY</sub>**. This aggregation behaviour is also observed in UV-vis absorption spectroscopy in CHCl<sub>3</sub> and THF solutions for **PF<sub>OXY</sub>DT-TPD<sub>OXY</sub>** and **PF<sub>OXY</sub>DT-TPD<sub>DMO</sub>**. The molecular weight results, however, were well defined after TEG substituents onto polyfluorenes were replaced with hydrophobic groups in **PF<sub>O</sub>DT-TPD<sub>DMO</sub>** and **PF<sub>O</sub>DT-TPD<sub>OXY</sub>**, which are much higher than **PF<sub>OXY</sub>DT-TPD<sub>DMO</sub>**. The optical spectra of polymer thin films showed two absorption bands, which indicated a pronounced vibronic structure for **PF<sub>OXY</sub>DT-TPD<sub>OXY</sub>**. This, in turn, indicates a highly crystalline arrangement within the polymer. These results are consistent with the results

of XRD analysis. Although the majority of interlayer chains of all the polymers observed by XRD analysis are located at the same angle, **PF<sub>OXY</sub>DT-TPD<sub>OXY</sub>** exhibited another intense peak and a slightly smaller  $\pi$ - $\pi$  stacking distance than **PF<sub>O</sub>DT-TPD<sub>DMO</sub>**. Furthermore, the electrochemical results suggest that the band gaps of those polymers substituted with TEG side chains are larger than those of polymers fully substituted with alkyl side chains (**PF<sub>O</sub>DT-TPD<sub>DMO</sub>**). This observation is attributed to the influence of TEG substitution in decreasing the LUMO and HOMO levels. The LUMOs are still high enough to transfer the electrons of the prepared conjugated polymers to the most widely used electron acceptor, PCBM. This work would open up new avenues for researchers to use such molecules on the side chains of conjugated polymers to design new alternating donor-acceptor conjugated polymer materials for OPV devices with less toxicity and optimal performance.

Like chapters II and III, chapter IV involved the preparation of a series of donor-acceptor alternating copolymers with varying number of triethylene glycol (**OXY**) chains, 3,7-dimethyloctane (**DMO**) chains, and 2-octyldodecyl (**ODD**) chains on thiophene and thieno[3,4-c]pyrrole-4,6-dione as pendant groups were prepared to afford **PT<sub>OXY</sub>-TPD<sub>OXY</sub>**, **PT<sub>OXY</sub>-TPD<sub>DMO</sub>**, and **PT<sub>ODD</sub>-TPD<sub>DMO</sub>** in order to study the effect of substitution on their optoelectronic properties, thermal stability, and molecular packing. The GPC results indicate that introducing hydrophilic side chains along conjugated polymer chains in **PT<sub>OXY</sub>-TPD<sub>OXY</sub>** led to the formation of insoluble aggregates within tetrachlorobenzene (TCB) solution, which impeded the solubility of the polymer and presented problems in the GPC measurements to determine its molecular weight. However, this problem was seemingly limited for **PT<sub>OXY</sub>-TPD<sub>DMO</sub>**, and **PT<sub>ODD</sub>-TPD<sub>DMO</sub>** in the TCB solution, where the hydrophilic chains were replaced with hydrophobic ones; the solubility of the two polymers was much improved which lead to relatively high molecular weight polymers. Investigation of the optical properties of **PT<sub>OXY</sub>-TPD<sub>OXY</sub>** and **PT<sub>OXY</sub>-TPD<sub>DMO</sub>** in various solutions shows that these polymers in CB, THF, and a mixture of THF/CHCl<sub>3</sub> solutions provide similar spectra to their films, indicating that polymer chains tend to form aggregates that begin as part of a packing of solid particles. Meanwhile, the optical spectra of these polymers in TCE and

CHCl<sub>3</sub> solutions provide a clear difference from solution to film where the large difference is observed in **PT<sub>OXY</sub>-TPD<sub>DMO</sub>** in TCE solution, unlike in **PT<sub>OXY</sub>-TPD<sub>OXY</sub>**, indicating that the polymer solubility decreased when the hydrophilic substituents grafted on TPD units. The absorption spectra of **PT<sub>OXY</sub>-TPD<sub>OXY</sub>** and **PT<sub>OXY</sub>-TPD<sub>DMO</sub>** films are significantly red-shifted compared to the **PT<sub>ODD</sub>-TPD<sub>DMO</sub>** film, resulting in a smaller band gap of 1.86 eV and 1.84 eV for **PT<sub>OXY</sub>-TPD<sub>OXY</sub>** and **PT<sub>OXY</sub>-TPD<sub>DMO</sub>**, respectively, due to having more coplanar polymer backbones as compared to **PT<sub>ODD</sub>-TPD<sub>DMO</sub>**. The oxidation potential of all three polymers was almost the same while the reduction potential was more positive for **PT<sub>OXY</sub>-TPD<sub>OXY</sub>** as a result of high flexible TEG side chains that caused a strong compact  $\pi$ - $\pi$  stacking in their backbones. Replacing the alkyl chain in **PT<sub>OXY</sub>-TPD<sub>DMO</sub>** with the less sterically demanding TEG chain in **PT<sub>OXY</sub>-TPD<sub>OXY</sub>** decreased the  $\pi$ - $\pi$  stacking distance between the polymer backbones in its solid state from 0.37 to 0.36 nm. Based on these findings, the new approach toward conjugated polymers with TEG side chains provides materials that could potentially provide higher power conversion efficiencies than analogous polymers with alkyl substituents. The photovoltaic properties of these materials are to be investigated in collaboration with colleagues in the Physics Department.

## 5.2 Future work

The results of chapter II provide important developments in the design of polymers with different regioregularity and novel physicochemical properties for application in OPV devices. Although a range of studies has been undertaken on these polymers, the photovoltaic properties and dipole moment measurements of these copolymers still need to be examined in order to analyse the relationship between  $\Delta\mu_{ge}$  and the PCE; it is believed that the high dipole moment positively affects the charge separation after photo-generated excitons in BHJ OPV. To further investigate these series, the external quantum efficiency of all polymers and PCBM blend films based on optimal preparation conditions of photovoltaic devices will be studied to evaluate the performance of these materials in devices. Furthermore, the measurement of the decay trace of similar polymer blend films used for the external quantum



efficiency measurement will be used to explore the electron transfer time from polymer to PCBM, as the driving force for electron transfer is substantially dependent upon the dipole moment of the polymers. To complete the picture of this chapter to its counterpart copolymers **[T-T] PT<sub>2OP</sub>-TPD<sub>O</sub>** and **[H-H] PT<sub>2OP</sub>-TPD<sub>O</sub>**, preparing highly regioregular **H-T** bithiophene is a future goal.

The existence of a hydrophilic side chain along the hydrophobic polymer backbone, as discussed in chapters III and IV, enabled the resulting polymers to reflect good optoelectronic properties and close polymer packing. Further enhancement on GPC measurements of **PF<sub>OXY</sub>DT-TPD<sub>OXY</sub>** and **PT<sub>OXY</sub>-TPD<sub>OXY</sub>** using a good solubilising solvent, (e.g. 1,1,2,2-TCE), to avoid aggregation will be needed to improve the accuracy in measuring the molecular weight of these polymers. As the research work used the hydrophilic side chain to develop the low dielectric constant ( $\epsilon_r$ ) in conjugated polymers and hence reduce bimolecular recombination in OPV devices, investigation into the effect of the substitution of the resulting polymers on the dielectric properties and photovoltaic performance will be required to elucidate the structure-property relationship as predicated—that efficiencies of more than 20% can be realized with high  $\epsilon_r$  materials.<sup>3</sup> Studies on the morphology of the active layer of all the conjugated polymers will also be desirable to better understand the operation of OPV devices using atomic force microscopy. From a chemical aspect, the resulting copolymers may help guide future designs to utilize different lengths of hydrophilic side chains appending to the acceptor or the donor backbones to explore the potential use of these materials in BHJ OPV devices processed with less toxic methods.

### 5.3 References

1. J.-H. Kim, J. B. Park, I. H. Jung, A. C. Grimsdale, S. C. Yoon, H. Yang and D.-H. Hwang, *Energy & Environmental Science*, 2015, **8**, 2352-2356.
2. A. Marrocchi, D. Lanari, A. Facchetti and L. Vaccaro, *Energy & Environmental Science*, 2012, **5**, 8457-8474.
3. S. Torabi, F. Jahani, I. Van Severen, C. Kanimozhi, S. Patil, R. W. A. Havenith, R. C. Chiechi, L. Lutsen, D. J. M. Vanderzande, T. J. Cleij, J. C. Hummelen and L. J. A. Koster, *Advanced Functional Materials*, 2015, **25**, 150-157.

>>  
**CHAPTER VI**  
**EXPERIMENTAL**

## 6.1 Materials and solvents

The chemical materials for this study were bought from Sigma-Aldrich, Alfa Aesar, and Fisher Scientific, and used without further purification unless otherwise stated. Anhydrous solvents were supplied by the Grubbs solvent system via the Department of Chemistry at the University of Sheffield. Reactions that required use of a metal catalyst were successfully achieved under an inert atmosphere unless otherwise stated. Confirmation of completed reactions was verified using thin layer chromatography (TLC), and silica gel (100-300 mesh) was used for column chromatography.

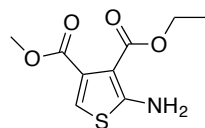
## 6.2 Analytical techniques

Melting points were determined using open-ended capillary tubes on a Gallenkamp Melting Point Apparatus.  $^1\text{H-NMR}$  and  $^{13}\text{C-NMR}$  spectra were carried out using the Bruker Avance 400 (400 and 100 MHz) at 21 °C, with chloroform- $\text{d}_1$ , acetone- $\text{d}_6$ , and dimethyl sulfoxide- $\text{d}_6$  as solvents.  $^1\text{H-NMR}$  data of all copolymers was recorded in 1,1,2,2-tetrachloroethane- $\text{d}_2$  as solvent on the Bruker Avance III HD 500 (500 MHz) at 100 °C. All  $J$  coupling values are quoted in hertz (Hz), the chemical shifts are expressed or calculated in parts per million (ppm) relative to tetramethylsilane (TMS) ( $\delta_{\text{H}}$  0.00), and the multiplicities of NMR signals are described as singlet (s), doublet (d), triplet (t), pentet (pent), sextet (se), quintet (qui), and multiplet (m). Elemental analysis of carbon, hydrogen, nitrogen, and sulphur analysis was performed using the Perkin Elmer 2400 series II while the analysis of Br was determined by using the oxygen flask combustion procedure. GPC curves were recorded on a system consisting of a Hewlett Packard Model 1090 HPLC, a Hewlett Packard Model 1037 Differential Refractive Detector, two Polymer Labs PLgel 5 $\mu$  Mixed-C (300 mm x 7.5 mm) columns and a guard (50 mm x 7.5 mm). GPC analysis was conducted on polymer solutions (2 mg/mL) in 1,2,4-trichlorobenzene at 140 °C and chloroform at 40 °C as eluents at a flow rate of 1 mL per minute. Polymer samples were spiked with toluene as a reference. GPC curves were obtained using the RI-detection method, which was calibrated with a number of polystyrene narrow standards (Polymer Laboratories). Thermal Gravimetric Analysis (TGA) curves were carried out

using a Perkin Elmer TGA-7 Thermogravimetric Analyser in heat from 25.00 °C to 800 °C at a rate of 10 °C min<sup>-1</sup> under an inert atmosphere of nitrogen. Powder X-ray diffraction samples were carried out on a Bruker D8 advance diffractometer with a Cu K $\alpha$  radiation source (1.5418 Å, rated as 1.6 kW). All measurements were performed in the angular range from 2 to 40 degree 2 $\theta$ . Ultraviolet-visible absorption spectra were recorded by a Hitachi U-2010 Double Beam UV/Visible Spectrophotometer. The absorbance of polymers was recorded in both a solution of chloroform, THF, chlorobenzene, and 1,1,2,2-tetrachloroethane using quartz cuvettes (path length= 10mm) and in the solid state (thin film) at room temperature. Measurement of polymers in the solid state for UV-visible absorption spectra was conducted by drop-casting solutions onto quartz plates using approximately 1 mg cm<sup>-3</sup> polymer solutions that were made up with the above solvents. Cyclic voltammograms were performed with a Model 263A Potentiostat-Galvanostat (Princeton Applied Research). A three electrodes setup consisting of a Pt disk as the working electrode, platinum wire as counter electrode, and Ag/AgCl as reference electrode was used. A solution of tetrabutylammonium perchlorate in acetonitrile (0.1 mol dm<sup>-3</sup>) was used as the electrolyte solution. Polymer films were prepared by drop casting polymer solution onto the Pt disk. Ferrocene was used as a reference redox system following IUPAC's recommendations. The energy level of Fc/Fc<sup>+</sup> was assumed to be -4.8 eV with respect to vacuum. The half-wave potential ( $E_{1/2}$ ) of Fc/Fc<sup>+</sup> redox couple was estimated to be 0.08 eV against Ag/Ag<sup>+</sup> reference electrode. The HOMO and LUMO energy levels of polymers were obtained by the equation:  $E_{\text{HOMO/LUMO}} = - (E_{\text{ox/red}}^{\text{onset}} - E_{1/2}) + 4.8$ .  $E_{\text{ox/red}}^{\text{onset}}$  is the onset oxidation/reduction potentials, respectively, relative to the Ag/Ag<sup>+</sup> reference electrode. Dynamic Light Scattering (DLS) measurements were recorded on a Malvern Nano-ZS zetasizer with a 633 nm He-Ne laser and an angle of 90°. The concentration of the samples for DLS measurement was set at 0.5 mg cm<sup>-3</sup>. The size distribution of the resulting particles and polydispersity index (PDI) were obtained.

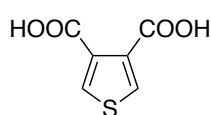
## 6.3 Preparation of monomers

### 3-Ethyl-4-methyl-2-aminothiophene-3,4-dicarboxylate (1)<sup>1</sup>



Ethyl cyanoacetate (23 mL, 24.49 g, 216.53 mmol), methyl pyruvate (21.64 mL, 24.31 g, 238.14 mmol) and sulphur (6.95 g, 216.71 mmol) were placed into two-neck round bottom flask and dissolved in 75 mL of *N,N*-dimethyl formamide (DMF) under N<sub>2</sub>. A solution of 19 mL of triethylamine (Et<sub>3</sub>N) in 38 mL of DMF was then added gently dropwise to the mixture. After adding the complete solution, the reaction was warmed to 50 °C overnight. Then, the mixture was cooled to room temperature and 500 mL of H<sub>2</sub>O was added and left for 48 h. The product was then filtered off to obtain an orange crystal (25 g, 50.54%). M.p. 110-111 °C; <sup>1</sup>H NMR (400 MHz, CDCl<sub>3</sub>) δ ppm 6.65 (s, 1H), 6.00 (s, 2H), 4.3 (q, 2H), 3.85 (s, 3H), 1.35 (t, 3H, *J* = 7.00 Hz); <sup>13</sup>C NMR (100 MHz, CDCl<sub>3</sub>) δ 165.5, 164.5, 162.7, 132.4, 111.3, 105.0, 60.2, 52.2, 14.2; Mass calc. for C<sub>9</sub>H<sub>11</sub>NO<sub>4</sub>S: 229.04. Found (ESI); (*m/z*): 230.1 (MH<sup>+</sup>); Elemental analysis (%): calc. for C<sub>9</sub>H<sub>11</sub>NO<sub>4</sub>S: C, 47.15; H, 4.84; N, 6.11; S, 13.98. Found: C, 46.47; H, 4.64; N, 5.84; S, 14.67.

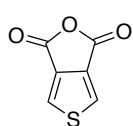
### Thiophene-3,4-dicarboxylic acid (2)<sup>2</sup>



A solution of 3-ethyl-4-methyl-2-aminothiophene-3,4-dicarboxylate (1) (3 g, 13.08 mmol) in dry THF (270 mL) was placed in a 500 mL round-bottom flask. Then, *t*-butyl nitrite (*t*-BuONO) (1.7 mL, 1.47 g, 13.73 mmol) in dry THF (360 mL) was placed in a 1L three-neck flask and warmed to 90 °C. The first solution was added gently dropwise to a boiling solution for about 2 h, and the reaction allowed refluxing for 4 h. The solvent was then removed and the concentrated product placed into a silica gel column (30% EA, 70% petroleum ether) to obtain brown oil (1.21 g). This brown oil was then charged in 100 mL of NaOH (2M) and stirred for 24 h at 95 °C. The solution was acidified by HCl to PH 1 and extracted with diethyl ether (8x 200 mL). The organic phase was then dried over MgSO<sub>4</sub> and evaporated to obtain a brown solid (1 g, 44.44 %). M.p. 225-226 °C; <sup>1</sup>H NMR (400 MHz, acetone-d<sub>6</sub>) δ ppm 8.54 (s, 2H); <sup>13</sup>C NMR (100 MHz, acetone-d<sub>6</sub>) δ 164.3, 138.8, 131.5; Mass calc. for C<sub>6</sub>H<sub>4</sub>O<sub>4</sub>S: 171.98. Found (ESI); (*m/z*):

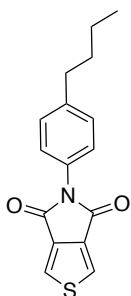
173.0 (MH<sup>+</sup>); Elemental analysis (%): calc. for C<sub>9</sub>H<sub>4</sub>O<sub>4</sub>S: C, 41.86; H, 2.34; S, 18.62. Found: C, 43.34; H, 2.60; S, 17.98.

### 3,4- Thiophene dicarboxylic anhydride (**3**)<sup>3, 4</sup>



(1.33 g, 7.73 mmol) of thiophene-3,4-dicarboxylic acid (**2**) was placed into a 100 mL round-bottom flask and dissolved in 12 mL of acetic anhydride. This reaction mixture was warmed to 110 °C and kept under N<sub>2</sub> for 1 h. Then, the mixture was cooled to room temperature, immediately forming crystals. After that, the product was filtered off and washed with hexane to obtain a dark green crystal (1 g, 84%). M.p. 156-157 °C; <sup>1</sup>H NMR (400 MHz, acetone-d<sub>6</sub>) δ ppm 8.54 (s, 2H); <sup>13</sup>C NMR (100 MHz, acetone-d<sub>6</sub>) δ 156.7, 136.3, 130.3; Mass calc. for C<sub>6</sub>H<sub>2</sub>O<sub>3</sub>S: 153.97. Found (EI); (m/z): 154.1 (MH<sup>+</sup>); Elemental analysis (%): calc. for C<sub>6</sub>H<sub>2</sub>O<sub>3</sub>S: C, 46.75; H, 1.31; S, 20.80. Found: C, 46.89; H, 1.60; S, 19.81.

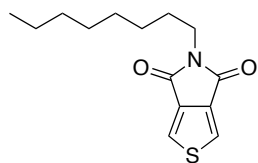
### 5-(4-Butylphenyl)-thieno[3,4-c]pyrrole-4,6-dione (**M1**)<sup>5</sup>



(1 g, 6.49 mmol) of 3,4- thiophene dicarboxylic anhydride (**3**) was placed into a 100 mL two-neck round-bottom flask charged with 5 mL of THF under an inert atmosphere (Ar). 4-butylaniline (1.09 g, 1.15 mL, 7.31 mmol) was then added dropwise to the stirred solution for about 10 min. The mixture was heated to 55 °C for 3 h, and then cooled to room temperature. 4.94 mL of thionyl chloride (SOCl<sub>2</sub>) was then charged into the mixture, which was heated again at the same temperature and then cooled to room temperature. The mixture slowly precipitated into a solution of (37.5 mL) of H<sub>2</sub>O and (75 mL) CH<sub>3</sub>OH. Then, the precipitated solution was filtered off to obtain a white solid and purified via chromatography on silica using 100% chloroform as the eluent to produce white solid (1.37 g, 74%). M.p. 216.5-217.5 °C; <sup>1</sup>H NMR (400 MHz, CDCl<sub>3</sub>) δ ppm 7.95 (s, 2H), 7.32 (d, 2H, J= 8.50 Hz), 7.29 (d, 2H, J= 8.50 Hz), 2.67 (t, 2H, J= 8.00 Hz), 1.64 (pent, 2H), 1.41 (se, 2H), 0.96 (t, 3H, J= 7.00 Hz); <sup>13</sup>C NMR (100 MHz, CDCl<sub>3</sub>) δ 161.7, 143.3, 136.2, 129.3, 129.1, 126.5, 35.3, 33.4, 22.3, 13.9; Mass calc. for C<sub>16</sub>H<sub>15</sub>NO<sub>2</sub>S: 285.08. Found (EI); (m/z):

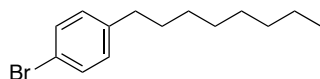
285.1 (M<sup>+</sup>); Elemental analysis (%): calc. for C<sub>16</sub>H<sub>15</sub>NO<sub>2</sub>S: C, 67.34; H, 5.30; N, 4.91; S, 11.23. Found: C, 67.32; H, 5.26; N, 4.86; S, 10.93.

### 5-Octyl-4H-thieno[3,4-c]pyrrole-4,6(5H)-dione (M2)<sup>5</sup>



(400 mg, 2.60 mmol) of 3,4-thiophene dicarboxylic anhydride (**3**) was placed in a 100 mL two-neck round-bottom flask charged with 4 mL of THF under an inert atmosphere (Ar). *n*-octylamine (503 mg, 0.64 mL, 2.98 mmol) was then added dropwise to the stirred solution for about 10 min. The mixture was then heated to 55 °C for 3 h, and then cooled to room temperature. 1.09 mL of thionyl chloride (SOCl<sub>2</sub>) was then charged into the mixture, which was heated again at the same temperature and then cooled to room temperature. The mixture slowly precipitated into a solution of (16 mL) of H<sub>2</sub>O and (50 mL) CH<sub>3</sub>OH. Then, the precipitated solution was filtered off to obtain a white solid and purified via chromatography on silica using 100% chloroform as the eluent to produce white solid (500 mg, 73%). M.p. 122-123 °C; <sup>1</sup>H NMR (400 MHz, CDCl<sub>3</sub>) δ ppm 7.82 (s, 2H), 3.62 (t, 2H, *J* = 7.00 Hz), 1.68-1.62 (m, 2H), 1.4-1.2 (m, 10H), 0.89 (t, 3H, *J* = 7.00 Hz); <sup>13</sup>C NMR (100 MHz, CDCl<sub>3</sub>) δ 160.7, 136.7, 125.4, 38.5, 31.7, 29.1, 28.4, 26.8, 22.6, 14.0; Mass calc. for C<sub>14</sub>H<sub>19</sub>NO<sub>2</sub>S: 265.37. Found (EI); (*m/z*): 265.4 (M<sup>+</sup>); Elemental analysis (%): calc. for C<sub>14</sub>H<sub>19</sub>NO<sub>2</sub>S: C, 63.37; H, 7.22; N, 5.28; S, 12.08. Found: C, 63.13; H, 7.17; N, 5.20; S, 11.87.

### 1-Bromo-4-*n*-octylbenzene (**4**)<sup>6</sup>

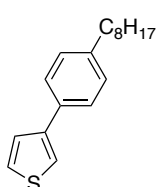


(15 g, 63.59 mmol) of 1,4-dibromobenzene were added to a two-neck round-bottom flask under N<sub>2</sub>. Then, 40 mL of anhydrous THF was charged in the flask. The mixture was degassed three times. After that, the reaction was cooled to -78 °C for 30 min. Then, (39.75 mL, 63.59 mmol) of *n*-BuLi (solution in hexane, 1.6M) were added dropwise and degassed again. The solution was left for 1 h at the same temperature. Next, 1-bromooctane (21.96 mL, 24.56 g, 127.18 mmol) was added to the solution. After cooling for two hours at -78 °C, the mixture was warmed to room temperature. The solvent was then



evaporated and the product extracted using (50 mL) diethyl ether and (3x 50) water. Then, the organic phase was placed over MgSO<sub>4</sub>. The solvent was filtered and evaporated to achieve slightly yellow oil. The yellow oil was distilled to remove the excess of 1-bromooctane (45–46 °C). The remaining product was placed into a silica gel column (petroleum ether) to achieve colourless oil (2.21 g, 12.91%). <sup>1</sup>H NMR (400 MHz, CDCl<sub>3</sub>) δ ppm 7.4 (d, 2H, *J*= 8.00 Hz), 7.1 (d, 2H, *J*= 8.00 Hz), 2.6 (t, 2H, *J*= 7.50 Hz), 1.6-1.3 (m, 12H), 0.9 (t, 3H, *J*= 7.00 Hz); <sup>13</sup>C NMR (100 MHz, CDCl<sub>3</sub>) δ 141.8, 130.7, 119.2, 35.3, 31.8, 31.3, 29.4, 29.2, 29.2, 22.6, 14.1; Mass calc. for C<sub>14</sub>H<sub>21</sub>Br: 268.08. Found (EI); (m/z): 268.1, 271.1 ([M<sup>+</sup>],[M+2<sup>+</sup>]); Elemental analysis (%): calc. for C<sub>14</sub>H<sub>21</sub>Br: C, 62.46; H, 7.86; Br, 29.68. Found: C, 62.51; H, 7.80; Br, 29.81.

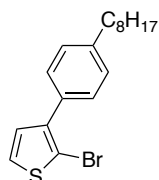
### 3-(4-Octylphenyl) thiophene (**5**)<sup>7</sup>



In a 100 mL two-neck round-bottom flask with reflux condenser, 4-n-octyl-bromobenzene (**4**) (1.21 g, 4.50 mmol) and 3-(4,4,5,5-tetramethyl)-1,3,2-dioxaborolan-2-yl) thiophene (0.76 g, 3.6 mmol) were placed and degassed. Next, 15 mL of anhydrous THF were added, followed by saturated NaHCO<sub>3</sub> (6 mL). After degassing of several times, this flask was charged with Pd(OAc)<sub>2</sub> (56.6 mg, 7% mmol) and tri(*o*-tolyl)phosphine (153.3 mg, 14% mol). The mixture was then degassed again, stirred and refluxed for 16 h. After cooling to room temperature, the reaction mixture was extracted with ethyl acetate (3x 50 mL). The organic phase was washed with water (2x 100 mL) and brine, and the aqueous phase was re-washed with ethyl acetate (3x 50 mL); the organic layer was then dried over MgSO<sub>4</sub>, filtered and concentrated. The crude compound was purified by flash column chromatography using petroleum ether as the eluent. The flash product was then recrystallized from ethanol to afford the corresponding product (590 mg, 60.23 %) as white flakes solid. M.p. 61-62 °C; <sup>1</sup>H NMR (400 MHz, CDCl<sub>3</sub>): δ ppm 7.52 (d, 2H, *J*= 8.00 Hz), 7.43 (t, 1H, *J*= 2.00 Hz), 7.41-7.38 (m, 2H), 7.23 (d, 2H, *J*= 8.00 Hz), 2.65-2.64 (t, 2H, *J*= 8.00 Hz), 1.67-1.3 (m, 12H), 0.91(t, 3H, *J*= 7.00 Hz); <sup>13</sup>C NMR (100 MHz, CDCl<sub>3</sub>) δ 142.4, 141.9, 133.3, 128.8, 126.3, 126.0, 119.6, 35.6, 31.9, 31.4, 29.5, 29.3, 29.2, 22.6, 14.1; Mass calc. for C<sub>18</sub>H<sub>24</sub>S: 272.16. Found

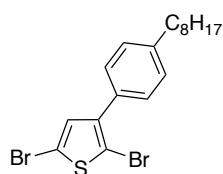
(EI); (m/z): 272.3 (M<sup>+</sup>); Elemental analysis (%): calc. for C<sub>18</sub>H<sub>24</sub>S: C, 79.35; H, 8.88; S, 11.77. Found: C, 79.06; H, 8.84; S, 10.99.

### 2-Bromo-3-(4-octylphenyl) thiophene (**6**)<sup>8</sup>



A solution of 3-(4-*n*-octylphenyl) thiophene (**5**) (500 mg, 1.84 mmol) in chloroform and acetic acid (20ml, 1:1 v/v) was placed into a 100 mL one-neck round-bottom flask. NBS (330 mg, 1.84 mmol) was then added at room temperature for 2 h. The brominated reaction was monitored by TLC to establish completion. After that, the reaction mixture was quenched with 1N NaOH and extracted with EtOAc (3x 50 mL), water (2x 50 mL), and brine. The organic phase was then combined, dried over MgSO<sub>4</sub> and concentrated in *vacuo*. The crude product was purified using a short pad of column chromatography (silica gel) with petroleum ether as the eluent to afford the corresponding product (560 mg, 87%) of colourless oil. <sup>1</sup>H NMR (400 MHz, CDCl<sub>3</sub>) δ ppm 7.50 (d, 2H, *J*= 8.00 Hz), 7.31 (d, 1H, *J*= 6.00 Hz), 7.26 (d, 2H, *J*= 8.00 Hz), 7.04 (d, 1H, *J*= 6.00 Hz), 2.66 (t, 2H, *J*= 8.00 Hz), 1.65-1.71 (m, 2H), 1.30-1.40 (m, 12H), 0.90 (t, 3H, *J*= 7.00 Hz); <sup>13</sup>C NMR (100 MHz, CDCl<sub>3</sub>) δ 142.5, 142.1, 132.3, 129.1, 128.4 (×2), 128.4(×2), 125.7, 108.1, 35.7, 31.9, 31.4, 29.5, 29.4, 29.2, 22.7, 14.1; Mass calc. for C<sub>18</sub>H<sub>23</sub>BrS: 350.07. Found (EI); (m/z): 350.3, 353.3 ([M<sup>+</sup>], [M+2<sup>+</sup>]); Elemental analysis (%): calc. for C<sub>18</sub>H<sub>23</sub>BrS: C, 61.53; H, 6.60; Br, 22.74; S, 9.12. Found: C, 61.44; H, 6.77; Br, 22.83; S, 8.24.

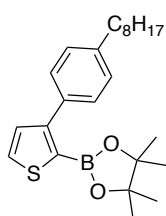
### 2,5-Dibromo-3-(4-octylphenyl) thiophene (**M3**)<sup>8</sup>



A solution of 3-(4-*n*-octylphenyl) thiophene (**6**) (300 mg, 0.86 mmol) in chloroform and acetic acid (10 ml, 1:1 v/v) was placed into a 100 mL one-neck round-bottom flask. NBS (305 mg, 1.71 mmol) was added and then warmed to reflux at 60 °C overnight. The brominated reaction was monitored by TLC to establish completion. After that, the reaction mixture was quenched with 1 N NaOH and extracted with CHCl<sub>3</sub> (3x 50 mL), water (2x 50 mL), and brine. The organic phase was then combined, dried over MgSO<sub>4</sub> and concentrated in *vacuo*. The crude product was purified using a short pad of column

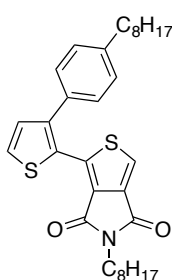
chromatography (silica gel) with petroleum ether as the eluent to afford the corresponding product (270 mg, 73.36%) of colourless oil.  $^1\text{H}$  NMR (400 MHz,  $\text{CDCl}_3$ )  $\delta$  ppm 7.43 (d, 2H,  $J = 8.00$  Hz), 7.25 (d, 2H,  $J = 8.00$  Hz), 7.03 (s, 1H), 2.66 (t, 2H,  $J = 8.00$  Hz), 1.65-1.71 (m, 2H), 1.30-1.40 (m, 12H), 0.90 (t, 3H,  $J = 7.00$  Hz);  $^{13}\text{C}$  NMR (100 MHz,  $\text{CDCl}_3$ )  $\delta$  143.0, 142.0, 131.7, 131.3, 128.5, 128.3, 111.0, 107.2, 35.7, 31.9, 31.3, 29.4, 29.4, 29.2, 22.7, 14.1; Mass calc. for  $\text{C}_{18}\text{H}_{22}\text{Br}_2\text{S}$ : 429.98. Found (EI); (m/z): 430, and 432. ( $[\text{M}^+]$ ,  $[\text{M}+2^+]$ ); Elemental analysis (%): calc. for  $\text{C}_{18}\text{H}_{22}\text{Br}_2\text{S}$ : C, 50.25; H, 5.15; Br, 37.14; S, 7.45. Found: C, 50.79; H, 5.44; Br, 36.99; S, 6.74.

#### 4,4,5,5-Tetramethyl-2-(3-(4-octylphenyl)thiophene-2-yl)-1,3,2-dioxaborolane (7)



In a 100 mL two-neck round-bottom flask with reflux condenser, 2-bromo-3-(4-octylphenyl) thiophene (**6**) (308 mg, 0.88 mmol) were placed and degassed. Then, 5 mL of anhydrous diethyl ether was added. After several times of degassing, the mixture was cooled to  $-78$  °C for 30 min. Next, (0.61 mL, 0.97 mmol) of *n*-BuLi (solution in hexane, 2.5M) was added dropwise, degassed and left for 3 h. After that, (0.22 ml, 1.25 mmol) of 2-Isopropoxy-4,4,5,5-tetramethyl-1,3,2-dioxaborolane was charged into the mixture and gradually warmed to room temperature overnight. The reaction mixture was extracted with diethyl ether (3x 50 mL), water (2x 50 mL) and brine. The organic layer was combined, dried over  $\text{MgSO}_4$ , and concentrated to produce brown oil (~ 230 mg).  $^1\text{H}$  NMR (400 MHz,  $\text{CDCl}_3$ ):  $\delta$  ppm 7.60 (d, 2H,  $J = 5.00$ ), 7.47 (d, 2H,  $J = 8.00$  Hz), 7.29 (d, 2H,  $J = 5.00$  Hz), 7.19 (d, 2H,  $J = 8.00$  Hz), 2.67-2.63 (t, 2H,  $J = 8.00$  Hz), 1.70-1.49 (m, 12H), 1.31(s, 21H), 0.91(t, 3H,  $J = 7.00$  Hz).

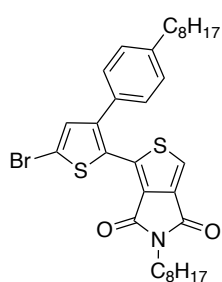
#### 5-Octyl-1-(3-(4-octylphenyl)thiophen-2-yl)-4H-thieno[3,4-c]pyrrole-4,6(5H)-dione (8)<sup>9</sup>



In a long pressure tube was charged with (200 mg, 0.57 mmol) of 2-bromo-3-(4-n-octylphenyl) thiophene (**6**), (605 mg, 2.28 mmol) of 5-octyl-4H-thieno[3,4-c]pyrrole-4,6(5H)-

dione (**M2**), (558 mg, 1.71 mmol) of Cs<sub>2</sub>CO<sub>3</sub>, (58 mg, 0.57 mmol) of PivOH, (6 mg, 4%mol) of PdCl<sub>2</sub>(MeCN)<sub>2</sub>, (8 mg, 4%mol) of P(C<sub>6</sub>H<sub>4</sub>-*o*-OMe)<sub>3</sub>, and 3 mL of dry THF. After that, the mixture was degassed and stirred at room temperature for 30 min, and then warmed up to 90 °C overnight. After cooling to room temperature, the reaction mixture extracted with CHCl<sub>3</sub> (5x 100 mL), water (5x 50 mL) and brine. The organic layer was collected, dried over MgSO<sub>4</sub>, and concentrated in *vacuo*. The crude product was columned using DCM and petroleum ether (1:1) as the eluent to achieve a yellow solid (100 mg, 33%). <sup>1</sup>H NMR (400 MHz, CDCl<sub>3</sub>) δ ppm 7.57 (s, 1H) 7.51 (d, 1H, *J*= 5.00 Hz), 7.26 (d, 2H, *J*= 8.00 Hz), 7.20 (d, 2H, *J*= 8.00 Hz), 7.11 (d, 1H, *J*= 5.00 Hz), 3.59 (t, *J*= 7.00 Hz, 2H), 2.65 (t, 2H, *J*= 8.00 Hz) 1.71-1.2 (m, 24H), 0.93-0.85 (m, 6H); <sup>13</sup>C NMR (100 MHz, CDCl<sub>3</sub>) δ 162.5, 162.4, 143.7, 143.1, 139.3, 136.2, 132.7, 130.4, 130.1, 129.3, 128.7, 127.7, 126.2, 124.4, 38.4, 35.7, 31.9, 31.8, 31.4, 29.7, 29.4, 29.3, 29.3, 29.2, 28.4, 26.9, 22.7, 22.6, 14.1, 14.1; Mass calc. for C<sub>32</sub>H<sub>41</sub>NO<sub>2</sub>S<sub>2</sub>: 535.26. Found (EI); (*m/z*): 535.3 [M<sup>+</sup>]; Elemental analysis (%): calc. for C<sub>32</sub>H<sub>41</sub>NO<sub>2</sub>S<sub>2</sub>: C, 71.73; H, 7.71; N, 2.61; S, 11.97. Found: C, 72.17; H, 7.89; N, 2.33; S, 11.08.

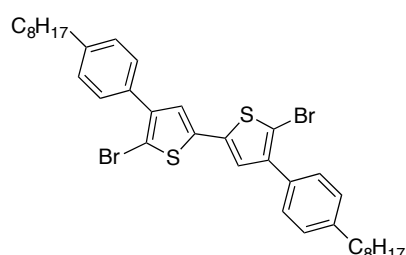
**1-(5-Bromo-3-(4-octylphenyl)thiophen-2-yl)-5-octyl-4*H*-thieno[3,4-*c*]pyrrole-4,6(5*H*)-dione (**M4**)**



A solution of 5-octyl-1-(3-(4-octylphenyl)thiophen-2-yl)-4*H*-thieno[3,4-*c*]pyrrole-4,6(5*H*)-dione (**8**) (120 mg, 0.224 mmol) in chloroform and acetic acid (6 mL, 1:1 v/v) was placed into a 50 mL one-neck round-bottom flask. NBS (39 mg, 0.224 mmol) was then added at 0 °C in two portions and warm up to room temperature for 30 min and then to 60 °C till the completion of the brominated reaction monitored by TLC (6 h). After that, the reaction mixture was quenched with 1.0 N NaOH and extracted with CHCl<sub>3</sub> (3x 50 mL), water (2x 50 mL), and brine. The organic phase was collected, dried over MgSO<sub>4</sub> and concentrated in *vacuo*. The concentrated product was purified by chromatography (silica gel) using petroleum ether as the eluent to afford the corresponding product (60 mg, 44%) of white solid. <sup>1</sup>H NMR (400 MHz, CDCl<sub>3</sub>) δ ppm 7.54 (s, 1H) 7.26-7.18 (m, 4H), 7.32-7.25 (m,

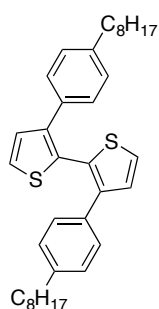
6H), 7.07 (s, 1H), 3.60 (t, 2H,  $J= 7.00$  Hz), 3.60 (t, 2H,  $J= 8.00$  Hz), 1.65 (m, 4H), 1.43-1.26 (m, 20H), 0.90 (m, 6H);  $^{13}\text{C}$  NMR (100 MHz,  $\text{CDCl}_3$ )  $\delta$  162.5, 162.3, 144.0, 143.8, 137.4, 136.1, 132.9, 131.6, 130.2, 129.3, 128.9, 127.7, 124.5, 115.7, 38.5, 35.7, 31.8, 31.8, 31.3, 29.4, 29.3, 29.2, 29.1, 28.4, 26.9, 22.6, 22.6, 14.1, 14.1; Mass calc. for  $\text{C}_{32}\text{H}_{40}\text{BrNO}_2\text{S}_2$ : 613.17. Found (EI); (m/z): 613.2, 615.2 ( $[\text{M}^+]$ ,  $[\text{M}+2^+]$ ); Elemental analysis (%): calc. for  $\text{C}_{32}\text{H}_{40}\text{BrNO}_2\text{S}_2$ : C, 62.53; H, 6.56; Br, 13.00; N, 2.28; S, 10.43. Found: C, 62.03; H, 6.46; N, 2.49; Br, 12.98; S, 10.44.

### 5,5'-Dibromo-4,4'-bis(4-octylphenyl)-2,2'-bithiophene (**M5**)<sup>10</sup>



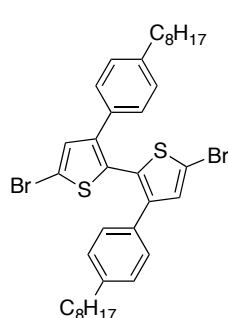
A dried 100 mL one-neck round bottom flask and stir bar was fitted with a condenser and argon Ar. (500 mg, 1.43 mmol) of 2-bromo-3-(4-n-octylphenyl) thiophene (**6**), (485 mg, 2.86mmol, 2 eq) of  $\text{AgNO}_3$ , (166 mg, 2.86 mmol, 2 eq) of potassium fluoride, and (39 mg, 7% mol) of bis(benzonitrile) palladium (II) chloride were added and dissolved in 8 mL of anhydrous DMSO. The reaction mixture was warmed up to 60 °C for 3 hours. After that, two extra equivalents of  $\text{AgNO}_3$  and potassium fluoride were also charged into this reaction and left to stir overnight. The reaction mixture was then filtered over Celite with diethyl ether. Then, the filtrate was washed with 1 mole/L HCl and water. The organic phase was combined and concentrated in *vacuo*. The crude product was columned using petroleum ether as eluent to give the title compound (275 mg, 27.5%) as a white solid. M.p. 80-81 °C;  $^1\text{H}$  NMR (400 MHz,  $\text{CDCl}_3$ )  $\delta$  ppm 7.50 (d, 4H,  $J= 8.00$  Hz) 7.28 (d, 4H,  $J= 8.00$  Hz), 7.07 (s, 2H), 2.67 (t, 4H,  $J= 8.00$  Hz), 1.73-1.61 (m, 4H), 1.47-1.23 (m, 20H), 0.91 (t, 6H,  $J= 7.00$  Hz);  $^{13}\text{C}$  NMR (100 MHz,  $\text{CDCl}_3$ )  $\delta$  142.9, 142.1, 136.1, 131.8, 128.5, 128.4, 125.5, 107.3, 35.8, 31.9, 31.4, 29.5, 29.4, 29.3, 22.7, 14.1; Mass calc. for  $\text{C}_{36}\text{H}_{44}\text{Br}_2\text{S}_2$ : 700.12. Found (MALDI-TOF); (m/z): 698.1, 699.1, 700.1, 701.1, 702.2 ( $[\text{M}^+]$ ,  $[\text{M}+1^+]$ ); Elemental analysis (%): calc. for  $\text{C}_{36}\text{H}_{44}\text{Br}_2\text{S}_2$ : C, 61.71; H, 6.33; Br, 22.81; S, 9.15. Found: C, 62.08; H, 6.50; Br, 24.08; S, 8.79.

### 3,3'-Bis(4-octylphenyl)-2,2'-bithiophene (**9**)<sup>11</sup>



(628 mg, 1.8 mmol) of 2-bromo-3-(4-n-octylphenyl) thiophene (**3**), (856 mg, 2.15 mmol) of 4,4,5,5-tetramethyl-2-(3-(4-octylphenyl)thiophene-2-yl)-1,3,2-dioxaborolane (**7**), (2M, 2ml) of  $K_2CO_3$ , and 5 mL of anhydrous toluene were placed in a dried 100 mL round-bottom flask and degassed three times. Then, 2 drops of Aliquat 336 and (103 mg, 5% mmol) of  $Pd(PPh_3)_4$  were added, degassed again and stirred at room temperature for 20 min. After that, the solution was warmed to 90 °C overnight. The mixture was then extracted with methylene chloride (3x 100 mL), water (3 × 50 mL) and brine. The organic layer was collected, dried over  $MgSO_4$  and concentrated in *vacuo*. The crude product was columned using petroleum ether as the eluent to achieve colourless oil (190 mg, 19.53%).  $^1H$  NMR (400 MHz,  $CDCl_3$ )  $\delta$  ppm 7.35 (d, 2H,  $J= 5.00$  Hz) 7.11 (d, 2H,  $J= 5.00$  Hz), 6.93-6.99 (m, 8H), 2.55 (t, 4H,  $J= 8.00$  Hz), 1.65-1.56 (m, 4H), 1.4-1.27 (m, 20H), 0.93 (t, 6H,  $J= 7.00$  Hz);  $^{13}C$  NMR (100 MHz,  $CDCl_3$ )  $\delta$  141.2, 141.0, 133.2, 129.7, 129.3, 128.1, 128.0, 125.7, 35.6, 31.9, 31.5, 29.5, 29.3, 29.2, 22.7, 14.1; Mass calc. for  $C_{36}H_{46}S_2$ : 542.30. Found (EI); (m/z): 542.6 [ $M^+$ ]; Elemental analysis (%): calc. for  $C_{36}H_{46}S_2$ : C, 79.65; H, 8.54; S, 11.81. Found: C, 79.49; H, 8.54; S, 11.47.

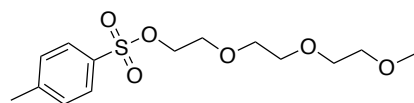
### 5,5'-Dibromo-3,3'-bis(4-octylphenyl)-2,2'-bithiophene (**M6**)



A solution of 3,3'-bis(4-octylphenyl)-2,2'-bithiophene (**9**) (87 mg, 0.16 mmol) in chloroform and acetic acid (6 mL, 1:1 v/v) was placed in a 100 mL one-neck round-bottom flask. NBS (578 mg, 0.32 mmol) was then added at room temperature and stirred for 2 h. The brominated reaction was monitored by TLC to establish completion. After that, the reaction mixture was quenched with 1.0 N NaOH and extracted with  $CHCl_3$  (3x 50 mL), water (2x50 mL), and brine. The organic phase was then combined, dried over  $MgSO_4$  and concentrated in *vacuo*. The crude oil was purified using a short pad of column chromatography (silica gel) with petroleum ether as the eluent to afford the corresponding product (85 mg, 76%) of colourless oil.  $^1H$  NMR (400 MHz,  $CDCl_3$ )  $\delta$  ppm 7.03 (s, 2H), 6.96 (d, 4H,  $J= 8.00$  Hz), 6.91 (d,

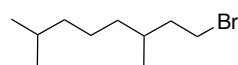
4H,  $J = 8.00$  Hz), 2.55 (t, 4H,  $J = 8.00$  Hz), 1.64-1.16 (m, 24H), 0.95-0.82 (m, 6H);  $^{13}\text{C}$  NMR (100 MHz,  $\text{CDCl}_3$ )  $\delta$  142.1, 142.0, 132.0, 131.8, 129.7, 128.2, 128.0, 112.9, 35.6, 31.9, 31.4, 29.7, 29.5, 29.3, 22.7, 14.1; Mass calc. for  $\text{C}_{36}\text{H}_{44}\text{Br}_2\text{S}_2$  : 700.12. Found (EI); (m/z): 700.1, and 702.1 ( $[\text{M}^+]$ ,  $[\text{M}+2^+]$ ); Elemental analysis (%): calc. for  $\text{C}_{36}\text{H}_{44}\text{Br}_2\text{S}_2$ : C, 61.71; H, 6.33; Br, 22.81; S, 9.15. Found: C, 61.44; H, 6.77; Br, 22.83; S, 8.24.

### 2-(2-(2-Methoxyethoxy)ethoxy)ethyl)-4-methylbenzenesulfonate (10)<sup>12</sup>



2-(2-(2-Methoxyethoxy)ethoxy)ethanol (20 g, 121.80 mmol) was placed in dried 250 mL two necked-round bottom flask and dissolved in 58 mL of anhydrous THF. The solution was cooled down to 0 °C. Then, a solution of NaOH (2.5M, 7.3 g in 73 mL water) was added and left the mixture to stir at this temperature for 2 hours. After that, (23.22 g, 121.80 mmol) of *p*-toluenesulfonyl chloride was dissolved in 58 mL of anhydrous THF and then added dropwise to the solution mixture. Upon complete addition, the reaction mixture was warmed up to room temperature overnight. Next, the solvent was evaporated and the product extracted with ethyl acetate (5x 50 mL). Then, the organic phase was washed with brine, combined, dried over  $\text{MgSO}_4$ , and concentrated to yield the product as colourless oil (33.05 g, 85.29%).  $^1\text{H}$  NMR (400 MHz,  $\text{CDCl}_3$ ):  $\delta$  ppm 7.80 (d, 2H,  $J = 8.00$  Hz), 7.35 (d, 2H,  $J = 8.00$  Hz), 4.17 (t, 2H,  $J = 5.00$  Hz), 3.69 (t, 2H,  $J = 5.00$  Hz), 3.63-3.59 (m, 6H), 3.54 (m, 2H), 3.38 (s, 3H), 2.46 (s, 2H);  $^{13}\text{C}$  NMR (100 MHz,  $\text{CDCl}_3$ )  $\delta$  144.8, 133.0, 129.8, 127.9, 72.4, 71.9, 70.7, 70.5, 70.5, 70.3, 69.2, 68.6, 59.0, 21.6; Mass calc. for  $\text{C}_{14}\text{H}_{22}\text{O}_6\text{S}$ : 318.11. Found (EI); (m/z): 318.1 ( $[\text{M}^+]$ ); Elemental analysis (%): calc. for  $\text{C}_{14}\text{H}_{22}\text{O}_6\text{S}$ : C, 52.81; H, 6.97; S, 10.07 Found: C, 52.61; H, 7.01; S, 9.09.

### 1-Bromo-3,7-dimethyl octane (11)<sup>13</sup>

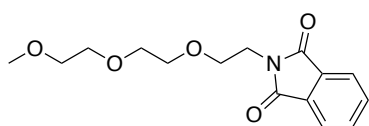


In 500 mL round bottom flask, 3,7-dimethyl-1-octanol (10 g, 63 mmol) and  $\text{PPh}_3$  (19.67 g, 75 mmol) were placed and dissolved in 250 mL of DCM. After that, NBS (50.70 g, 63 mmol) was added to the solution mixture in small portions over 30 min and left to stir at room for

2 hours. After that, the reaction mixture was quenched with a solution of NaHCO<sub>3</sub> and extracted with DCM (3x 50 mL). The organic phase was combined, dried over MgSO<sub>4</sub>, filtered and concentrated in *vacuo*. Next, the concentrated product was treated with some petroleum ether and then filtered. The filtrate solution was further purified by chromatography (silica gel) using petroleum ether as an eluent to obtain the desired product as colourless oil (11.81 g, 84,78%). <sup>1</sup>H NMR (400 MHz, CDCl<sub>3</sub>) δ ppm 3.49 (m, 2H), 1.91 (m, 2H), 1.71 (m, 2H), 1.57 (m, 1H), 1.33 (m, 3H), 1.19 (m, 3H), 0.91 (t, 9H, *J* = 7.00 Hz); <sup>13</sup>C NMR (100 MHz, CDCl<sub>3</sub>) δ 40.0, 39.1, 36.7, 32.2, 31.6, 27.9, 24.5, 22.6, 22.5, 18.9; Mass calc. for C<sub>10</sub>H<sub>21</sub>Br: 221.18. Found (EI); (*m/z*): 222.1 ([MH<sup>+</sup>]); Elemental analysis (%): calc. for C<sub>10</sub>H<sub>21</sub>Br: C, 54.30; H, 9.57; Br, 36.13. Found: C, 54.37; H, 9.45; Br, 36.10.

### 2-(2-(2-(2-Methoxyethoxy)ethoxy)ethyl)isoindoline-1,3-dione (**12**)<sup>14</sup>

A mixture of 2-(2-(2-methoxyethoxy)ethoxy)ethyl-4-methylbenzenesulfonate

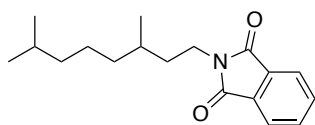


(**10**) (5 g, 15.72 mmol), potassium phthalimide (5.82 g, 31.44 mmol), and 95 mL of dry DMF was stirred at 100°C for 24 hours. After cooled

down to room temperature, 100 mL of distilled water was added and the solution mixture was extracted with DCM (3x 50 mL). The organic phase was combined and washed with 1M of NaOH followed by saturated NaCl solution. After this treatment, the combined organic layer was dried over MgSO<sub>4</sub>, filtered and concentrated in *vacuo* to yield the desired product as pale yellow oil (2.9 g, 63%). <sup>1</sup>H NMR (400 MHz, CDCl<sub>3</sub>): δ ppm 7.86 (m, 2H), 7.73 (m, 2H), 3.91 (t, 2H, *J* = 6.00 Hz), 3.75 (t, 2H, *J* = 6.00 Hz), 3.67 (m, 2H), 3.61 (m, 4H), 3.49 (m, 2H), 3.35 (s, 3H); <sup>13</sup>C NMR (100 MHz, CDCl<sub>3</sub>) δ 168.27, 133.9, 132.1, 123.2, 71.8, 70.5, 70.5, 70.1, 67.9, 59.0, 37.2; Mass calc. for C<sub>15</sub>H<sub>19</sub>NO<sub>5</sub>: 293.13. Found (ES); (*m/z*): 294.3 ([MH<sup>+</sup>]); Elemental analysis (%): calc. for C<sub>15</sub>H<sub>19</sub>NO<sub>5</sub>: C, 61.42; H, 6.53; N, 4.78. Found: C, 60.92; H, 6.39; N, 4.79.

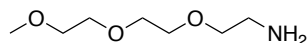


### 2-(3,7-Dimethyl octyl)isoindol-1,3-dione (13)<sup>13</sup>



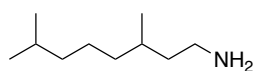
A mixture of 1-bromo-3,7-dimethyl octane (**11**) (3 g, 13 mmol), potassium phthalimide (2.01 g, 10 mmol) and 20 mL of anhydrous DMF was stirred at 135°C for 4 hours. After cooled down to room temperature. 100 mL of distilled water was added and the solution mixture was extracted with DCM (4x 100 mL) and brine. The organic phase was combined and washed with water (10x 200 mL). After this step, the combined organic layer was dried over MgSO<sub>4</sub>, filtered and concentrated in *vacuo* to yield the desired product as colourless oil (8.47 g, 86.67%). <sup>1</sup>H NMR (400 MHz, CDCl<sub>3</sub>) δ ppm 7.86 (m, 2H), 7.72 (m, 2H), 3.73 (t, 2H, *J* = 7.00 Hz), 1.72-1.12 (m, 10H), 0.98 (d, 3H, *J* = 6.00 Hz), 0.87 (d, 6H, *J* = 7.00 Hz); <sup>13</sup>C NMR (100 MHz, CDCl<sub>3</sub>) δ 168.4, 133.8, 132.3, 123.1, 39.2, 36.9, 36.3, 35.5, 30.7, 27.9, 24.5, 22.6, 22.5, 19.3; Mass calc. for C<sub>18</sub>H<sub>25</sub>NO<sub>2</sub>: 287.19. Found (EI); (*m/z*): 287.2. ([M<sup>+</sup>]); Elemental analysis (%): calc. for C<sub>18</sub>H<sub>25</sub>NO<sub>2</sub>: C, 75.22; H, 8.77; N, 4.87. Found: C, 74.87; H, 8.90; N, 4.63.

### 2-(2-(2-Methoxyethoxy)ethoxy)ethanamine (14)<sup>14</sup>



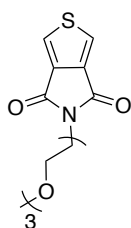
2-(2-(2-(2-Methoxyethoxy)ethoxy)ethyl)isoindoline-1,3-dione (**12**) (1.98 g, 6.75 mmol) was dissolved in 8 mL of methanol. Then, hydrazine monohydrate (0.8 mL, 64%) was added to the mixture and left to stir at reflux temperature for 24hrs, then cooled down to room temperature, 1M of NaOH solution was added to the reaction mixture. The solution mixture was then extracted with DCM (5x 50 mL). The organic phase was combined, dried over MgSO<sub>4</sub>, filtered and concentrated in *vacuo* to obtain the desired product as colorless oil (770 mg, 79%). <sup>1</sup>H NMR (400 MHz, CDCl<sub>3</sub>): δ ppm 3.68 (m, 6H), 3.57 (m, 2H), 3.52 (t, 2H, *J* = 5.00 Hz), 3.38 (s, 3H), 2.87 (t, 2H, *J* = 5.00 Hz); <sup>13</sup>C NMR (100 MHz, CDCl<sub>3</sub>) δ 73.4, 71.9, 70.5, 70.2, 59.0, 41.7; Mass calc. for C<sub>7</sub>H<sub>17</sub>NO<sub>3</sub>: 163.12. Found (EI); (*m/z*): 164.1 ([MH<sup>+</sup>]); Elemental analysis (%): calc. for C<sub>7</sub>H<sub>17</sub>NO<sub>3</sub>: C, 51.51; H, 10.50; N, 8.58. Found: C, 45.00; H, 9.86; N, 7.03.

### 3,7-Dimethyl-1-octyl amine (**15**)<sup>13</sup>



2-(3,7-Dimethyl octyl)isoindol-1,3-dione (**13**) (6 g, 20 mmol) was dissolved in 62 mL of ethanol. Then, Hydrazine monohydrate (2 mL, 64%) was added to the mixture and left to stir at reflux temperature for 3 hours. After cooled down to room temperature, 1 mL of HCl was added to the reaction mixture. Then, the solution mixture was filtered and followed by quick wash with ethanol. The filtrated solution was collected and treated with 1M of NaOH. After this treatment, the solution mixture was extracted with DCM (5x 50 mL). The organic phase was then combined and concentrated in *vacuo* to obtain the desired product as sticky oil (2.78 g, 88.40%). <sup>1</sup>H NMR (400 MHz, CDCl<sub>3</sub>) δ ppm 2.77 (m, 2H), 1.58-1.08 (m, 12 H), 0.887 (dd, 9H, *J*= 6.50, *J*= 1.00 Hz); <sup>13</sup>C NMR (100 MHz, CDCl<sub>3</sub>) δ 41.2, 40.1, 39.2, 37.3, 30.5, 27.9, 24.7, 22.7, 22.6, 19.6. Mass calc. for C<sub>10</sub>H<sub>23</sub>N: 157.18. Found (EI); (m/z): 158.2 ([MH<sup>+</sup>]); Elemental analysis (%): calc. for C<sub>10</sub>H<sub>23</sub>N: C, 76.36; H, 14.74; N, 8.90. Found: C, 68.35; H, 13.92; N, 6.40.

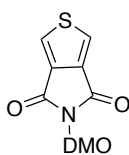
### 5-(2-(2-(2-Methoxyethoxy)ethoxy)ethyl)-4H-thieno[3,4-c]pyrrole-4,6(5H)-dione (**M7**)



In a dried two-necked round bottom flask under an inert atmosphere, thieno[3,4-c]furan-1,3-dione (**3**) (500 mg, 3.24mmol) and 2-(2-(2-methoxyethoxy)ethoxy)ethanamine (**14**) (590 mg, 3.60 mmol) were placed and dissolved using 13 mL of anhydrous THF. The solution mixture was then left to stir at room temperature for 10 min. After that, 2mL of thionyl chloride (SOCl<sub>2</sub>) was charged into the mixture. The reaction mixture was then left to stir at 55°C overnight. After that, the reaction mixture was cooled down and added slowly dropwise into a solution of (75 mL) H<sub>2</sub>O and (25 mL) CH<sub>3</sub>OH. Then, the solution mixture was extracted with ethyl acetate (6x 100mL). The organic phase was combined, dried over MgSO<sub>4</sub> overnight, filtered and concentrated in *vacuo*. The resulting crude product was then purified via chromatography on silica using DCM: EA (3:2) as eluents to produce pale brown solid (680 mg, 70%). M.p. 71-73 °C; <sup>1</sup>H NMR (400 MHz, CDCl<sub>3</sub>): δ ppm 7.83 (s, 2H),

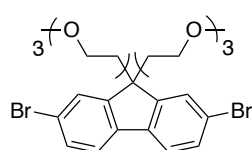
3.86 – 3.83 (m, 2H), 3.74 – 3.70 (m, 2H), 3.68 - 3.49 (m, 8H), 3.36 (s, 3H); <sup>13</sup>C NMR (100 MHz, CDCl<sub>3</sub>) δ 162.7, 136.5, 125.5, 71.9, 70.5, 70.0, 67.8, 59.0, 53.4, 37.7; Mass calc. for C<sub>13</sub>H<sub>17</sub>NO<sub>5</sub>S: 299.08. Found (EI); (m/z): 299.1 ([M<sup>+</sup>]); Elemental analysis (%): calc. for C<sub>13</sub>H<sub>17</sub>NO<sub>5</sub>S: C, 52.16; H, 5.72; N, 4.68; S 10.71. Found: C, 52.25; H, 5.64; N, 4.66; S 10.56.

### 5-(3,7-Dimethyloctyl)-4H-thieno [3,4-c] pyrrole-4,6(5H)-dione (**M8**)<sup>15</sup>



In a dried two-necked round bottom flask and inert atmosphere, thieno[3,4-c]furan-1,3-dione (**3**) (2 g, 12.9 mmol) and 3,7-dimethyl-1-octyl amine (**15**) (2.45 g, 15.5 mmol) were placed and dissolved using 20 mL of dry THF. The solution mixture was then warmed up to 55°C for 3 hours. After that, the reaction mixture was cooled down and 2 mL of thionyl chloride (SOCl<sub>2</sub>) was charged into the mixture, which was heated again at the same temperature overnight and then cooled to room temperature. The mixture slowly precipitated into a solution of (75 mL) of H<sub>2</sub>O and (25 mL) CH<sub>3</sub>OH. Then, the precipitated solution was filtered off to obtain a white solid and purified via chromatography on silica using hexane and ethyl acetate (9:1) as eluents to produce white solid (2.45 g, 83.60%). M.p. 69 -71 °C; <sup>1</sup>H NMR (400 MHz, DMSO-d<sub>6</sub>) δ ppm 8.33 (s, 2H), 3.52 (t, 2H, J= 7.00), 1.60 – 1.04 (m, 10H), 0.89 (d, 3H, J= 6.00), 0.82 (d, 6H, J= 7.00); <sup>13</sup>C NMR (100 MHz, DMSO-d<sub>6</sub>) δ 162.7, 136.1, 128.3, 36.7, 36.3, 35.0, 30.3, 27.7, 24.4, 23.0, 19.8; Mass calc. for C<sub>16</sub>H<sub>23</sub>NO<sub>2</sub>S: 293.14. Found (EI); (m/z): 293.1 ([M<sup>+</sup>]); Elemental analysis (%): calc. for C<sub>16</sub>H<sub>23</sub>NO<sub>2</sub>S: C, 65.49; H, 7.90; N, 4.77; S, 10.93. Found: C, 58.17; H, 7.29; N, 3.77; S, 9.81.

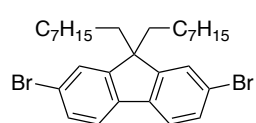
### 2,7-Dibromo-9,9-bis(2-(2-(2-methoxyethoxy)ethoxy)ethyl)-9H-fluorene (**16**)<sup>12</sup>



2,7-Dibromofluorene (5 g, 15.43 mmol), 2(2-(2-methoxyethoxy)ethoxy)ethyl-4-methyl benzenesulfonate (**10**) (13.25 g, 41.66 mmol), TBAB (1.02 g, 3.19 mmol) were charged in a dried 250 mL round bottom flask. Then, a solution of NaOH (25 mL, 50%) was added. The mixture was dissolved in 45 mL of anhydrous

toluene and stirred at 80 °C for 15 hours. After cooling down to room temperature, the mixture was extracted with DCM (5x 100 mL) and water (5x 50 mL). The organic phase was washed with brine, combined, dried over MgSO<sub>4</sub>, and concentrated. The concentrated product was purified by silica gel chromatography using DCM and ethyl acetate (3:2) as eluent to yield the desired product as a pale yellow solid (7.22 g, 76%). M.p. 49-50 °C; <sup>1</sup>H NMR (400 MHz, CDCl<sub>3</sub>): δ ppm 7.54 (d, 2H, *J* = 2.00 Hz), 7.52 (d, 2H, *J* = 8.00 Hz), 7.48 (dd, 2H, *J* = 2.00 Hz, *J* = 8.00 Hz), 3.54 (m, 4H), 3.51 (m, 4H), 3.41 (m, 4H), 3.36 (s, 6H), 3.22 (m, 4H), 2.79 (t, 4H, *J* = 7.00 Hz), 2.35 (t, 4H, *J* = 7.00 Hz); <sup>13</sup>C NMR (100 MHz, CDCl<sub>3</sub>) δ 150.9, 138.4, 130.6, 126.7, 121.6, 121.2, 71.8, 70.4, 70.4, 70.0, 66.7, 59.0, 51.8, 39.5; Mass calc. for C<sub>27</sub>H<sub>36</sub>Br<sub>2</sub>O<sub>6</sub>: 616.09. Found (EI); (m/z): 616.1, and 618.1 ([M<sup>+</sup>],[M+2<sup>+</sup>]); Elemental analysis (%): calc. for C<sub>27</sub>H<sub>36</sub>Br<sub>2</sub>O<sub>6</sub>: C, 52.61; H, 5.89; Br, 25.93. Found: C, 52.60; H, 5.68; Br, 26.06.

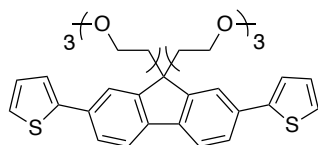
### 2,7-Dibromo-9,9-dioctyl)-9H-fluorene (17)<sup>16, 17</sup>



2,7-Dibromofluorene (1 g, 3.09 mmol), potassium hydroxide (804 mg, 12.36 mmol) and potassium iodide (25 mg, 0.154 mmol) were placed in dried two-necks round bottom flask. 10 mL of DMSO was added under nitrogen atmosphere. Then, 1-bromooctane (1.26 g, 6.5 mmol) was added gently dropwise. The reaction mixture was left to stir at room temperature overnight. After that, the mixture was poured into 500 mL of distilled water and extracted with DCM (3x 25 mL). The organic phase was collected, dried over MgSO<sub>4</sub>, filtered, and concentrated in *vacuo*. The concentrated product was then purified by silica gel chromatography using DCM as an eluent to yield the desired product as pale yellow solid (1.40 g, 83%). M.p. 56-57 °C; <sup>1</sup>H NMR (400 MHz, CDCl<sub>3</sub>): δ ppm 7.54 (m, 2H), 7.48 (m, 2H), 7.46 (s, 2H), 1.93 (m, 4H), 1.27-1.07 (m, 20H), 0.85 (t, 6H, *J* = 7.00 Hz), 0.60 (m, 4H); <sup>13</sup>C NMR (100 MHz, CDCl<sub>3</sub>) δ 152.5, 139.0, 130.1, 126.1, 121.4, 121.1, 55.7, 40.1, 31.7, 29.8, 29.1, 29.1, 23.6, 22.6, 14.0; Mass calc. for C<sub>29</sub>H<sub>40</sub>Br<sub>2</sub>: 548.15. Found (EI); (m/z): 548.2, and 550.2 ([M<sup>+</sup>],[M+2<sup>+</sup>]); Elemental analysis (%): calc. for C<sub>29</sub>H<sub>40</sub>Br<sub>2</sub>: C, 63.51; H, 7.35; Br, 29.14. Found: C, 64.78; H, 7.40; Br, 28.15.

### 2,2'-(9,9-Bis(2-(2-(2-methoxyethoxy)ethoxy)ethyl)-9H-fluorene-2,7-diyl)di thiophene (18)

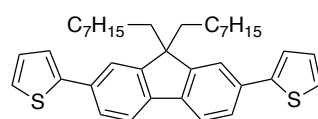
2,7-Dibromo-9,9-bis(2-(2-(2 methoxyethoxy)ethoxy)ethyl)-9H-fluorene (16) (2



g, 3.24 mmol), 2-(tributylstannyl) thiophene (2.54 g, 6.80 mmol), Pd<sub>2</sub>(dba)<sub>3</sub> (208 mg, 7% mol) and tri(*o*-tolyl) phosphine (138 mg, 14% mol) were placed in

round bottom flask and dissolved in 10 mL of dry toluene under inert atmosphere. The solution mixture was then left to stir at reflux temperature overnight. After cooling the reaction mixture to room temperature, the solution was extracted with ethyl acetate (3x 50 mL) and water (2x 50 mL). The organic phase was collected, dried over MgSO<sub>4</sub>, filtered, and concentrated. The concentrated product was purified by silica gel chromatography using ethyl acetate and DCM (2:3) as eluents to yield the desired product as green liquid (1.40 g, 70%). <sup>1</sup>H NMR (400 MHz, CDCl<sub>3</sub>): δ ppm 7.67 (m, 6H), 7.42 (d, 2H, *J*= 4.00 Hz), 7.33 (d, 2H, *J*= 5.00 Hz) 7.14 (t, 2H, *J*= 4.00 Hz), 3.50 (m, 4H), 3.46-3.39 (m, 8H), 3.32 (s, 6H), 3.24 (t, 4H, *J*= 5.00 Hz), 2.86 (t, 4H, *J*= 7.50 Hz), 2.48 (t, 4H, *J*= 7.50 Hz); <sup>13</sup>C NMR (100 MHz, CDCl<sub>3</sub>) δ 149.9, 144.6, 139.4, 133.6, 128.1, 125.3, 124.7, 120.4, 120.2, 71.8, 70.4, 70.4, 70.0, 67.0, 58.9, 51.4, 39.8; Mass calc. for C<sub>35</sub>H<sub>42</sub>O<sub>6</sub>S<sub>2</sub>: 622.24. Found (EI); (*m/z*): 622.2 ([M<sup>+</sup>]); Elemental analysis (%): calc. for C<sub>35</sub>H<sub>42</sub>O<sub>6</sub>S<sub>2</sub>: C, 67.50; H, 6.80; S, 10.29. Found: C, 67.00; H, 6.89; S, 9.92.

### 2,2'-(9,9-Dioctyl-9H-fluorene-2,7-diyl)dithiophene (19)<sup>18</sup>



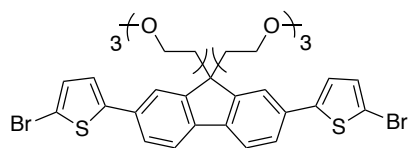
2,7-Dibromo-9,9-dioctyl)-9H-fluorene (17) (1 g, 1.82 mmol), 2-(tributylstannyl) thiophene (1.36 g, 3.65 mmol), Pd(OAc)<sub>2</sub> (28 mg, 7% mol) and P(*o*-tolyl)<sub>3</sub> (39

mg, 7% mol) were placed in round bottom flask and dissolved in 5 mL of dry toluene under inert atmosphere. The solution mixture was then left to stir at 120°C overnight. After cooling the reaction mixture to room temperature, the solution was extracted with diethyl ether (3x 50 mL) and water (2x 50 mL). The organic phase was collected and then washed with a brine solution. After that, the organic layer was combined, dried over MgSO<sub>4</sub>, filtered, and concentrated. The concentrated product was purified by silica gel

chromatography using petroleum ether and DCM (10:1) as eluents to yield the desired product as green liquid (910 mg, 90%).  $^1\text{H}$  NMR (400 MHz,  $\text{CDCl}_3$ ):  $\delta$  ppm 7.72 (d, 2H,  $J$  = 8.00 Hz), 7.63 (dd, 2H,  $J$  = 2.00 Hz,  $J$  = 1.50 Hz), 7.60 (d, 2H,  $J$  = 1.50 Hz), 7.43 (dd, 2H,  $J$  = 1.00 Hz,  $J$  = 1.00 Hz), 7.33 (dd, 2H,  $J$  = 1.00 Hz,  $J$  = 1.00 Hz), 7.14 (m, 2H), 2.03 (m, 4H), 1.39-0.98 (m, 24H), 0.82 (t, 6H,  $J$  = 7.00 Hz);  $^{13}\text{C}$  NMR (100 MHz,  $\text{CDCl}_3$ )  $\delta$  145.8, 142.9, 133.1, 128.9, 128.0, 126.2, 124.5, 123.0, 120.6, 117.7, 55.4, 33.7, 31.7, 29.4, 29.3, 29.1, 26.7, 22.5, 14.0; Mass calc. for  $\text{C}_{37}\text{H}_{46}\text{S}_2$ : 554.30. Found (EI); (m/z): 554.4 ( $[\text{M}^+]$ ); Elemental analysis (%): calc. for  $\text{C}_{37}\text{H}_{46}\text{S}_2$ : C, 80.09; H, 8.36; S, 11.55. Found: C, 79.88; H, 8.24; S, 11.33.

**5,5'-(9,9-Bis(2-(2-(2-methoxyethoxy)ethoxy)ethyl)-9H-fluorene-2,7-diyl)bis(2-bromothiophene) (M9)**

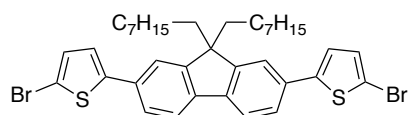
A solution of 2,2'-(9,9-bis(2(2(2methoxyethoxy)ethoxy)ethyl)-9H-fluorene-2,7-diyl)dithiophene (**18**) (1.35 g, 2.17 mmol) in chloroform and acetic acid (40 mL, 1:1 v/v) was placed into a 100 mL one-neck round-bottom flask. NBS (772 mg, 4.34 mmol) was then



added at room temperature for 2 h. The brominated reaction was monitored by TLC to establish completion. After that, the reaction mixture was quenched with 100 mL of  $\text{Na}_2\text{CO}_3$  solution and extracted with DCM (3x 50 mL), water (2x 50 mL), and brine. The organic phase was then combined, dried over  $\text{MgSO}_4$  and concentrated in *vacuo*. The concentrated product was purified by silica gel chromatography using ethyl acetate and DCM (2:3) as eluents to yield the desired product as green solid (1.01 g, 60%). M.p. 60-61  $^\circ\text{C}$ ;  $^1\text{H}$  NMR (400 MHz,  $\text{CDCl}_3$ ):  $\delta$  ppm 7.67 (d, 2H,  $J$  = 8.00 Hz), 7.56 (d, 2H,  $J$  = 2.00 Hz), 7.52 (dd, 2H,  $J$  = 8.00 Hz,  $J$  = 2.00 Hz), 7.15 (d, 2H,  $J$  = 4.00 Hz), 7.09 (d, 2H,  $J$  = 4.00 Hz), 3.50 (m, 4H), 3.45 (m, 4H), 3.40 (m, 4H), 3.33 (s, 6H), 3.24 (m, 4H), 2.83 (t, 4H,  $J$  = 7.50 Hz), 2.45 (t, 4H,  $J$  = 7.50 Hz);  $^{13}\text{C}$  NMR (100 MHz,  $\text{CDCl}_3$ )  $\delta$  150.1, 146.0, 139.6, 132.9, 130.9, 125.1, 120.4, 120.0, 111.4, 71.8, 70.4, 70.0, 66.9, 58.9, 51.5, 39.7, 29.5; Mass calc. for  $\text{C}_{35}\text{H}_{40}\text{Br}_2\text{O}_6\text{S}_2$ : 780.06. Found (AP); (m/z): 781.2, and 783.2 ( $[\text{M}^+]$ ,  $[\text{M}+2^+]$ ); Elemental analysis

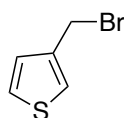
(%): calc. for C<sub>35</sub>H<sub>40</sub>Br<sub>2</sub>O<sub>6</sub>S<sub>2</sub>: C, 53.85; H, 5.17; Br, 20.47; S, 8.21. Found: C, 53.68; H, 5.21; Br, 21.48; S, 7.80.

### 5,5'-(9,9-Dioctyl-9H-fluorene-2,7-diyl)bis(2-bromothiophene) (**M10**)<sup>19</sup>



A solution of 2,2'-(9,9-dioctyl-9H-fluorene-2,7-diyl)dithiophene (**19**) (400 mg, 0.72 mmol) in chloroform and acetic acid (20 mL, 1:1 v/v) was placed into a 100 mL one-neck round-bottom flask. NBS (257 mg, 1.44 mmol) was then added and left the mixture to stir at 70° C for 4 h. The brominated reaction was monitored by TLC to establish completion. After that, the reaction mixture was quenched with 25 mL of Na<sub>2</sub>CO<sub>3</sub> solution and extracted with DCM (3x 50 mL), water (2x 50 mL), and brine. The organic phase was then combined, dried over MgSO<sub>4</sub> and concentrated in *vacuo*. The product was then washed with acetone to yield the desired product as pale yellow solid (436 mg, 85%). M.p. 70-71 °C; <sup>1</sup>H NMR (400 MHz, CDCl<sub>3</sub>): δ ppm 7.69 (d, 2H, *J*= 8.00 Hz), 7.52 (dd, 2H, *J*= 8.00 Hz, *J*= 2.00 Hz), 7.47 (d, 2H, *J*= 2.00 Hz), 7.15 (d, 2H, *J*= 4.00 Hz), 7.08 (d, 2H, *J*= 4.00 Hz), 2.01 (m, 4H), 1.24-1.05 (m, 20H), 0.82 (t, 6H, *J*= 7.00 Hz), 0.67 (m, 4H); <sup>13</sup>C NMR (100 MHz, CDCl<sub>3</sub>) δ 151.8, 146.5, 140.4, 132.6, 130.8, 124.6, 123.0, 120.3, 119.8, 111.1, 55.3, 40.3, 31.7, 29.9, 29.2, 29.1, 23.7, 22.6, 14.0; Mass calc. for C<sub>37</sub>H<sub>44</sub>Br<sub>2</sub>S<sub>2</sub>: 712.12. Found (EI); (*m/z*): 712.1, and 714.1 ([M<sup>+</sup>],[M+2<sup>+</sup>]); Elemental analysis (%): calc. for C<sub>37</sub>H<sub>44</sub>Br<sub>2</sub>S<sub>2</sub>: C, 62.36; H, 6.22; Br, 22.42; S, 9.00. Found: C, 62.57; H, 6.23; Br, 22.98; S, 8.95.

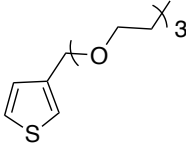
### 3-(Bromomethyl)thiophene (**20**)<sup>20</sup>



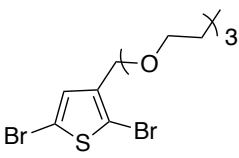
A solution of 3-thiophenemethanol (4.5 g, 39.4 mmol) and phosphorous tribromide (4.06 g, 14.9 mmol) in 20 ml of anhydrous DCM was placed in 100 mL round bottom flask under an inert atmosphere. The mixture was then left to stir at room temperature for 16 hours and then treated with saturated NaHCO<sub>3</sub>. The mixture was extracted with diethyl ether (3x 50 mL) and the organic phase was combined, dried over MgSO<sub>4</sub>, filtered and evaporated to dryness in *vacuo* to yield the desired product as light yellow liquid (4.65 g, 87.75%). <sup>1</sup>H NMR (400 MHz, CDCl<sub>3</sub>) δ

ppm 7.35 (m, 2H), 7.16 (dd, 1H,  $J= 5.00$  Hz,  $J= 3.50$  Hz), 4.55 (s, 2H).  $^{13}\text{C}$  NMR (100 MHz,  $\text{CDCl}_3$ )  $\delta$  138.3, 128.4, 127.0, 124.5, 27.7; Mass calc. for  $\text{C}_5\text{H}_5\text{BrS}$ : 175.93. Found (EI);(m/z): 175.9. ( $[\text{M}^+]$ ); Elemental analysis (%): calc. for  $\text{C}_5\text{H}_5\text{BrS}$ : C, 33.92; H, 2.85; Br, 45.12; S, 18.11. Found: C, 33.57; H, 2.99; Br, 44.92; S, 17.78.

### 3-((2-(2-Methoxyethoxy)ethoxy)methyl)thiophene (**21**)<sup>21</sup>

 (1 g, 42 mmol) of sodium hydride and 40 mL of anhydrous THF were placed in a 250 mL round bottom flask under an inert atmosphere. The mixture was then cooled to 0°C and (5.08 g, 42.2 mmol) of di(ethyleneglycol) monomethyl ether was added dropwise. After 30 min of stirring, (5 g, 28.2 mmol) of 3-(bromomethyl)thiophene (**20**) was added to the solution mixture and left to stir for 3 hours at room temperature. Then, the mixture was poured into distilled water and extracted with ethyl acetate (3x 300 mL). The organic phase was then combined, dried over  $\text{MgSO}_4$  overnight, filtered and concentrated in *vacuo*. The concentrated product was purified by silica gel chromatography using ethyl acetate and hexane (1:1) as eluents to yield the desired product as colourless liquid (3.64 g, 84%).  $^1\text{H}$  NMR (400 MHz,  $\text{CDCl}_3$ )  $\delta$  ppm 7.32 (m,1H), 7.24 (s, 1H), 7.10 (dd, 1H,  $J= 5.00$  Hz,  $J= 3.50$  Hz), 4.59 (s, 2H), 3.70 (m, 6H), 3.59 (m, 2H), 3.40 (s, 3H);  $^{13}\text{C}$  NMR (100 MHz,  $\text{CDCl}_3$ )  $\delta$  139.6, 127.7, 126.2, 132.1, 72.1, 70.8, 69.5, 68.6, 59.2; Mass calc. for  $\text{C}_{10}\text{H}_{16}\text{O}_3\text{S}$ : 216.08 Found (EI); (m/z): 217.1 ( $[\text{MH}^+]$ ); Elemental analysis (%): calc. for  $\text{C}_{10}\text{H}_{16}\text{O}_3\text{S}$ : C, 55.53; H, 7.46; S, 14.82. Found C, 54.86; H, 7.49; S, 11.35.

### 2,5-Dibromo-3-((2-(2-methoxyethoxy)ethoxy)methyl)thiophene (**M11**)<sup>21</sup>

 (1.5 g, 6.9 mmol) of 3-((2-(2-methoxyethoxy)ethoxy)methyl)-thiophene (**21**) and 20 mL of  $\text{CHCl}_3$  were charged in 100mL two-necks round bottom flask. NBS (2.135 g, 11 mmol) in 10 mL of DMF was added dropwise to the reaction mixture and left to stir in the dark at 60 °C for 24 hours. The brominated reaction was monitored by TLC to establish completion. After that, distilled water was added. The mixture was separated using  $\text{CHCl}_3$  (3x 30 mL). The organic

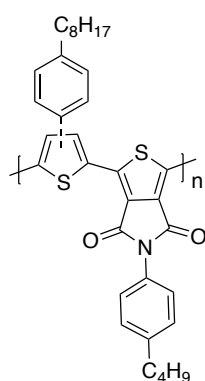


phase was then combined, dried over  $\text{MgSO}_4$ , filtered and concentrated in *vacuo*. The concentrated product was purified by silica gel chromatography using ethyl acetate: Hexane (7:3) as eluents to yield the desired product as colourless liquid (800 mg, 36%).  $^1\text{H}$  NMR (400 MHz,  $\text{CDCl}_3$ )  $\delta$  ppm 7.0 (s, 1H), 4.45 (s, 2H), 3.69 (m, 6H), 3.59 (m, 2H), 3.41 (s, 3H);  $^{13}\text{C}$  NMR (100 MHz,  $\text{CDCl}_3$ )  $\delta$  139.2, 130.8, 11.2, 109.9, 72.1, 70.6, 69.4, 66.9, 59.0; Mass calc. for  $\text{C}_{10}\text{H}_{14}\text{Br}_2\text{O}_3\text{S}$ : 374.09. Found (EI); (m/z): 375 ( $[\text{MH}^+]$ ); Elemental analysis (%): calc. for  $\text{C}_{10}\text{H}_{14}\text{Br}_2\text{O}_3\text{S}$ : C, 32.11; H, 3.77; Br, 42.72; S, 8.57. Found: C, 32.15; H, 3.94; Br, 38.42; S, 8.69.

## 6.4 Preparation of polymers

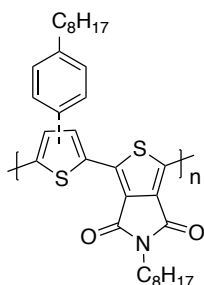
### Poly(3-(4-n-octylphenyl)thiophene-*alt*-5-(4-butylphenyl)-thieno-[3,4-c]pyrrole-4,6-dione) (rir-PT<sub>OP</sub>-TPD<sub>BP</sub>)

In a Schlenk tube was charged 5-(4-butylphenyl)-thieno[3,4-c]pyrrole-4,6-dione (**M1**) (120 mg, 0.42 mmol), 2,5-dibromo-3-(4-octylphenyl)thiophene (**M3**), (180 mg, 0.42 mmol),  $\text{Cs}_2\text{CO}_3$  (409 mg, 1.26 mmol), PivOH (43 mg, 0.42 mmol),  $\text{PdCl}_2(\text{MeCN})_2$  (4.3 mg, 4%mol),  $\text{P}(\text{C}_6\text{H}_4\text{-}o\text{-OMe})_3$  (5.9 mg, 4%mol), and anhydrous THF (1.8 mL) under an inert atmosphere. The mixture was stirred at room temperature for 30 min, and then warmed up to 90 °C for 2.5h. The mixture was cooled to room temperature, diluted with  $\text{CHCl}_3$  (250 mL) to dissolve the polymer deposited from the solution, and concentrated in *vacuo*. The concentrated solution was precipitated into vigorously stirred methanol. The precipitated solid was collected by membrane filter. The collected polymer was fractionated using methanol, acetone, hexane, toluene, chloroform in a Soxhlet apparatus. The chloroform fraction was concentrated *in vacuo*, and precipitated into vigorously stirred methanol. The precipitated fraction was filtered by a membrane filter to yield the copolymer as a dark red solid (144 mg, 62%). GPC chloroform fraction:  $M_n = 4400$  Da;  $M_w = 11700$  Da, PDI = 2.60;  $^1\text{H}$  NMR (500 MHz,  $\text{C}_2\text{D}_2\text{Cl}_4$ , 100 °C)  $\delta$  ppm 7.28 (m, 8H), 7.13-7.12 (m, 1H), 2.66 (br.m, 4H), 1.73-1.20 (br, 16H), 0.96 (t, 3H), 0.88 (t, 3H);



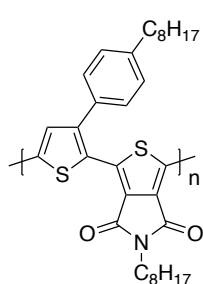
Elemental analysis (%): calc. for C<sub>34</sub>H<sub>35</sub>NO<sub>2</sub>S<sub>2</sub>: C, 73.74; H, 6.37; N, 2.53; S, 11.58. Found: C, 71.27; H, 6.03; N, 2.39; S, 11.26.

### Poly(3-(4-*n*-octylphenyl)thiophene-*a/t*-5-(octyl)-thieno-[3,4-*c*]pyrrole-4,6-dione) (rir-PT<sub>OP</sub>-TPD<sub>O</sub>)



PT<sub>OP</sub>-TPD<sub>O</sub> was synthesized following the similar procedure reported for PT<sub>OP</sub>-TPD<sub>BP</sub>, using a mixture of (**M2**) (81 mg, 0.31 mmol), (**M3**) (132 mg, 0.31 mmol), Cs<sub>2</sub>CO<sub>3</sub> (301 mg, 0.93 mmol), PivOH (31 mg, 0.31 mmol), PdCl<sub>2</sub>(MeCN)<sub>2</sub> (5.5 mg, 7%mol), P(C<sub>6</sub>H<sub>4</sub>-*o*-OMe)<sub>3</sub> (7.5 mg, 7%mol), and THF (1.8 mL). The mixture was stirred and warmed up to 90 °C for 5h. The copolymer was obtained as a dark purple solid (73 mg, 44%). GPC chloroform fraction: *M<sub>n</sub>* = 19800 Da; *M<sub>w</sub>* = 48000 Da; PDI= 2.40; <sup>1</sup>H NMR (500 MHz, C<sub>2</sub>D<sub>2</sub>Cl<sub>4</sub>, 100 °C) δ ppm 7.20 (m, 4H), 7.13-7.12 (m, 1H), 3.60 (br, 2H) 2.66 (t, 2H), 1.78-1.21 (br.m, 24H), 0.89 (t, 6H); Elemental analysis (%): calc. for C<sub>32</sub>H<sub>39</sub>NO<sub>2</sub>S<sub>2</sub>: C, 72.00; H, 7.36; N, 2.62; S, 12.01. Found: C, 71.19; H, 7.15; N, 2.51; S, 11.77.

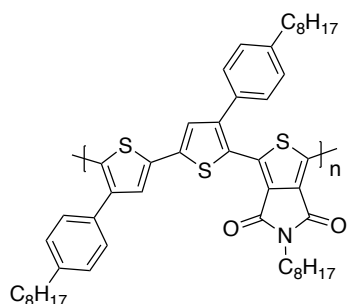
### Poly(3-(4-*n*-octylphenyl)thiophene-*a/t*-5-(octyl)-thieno-[3,4-*c*]pyrrole-4,6-dione) (rr-PT<sub>OP</sub>-TPD<sub>O</sub>)



PT<sub>OP</sub>-TPD<sub>O</sub> was synthesized following the similar procedure reported for PT<sub>OP</sub>-TPD<sub>BP</sub>, using 1-(5-bromo-3-(4octylphenyl)thiophen-2-yl)-5-octyl-4*H*-thieno[3,4-*c*]pyrrole-4,6(5*H*)-dione (**M4**) (58 mg, 0.094 mmol), Cs<sub>2</sub>CO<sub>3</sub> (92 mg, 0.283 mmol), PivOH (9.6 mg, 0.094 mmol), PdCl<sub>2</sub>(MeCN)<sub>2</sub> (1.7 mg, 7%mol), P(C<sub>6</sub>H<sub>4</sub>-*o*-OMe)<sub>3</sub> (2.33 mg, 7%mol), and THF (1.8 mL). The mixture was stirred and warmed up to 90 °C for 3h. The homopolymer was achieved as a dark purple solid (25 mg, 50%). GPC chloroform fraction: *M<sub>n</sub>* = 2700 Da; *M<sub>w</sub>* = 3600 Da; PDI= 1.32; <sup>1</sup>H NMR (500 MHz, C<sub>2</sub>D<sub>2</sub>Cl<sub>4</sub>, 100 °C) δ ppm 7.24 (br, 1H), 7.21-7.12 (br.dd, 4H), 3.64 (br, 2H), 2.71 (br.t, 2H), 1.78-1.23 (br.m, 24H), 0.94 (br.t, 6H); Elemental analysis (%): calc. for C<sub>32</sub>H<sub>39</sub>NO<sub>2</sub>S<sub>2</sub>: C, 72.00; H, 7.36; N, 2.62; S, 12.01. Found: C, 69.64; H, 6.90; N, 2.44; S, 11.08.

**Poly(4,4'-bis(4-octylphenyl)-2,2'-bithiophene-*alt*-5-(octyl)-thieno-[3,4-  
c]pyrrole-4,6-dione) (PBT<sub>OP</sub>-TPD<sub>O</sub> [TT])**

PBT<sub>OP</sub>-TPD<sub>O</sub> was synthesized following the similar procedure reported for

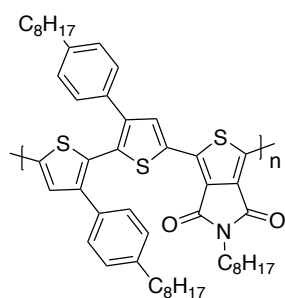


PT<sub>OP</sub>-TPD<sub>BP</sub>, using a mixture of 5,5'-dibromo-4,4'-bis(4-octylphenyl)-2,2'-bithiophene (**M5**) (90 mg, 0.129 mmol), (**M3**) (34 mg, 0.129 mmol), Cs<sub>2</sub>CO<sub>3</sub> (125 mg, 0.386 mmol), PivOH (13 mg, 0.129 mmol), PdCl<sub>2</sub>(MeCN)<sub>2</sub> (2.33 mg, 7%mol), P(C<sub>6</sub>H<sub>4</sub>-*o*-OMe)<sub>3</sub> (3.2 mg, 7%mol), and THF (1.8 mL). The

mixture was stirred and warmed up to 90 °C for 24h. The main polymer fraction was collected in toluene. The copolymer was acquired as a dark red solid (35 mg, 34%). GPC toluene fraction:  $M_n = 31600$  Da;  $M_w = 12900$  Da; PDI = 4.10; <sup>1</sup>H NMR (500 MHz, C<sub>2</sub>D<sub>2</sub>Cl<sub>4</sub>, 100 °C) δ ppm 8.01 (br.s, 2H), 7.01 (br.dd, 8H), 3.70 (br, 2H), 2.60 (br.t, 4H), 1.78-1.21 (br.m, 34H), 0.94 (br.t, 9H); Elemental analysis (%): calc. for C<sub>50</sub>H<sub>61</sub> NO<sub>2</sub>S<sub>3</sub>: C, 74.67; H, 7.65; N, 1.74; S, 11.96. Found: C, 73.24; H, 7.46; N, 1.54; S, 11.31.

**Poly(3,3'-bis(4-octylphenyl)-2,2'-bithiophene-*alt*-5-(octyl)-thieno-[3,4-  
c]pyrrole-4,6-dione) (PBT<sub>OP</sub>-TPD<sub>O</sub> [HH])**

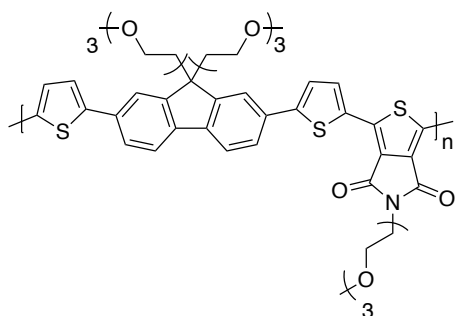
PBT<sub>OP</sub>-TPD<sub>O</sub> was synthesized following the similar procedure reported for



PT<sub>OP</sub>-TPD<sub>BP</sub>, using a mixture of 5,5'-dibromo-3,3'-bis(4-octylphenyl)-2,2'-bithiophene (**M6**) (86 mg, 0.123 mmol), (**M3**) (34 mg, 0.123 mmol), Cs<sub>2</sub>CO<sub>3</sub> (119 mg, 0.369 mmol), PivOH (12.5 mg, 0.123 mmol), PdCl<sub>2</sub>(MeCN)<sub>2</sub> (2.23 mg, 7%mol), P(C<sub>6</sub>H<sub>4</sub>-*o*-OMe)<sub>3</sub> (3 mg, 7%mol), and anhydrous THF (1.8 mL). The

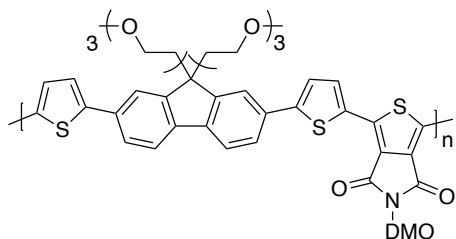
mixture was stirred and warmed up to 90 °C for 72h. The main polymer fraction was collected in toluene. The copolymer was obtained as a dark red solid (18 mg, 17.4%). GPC toluene fraction:  $M_n = 10500$  Da;  $M_w = 20000$  Da; PDI = 1.90; <sup>1</sup>H NMR (500 MHz, C<sub>2</sub>D<sub>2</sub>Cl<sub>4</sub>, 100 °C) δ ppm 7.91 (br, 2H), 7.30 (br, 8H), 3.64 (br, 2H), 2.70 (br.t, 4H), 1.81-1.25 (br.m, 36H), 0.94 (br.t, 9H); Elemental analysis (%): calc. for C<sub>50</sub>H<sub>61</sub> NO<sub>2</sub>S<sub>3</sub>: C, 74.67; H, 7.65; N, 1.74; S, 11.96. Found: C, 71.23; H, 7.42; N, 1.69; S, 11.24.

**Poly(5-(9,9-bis(2-(2-(2-methoxyethoxy)ethoxy)ethyl)-7-(thiophene-2-yl)-9H-fluorene-2-yl)thiophene-2-yl)-alt-5-(2-(2-(2-methoxyethoxy)ethoxy)ethyl)-thieno[3,4-c]pyrrole-4,6-dione) (PF<sub>OXY</sub>DT-TPD<sub>OXY</sub>)**



PF<sub>OXY</sub>DT-TPD<sub>OXY</sub> was prepared according to a procedure proposed for PT<sub>OP</sub>-TPD<sub>BP</sub>, using a mixture of 5,5'-(9,9-bis(2-(2-(2-methoxyethoxy)ethoxy)ethyl)-9H-fluorene-2,7-diyl)bis(2-bromothiophene) (**M7**) (100 mg, 0.128 mmol), 5-(2-(2-(2-methoxyethoxy)ethoxy)ethyl)-4H-thieno[3,4-c]pyrrole-4,6(5H)-dione (**M10**) (38.34 mg, 0.128 mmol), Cs<sub>2</sub>CO<sub>3</sub> (125.30 mg, 0.385 mmol), PivOH (13 mg, 0.128 mmol), Pd<sub>2</sub>(dba)<sub>3</sub> (8.2 mg, 7%mol), P(C<sub>6</sub>H<sub>4</sub>-o-OMe)<sub>3</sub> (3.17 mg, 7%mol), and THF (2 mL). The mixture was stirred and warmed up to 90 °C for 8h. The polymer was achieved as a dark red solid (40 mg, 34%). GPC chloroform fraction: *M<sub>n</sub>* = 4000 Da; *M<sub>w</sub>* = 4900 Da; PDI = 1.21 (Incorrect); <sup>1</sup>H NMR (500 MHz, C<sub>2</sub>D<sub>2</sub>Cl<sub>4</sub>, 100 °C) δ ppm 8.11 (br, 2H), 7.85-7.68 (br.m, 6H), 7.45 (br, 2H), 3.85 (br, 2H) 3.76-3.62 (m, 6H), 3.60-3.25 (m, 29H), 3.07 (br, 4H), 2.52 (br, 4H); Elemental analysis (%): calc. for C<sub>48</sub>H<sub>55</sub>NO<sub>11</sub>S<sub>3</sub>: C, 62.79; H, 6.04; N, 1.53; S, 10.48. Found: C, 61.44; H, 5.94; N, 1.35; S, 9.88.

**Poly(5-(9,9-bis(2-(2-(2-methoxyethoxy)ethoxy)ethyl)-7-(thiophene-2-yl)-9H-fluorene-2-yl)thiophene-2-yl)-alt-5-(-(3,7-dimethyloctyl))-thieno-[3,4-c]pyrrole-4,6-dione) (PF<sub>OXY</sub>DT-TPD<sub>DMO</sub>)**

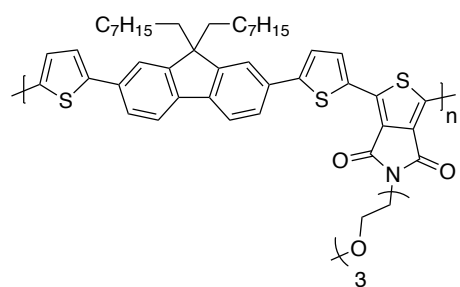


PF<sub>OXY</sub>DT-TPD<sub>DMO</sub> was prepared according to a procedure proposed for PT<sub>OP</sub>-TPD<sub>BP</sub>, using a mixture of 5,5'-(9,9-bis(2-(2-(2-methoxyethoxy)ethoxy)ethyl)-9H-fluorene-2,7-diyl)bis(2-bromothiophene) (**M7**) (104 mg, 0.13 mmol), 5-(3,7-dimethyloctyl)-4H-thieno[3,4-c]pyrrole-4,6(5H)-dione (**M9**) (39.08 mg, 0.13 mmol), Cs<sub>2</sub>CO<sub>3</sub> (130.31 mg, 0.40 mmol), PivOH (13.61 mg, 0.13 mmol), Pd<sub>2</sub>(dba)<sub>3</sub> (8.5 mg, 7 %mol), P(C<sub>6</sub>H<sub>4</sub>-o-OMe)<sub>3</sub> (3.3 mg, 7 %mol), and THF (2 mL). The mixture was stirred

and warmed up to 90 °C for 5h. The polymer was achieved as a dark red solid (40 mg, 33.5%). GPC chloroform fraction:  $M_n$  = 29100 Da;  $M_w$  = 49000 Da; PDI = 1.68;  $^1\text{H}$  NMR (500 MHz,  $\text{C}_2\text{D}_2\text{Cl}_4$ , 100 °C)  $\delta$  ppm 8.12 (br.d, 2H), 7.82-7.73 (m, 6H), 7.48 (br.d, 2H), 3.78 (br, 2H) 3.54-3.38 (m, 12H), 3.35-3.29 (10H), 3.08 (br.t, 4H), 2.52 (br, 4H) 1.80-1.20 (br.m, 10H) 1.08 (br.d, 3H) 0.94 (dd, 6H); Elemental analysis (%): calc. for  $\text{C}_{51}\text{H}_{61}\text{NO}_8\text{S}_3$ : C, 67.15; H, 6.74; N, 1.54; S, 10.54. Found: C, 66.02; H, 6.87; N, 1.16; S, 9.68.

**Poly(5-(9,9-dioctyl-7-(thiophene-2-yl)-9H-fluorene-2-yl)thiophene-2-yl)-*alt*-5-(2-(2-(2-methoxyethoxy)ethoxy)ethyl)-thieno[3,4-*c*]pyrrole-4,6-dione) (PF<sub>o</sub>DT-TPD<sub>oxy</sub>)**

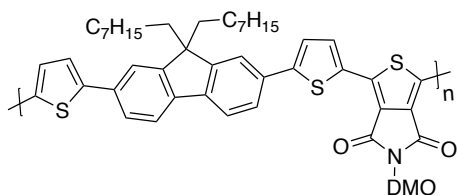
PF<sub>o</sub>DT-TPD<sub>oxy</sub> was prepared according to a procedure proposed for PT<sub>OP</sub>-



TPD<sub>BP</sub>, using a mixture of 5,5'-(9,9-dioctyl-9H-fluorene-2,7-diyl)bis(2-bromothiophene) (**M8**) (101 mg, 0.14 mmol), 5-(2-(2-(2-methoxyethoxy)ethoxy)ethyl)-4H-thieno[3,4-*c*]pyrrole-4,6(5H)-dione (**M10**) (42.42 mg, 0.14 mmol),  $\text{Cs}_2\text{CO}_3$  (138.63 mg, 0.425

mmol), PivOH (14.5 mg, 0.14 mmol),  $\text{Pd}_2(\text{dba})_3$  (9.1 mg, 7%mol),  $\text{P}(\text{C}_6\text{H}_4\text{-}o\text{-OMe})_3$  (3.5 mg, 7%mol), and THF (2 mL). The mixture was stirred and warmed up to 90 °C for 5h. The polymer was achieved as a dark red solid (52.80 mg, 42.35 %). GPC chloroform fraction:  $M_n$  = 46600 Da;  $M_w$  = 102800 Da; PDI = 2.20;  $^1\text{H}$  NMR (500 MHz,  $\text{C}_2\text{D}_2\text{Cl}_4$ , 100 °C)  $\delta$  ppm 8.13 (br.d, 2H), 7.79 (br.d, 2H), 7.72 (br.d, 2H), 7.69 (br.s, 2H), 7.46 (br.d, 2H), 3.97 (br, 2H) 3.85 (br.t, 2H), 3.76-3.62 (m, 6H), 3.55 (br.t, 2H), 3.37 (s, 3H) 2.15 (br, 4H) 1.70-1.10 (br.m, 20H) 0.94 (br.d, 4H) 0.87 (br.t, 6H); Elemental analysis (%): calc. for  $\text{C}_{50}\text{H}_{59}\text{NO}_5\text{S}_3$ : C, 70.64; H, 7.00; N, 1.65; S, 11.31. Found: C, 70.24; H, 6.40; N, 1.46; S, 10.24.

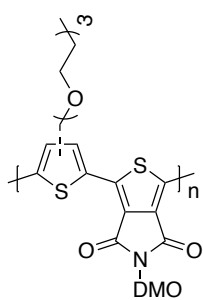
**Poly(5-(9,9-dioctyl-7-(thiophene-2-yl)-9H-fluorene-2-yl)thiophene-2-yl)-*alt*-5-(3,7-dimethyloctyl)-thieno-[3,4-c]pyrrole-4,6-dione)(PF<sub>0</sub>DT-TPD<sub>DMO</sub>)**



PF<sub>0</sub>DT-TPD<sub>DMO</sub> was prepared according to a procedure proposed for PT<sub>OP</sub>-TPD<sub>BP</sub>, using a mixture of 5,5'-(9,9-dioctyl-9H-fluorene-2,7-diyl)bis(2-bromothiophene) (**M8**) (101 mg,

0.14 mmol), 5-(3,7-dimethyloctyl)-4*H*-thieno [3,4-*c*] pyrrole-4,6(5*H*)-dione (**M9**) (41.57 mg, 0.14 mmol), Cs<sub>2</sub>CO<sub>3</sub> (138.63 mg, 0.425 mmol), PivOH (14.5 mg, 0.14 mmol), Pd<sub>2</sub>(dba)<sub>3</sub> (9.1 mg, 7%mol), P(C<sub>6</sub>H<sub>4</sub>-*o*-OMe)<sub>3</sub> (3.5 mg, 7%mol), and THF (2 mL). The mixture was stirred and warmed up to 90 °C for 7h. The polymer was achieved as a dark red solid (25 mg, 21.17 %). GPC chloroform fraction:  $M_n = 41200$  Da;  $M_w = 93900$  Da; PDI = 2.28; <sup>1</sup>H NMR (500 MHz, C<sub>2</sub>D<sub>2</sub>Cl<sub>4</sub>, 100 °C) δ ppm 8.13 (br, 2H), 7.78 (br.d, 2H), 7.72 (br.d, 2H), 7.69 (br.s, 2H), 7.46 (br.d, 2H), 3.79 (br, 2H), 2.14 (br, 4H) 1.70-1.04 (br.m, 32H), 0.96 (br.d, 4H), 0.87 (br.t, 9H); Elemental analysis (%): calc. for C<sub>53</sub>H<sub>65</sub>NO<sub>2</sub>S<sub>3</sub>: C, 75.40; H, 7.76; N, 1.66; S, 11.39. Found: C, 74.79; H, 8.02; N, 1.19; S, 9.38.

**Poly((3-((2-(2-methoxyethoxy)ethoxy)methyl)thiophene2,5-diyl)-*alt*-5-(3,7-dimethyloctyl)-thieno [3,4-*c*] pyrrole-4,6-dione) (PT<sub>OXY</sub>-TPD<sub>DMO</sub>)**



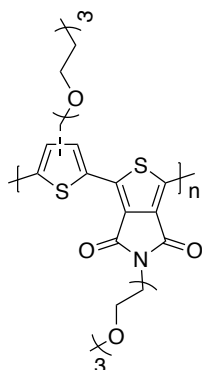
PT<sub>OXY</sub>-TPD<sub>DMO</sub> was synthesized following the similar procedure reported for PT<sub>OP</sub>-TPD<sub>BP</sub>, using a mixture of 5-(3,7-dimethyloctyl)-4*H*-thieno [3,4-*c*] pyrrole-4,6(5*H*)-dione (**M9**) (100 mg, 0.34 mmol), 2,5-dibromo-3-((2-(2-methoxyethoxy)ethoxy)methyl)thiophene (**M11**) (127 mg, 0.34 mmol), PdCl<sub>2</sub>(MeCN)<sub>2</sub> (6 mg, 7%mol), P(C<sub>6</sub>H<sub>4</sub>-*o*-OMe)<sub>3</sub>

(8 mg, 7%mol), Cs<sub>2</sub>CO<sub>3</sub> (333 mg, 1.02 mmol), PivOH (34.70 mg, 0.34mmol), and anhydrous THF (1.5 mL). The mixture was stirred and warmed up to 90 °C for 4h. The copolymer was obtained as a dark purple solid (167 mg, 91%). GPC chloroform fraction:  $M_n = 29400$  Da;  $M_w = 48100$  Da; PDI = 1.63; <sup>1</sup>H NMR (500 MHz, C<sub>2</sub>D<sub>2</sub>Cl<sub>4</sub>, 100 °C) δ ppm 8.08 (br, 1H), 4.74 (br, 2H), 3.76-3.60 (m, 8H), 3.53 (br, 2H), 3.34 (br. 3H), 1.80 (br, 2H), 1.62-1.15 (br.m, 8H),

1.01 (br, 3H), 0.92 (br.d, 6H); Elemental analysis (%): calc. for C<sub>26</sub>H<sub>35</sub>NO<sub>5</sub>S<sub>2</sub>: C, 61.75; H, 6.98; N, 2.77; S, 12.68. Found: C, 62.69; H, 7.15; N, 2.58; S, 11.83.

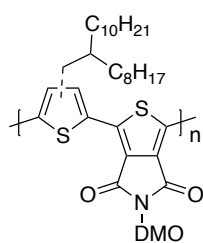
**Poly((3-((2-(2-methoxyethoxy)ethoxy)methyl)thiophene-2,5-diyl)-alt-5-[2-  
[2-(2-methoxyethoxy)ethoxy]ethyl]-thieno[3,4-c]pyrrole-4,6-dione)**

**(PT<sub>OXY</sub>-TPD<sub>OXY</sub>)**



PT<sub>OXY</sub>-TPD<sub>OXY</sub> was synthesized following the similar procedure reported for PT<sub>OP</sub>-TPD<sub>BP</sub>, using a mixture of 5-(2-(2-(2-methoxyethoxy)ethoxy)ethyl)-4*H*-thieno[3,4-*c*]pyrrole-4,6(5*H*)-dione (**M10**) (100 mg, 0.34 mmol), 2,5-dibromo-3-((2-(2-methoxyethoxy)ethoxy)methyl)thiophene (**M11**) (127 mg, 0.34 mmol), PdCl<sub>2</sub>(MeCN)<sub>2</sub> (6 mg, 7%mol), P(C<sub>6</sub>H<sub>4</sub>-*o*-OMe)<sub>3</sub> (8mg, 7%mol), Cs<sub>2</sub>CO<sub>3</sub> (333 mg, 1.02 mmol), PivOH (34.70 mg, 0.34mmol), and anhydrous THF (1.5 mL). The mixture was stirred and warmed up to 90 °C for 5h. The copolymer was obtained as dark purple solid (105 mg, 58%). GPC chloroform fraction: *M<sub>n</sub>* = 1600 Da; *M<sub>w</sub>* = 1700 Da; PDI = 1.07 (Incorrect); <sup>1</sup>H NMR (500 MHz, C<sub>2</sub>D<sub>2</sub>Cl<sub>4</sub>, 100 °C) δ ppm 8.08 (br, 1H), 4.75 (br.s, 2H), 3.89 (br, 2H), 3.81- 3.45 (m, 18H), 3.36-3.31 (br.m, 6H); Elemental analysis (%): calc. for C<sub>23</sub>H<sub>29</sub>NO<sub>8</sub>S<sub>2</sub>: C 54.00, H 5.71, N 2.74, S 12.53; found C 52.09, H 5.69, N 2.47, S 11.83.

**Poly((3-(2-octyldodecyl)thiophene-2,5-diyl)-alt-5-(3,7-dimethylotyl)  
thieno[3,4-c]pyrrole-4,6-dione) (PT<sub>ODD</sub>-TPD<sub>DMO</sub>)**



PT<sub>ODD</sub>-TPD<sub>DMO</sub> was synthesized following the similar procedure reported for PT<sub>OP</sub>-TPD<sub>BP</sub>, using a mixture of 5-(3,7-dimethyloctyl)-4*H*- thieno [3,4-*c*] pyrrole-4,6(5*H*)-dione (**M9**) (100 mg, 0.34 mmol), 2,5-dibromo-3-(2-octyldodecyl)thiophene (177.53 mg, 0.34 mmol), PdCl<sub>2</sub>(MeCN)<sub>2</sub> (6 mg, 7%mol), P(C<sub>6</sub>H<sub>4</sub>-*o*-OMe)<sub>3</sub> (8mg, 7%mol), Cs<sub>2</sub>CO<sub>3</sub> (333 mg, 1.02 mmol), PivOH (34.70 mg, 0.34mmol), and anhydrous THF (1.5 mL). The mixture was stirred and warmed up to 90 °C for 48h. The copolymer was

obtained as dark purple solid (210 mg, 94.50%). GPC chloroform fraction:  $M_n$  = 13300 Da;  $M_w$  = 18000 Da; PDI = 1.40;  $^1\text{H}$  NMR (500 MHz,  $\text{CDCl}_3$ )  $\delta$  ppm 7.94 (br.d, 1H), 3.70 (br, 4H), 2.82 (br, 2H), 1.97-1.05 (br.m, 18H), 0.99 (br, 3H), 0.87 (br, 12H); Elemental analysis (%): calc. for  $\text{C}_{40}\text{H}_{63}\text{NO}_2\text{S}_2$ : C 73.45, H 9.71, N 2.14, S 9.80; found C 72.35, H 9.53, N 2.03, S 8.69.



## 6.5 References

1. P. Berrouard, F. Grenier, J.-R. Pouliot, E. Gagnon, C. Tessier and M. Leclerc, *Organic Letters*, 2011, **13**, 38-41.
2. P. Berrouard, S. Dufresne, A. Pron, J. Veilleux and M. Leclerc, *Journal of Organic Chemistry*, 2012, **77**, 8167-8173.
3. E. W. Zhu, B. Ni, B. F. Zhao, J. F. Hai, L. Y. Bian, H. B. Wu and W. H. Tang, *Macromolecular Chemistry and Physics*, 2014, **215**, 227-234.
4. C. Piliago, T. W. Holcombe, J. D. Douglas, C. H. Woo, P. M. Beaujuge and J. M. J. Frechet, *Journal of the American Chemical Society*, 2010, **132**, 7595-+.
5. J. Warnan, A. El Labban, C. Cabanetos, E. T. Hoke, P. K. Shukla, C. Risko, J. L. Bredas, M. D. McGehee and P. M. Beaujuge, *Chemistry of Materials*, 2014, **26**, 2299-2306.
6. I. Barlow, S. Sun, G. J. Leggett and M. Turner, *Langmuir*, 2010, **26**, 4449-4458.
7. H. Yi, S. Al-Faifi, A. Iraqi, D. C. Watters, J. Kingsley and D. G. Lidzey, *Journal of Materials Chemistry*, 2011, **21**, 13649-13656.
8. A. Britze, V. Moellmann, G. Grundmeier, H. Luftmann and D. Kuckling, *Macromolecular Chemistry and Physics*, 2011, **212**, 679-690.
9. M. Wakioka, Y. Kitano and F. Ozawa, *Macromolecules*, 2013, **46**, 370-374.
10. M. Takahashi, K. Masui, H. Sekiguchi, N. Kobayashi, A. Mori, M. Funahashi and N. Tamaoki, *Journal of the American Chemical Society*, 2006, **128**, 10930-10933.
11. X. Guo, H. N. Tsao, P. Gao, D. Xia, C. An, M. K. Nazeeruddin, M. Baumgarten, M. Graetzel and K. Muellen, *RSC Advances*, 2014, **4**, 54130-54133.
12. B. Meng, H. Y. Song, X. X. Chen, Z. Y. Xie, J. Liu and L. X. Wang, *Macromolecules*, 2015, **48**, 4357-4363.
13. S. J. Liu, Z. P. Kan, S. Thomas, F. Cruciani, J. L. Bredas and P. M. Beaujuge, *Angewandte Chemie-International Edition*, 2016, **55**, 12996-13000.
14. A. S. Jalilov, L. G. Nilewski, V. Berka, C. H. Zhang, A. A. Yakovenko, G. Wu, T. A. Kent, A. L. Tsai and J. M. Tour, *ACS Nano*, 2017, **11**, 2024-2032.
15. J. Warnan, A. El Labban, C. Cabanetos, E. T. Hoke, P. K. Shukla, C. Risko, J.-L. Bredas, M. D. McGehee and P. M. Beaujuge, *Chemistry of Materials*, 2014, **26**, 2299-2306.
16. G. F. Zhang, T. Chen, Z. Q. Chen, M. P. Aldred, X. G. Meng and M. Q. Zhu, *Chinese Journal of Chemistry*, 2015, **33**, 939-947.
17. M. Irfan, K. D. Belfield and A. Saeed, *RSC Advances*, 2015, **5**, 48760-48768.

18. M. J. Baek, W. Jang, S. H. Lee and Y. S. Lee, *Synthetic Metals*, 2012, **161**, 2785-2791.
19. W. B. Ma, Y. Q. Wu, J. H. Han, J. H. Liu, D. H. Gu and F. X. Gan, *Chinese Physics*, 2006, **15**, 750-755.
20. L. Wang, Y. Zhai, X. Wang, Q. Feng, M. Pei, G. Zhang, *Advanced in Polymer Technology*, 2013, 32, E612-E623.
21. M. P. Ouattara, S. Lenfant, D. Vuillaume, M. Pezolet, J. F. Rioux-Dube, J. Brisson and M. Leclerc, *Macromolecules*, 2013, **46**, 6408-6418.

>>

**CHAPTER VII  
SUPPLEMENTARY  
INFORMATION**

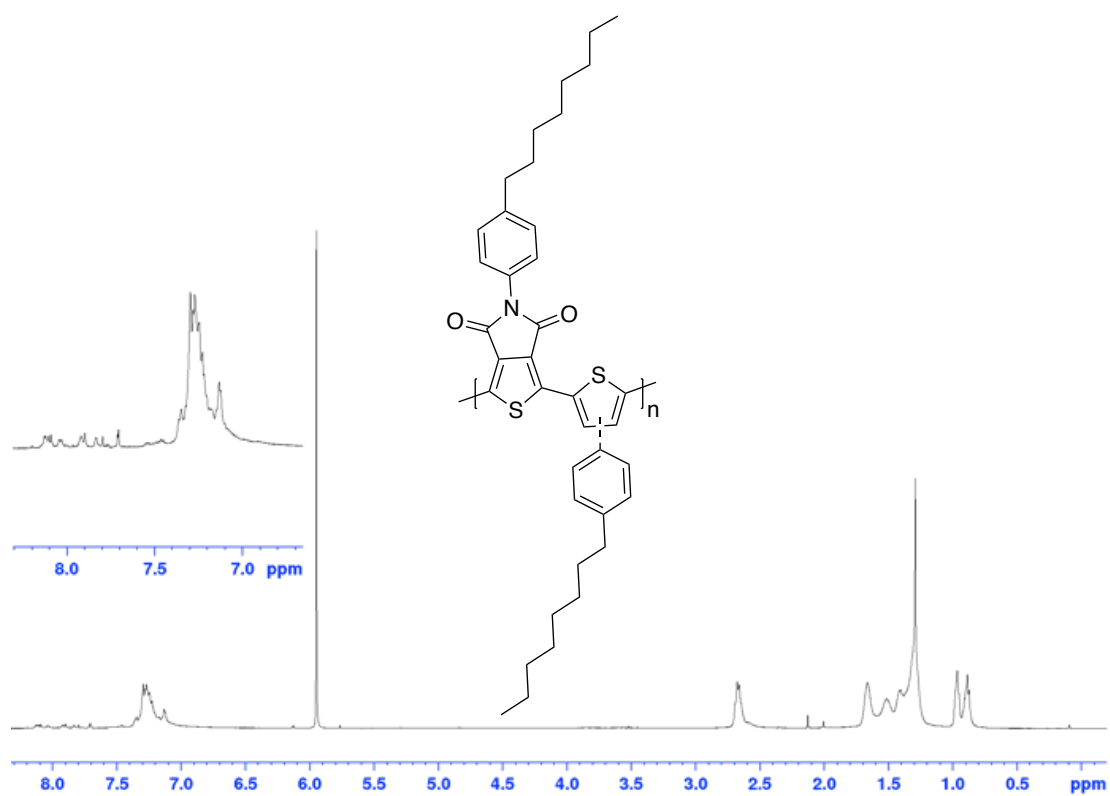


**Figure S 1.**  $^1\text{H}$  NMR spectrum of RIR-PBT<sub>OP</sub>-TPD<sub>BP</sub> in  $\text{C}_2\text{D}_2\text{Cl}_4$  at  $100^\circ\text{C}$ .

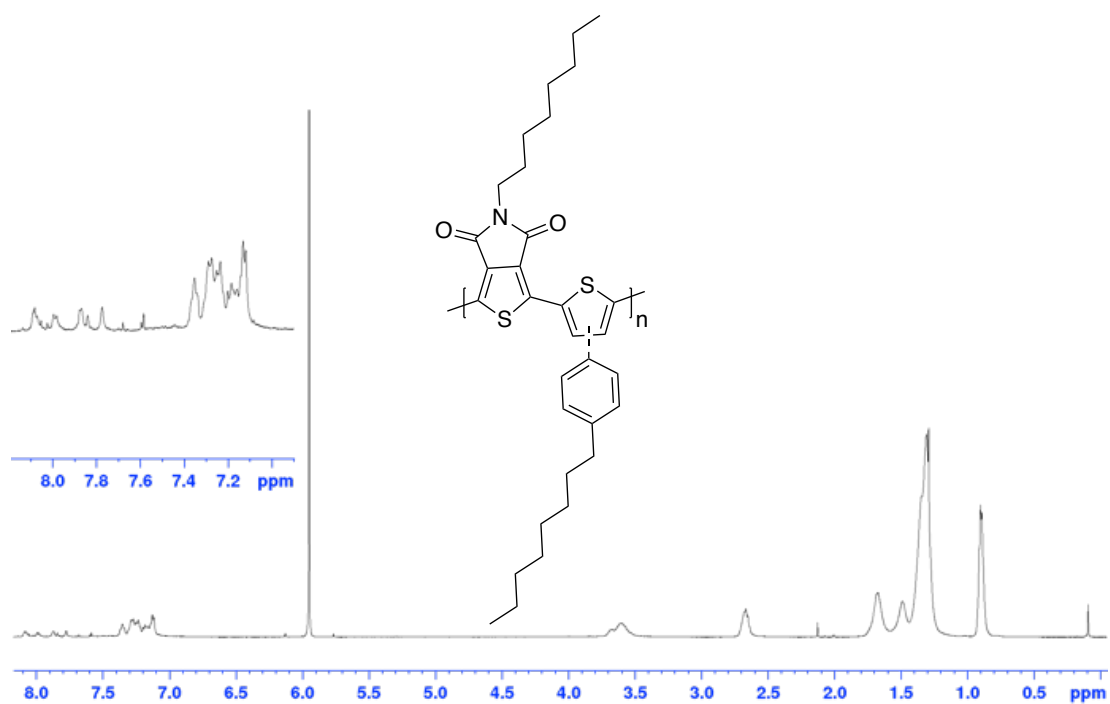


**Figure S 2.**  $^1\text{H}$  NMR spectrum of RIR-PBT<sub>OP</sub>-TPD<sub>O</sub> in  $\text{C}_2\text{D}_2\text{Cl}_4$  at  $100^\circ\text{C}$ .

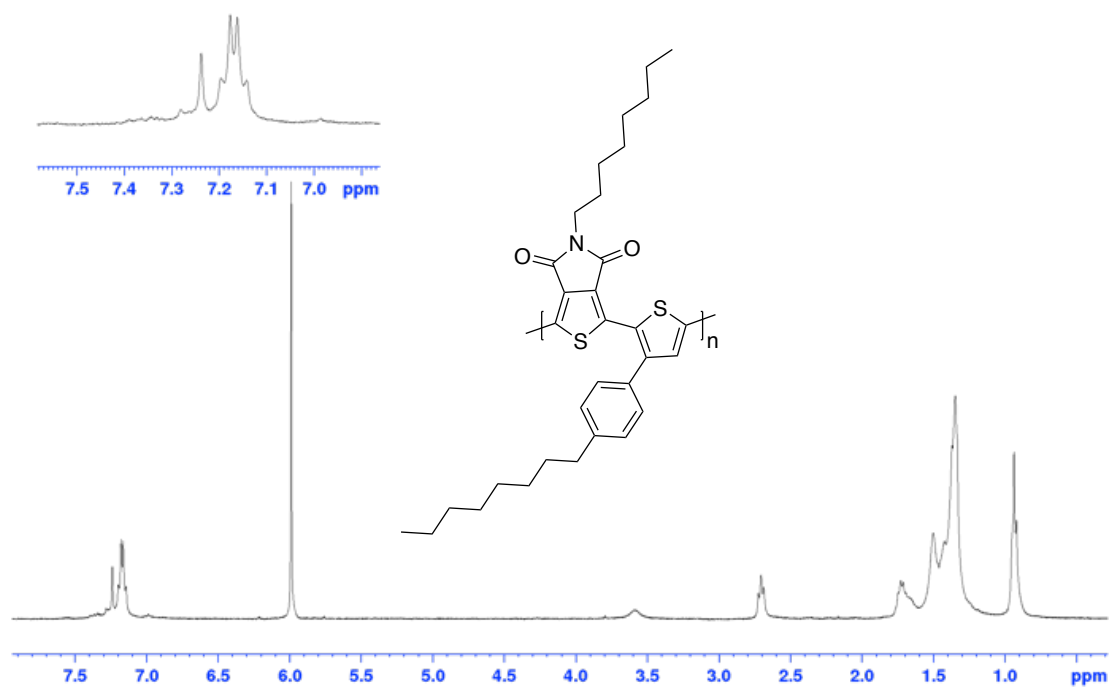


**Figure S 3.**  $^1\text{H}$  NMR spectrum of RR-PBT<sub>OP</sub>-TPD<sub>O</sub> in  $\text{C}_2\text{D}_2\text{Cl}_4$  at  $100\text{ }^\circ\text{C}$ .

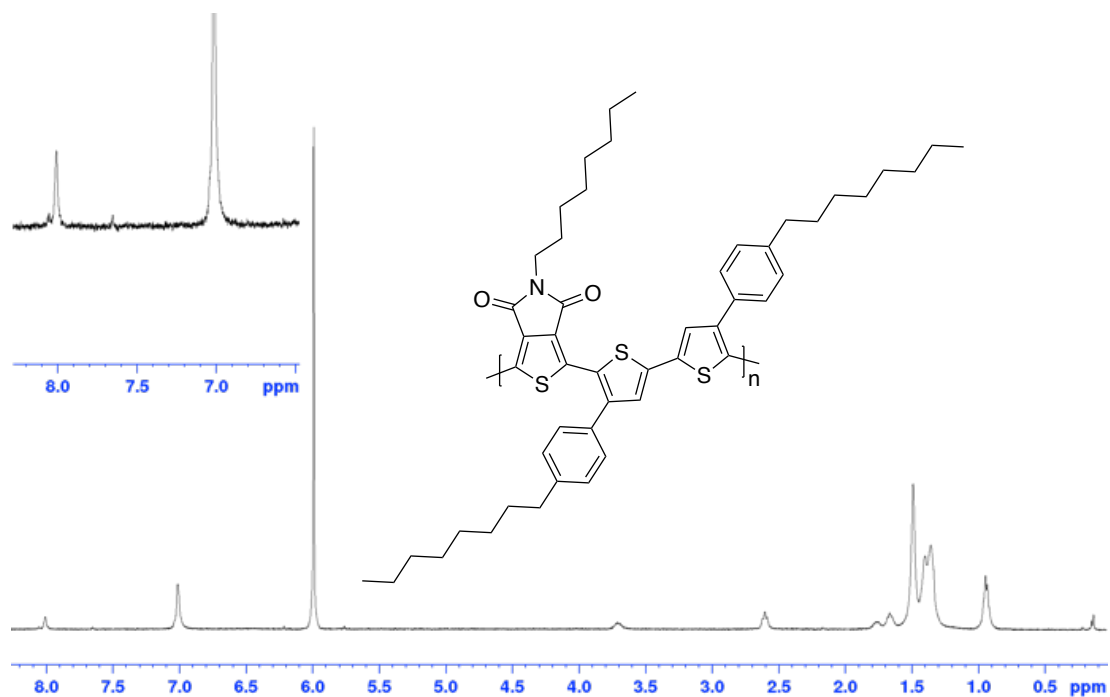


**Figure S 4.**  $^1\text{H}$  NMR spectrum of TT-PBT<sub>OP</sub>-TPD<sub>O</sub> in  $\text{C}_2\text{D}_2\text{Cl}_4$  at  $100\text{ }^\circ\text{C}$ .

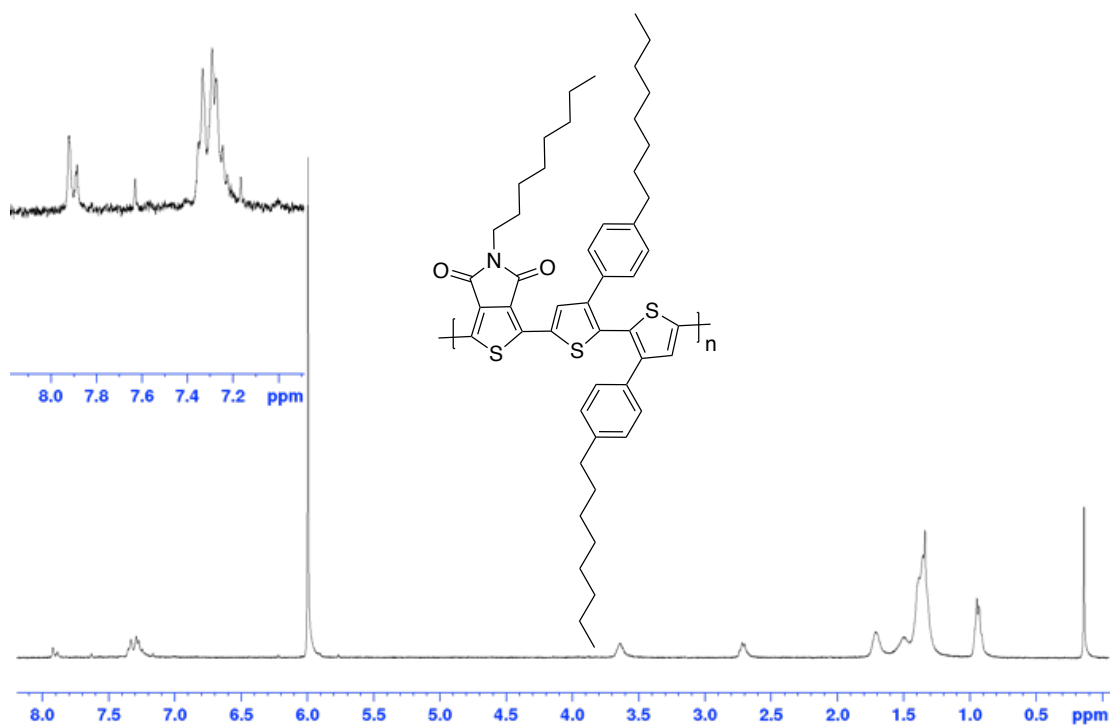


**Figure S 5.** <sup>1</sup>H NMR spectrum of **HH-PBT<sub>OP</sub>-TPD<sub>O</sub>** in C<sub>2</sub>D<sub>2</sub>Cl<sub>4</sub> at 100 °C.

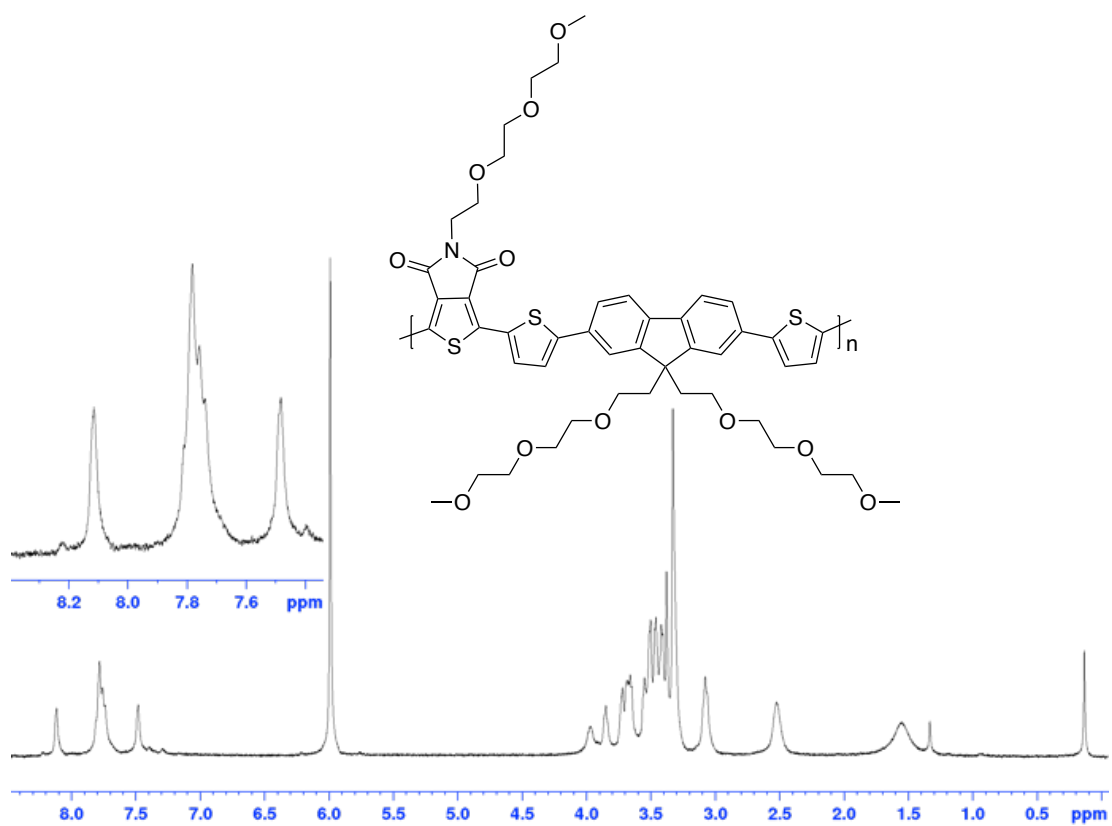


**Figure S 6.** <sup>1</sup>H NMR spectrum of **PF<sub>oxy</sub>DT-TPD<sub>oxy</sub>** in C<sub>2</sub>D<sub>2</sub>Cl<sub>4</sub> at 100 °C.

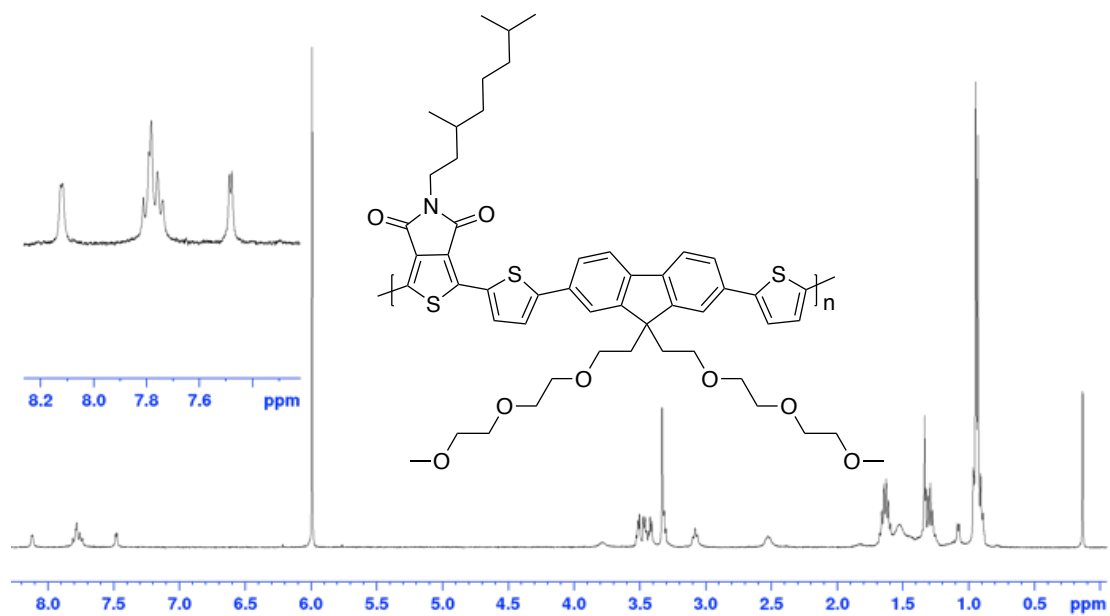


**Figure S 7.**  $^1\text{H}$  NMR spectrum of  $\text{PF}_{\text{oxy}}\text{DT-TPD}_{\text{DMO}}$  in  $\text{C}_2\text{D}_2\text{Cl}_4$  at  $100\text{ }^\circ\text{C}$ .

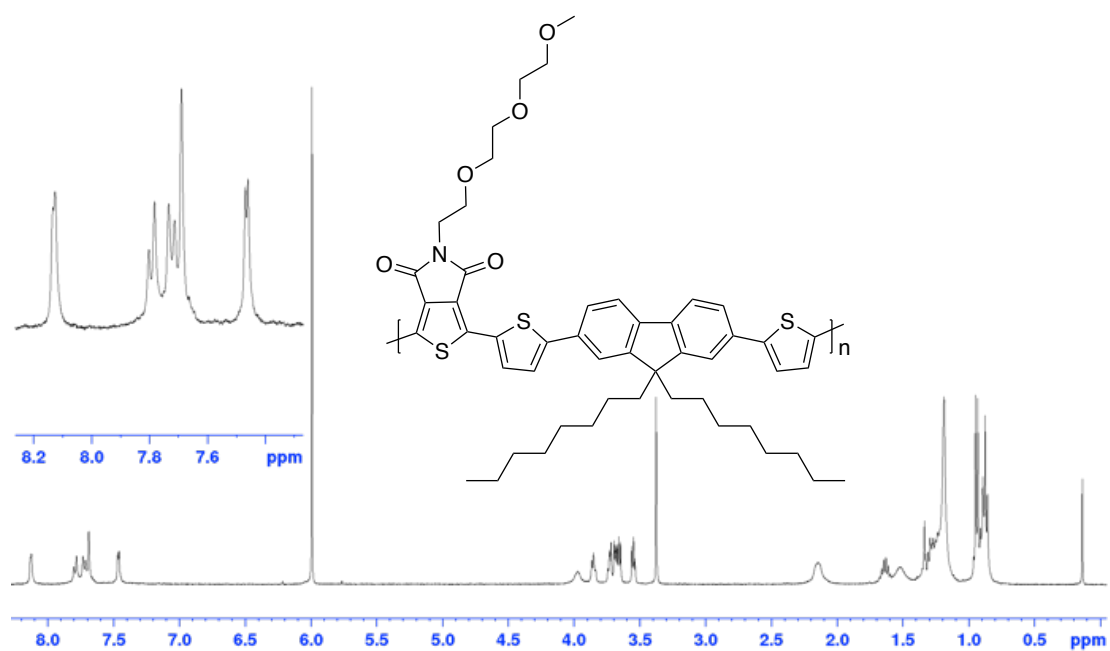


**Figure S 8.**  $^1\text{H}$  NMR spectrum of  $\text{PF}_0\text{DT-TPD}_{\text{oxY}}$  in  $\text{C}_2\text{D}_2\text{Cl}_4$  at  $100\text{ }^\circ\text{C}$ .

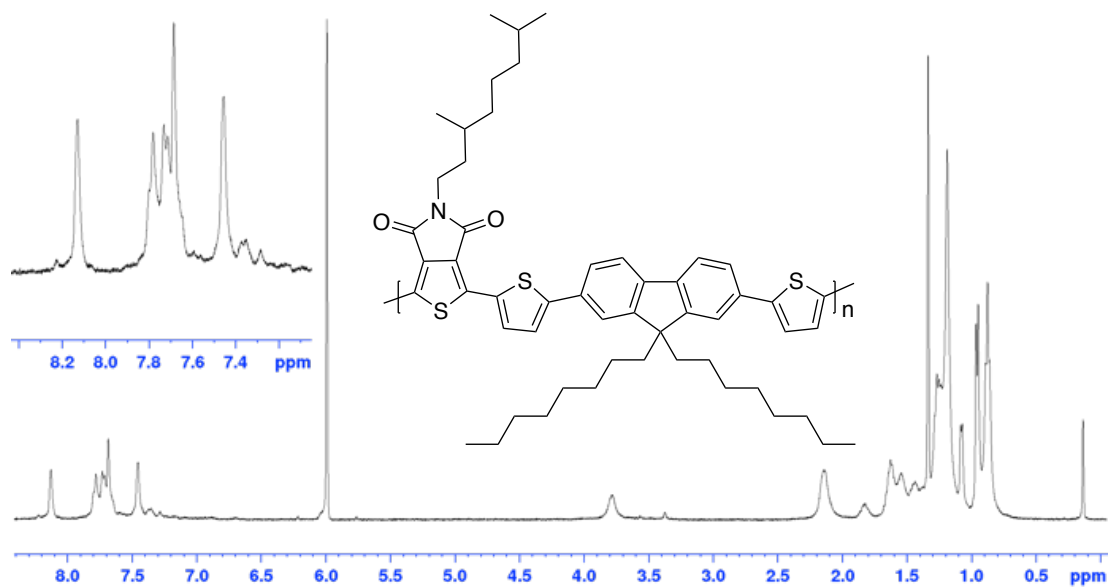


**Figure S 9.**  $^1\text{H}$  NMR spectrum of  $\text{PF}_0\text{DT-TPD}_{\text{DMO}}$  in  $\text{C}_2\text{D}_2\text{Cl}_4$  at  $100\text{ }^\circ\text{C}$ .

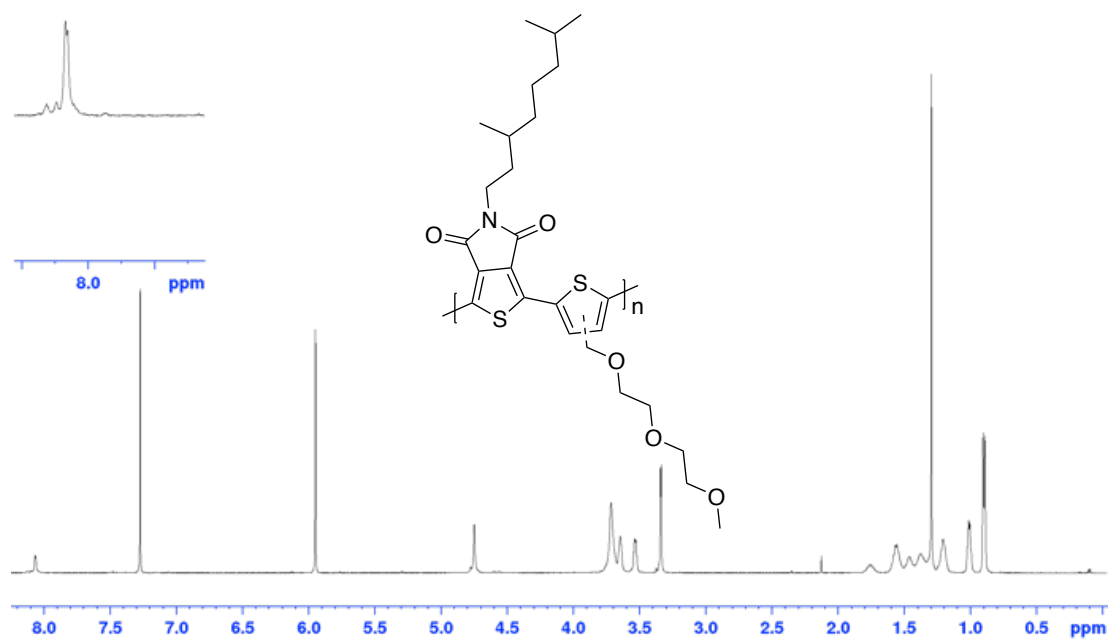


**Figure S 10.**  $^1\text{H}$  NMR spectrum of  $\text{PT}_{0\text{xy}}\text{-TPD}_{\text{DMO}}$  in  $\text{C}_2\text{D}_2\text{Cl}_4$  at  $100\text{ }^\circ\text{C}$ .



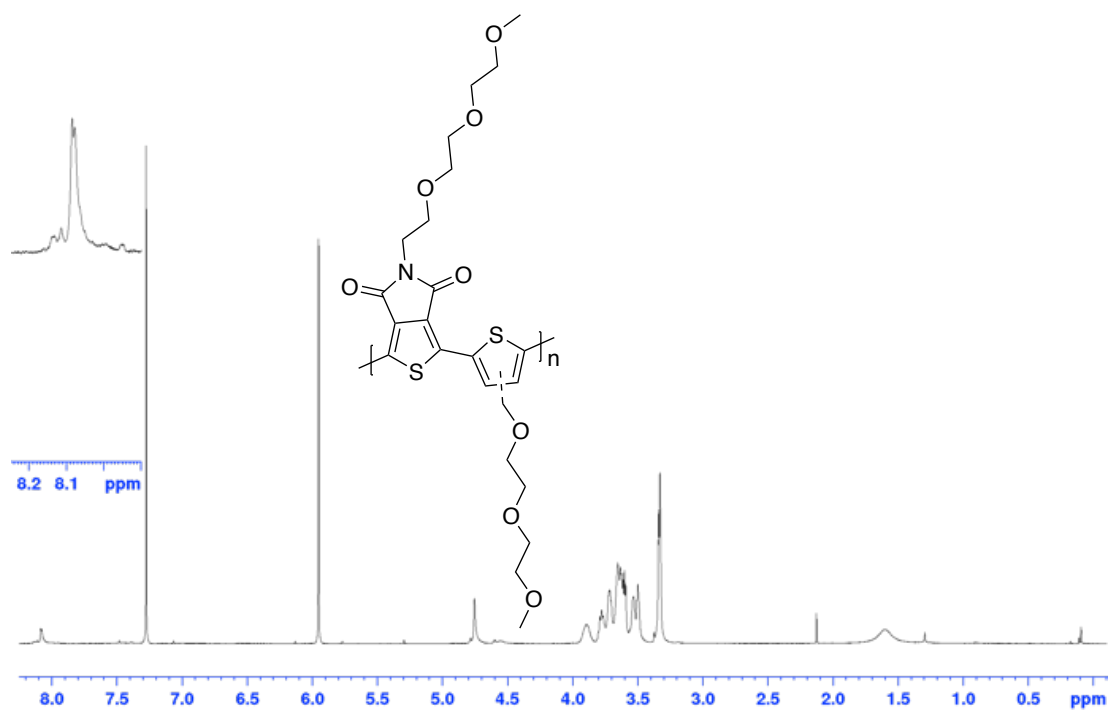


**Figure S 11.** <sup>1</sup>H NMR spectrum of PT<sub>oxy</sub>-TPD<sub>oxY</sub> in C<sub>2</sub>D<sub>2</sub>Cl<sub>4</sub> at 100 °C.

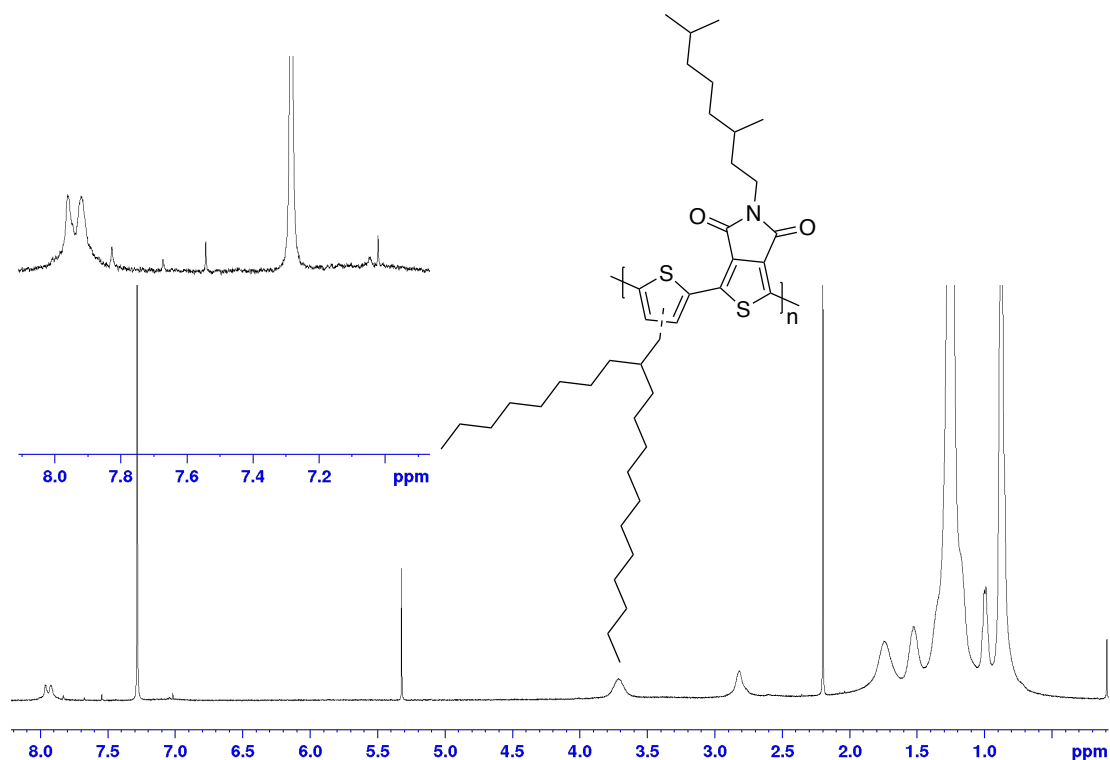
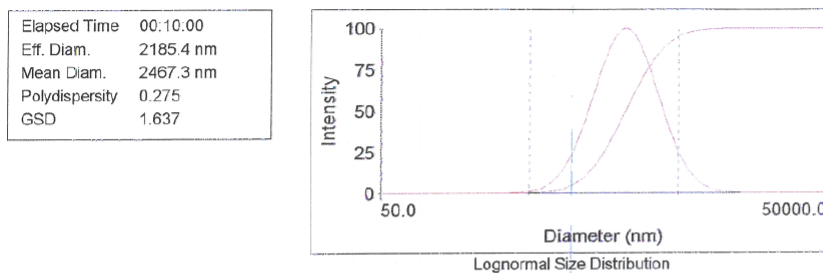


**Figure S 12.** <sup>1</sup>H NMR spectrum of PT<sub>ODD</sub>-TPD<sub>DMO</sub> in CDCl<sub>3</sub> at 25 °C.

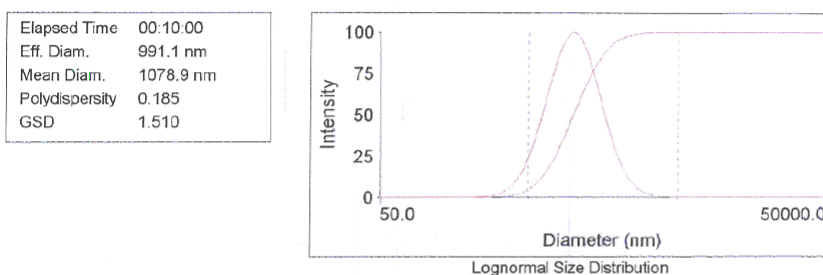
**PToxy-TPDmo in 100% CHCl3 at 0.5 mg/ml**



| d(nm)  | G(d) | C(d) | d(nm)  | G(d) | C(d) | d(nm)  | G(d) | C(d) |
|--------|------|------|--------|------|------|--------|------|------|
| 972.0  | 26   | 5    | 1929.4 | 97   | 40   | 3045.9 | 80   | 75   |
| 1162.2 | 44   | 10   | 2053.9 | 99   | 45   | 3308.7 | 70   | 80   |
| 1312.0 | 58   | 15   | 2185.4 | 100  | 50   | 3640.5 | 58   | 85   |
| 1443.5 | 70   | 20   | 2325.4 | 99   | 55   | 4109.4 | 44   | 90   |
| 1568.1 | 80   | 25   | 2475.5 | 97   | 60   | 4914.0 | 26   | 95   |
| 1688.3 | 87   | 30   | 2641.8 | 93   | 65   |        |      |      |
| 1807.9 | 93   | 35   | 2829.0 | 87   | 70   |        |      |      |

**Figure S 13.** Particles size analysis of **PT<sub>OXY</sub>-TPD<sub>DMO</sub>** with DLS in CHCl<sub>3</sub> solution.

**PToxy-TPDmo in 100% TCE at 0.5 mg/ml**



| d(nm) | G(d) | C(d) | d(nm)  | G(d) | C(d) | d(nm)  | G(d) | C(d) |
|-------|------|------|--------|------|------|--------|------|------|
| 503.2 | 26   | 5    | 893.0  | 97   | 40   | 1308.3 | 80   | 75   |
| 584.4 | 44   | 10   | 940.9  | 99   | 45   | 1402.1 | 70   | 80   |
| 646.8 | 58   | 15   | 991.1  | 100  | 50   | 1518.7 | 58   | 85   |
| 700.6 | 70   | 20   | 1043.9 | 99   | 55   | 1680.7 | 44   | 90   |
| 750.8 | 80   | 25   | 1100.0 | 97   | 60   | 1951.8 | 26   | 95   |
| 798.6 | 87   | 30   | 1161.4 | 93   | 65   |        |      |      |
| 845.7 | 93   | 35   | 1229.9 | 87   | 70   |        |      |      |

**Figure S 14.** Particles size analysis of **PT<sub>OXY</sub>-TPD<sub>DMO</sub>** with DLS in TCE solution.